CRANFIELD INSTITUTE OF TECHNOLOGY

SCHOOL OF MECHANICAL ENGINEERING

PhD THESIS

Academic Year 1991-92

C S WELCH

Servicing polar platforms using electric propulsion

Supervisor: Prof. J.B. Moss

February 1992

Abstract

The future of space development has been examined in the context of the infrastructure necessary to support it. It is concluded that the selection of propulsion systems for in-orbit transportation requires the development of general computer codes capable of simulating the use of a wide range of propulsion systems on near-Earth missions.

It is also concluded that, even if limited infrastructural development occurs, polar orbiting spacecraft will be an important feature of future space activities. Replacing current single-use polar spacecraft with extended-life serviceable platforms is attractive. However, the very limited manned access to polar orbits in the mid-term future suggests that such platforms will only be possible if remote telerobotic/autonomous servicing can be carried out. To this extent polar platforms are considered to provide a useful driver and first testbed for the development of technologies designed to extend human capability in those regimes where direct mediation is not possible.

Options for such remote servicing are examined, the concept of performing nodal transfers by enhanced differential nodal drift is introduced and the application of electric propulsion to this discussed. Low-thrust orbital manoeuvres are analyzed in this context and the conditions for optimum nodal transfer defined. Particular service vehicle configurations are then defined against a projected infrastructure and baseline polar platform constellation. A model for the service vehicle is defined and its performance investigated using a number of electric propulsion systems. Simulations of transfer manoeuvres have been carried out and the effects and relative importance of the various orbit perturbations identified. It is concluded that a service vehicle propelled by a Xenon ion system offers the capability required and two final configurations are identified characterising different servicing mission upload schemes.

Contents

List of figures

List of tables

List of abbreviations

APSA Advanced photovoltaic solar array

BOL Beginning of life

CADV Crew-only ascent/descent vehicle

EDRS European data relay satellites

ELV Expendable launch vehicle

EOL End of life

EOS Earth observing system

EOTV Electric orbit transfer vehicle

GaAs Gallium arsenide

GN&C Guidance, navigation and control

GPS Global positioning system

InP Indium phosphide

LP Logistics platform

MMH Monomethylhydrazine

MPD Magnetoplasmadynamic

N_2O_4 Nitrogen tetroxide

NASP National aerospace plane

NLS National launch system

OMV Orbit manoeuvering vehicle

ORU Orbital replacement unit

OTSV Orbit transfer and servicing vehic;e

OTV Orbit transfer vehicle

PAM Payload assist module

RTG Radioisotope thermal generator

RDV Rendezvous and docking vehicle

Si Silicon

STME Space transportation main engines

SV Service vehicle

TRDSS Tracking and data relay satellite system

TRMS Teloperated remote manipulator system

TT&C Telemetry, tracking and command

Notation

a	semimajor axis
a_{ps}	area of power source
a'	acceleration
a'_{east}	acceleration level for eastward transfer
a'_{max}	maximum acceleration level
a'_{q}	acceleration due to solar radiation pressure
a'_{west}	acceleration level for westward transfer
a'_{n}	acceleration component normal to orbit plane
a'_{r}	acceleration component in radial direction
a'_{t}	acceleration component in plane, at 90° to radius in direction of motion
A	area
A(L)	function of equinoctial elements f_e and L and W
b_o	arbitrary constant to give zero error for calculated density
B	magnetic field strength
B(L)	function of equinoctial elements g_e and L and W
c_p	specific heat
C_d	drag coefficient
C_{22}	first tesseral harmonic in geopotential field
e	eccentricity
e_o	initial eccentricity
e_1	final eccentricity
E	eccentric anomaly
E	electric field strength
f_e	equinoctial orbital element and unit axis
f_{ac}	attitude control propellant fraction

f_{dg} array annual degradation factor

f_{ec} eclipse factor

f_s structure fraction

f_{tk} tankage fraction

F thrust

F_a density amplitude fluctuation

F_d drag force

F_e position co-ordinate in equinoctial frame

$\dot{F}_e$ velocity co-ordinate in equinoctial frame

F' function of r_p, v_p, i, ω'

g_e equinoctial orbital element and unit axis

G_e position co-ordinate in equinoctial frame

$\dot{G}_e$ velocity co-ordinate in equinoctial frame

G universal gravitational constant

h_e equinoctial orbital element

h altitude

h' specific angular momentum

h_o reference altitude

H_o density scale height at reference altitude

i inclination

i_A inclination of reference orbit

i_B inclination of drift orbit

I current

j current density

J_2 first zonal harmonic in geopotential field

J_3 second zonal harmonic in geopotential field

J_4 third zonal harmonic in geopotential field

k_e equinoctial orbital element

k_r reflection factor

k function of Θ, β_{opt}

k' function of k

l_t lifetime of thruster units

L true longitude

n number of orbits

m number of days before groundtrack repeats

$\dot{m}$ mass flow rate

m_{aum} all-up mass

m_f final mass of rocket

$m_{m.prop}$ mass of manoeuvre propellant

m_{ms} mass of manoeuvring system

$m_{m.th}$ mass of manoeuvre thrusters

$m_{m.tk}$ mass of manoeuvre propellant tankage

m_o initial mass of rocket

m_p mass of propellant

m_{pp} mass of power processor

m_{ps} mass of power source

m_s mass of structure

m_{sc} mass of spacecraft

m_{sv} mass of service vehicle

m_t mass of thrusters

m_{tc} mass of thermal control system

m_{tk} mass of tankage

m_{ttc} mass of TT&C and GN&C systems

M mean anomaly

M'	matrix relating equatorial to equinoctial frame
M_e	mass of Earth
N	number of thrusters in network
N'	matrix relating equinoctial to spacecraft frame
p	semilatus rectum
P	power
P_b	beam power
P_{bol}	power at beginning of life
P_{eol}	power at end of life
P_t	power supplied to thrusters
P_{tc}	power rejected as heat to thermal control system
q	charge
q_o	solar radiation pressure at 1 AU
Q	disturbing potential
r	radius
r_a	radius of apoapsis
r_A	radius of reference orbit
r_B	radius of drift orbit
r_e	mean equatorial radius of Earth
r_p	radius of periapsis
R	mass ratio
S	reference area of spacecraft
S_{array}	reference area of spacecraft arrays
S_{front}	reference area of side of spacecraft
S_{side}	reference area of side of spacecraft
S_{22}	second tesseral harmonic in geopotential field
t	total trip time

t_b total thruster burn time (i.e cumulative total)

t_b' overall mission burn time (i.e. including eclipsed periods)

t_d time in drift orbit

t_m mission duration

t_t transfer time

T_c chamber temperature

T_e exit temperature

u argument of latitude

u_s thrust reversal angle

U shadowing factor

U_g gravitational potential

v velocity

v_c circular orbit velocity

v_{ch} characteristic velocity

v_e exhaust velocity

V_a potential difference across accelerator grid

w_e equinoctial unit axis

W function of equinoctial elements f_e,g_e,L

W_e position co-ordinate in equinoctial frame

$\dot{W}_e$ velocity co-ordinate in equinoctial frame

X function of equinoctial elements h_e,k_e

α right ascension

α_s earth-spacecraft-sun angle

α' In-plane thrust angle

$\alpha_{m.th}$ specific mass of manoeuvre thrusters

α'_{opt} Optimum in-plane thrust angle

α_{pp} inverse specific power of power processor

α_{ps} inverse specific power of power source

α_{tc} inverse specific power of thermal control system

$\dot{\alpha}$ mean angular velocity of earth about sun

β wedge angle of intersection between two orbits

β' Out of plane thrust angle

β'_{opt} Optimum out of plane thrust angle

β_{ps} area to power ratio of power source

δ function of F', S, C_d, m_s

Δv characteristic velocity

Δv_{east} Δv for eastward transfer

Δv_{west} Δv for westward transfer

Δv_{drag} Δv required for drag make-up

ϵ angle between equatorial and ecliptic planes

η overall efficiency

η_e electrical efficiency

η_f efficiency factor due to frozen flow losses

η_h efficiency factor due to heat transfer losses

η_m mass utilisation efficiency

η_n efficiency factor due to propellant expansion in nozzle

η_{pp} efficiency of power processing

η_t efficiency of thruster

θ true anomaly

λ_g geographic longitude

λ_n lagrangian multiplier

μ gravitational parameter

ρ atmospheric density

ρ_o atmospheric density at reference altitude

ρ mean atmospheric density over diurnal period

σ angle between velocity vector and sun vector

σ_c conductivity

τ time of periapsis passage

ϕ geographic latitude

ϕ' geographic co-latitude

ψ_1 in-plane thrust angle

ψ_2 out-of-plane thrust angle

Ω right ascension of the ascending node

$\dot{\Omega}_A$ nodal drift rate of reference orbit

$\dot{\Omega}_B$ nodal drift rate of drift orbit

$\dot{\Omega}_d$ differential nodal drift rate

$\dot{\Omega}_{md}$ mean differential nodal drift rate

ω argument of periapsis

ω' angular velocity of atmosphere

Acknowledgements

I would like to thank the following people:

Professor J.B. Moss, my supervisor, who gave me invaluable help, advice and encouragement throughout my time at Cranfield and afterwards.

Mr. C. Moller who kindly volunteered to 'project manage' me through the last year.

Dr. P.S. Welch, my late father, for the example he set me.

Sue, my wife, for the diagrams, the proof-reading and, most of all, her extreme patience.

Chapter 1 - Introduction

1.1 Introduction

This chapter describes the background to the work in the thesis. It presents a view of the development of space activities from inception to maturity and then delineates a possible form for a long term future space architecture. The importance of effective space transportation systems in the operation of such is then highlighted as an area worthy of more study. This necessitates the development of simulation tools to allow different propulsion systems and missions to be evaluated against a common background, in this case with particular reference to the space segment. The resulting development of such a simulation tool is then briefly described before the particular prospect of the servicing of polar platforms is introduced, specifically that using electric propulsion systems. The broad approach to this problem is then summarised and, finally, the structure of the thesis described.

1.2 Trends in space development

Despite the continuing difficulties that the world space community has experienced in implementing its larger-scale and longer-term goals, there is an obvious trend in all future programmes and plans. This trend, which can be argued to be an evolutionary one, is a move away from the undertaking of space-orientated activities with little or no reference to each other and towards a situation in which the different elements form mutually interdependent parts of a larger whole.

This trend is not exclusive to the development and utilisation of space and can be observed to a greater or lesser extent in the advancement of other fields of technological endeavour (Sadin [1]). Although there are numerous factors which may contribute to the trend, two fundamental drivers are cost and capability. In broad terms, the smaller the ratio of cost to capability, the faster the field will progress. This effect can be observed in some 'sub-fields' of space development which have moved forward at a significantly faster rate than others as their cost-capability ratio has reduced with time. Perhaps the prime

example of this is the development of communication and direct broadcast satellites.

The development of a new and promising field of technology can be described in terms of the following development cycle. At the start, a high-level of funding is usually needed to stimulate work in the field (i.e. 'pump-priming'). In this climate the amount of activity in the field expands, with the emphasis on groundbreaking work. In a comparatively short time a basic capability may be obtained, albeit at a very high cost.

Examining the development of space activities in the light of the above, the first, 'immature' stage can be considered broadly to be the period from 1957 to the early 1970's. During this period NASA was created in the US and ELDO (European Launcher Development Organisation) and ESRO (European Space Research Organisation) in Europe. The fundamentals of manned spaceflight were defined, Man landed on the Moon, numerous unmanned interplanetary missions were dispatched, two space-stations established and six nations placed satellites into orbit through independent effort. This period also encompasses the first use of Earth applications satellites with geostationary communications satellites becoming commercially viable after a comparatively short period.

However, once a field has matured somewhat, initial groundbreaking work starts to be replaced by projects which aim to extend the basic knowledge and capabilities developed in the first part of the development cycle. Usually the rate of funding increase, or even the total funding itself, drops off. In simplistic terms this is because the field now has to compete with other already-established fields, or possibly with completely external undertakings, for the attention of the funding provider. At this stage 'value for money' (i.e reducing the cost-capability ratio) starts to become more important than breaking new ground. This can result in substantial forward-planning activities aimed at defining a series of objectives to support a general strategy for development. Concomitant with this, the first real practical applications of the field may be developed and commercial investment can start.

If funding for space had continued at its initial high level then the first stage could have continued well into the 1970's but, for numerous societal and political reasons that will not be addressed here, this did not happen. The development of space entered the second stage, at least as far as the near-Earth activities were concerned. The two main cost drivers for the development of this sphere were and are those governing transportation into orbit and manned space operations. In addition, the latter requires detailed knowledge of the long-term effects of microgravity and the space environment on humans before placing significant numbers of them in orbit. The second stage of space development in the USA and the USSR reflected these concerns (and possibly national preoccupations, also) with the former concentrating most visibly on the development of the Space Shuttle and the latter on additional manned space stations. In Europe the formation of the European Space Agency from ELDO and ESRO, with the aim of achieving and maintaining independent space capability, engendered local first stage activity culminating in the first Ariane launch in 1979. More recently, Japan entered its own first stage (and should probably be considered to have achieved the second stage by now). Interplanetary exploration continued, more earth resources missions were orbited, and launch systems developed into a commercial undertaking designed to support, in the main, the ever expanding geostationary satellite market. This last is more highly developed than any other sector of space development and, to the extent that satellite communications, direct broadcast TV and images from weather satellites are considered commonplace, may be considered to have entered the third stage of development (described below). More recently, earth resources applications have started to come to the fore and this field is also starting to develop commercially.

The final stage of the development cycle comes about when the knowledge-base is sufficiently large that activities within the field may be performed on a routine basis. Here those undertakings that characterise the field are starting to become part of normal human activities. Alongside such integration with the mainstream comes the definite economic requirement for the field, if not to pay its way, at least to aim to perform in as efficient a way as possible. By this stage the capabilities of the field have developed quite considerably and any given task may be performed in a number of ways. This factor,

combined with the drive to maximise cost benefit predicates the design of assets to enable them to be used in as flexible a manner as possible. This, in turn, means that a much wider view must be taken of the field. Tasks are no longer conceived and undertaken independently, but against the background of some definite architecture or infrastructure. This makes the overall capabilities of the field very wide, but also makes each sub-field much more dependent on the others than previously. From this point on the field may be considered to be mature.

As far as the overall development and utilisation of space is concerned, the stage third stage has not yet been achieved, with most launch systems and satellites remaining disposable assets. The prime reason for this is connected with the cost of access to orbit. Although this cost has fallen by a factor of five over the last twenty-five years (Parkinson [2]), most of the improvement occurred earlier rather than later in this timespan. Although the Space Shuttle is technically more advanced than expendable launch vehicles, it is not significantly cheaper in terms of dollars per kilogramme in orbit because its development was severely constrained financially. This has kept the cost-capability ratio low over the short-term at the expense of inhibiting significant further development. If a completely re-useable Earth-to-orbit transportation system were to be developed launch costs would be reduced. This would make access to space significantly easier and cheaper and hence bolster the economic attractiveness of re-useable space resources. Although 'one-shot technology' may be eminently practical for specific small-scale applications, it is apparent that the capabilities of the space sector will not be fully utilised until some form of permanent space infrastructure has been achieved. Albeit that the various space authorities have invested significant amounts of effort in the planning of this, they have been faced with the difficulty that the integrated nature of the infrastructure means that it must be purchased en masse since the components are much less valid as systems when taken individually. The cost of doing this has, in all cases so far, deterred governments from implementing the plans. Nevertheless, as the applications of space development and the general world level of space technology have increased, the argument for the creation of a permanent space infrastructure has become increasingly compelling.

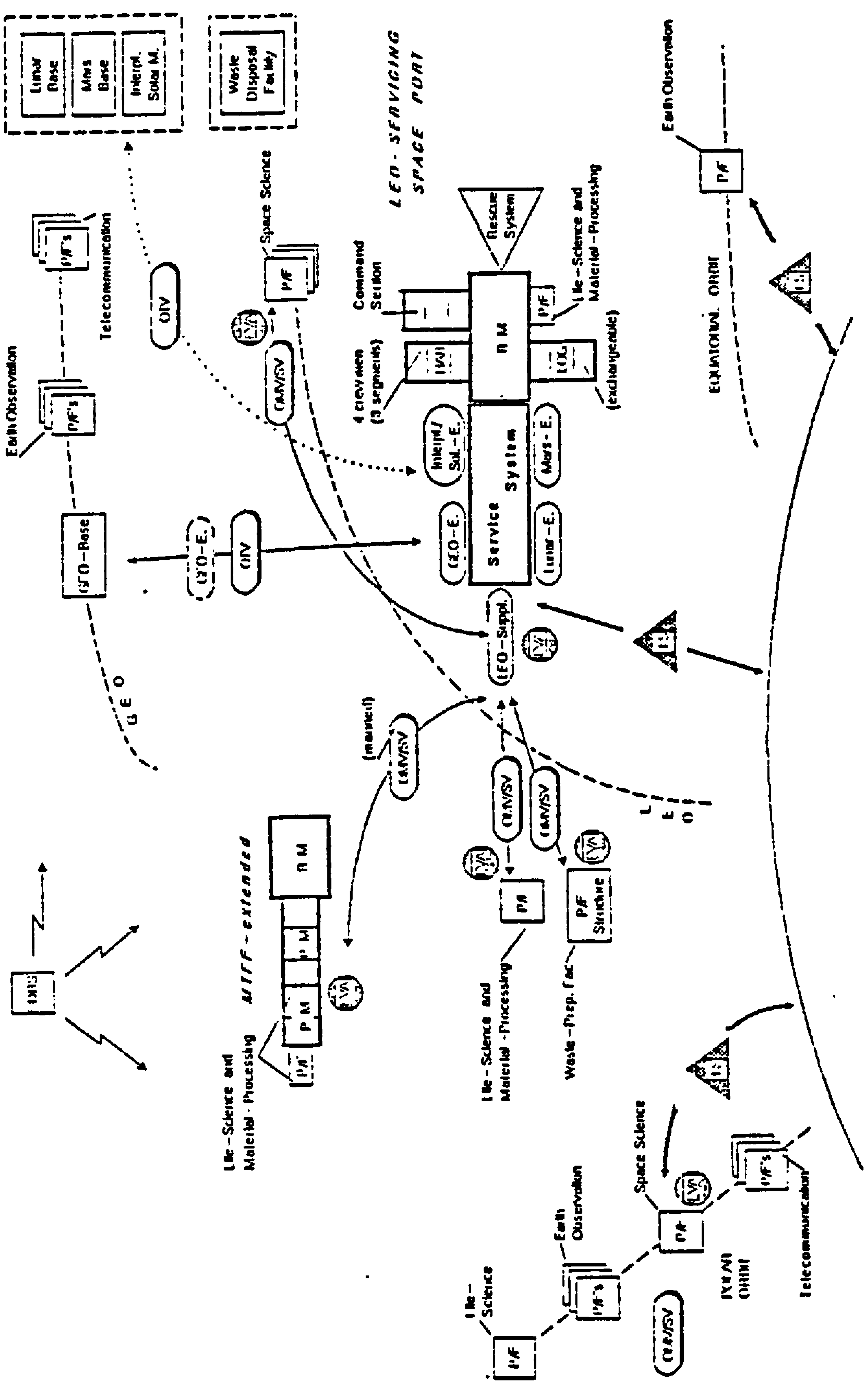

Figure 1.1 Global scenario chart for a future space infrastructure (Riedel [4]).

The long-term orbital infrastructure will almost certainly feature Man as an essential asset (Kline [3]). Initially he/she will be based in space stations in low earth orbit, later on in geostationary and polar orbits and finally on the Moon and beyond (Riedel [4]). The size, scope and complexity of space systems deployed is liable to increase substantially and single-use satellites will eventually be replaced by reconfigurable platforms. The mass of these may well eventually exceed the capability of single launches, leading to in-orbit assembly followed by transfer to operational orbit. In parallel with this, in-orbit servicing and repair operations will become very important (Reuter [5]). However, the cost of supporting Man in space will also mean that he/she will not necessarily be directly involved in all activities. Where it is not possible or economic for Man to perform servicing and repairs, use will be made of telerobotic or autonomous servicing techniques, a field that will become increasingly important as the infrastructure develops (Varsi [6]). A schematic of such an infrastructure is given on the preceding page in Figure 1.1.

In support of the space-based infrastructure assets a well-integrated communications infrastructure will also be needed. This will to have provide for reliable communications between space and ground and between the various in-orbit assets. Without such communications, the coherent nature of the space infrastructure would be significantly degraded. (Dickinson et al. [7]).

The third part of the total space infrastructure is a transportation infrastructure. This can be broadly considered in two parts. The Earth-Space component will provide access to orbit for the payloads and astronauts. Initially this will continue to be serviced by conventional expendable launch vehicles (ELVs), the US Shuttle and the European Hermes. Eventually, however, fully reusable, air-breathing horizontal-take-off-and-landing vehicles may be expected to replace these, possibly complemented by re-usable vertical take-off launch systems to provide heavy-lift capability. In-space transportation will be achieved by use of space-based Orbit Transfer Vehicles (OTVs) which will meet the requirement for transfer of payload and personnel between parts of the in-orbit infrastructure. Again, the transportation infrastructure is an integral part of the overall space infrastructure, the efficiency of which significantly effects the overall performance of the whole.

Although the detailed implementation of the space infrastructure outlined above is open to debate, its overall nature and scope is generally accepted. Much more uncertain, however, is the timescale over which it may be achieved since this is dependent on the vicissitudes of world affairs more than on technological expertise. This aside, the advent of the International Space Station with its US, Japanese and European components and the development of further partially reusable launch systems indicates that there is liable to be at least a minimum stage three space infrastructure by early in the next century.

1.3 Background to thesis

It has been stated that space transportation is an important part of a future space infrastructure. It follows, therefore, that the design and operation of the relevant transportation systems is worthy of careful consideration. The two portions of the transport infrastructure, Earth-space and in-space, are characterised by very different requirements. Of the two, the former is the more easily defined since the basic task to be undertaken is always the same. The latter is more complex to define because there is wide variation in the capabilities required to perform different missions which are defined, in the main, by the orbital mechanics of the situation. Furthermore, different types of propulsion system may be adopted, each with their own particular characteristics. As well as conventional and advanced chemical propulsion systems, other systems suggested include solar thermal, laser thermal, electric propulsion and nuclear propulsion (see Caveny [8]), Fearn [9], George [10]).

This diverse range of propulsion technologies has meant that many designs for orbit manoeuvring, raising, and transfer vehicles (hereafter referred to collectively as OTVs) have been suggested. These have been designed to undertake tasks such as placement/recovery/servicing of satellites in low-earth and geostationary orbits, transfer between a space station and other facilities in low-earth orbit and injection of payloads into translunar and interplanetary trajectories (for examples see Caluori and Saxton [11], Charhut and Ketchun [12], Dickey et al [13] and Thomas and Thirkettle [14]). It should be noted that the study of servicing and resupply missions, particularly those in low orbit, is a broad area since a wide range of general strategies exist. The options for resupplying a satellite using an OTV

include; using it to deliver resupply crew to satellite; using it to perform autonomous/teleoperated resupply; using it to recover the satellite to the Space Station; using it to deliver the satellite to some other resupply node, with the options all open to influence by other factors such as the total number of platforms to be resupplied, the resupply period and the ease of access to the platforms from other points in the infrastructure.

Some of the studies into OTV missions include orbit mechanical analyses of the operation of the vehicles that they deal with, but in many cases this does not extend beyond the calculation the of Δv's necessary to perform the missions. Although acceptable for defining the broad operational limits needed in forward planning/systems-level studies, these calculations are not sufficient for the detailed investigation and optimisation of vehicle and mission configurations. In addition, in those cases where more detailed vehicle and mission analysis has been carried out, this is done using simulations developed particularly for the case in hand. In general terms the strategy for such studies is to approximate some characteristic of the orbital mechanics in an attempt to simplify the analysis. Two common examples of this are; the assumption of instantaneous application of velocity changes to a spacecraft by a high-thrust propulsion system; and the approximation of the effects of perturbations over time by semi-empirical formulae. This is both understandable and valid since the adoption of specific application-orientated techniques allows the performance of individual assessments to be carried out both more easily and more effectively than a full-scale simulation would be. Unfortunately, though, this makes comparison of the results of the different studies difficult since they will have different underlying assumptions and utilise different approximations to reality. In the end there is a necessity for all mission simulations to be evaluated using a common standard.

The first part of this thesis, then, originates in the wish to develop a very general framework against which to model the performance and orbit mechanics of spacecraft equipped with a wide range of propulsion and control systems. The broad approach taken has been to model the effects of thrust as one of the perturbations acting on an orbit described in terms of an orbital co-ordinate system not subject

to singularities for circular orbits (since these form a major area of interest). This idea has been implemented in a computer program designed with the underlying philosophy of generality in mind. To a certain extent this philosophy proved to be at variance with the parallel aim of designing the program to be as easy to use as possible. Bearing in mind this conflict, the final program represents an acceptable compromise between the two extremes.

There were and are a wide range of existing studies that could be examined in more detail. In the light of the previously expressed interest in the future development of a space transportation infrastructure, a number of near and mid-term mission scenarios were considered for further investigation in parallel with the program development. In particular, at this time early work was being done in the US and Europe on co-orbiting and polar orbiting platforms as part of the International Space Station and Columbus definition, the first manifestation of a third-stage space infrastructure. Examining the scenarios then under discussion suggested that, even if they were not to come to fruition as then conceived, they were probably representative of future infrastructure developments.

Coincident with this, concern over the global environment was starting to become more widespread and the application of remote sensing and earth resources satellites to the monitoring of this was starting to become more widespread. The development of expertise in this area was part of declared UK space policy and, worldwide, the field was starting to move towards a more commercial footing than hitherto. Given this, it was concluded that analysis of Freedom/Columbus polar platform plans would prove a useful guide to future infrastructure concerns and, furthermore, that even if the major parts of Freedom/Columbus were to be deleted at a future stage the polar platforms were unlikely to be included in this because of the dual commercial and environmental pressures for more remote sensing payloads to be orbited. From this viewpoint, it may be argued that polar platforms are a most fundamental part of a future space infrastructure since they appear to be on the verge of becoming part of the mainstream of human activities and capable of entering their own third stage even if the larger sphere of space development remains stalled. Advantageously, however, many of the problems to be addressed and solved

in the servicing of polar platforms have much wider applications in space and so, were this unfortunate scenario to come about, progress could still be made on these topics.

At this stage in the work it was anticipated that the polar platforms under consideration would be serviced at regular intervals. It was apparent that this process was significantly more demanding than that for the space station co-orbiting platforms (this, and other matters outlined here, are discussed in more detail in Chapter 4). It was also concluded that some of the issues that will become more relevant and important as a full third stage infrastructure develops are already exhibited in this field. These include difficulty in achieving regular access (manned or unmanned), minimising disruption to normal operations, provision of suitable in-orbit spares, and the selection of suitable propulsion systems to perform transport/servicing in as efficient a manner as possible. Given this emergence of polar platforms and their servicing as a field of strong future interest, this area was selected for further investigation in order to determine a suitable sphere of study. Attention was then focused on this as a worthwhile area for further investigation. Because of servicing vehicle limitations the scenarios then under consideration were heavily constrained propulsively and required high thrust propulsion systems. Ultimately, however, the decision was taken to make the new generation of polar platform disposable rather than serviceable. Although this reduced the immediate interest in polar platform servicing, it also widened the scope of the topic since it reinforced the basic argument for considering the servicing of polar platforms as an encapsulation of future infrastructure needs.

As part of the process of examining this wider scope, the application of different propulsion systems was considered. As a result of this the use of electric propulsion appeared to be of interest. This type of propulsion, which is characterised by high exhaust velocities, low propellant consumption, low thrust and high payload fractions, has been in existence for nearly thirty years, but still has to find widespread use despite the benefits it offers. Nevertheless the technology is under active development and in-flight demonstrations are currently planned/proposed by both the Europe (Bartoli and Berry [15]) and the United States (Dickey et al. [13] and Deininger and Vondra [16]). Many studies of the use of electric

propulsion have been carried, mainly covering the emplacement of satellites in geostationary orbit (some of these are discussed in Chapter 6). Less attention has been paid to the application in low earth orbits, generally because the Δv requirements tend not to be large enough to make the use of electric propulsion attractive. However, examination by the author of the use of electric propulsion as the motive force for a servicing vehicle designed to resupply a polar platform constellation showed that this was worthy of closer examination. This subject, then, forms the second part of the thesis.

1.4 Method of approach

It may be useful to outline the approach taken to the polar platform servicing study. Initially a familiarisation exercise was undertaken which involved developing an appreciation of their particular orbital mechanics, the general characteristics of platform servicing and retrieval, and how these were determined by particular space transportation infrastructure configurations. Once these had been established the task of determining the fundamental techniques for performing the necessary orbital manoeuvres was pursued, together with the investigation of how such manoeuvres might be optimised.

Although it has already been stated in general terms that no part of a future space infrastructure can be considered independently of any other it was ascertained quite early that this is somewhat less true for polar orbiting spacecraft than for those in low inclination orbits. A Δv of approximately 9 $km.s^{-1}$ is required to transfer from low inclination low-earth orbits to polar ones and this effectively precludes any commerce between the two in the near future (this can be seen in Figure 1.1 where no links are shown between the two realms). Given this, a baseline was developed against which platform servicing could be examined. Working with the assumption that 'second generation' serviceable polar platforms would be introduced in the 2015-2025 timeframe, and given current knowledge of future programmes, it was determined that the transportation infrastructure is unlikely to be well-developed as far as access to polar orbits is concerned. From this it was concluded that polar platform servicing could be accomplished only by use of expendable launch vehicles and remote servicing techniques. Given these limitations, a baseline polar platform and constellation configurations were established and four servicing scenarios delineated.

A systems level design for an electrically propelled service vehicle was then performed and incorporated in a general model, and the performance of the different electrical propulsion systems were characterised. The propulsive requirements for each of the servicing scenarios were then determined. Integrating these with the vehicle model allowed evaluation of the relative merits of the various scenario/vehicle combinations, leading to two worthy of more detailed investigation.

The actual operation of one of these service vehicles was then investigated using the computer program to determine how closely its performance matched that predicted by the general model of nodal transfer manoeuvres already derived. The effects of earth asphericity, atmospheric drag and solar radiation pressure were identified and the implication of these for the servicing mission and vehicle design identified.

1.5 Structure of thesis

The broad structure of the thesis is as follows; this, the first chapter, describes the background to the work, the method of approach and the structure of the thesis. The second chapter introduces polar platforms and discusses both the general techniques and propulsive options for servicing them. Chapter 3 establishes the basis for the modelling of perturbed orbital motion which is incorporated into the computer programs described in Chapter 4. The next chapter gives a general coverage of electric propulsion technologies and the characteristics of solar photovoltaic power sources. The sixth chapter investigates the performance of orbital manoeuvres using low-thrust propulsion with particular reference to quasi-circular orbits and then examines how differential nodal drift may be used to effect nodal transfers. Chapter 7 makes predictions as to the likely state of the relevant portions of space infrastructure in the timeframe of interest and, from this, then defines a baseline polar platform constellation against which to examine servicing and a number of possible servicing scenarios. From this, and the concepts developed in Chapter 6, a service vehicle model is defined in Chapter 8. This is then used to evaluate the performance of a number of electric propulsion systems in conjunction with the servicing scenarios. Chapter 9 describes the results of transfer manoeuvre simulation using the ORBIT_CALC program, the

effects on this of the various perturbations and the significance of these to mission and vehicle design.

The final chapter, 10, summarises and discusses the results of the work.

Chapter 2 - Polar platforms and servicing

2.1 Introduction

This chapter introduces the concept of serviceable orbiting platforms as an evolutionary development from current single-use satellites, delineating some of the benefits to be gained from their use and outlining their history with particular reference to those related to Freedom/Columbus. The orbit mechanics of polar orbiting earth resources satellites are described and the implications of these for platform servicing are discussed. Servicing options are shown to be capable of being classed as one of two types, off-orbit or on-orbit, and the existing work carried out in the areas is surveyed.

2.2 The necessity for satellite servicing

The evolution of satellites so far has featured a steady growth in payload mass and power requirements (Smith [17]). However, during this evolution satellites have remained essentially disposable items planned to have limited lifetimes. Over the last decade discussion has focused on alternative methods for performing the tasks that conventional satellites currently undertake. Two basic approaches have developed. The first of these is to make satellites much smaller and to replace one old-style satellite with a number of the newer ones. Such satellites (known variously as lightsats, smallsats etc.) have much simpler system architectures and achieve reliability through simplicity rather than redundancy, can be developed more quickly and more economically than conventional satellites and can also be launched easily and comparatively cheaply on existing launch systems (Fleeter and Warner [18]). This approach offers considerable benefits, particularly in the short-term. Lightsats nevertheless remain essentially disposable items, embodying no real increase in space technological maturity, and, although useful in many cases, do not represent a complete solution to all future satellite requirements.

The second approach to overcoming the present satellite limitations (e.g. limited lifespan, no opportunities for resupply/repair or upgrading of capabilities) represents a longer term approach and

exploits the benefits to be gained from making satellites fully reusable. Instead of being designed to be single-use, disposable, units it is anticipated that satellites will evolve into what are known as platforms. These will feature easily-maintainable systems and payloads and will be modular in design to enable long term cost reduction through commonality of units, ease of resupply and/or repair through replacement of modules, and reconfiguration over longer periods of time by changing and/or updating payloads. This move towards reusable platforms over disposable satellites can already be seen in the (original) planned infrastructure for the Freedom space station and Columbus which included a man-tended free-flyer and co-orbiting and polar-orbiting platforms (Longhurst [19]). This platform strategy requires a significantly more advanced infrastructure than the lightsat one since the platforms must not only be launched, but also serviced (i.e. be refuelled with AOCS propellant, have faulty components replaced and similar) in orbit at regular intervals. Although such capabilities will be more expensive than those for lightsats, they represent both an important, and ultimately completely necessary, part of any development of space activities in the longer term.

In order to maximise the benefits that may be accrued from this more mature approach it will be necessary to employ systems and strategies that are as efficient, both technically and economically, as possible. Investigations into this have already been performed, with the emphasis on the servicing of platforms in low altitude, low inclination orbits (e.g. Kline and Adornato [20], Meissinger [21], Lutze [22]). This is chiefly because of the comparative ease with which realistic payloads (including men) can be placed into this type of orbit using existing launch systems. The servicing of platforms in near-polar (i.e high-inclination) orbits is significantly more difficult, the situation being exacerbated by the fact that most of the orbits of interest are retrograde ones. Inclination changes are extremely expensive manoeuvres in terms of Δv, particularly in low orbits where the circular orbit velocity is high. This forces launchers of such platforms to use direct injection from a launch site at which a northerly or southerly launch azimuth is permitted, rather than adjusting the inclination after injection. Even launching direct into the necessary orbit imposes heavy penalties. By way of example, the space shuttle can launch approximately 30,000 kg into a 300 km 28.5° orbit, but only about half of this into a 300 km 97° orbit. These mass

penalties appear to preclude manned rendezvous with polar platforms using either existing or planned launch vehicles and were largely responsible for the adoption of a platform deorbit-rendezvous-reorbit strategy (to be discussed in more detail later) for the Freedom/Columbus polar platforms. In any event, the serviceable polar platform concept has now been deleted from the Freedom/Columbus plans. The two platforms involved will now be single use/disposable and will not be serviced (although the 'platform' description remains attached to them).

2.3 The history of space platforms

The origins of the space platform concept can be traced back to a NASA Workshop on Solar and Terrestrial Physics in 1977 (Parkinson [23]). At this time the platform was seen as a technique to extend Spacelab-type missions. It would be revisited twice a year to have instruments exchanged and be refuelled. This would allow considerable benefits over conventional satellites with fixed payload allocations. The original platform concept continued to evolve and by the early 1980s had been formally defined as the Science and Microgravity Applications Platform. It was in this form that the concept was formally adopted as an adjunct to NASA's plans for its space station. Although it was originally envisaged that the platform would have the same orbit inclination as the space station (28.5°) it was discovered that a significant proportion of the platform's potential users had a requirement for a platform in a polar orbit. This was the start of the polar platform.

In parallel with the NASA studies, ESA was investigating what it expected to need for long term orbit infrastructure. When the agency started to consider which elements it might contribute to a joint space station programme with the US, the use of unmanned platforms appeared attractive. At the conclusion of the Columbus B1 studies ESA proposed a number of elements including a polar platform dedicated primarily to earth observation (Shapland [24]). This platform, sized to be launched on an Ariane 5, was anticipated to operate in a morning orbit, complemented by one or more American platforms in an afternoon orbit. At this stage the platform was envisaged as outlined overleaf in Table 2.1 (Sawdon et al. [25]);

Table 2.1 - Columbus polar platform definition at conclusion of B1 stage

Modular platform design:	
Payload module	2904 kg
Utilities module	382 kg
Propulsion module	408 kg (dry mass)
	5208 kg (wet mass)
Orbit characteristics	
Altitude	500-900 km, nominal 850 km
Inclination	97.4-99.8°, nominal 98.8°
Period	94.6-105.1 min, nominal 102 min
Repeat Period	9 days (for 850 km)
Equator crossing time	9.30 - 10.30 am (descending)
Eclipse period	20-36 min
Lifetime	15 years

The platform was to be serviced at regular intervals throughout its lifetime using either the Space Shuttle or Hermes (though the latter option was deleted when design modifications to Hermes removed its payload bay). The nominal servicing scenario developed was to launch the shuttle into a low servicing orbit of 275 km. Once the shuttle was on station the platform was then to be deboosted from its operational orbit and captured by the shuttle. The platform would then be serviced and reboosted back into its original orbit. Because of operational requirements connected with regaining the original orbit (see later) the platform outage could not exceed 14 days (though shuttle operational constraints limited the actual service period, from the platform leaving its operational orbit to regaining it, to 7 days.)

However, despite the obvious advantages of replenishable polar platforms, combined technical and economic difficulties led in 1988 to both of the Freedom/Columbus platforms being redefined as single use/disposable platforms. These platforms, two American and one European, together with a Japanese platform now form the basis of an international Earth Observing System (EOS) to be launched in the late 1990s. This is discussed further in Chapter 7.

2.4 Orbit mechanics of polar platforms

High inclination, retrograde orbits are chosen for remote sensing/earth observation payloads as a result of their orbit mechanics, while the particular orbit selected is driven by a number of operational constraints. (De Villiers [26], Meissinger et al [27]). Both of these have implications for the servicing of platforms in such orbits.

In order to maximise the coverage of the earth given by the platform, the orbit should obviously have as high an inclination as possible. In addition, it is advantageous that the orbit should be both earth and sun-synchronous, that is that its ground track should repeat after some period of time so that it will repeatedly view the same point on the ground from the same relative position in space, and the sub-platform point should always be illuminated by the Sun from the same direction.

For the platform to be earth-synchronous the following condition must be fulfilled,

$$n\Delta\lambda_g = m2\pi \qquad \text{Eq. 2.1}$$

where n is the number of orbits, and m is the number of days that must pass before the ground track repeats. The $\Delta\lambda_g$ factor, the longitudinal separation of successive grountracks at the equator, has two components, one due to the rotation of the Earth, the other due to the rotation of the orbital plane because of the oblateness of the Earth and given by the equation

$$\frac{d\Omega}{dt} = \frac{-3\pi J_2 r_e^2 \cos i}{a^2(1-e^2)^2} \quad rad/rev \qquad \text{Eq. 2.2}$$

Ω is the right ascension of the ascending node and describes the orientation of the orbit plane in space. It is one of the classical orbital elements and is described in more detail with the rest of these in Chapter 3.

The effect of oblateness on the orbit is also usually the mechanism that finally defines the inclination of the orbit once the operational altitude and the repeat period have been defined. This is because the

requirement that the orbit be sun-synchronous is fulfilled by making the orbit plane precess at the same angular rate as that of the Earth about the sun (0.986° per day). This can be achieved without the use of propellant by selecting the appropriate altitude and inclination for the orbit. Equation 2.1 can be rewritten to give

$$\frac{d\Omega}{dt} = \frac{-9.975}{(1-e^2)^2}\left(\frac{r_e}{a}\right)^{7/2}\cos i \qquad °/day \qquad \text{Eq. 2.3}$$

Fig. 2.1 overleaf shows the nodal regression rate as a function of inclination for a number of altitudes. For prograde orbits the line of nodes moves westwards, for retrograde ones eastwards. Over the altitude range of interest for polar platforms, say 250-1000 km, the inclinations necessary for sun-synchronicity lie between 96.5-99.5°. The repeat period (in days) of an orbit that is both Sun and earth-synchronous can be shown to be

$$m = \frac{n\,a^{3/2}}{8.68 \times 10^6} \qquad \text{Eq. 2.4}$$

where the semi-major axis is measured in kilometres.

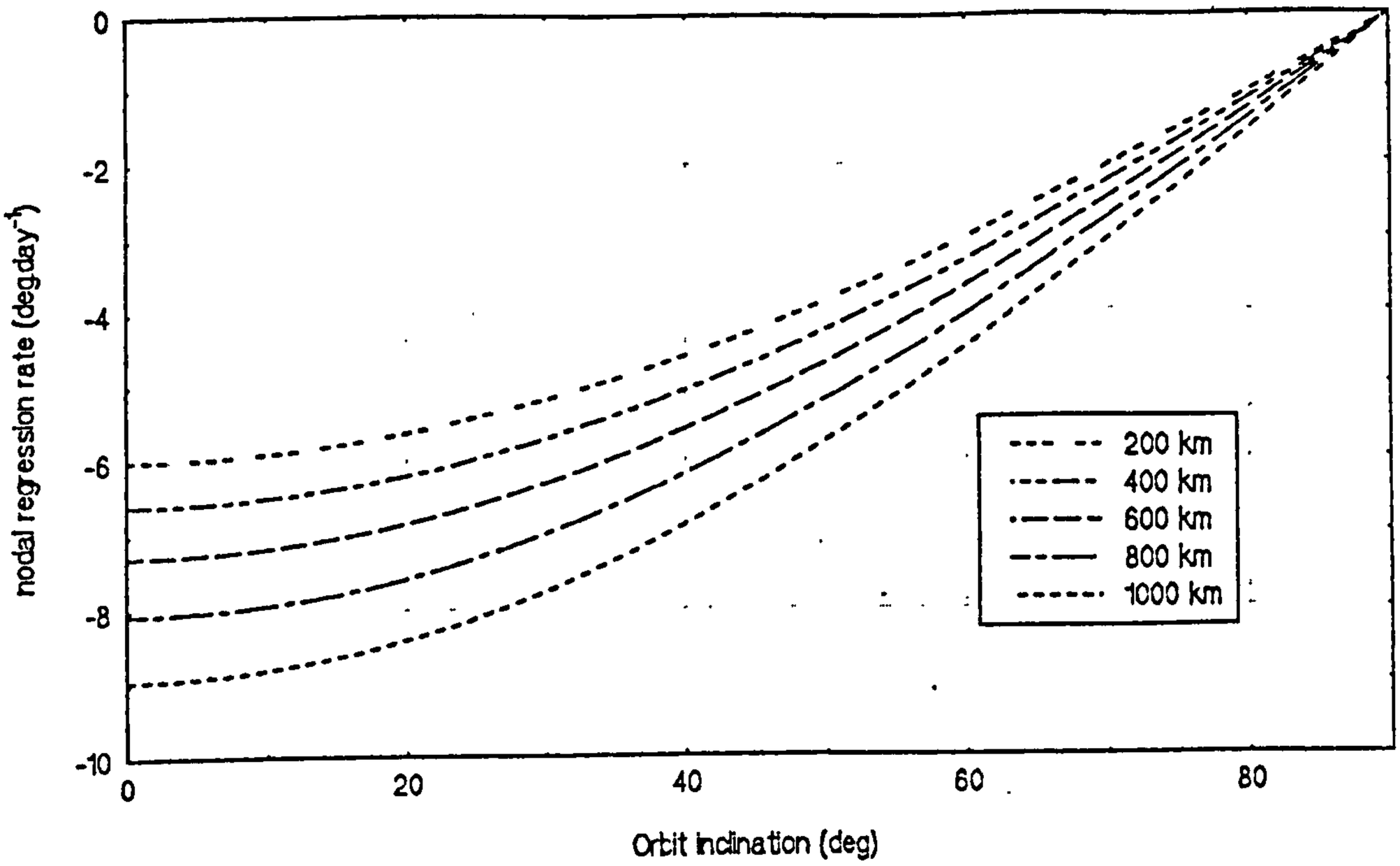

Figure 2.1 Nodal regression vs. inclination for different altitudes.

2.5 Polar platform servicing

It can be seen that the right ascension of the ascending node, Ω, (explained in the next chapter) of a polar platform orbit is a very important parameter, since it defines whether the platform is sun-synchronous or not. Equator crossing conditions for a platform may described either in terms of the local time of day at which the platform crosses, or in terms of right ascension of the ascending node. Hence, for the Freedom/Columbus platforms Ω must be kept within ± 5 minutes/$\pm 0.25^{\circ}$ of its nominal value both during normal operation and between the beginning and end of servicing. Otherwise the platform will be following what is effectively a different orbit. Although it will pass over the same points on the Earth's surface it will do this at different times of day, thereby making comparison of pre- and post-servicing data difficult. Whatever servicing strategies are employed, therefore, this integrity of the ascending node value must be retained.

To service the platform the basic requirement is that the supplies and the platform be brought together in some manner. In broad terms this defines three sorts of resupply strategy;

i) The supplies are taken to the platform.

ii) The platform is taken to the supplies.

iii) The platform and the supplies are both taken to a third point.

In terms of platform operation the third option is functionally equivalent to the second one since they both require taking the platform off-station, thereby making it unavailable for use. Because of this the third option can effectively be considered as a subset of the second.

The first option posits the use of some form of service vehicle capable of rendezvous with the platform. The origin of the service vehicle could be, in theory, any one of a number of sources - the space shuttle, the space station, an expendable launch vehicle, a dedicated resupply base. The choice of which of these is used is dependent on the scenario selected, i.e. the number of platforms to be serviced,

the propulsive capabilities of the servicing vehicle, the lifetime of the polar platforms and similar. In general the first option is attractive because of its inherent flexibility and the fact that the platform does not need to be taken off-station. It is especially attractive in the long term as the number of platforms to be serviced increases. This is discussed further in section 2.7.

The second option requires the use of another spacecraft/station as a (possibly temporary) service depot. This is the option that was originally selected for the Freedom/Columbus polar platforms. It has the disadvantage that it requires the platform to be taken off-station and then repositioned after servicing because of the differential nodal drift between the servicing orbit and operational orbit that will have occurred over the period of servicing. For impulsive manoeuvres the Δv required to perform this node change is dependent on β, the angle between the the two orbits at the point where they intersect (sometimes also called the wedge angle - see Figure 2.2 overleaf). This is given by

$$\beta = \cos^{-1}[\cos^2 i + \sin^2 i \cos \Delta\Omega] \qquad \text{Eq. 2.5}$$

where $\Delta\Omega$ is the nodal difference between the orbits. This is the product of the service period and the differential drift rate between the operational and service orbits. The node change Δv is then given by

$$\Delta v = \sqrt{2v_c^2(1-\cos\beta)} \qquad \text{Eq. 2.6}$$

where v_c is the circular orbit velocity. It is effectively a sinusoidal function of service time and therefore increases most steeply at small values of this.

For a platform with operational altitude 800 km, inclination 98.5° being serviced in an orbit of altitude 200 km the nodal correction Δv starts to exceed the two-way orbit transfer Δv after about two weeks in the servicing orbit (shown in Figure 2.3 overleaf). This Δv requirement severely limits off-station servicing. This option is, however, the only one that can be used if no servicing vehicle exists that is capable of reaching the platform operational altitude. This is most likely to be the case when both the number of platforms and the amount of in-orbit infrastructure is limited (as is the case at the moment).

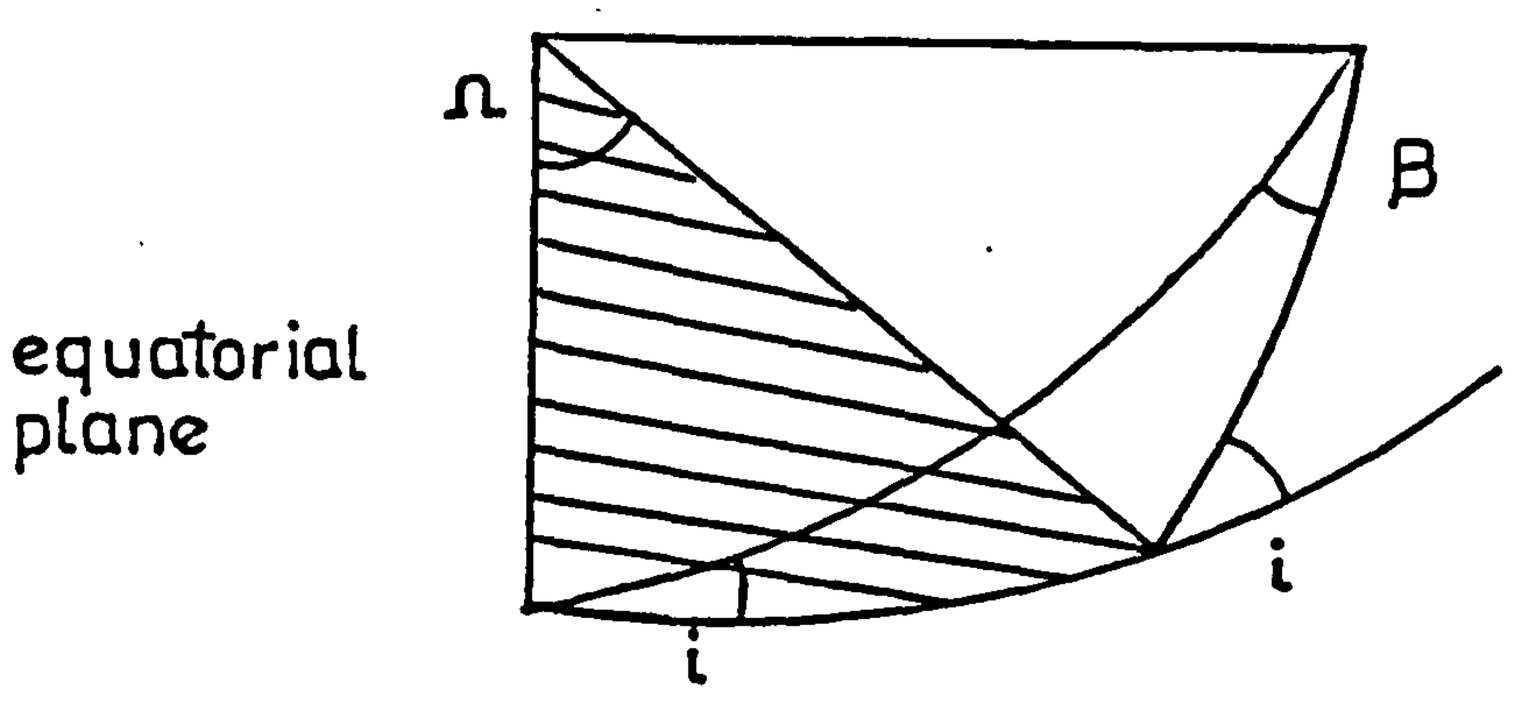

Figure 2.2 Wedge angle for two orbits of same inclination but different node

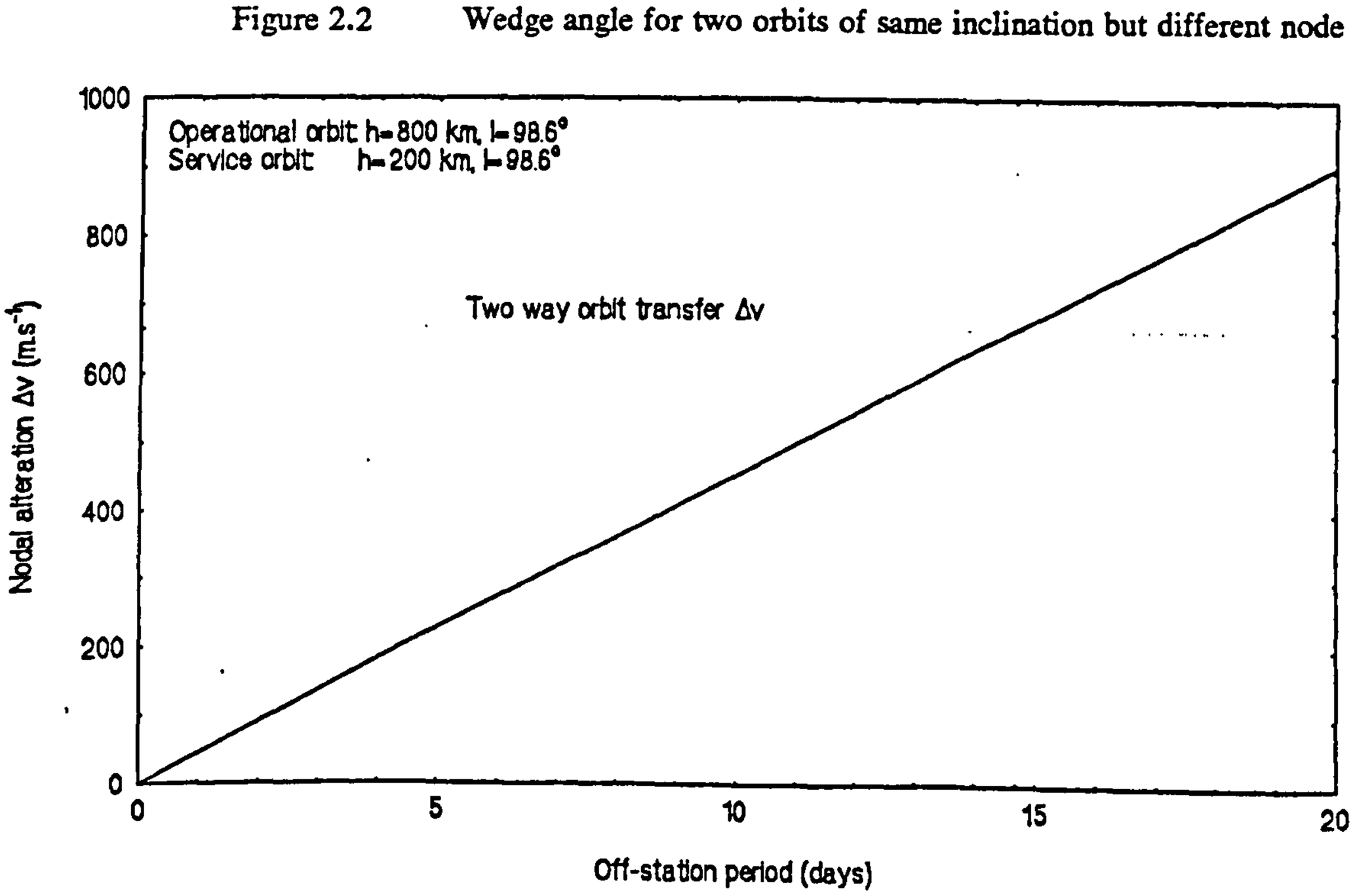

Figure 2.3 Impulsive nodal correction Δv vs. off-station period

2.6 Propulsion options for de-orbitable polar platforms

Of the two main options for servicing outlined in the previous section, most work has so far concentrated on the second because of its selection for Freedom/Columbus. A sizeable body of work exists covering the area in some detail until approximately 1988 when the decision was made to use disposable platforms instead of serviceable ones. This work can be typified by a number of studies of the best form of propulsion module to be attached to the platforms summarised hereafter.

The work carried out by Boriello et al. [28] formed part of the B1 phase of the Columbus polar platform study. A number of propulsion technologies are considered, both electric systems (ion, magnetoplasmadynamic (MPD), field emission and electrothermal arcjet) and chemical systems (solid, bipropellant, monopropellant and cold gas). Despite the considerable mass savings obtainable by using electric propulsion systems, only the MPD system was considered a candidate propulsion system, ion propulsion being considered to have exhaust velocities far above the optimum for this sort of application, and arcjets being considered to provide exhaust velocities that were too low. In the final event a bipropellant monomethylhydrazine (MMH) and nitrogen tetroxide (N_2O_4) system was selected as the best option. This formed the basis of a dual gimballed thruster, 800 N, pressure fed propulsion system mounted in a strut network which also housed the propellant tanks (2, 4, or 6 for a platform of mass 9, 15, or 25 tonnes respectively). This reference also defines the advantages of the disposable orbit replacement unit (ORU) type of propulsion module over in-orbit refuelling of platform propulsion systems. This design is shown in Figure 2.4 overleaf.

Palaszewski [29] examines a number of advanced propulsion systems for both co-orbiting and polar orbiting platforms. These include resistojets, thermal and microwave arcjets, ion and MPD systems, as well as the possible usage of cryogenic propellants scavenged from the space shuttle external tank. He concludes that, for polar platforms, although the advanced propulsion systems offer significant mass savings, that their low levels of thrust make them inherently unsuitable for this application since they are

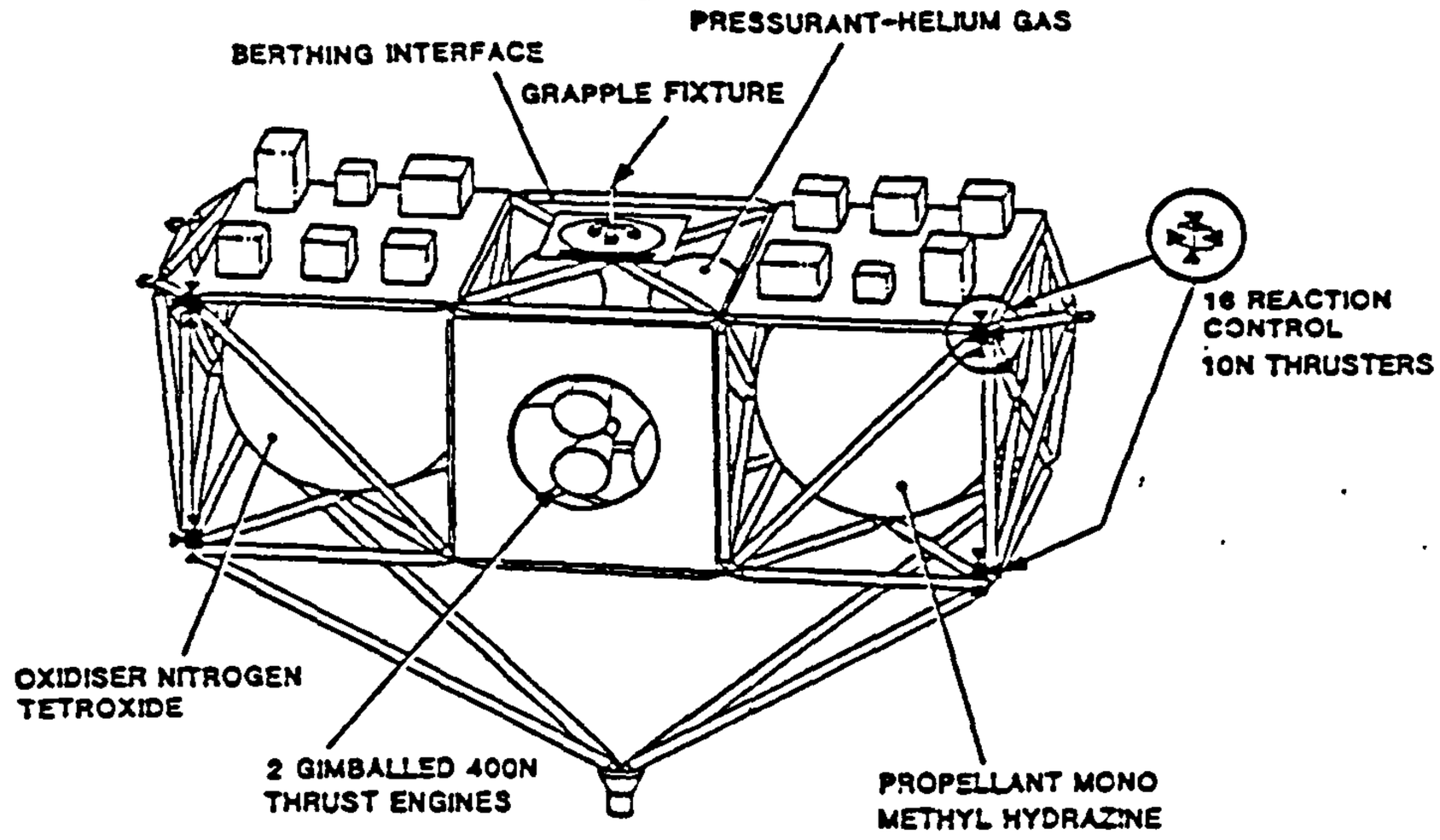

Figure 2.4 Bipropellant propulsion module for polar platform (Boriello et al [29]).

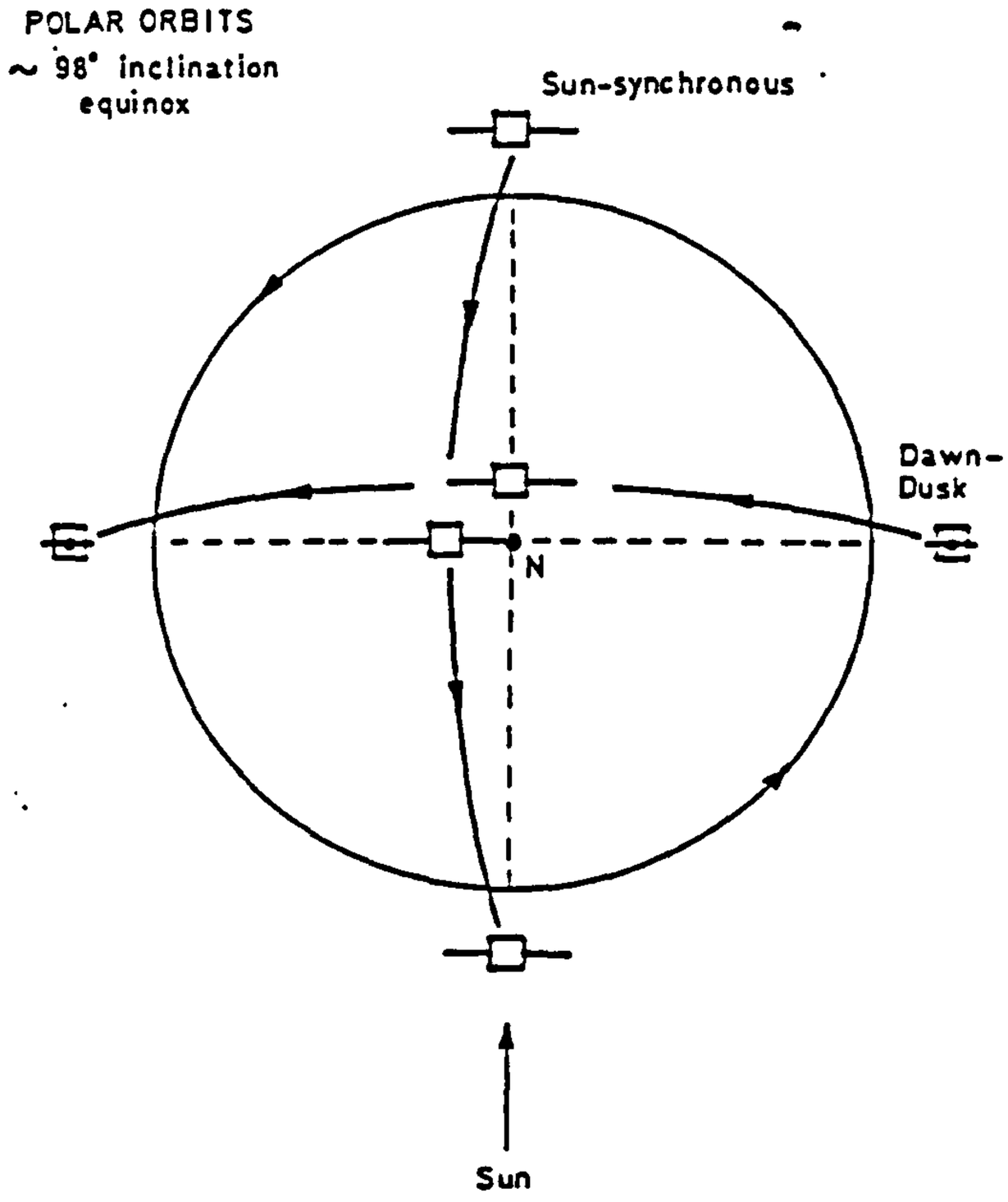

Figure 2.5 Dawn-dusk and day-night orientations for sun-synchronous orbits (Fearn and Wallace, [31]).

unable to fulfil the condition that the polar platform be de-orbited, serviced, and re-orbited with the space shuttle on station in the servicing orbit, taken here as seven days. As a result, a bipropellant MMH/N_2O_4 system is suggested and favoured over a monpropellant system because of its higher performance.

Feconda and Rauscher [30] also examine space station platform propulsion options; MMH thrusters in normal, resistojet and arcjet configurations, a bipropellant MMH/N_2O_4 system, and gaseous oxygen and hydrogen thrusters using either supercritical gas storage or water electrolysis to provide propellant. It is stated here, also, that resistojet and arcjet systems (both of 6 kW power, but 5 and 1.4 N thrust respectively) are incapable of achieving the necessary short transfer times, here taken to be two days for a one way trip up or down. After performing a trade-off study based on a number of criteria including transfer time, system mass, development and operational costs, risk, and serviceability, they determine that earth-storable liquid propellant systems are by far the most advantageous with the bipropellant system once again selected as the best.

It can be seen that the limitation on the duration of the orbit transfer and the overall time off-station is a very powerful one and, if it were not for this, that electric propulsion systems could offer important benefits. Some work has been done on this basis.

For electric propulsion, Fearn and Wallace [31] show that propellant mass savings of 400-900 kg can be made for a shuttle launched polar platform, albeit at the expense of transfer times of between 30 and 120 days. They also identify the importance of orbit orientation for electrically propelled polar platforms. Operational sun-synchronous remote sensing satellites usually have day-night orbits so that the earth below the satellite is fully illuminated by the sun. Under these conditions, however, the satellite's solar arrays are eclipsed for a substantial part of the orbit and are incapable of generating power for the engines. For spacecraft using electric propulsion the dawn-dusk orbit (See Figure 2.5 previous page) is much superior. In this configuration the solar arrays are illuminated throughout the orbit and thrust may be generated continuously. An additional advantage is that the solar arrays are aligned with the velocity

vector of the spacecraft throughout the orbit which minimises the effects of atmospheric drag.

They conclude that there are considerable advantages in the use of the dawn-dusk orbit although a certain amount of propulsive effort is needed to maintain the orientation of the dawn-dusk orbit plane as the altitude changes. Also since this is not a satisfactory orbit for earth resources missions (as the sub-satellite point will suffer from constant long shadows and low illumination levels) the dawn-dusk orbit is only appropriate for the orbit transfer phase. Eventually the satellite will have to be allowed a 90° drift of right ascension towards the end of the orbit raising period if a conventional day-night sun-synchronous orbit is to be used operationally.

This work is extended by Martin and Cresdee [32] who analyse the effects of atmospheric drag in more detail and determine the minimum altitude from which electric propulsion can be used. This is approximately 300 km. At this altitude the thrust provided by a typical electric propulsion system is only just enough to counteract drag and leads to transfer times in excess of 200 days. For initial altitudes of 400 to 500 km this figure reduces to 105 to 135 days. They also consider the use of non dawn-dusk orbits and show the effects of shadowing factor on transfer times. See Figure 2.6 overleaf. They conclude that the use of electric propulsion on a de-orbitable, space shuttle-serviced polar platform is not appropriate since this would have to be carried out at an altitude of 275 km, but comment that the development of solar arrays with higher specific powers than those currently available might alter this situation.

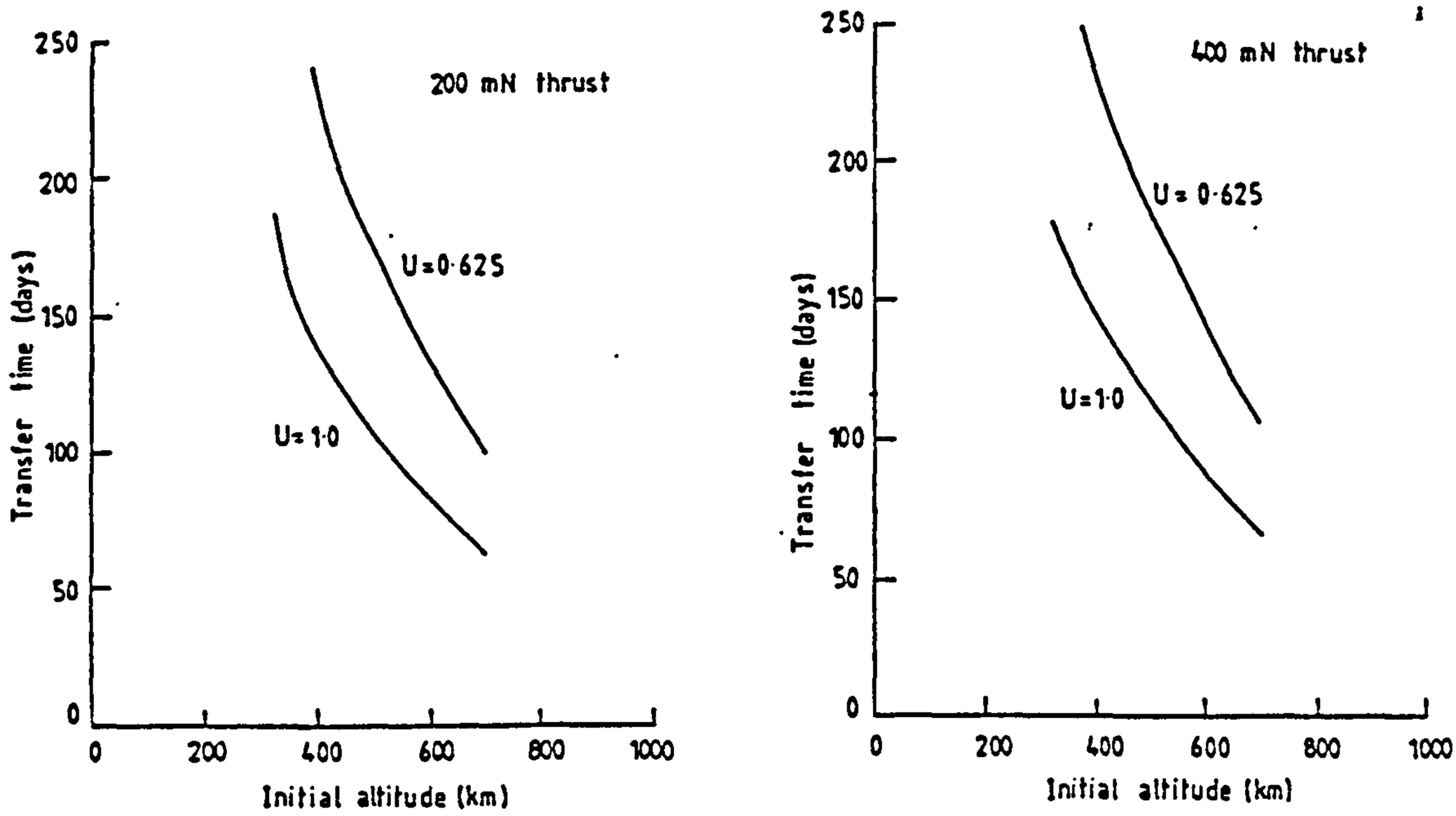

Figure 2.6 Transfer times to 1000 km for nominal (left) and enhanced (right) polar platforms with shadowing (U = 0.625) and without shadowing (U = 1.0) (Martin and Cresdee [32]).

2.7 Options for remote servicing

The first servicing option outlined earlier, the use of some form of servicing vehicle (SV) has not been examined in as much depth as the second option. This is because it requires a more mature technological base. Either the capability to place a manned vehicle into high polar orbits or the capability to conduct autonomous or teleoperated servicing must be developed before this concept is realisable. Current trends indicate that a teleoperated SV approach is most likely to be adopted since work on the necessary techniques is already under way for other, similar, orbital applications. This is discussed further in Chapter 7.

Remote servicing of polar platforms was considered as an option early in the Freedom/Columbus design studies. Klemetson [33] examines both remote servicing and servicing in a lower orbit, considering in particular the use of platform-space shuttle rendezvous effected by either on-platform propulsion or by the use of the projected (but now cancelled) Orbit Manoeuvring Vehicle (OMV) to 'fetch and carry' the platform, and also remote servicing by the OMV. He analyses these service modes for two sorts of platforms; small ones of mass 12000 kg and large ones of mass 37000 kg.

His results may be summarised as follows. Small platforms are considered more advantageous than large ones as they can achieve initial operating capability in a single shuttle launch. Remote servicing of platforms is the preferable mode since it minimises outage, and this becomes increasingly important the higher the platform mass. Smaller platforms may be serviced in a lower orbit if remote servicing is not possible. Under these circumstances on board propulsion is significantly preferable to the use of the OMV.

Kleinau et al. [34] consider a European Orbital Transfer and Service Vehicle (OTSV) to be used for a wide range of missions related to the various Freedom/Columbus segments, including polar platform servicing. The OTSV is considered for either manned or teleoperated operation and for launch on the space shuttle, Ariane 5 or Hermes (though the latter would no longer be possible). They conclude that

although an OTSV is not mandatory for Freedom/Columbus it improves considerably the operational flexibility in the short term. In the long term such a vehicle will prove necessary to extend orbital activities beyond those orbits reachable by the Shuttle and Hermes. Figure 2.7 (overleaf) shows one of the concepts examined.

The use of the space shuttle to deliver service vehicles into suitable polar orbits assumed by both Klemetson and Kleinau et al. has become very much less likely. The after effects of the Challenger accident triggered off a review of the necessity and economics behind using the shuttle to launch payloads that could be launched on expendable launch vehicles (ELVs). This, combined with the indefinite mothballing of the shuttle launch site at the Western Test Range, has reduced the likelihood of significant numbers of shuttle launches into polar orbits to zero for the foreseeable future. For these reasons, interest has emerged in the use of ELV launched polar platform servicing missions.

Graves and Rosen [35] have suggested using a telerobotic rendezvous and docking vehicle (RDV) based on the OMV. This can be used in two modes. Firstly, the RDV and supplies can be launched together and the RDV used to dock and resupply the platform, after which it is either left attached in inactive mode or detached, deorbited and expended. Secondly, the RDV and supplies and RDV propellant are launched separately. The RDV rendezvouses with the supplies and propellant, refuels itself, and takes the supplies to the platform. After resupply is complete the RDV detaches itself, deboosts the old ORUs and remains in orbit ready to ferry future ELV launched supplies when necessary.

Graves et al. [36] have extended this work further to cover the servicing of multiple polar platforms. The main difficulty in doing this is the alteration of the ascending node of the servicing vehicle to match the nodes of the different platforms. As discussed earlier, such manoeuvres are highly Δv intensive and would normally preclude performing this propulsively. If, however, the servicing schedule is of a sufficiently long period (36 months is assumed here) then it is possible to use the natural change in Ω dues to the earth's oblateness to perform this change over a longer period of time. They also

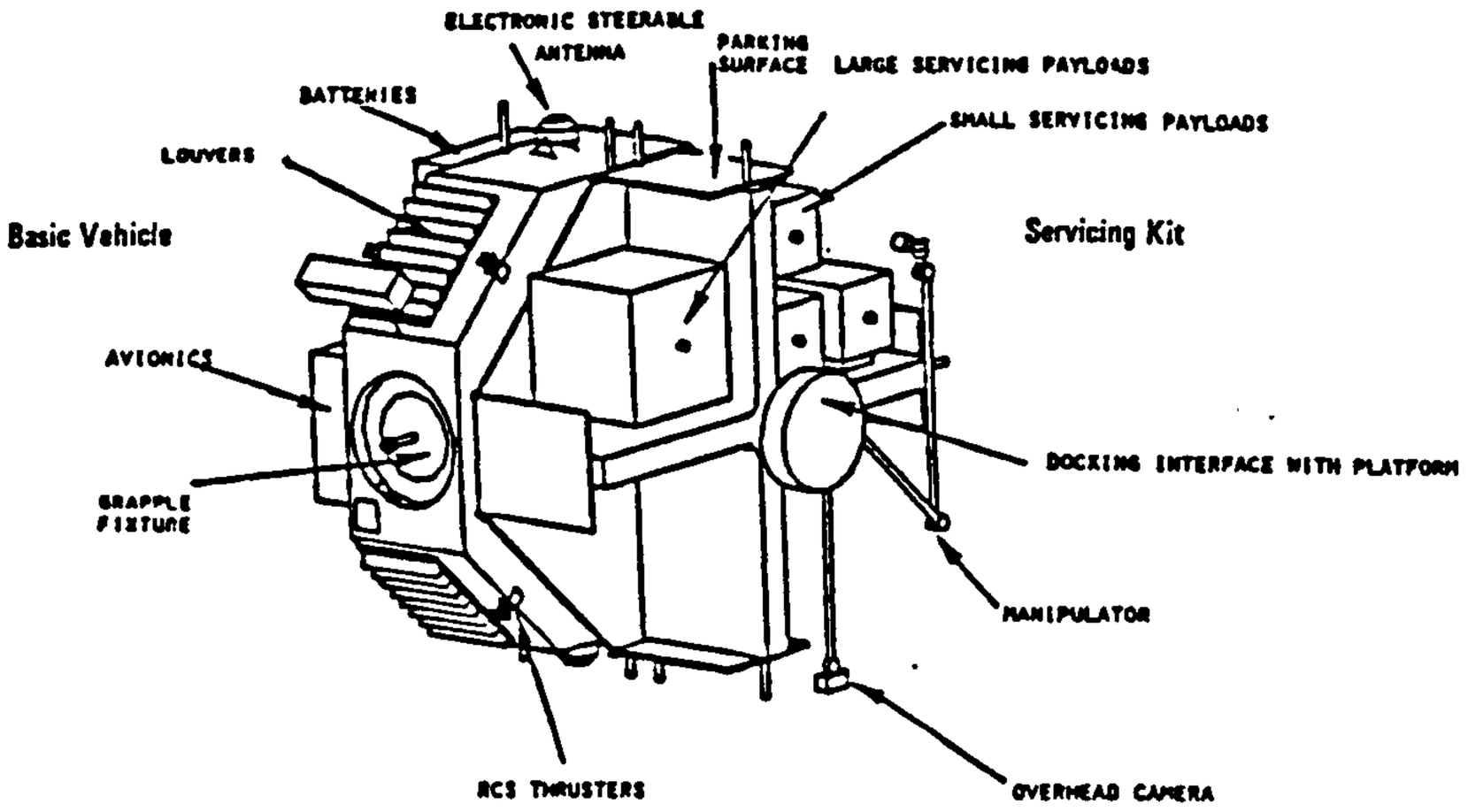

Figure 2.7 Concept for a European Orbital Transfer and Service Vehicle (Kleinau et al. [34]).

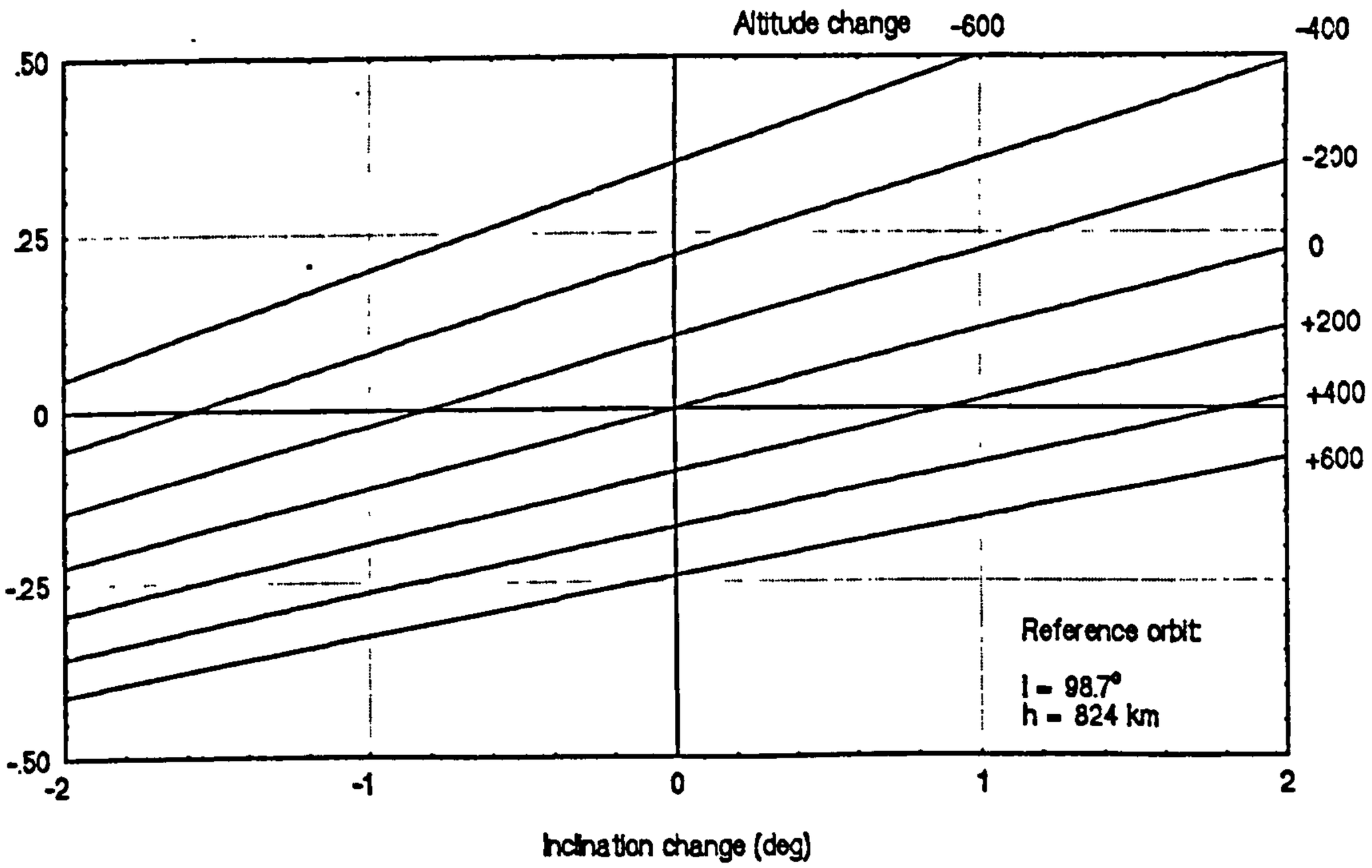

Figure 2.8 Effect of small changes on differential nodal regression rate for a typical polar platform orbit.

note that the nodal drift can be enhanced by up to 35% for polar orbits by making comparatively small alterations to the orbital altitude and/or inclination. (Mugellesi [37] has also suggested this approach for matching nodes between Eureca and the shuttle during retrieval manoeuvres.) Figure 2.8 on the previous page shows the effects of small changes in h and i on nodal drift rate for a 98.6°, 800 km orbit.

Graves et al. identify three possible scenarios for servicing four platforms over a fifteen year period using this technique. The first scenario uses a single (smaller) ELV launch for each platform to be serviced, carrying the necessary ORUs and RDV propellant. The second two scenarios use a larger ELV launch to carry enough ORUs and RDV propellant for the servicing of four platforms into orbit. The second and third scenarios differ in their transfer sequences. In the second scenario the RDV carries all remaining supplies with it and visits the platforms sequentially. In the third scenario the RDV deposits the bulk of its supplies at the first platform and then performs sorties to the other platforms from this newly established base.

In terms of mass supplied to platforms there is little to choose between the different scenarios. In each case, however, the amount of the propellant used by the RDV is significantly greater than that of the supplies launched at the same time. For the first scenario the payload mass is 1000 lbs and the propellant mass 1850 lbs, for the second and third scenarios payload mass is 3000 lbs and propellant mass 16200 lbs. Despite this the large ELV launch option is preferred as this will require only four launches to resupply the platforms over the fifteen years, as opposed to sixteen launches of the smaller ELV, and this gives a smaller overall cost.

Other concepts for remote servicing revolve around basing an SV at some other location in space, usually either the Freedom space station or, in the longer term, some form of dedicated maintenance/logistics platform.

For medium response time servicing, basing an SV at Freedom may initially seem quite attractive as the differential nodal drift between the platform and the space station means that the nodes will line up every forty days or so. The major restriction on this scenario is the very great Δv needed to transfer from the Freedom's orbit to that of a typical polar platform. If it is assumed that the inclination change takes place at the platform's operational altitude then the Δv for an impulsive inclination change is approximately 8.5 $km.s^{-1}$. To make a round trip to a platform, let alone a number of them, would be prohibitively expensive in terms of propellant unless some form of advanced propulsion was used. Factors governing general platform servicing from Freedom are dealt with by Fisher and Forsberg [38].

Servicing a platform from a dedicated logistics platform (LP) requires an advanced infrastructure. Two conceptual LPs are outlined by Qualls and Ferebe [39], one manned and one unmanned. In both cases they envisage the use of an OMV/OTV-like vehicle to either visit the polar platforms or return to them to the LP for servicing when necessary.

Selection of an orbit for an LP would depend on the number of platforms to be serviced and the interval between servicing. Ideally the LP would have an altitude and inclination sufficient to cause differential nodal regression to match its node with those of each platform in turn, leaving an SV to perform comparatively small Δv manoeuvres. However, the necessity to deliver supplies to an unmanned LP in the first place makes it unclear what benefits this approach has over Graves et alias's ELV launched/resupplied RDV approach unless there is an extremely high number of platforms giving rise to a smaller mean time between failures for the population taken as a whole. If this is the case then it may be presumed that a manned platform may be more advantageous. For timely effecting of repairs it may well be more useful to undertake a dedicated launch from the ground to rendezvous with a platform.

2.8 Servicing polar platforms by electric propulsion

The work outlined in previous sections suggests that electric propulsion may be applied to the servicing of polar platform constellations. The propellant mass savings electric propulsion offers make it attractive for orbit raising activities where transfer time is not a critical factor. Given this, it is not suitable as primary propulsion for platforms to be serviced off-station because this would extend the operational outage beyond an acceptable period.

This suggests, then, that the major area of interest would then be the use of electric propulsion as the primary propulsion for a service vehicle. This also appears attractive because we have determined that the Δv's for performing nodal transfers are high. For the Earth Observing System the impulsive Δv necessary to perform the nodal alterations for a single servicing cycle (one servicing of each satellite in the constellation) is 34 $km.s^{-1}$.

We have also seen that, where a rapid transfer between orbits of different ascending node is not required, use can be made of orbits that provide a differential nodal drift, hence mitigating the the high propulsive cost of nodal alteration. To date, only impulsive transfers between orbits have been considered. However, it seems possible that the long transfer periods typical of such scenarios would fit well with the long burn times typical of electrically propelled missions. Missions undertaken in such a manner would then have the potential to gain both from the differential nodal drift and the high mass efficiency of electric propulsion systems together with the benefits (e.g. reduced overall upload requirement, extended service vehicle lifetime) that this would offer.

Chapter 3 - Modelling perturbed orbital motion

3.1 Introduction

In order to investigate the operation of vehicles suitable for the on-orbit servicing of polar platforms it is necessary to develop a model to describe the vehicle orbital motion. This chapter deals with the basis of the simulation model used in this work. The chapter is divided into two halves. The first deals with orbital modelling in general and the equations of motion using the classical and equinoctial orbital elements. The second section covers the perturbations of the orbit by a number of effects (the asphericity of the earth, the drag of an oblate rotating atmosphere, solar radiation pressure and the thrust of the spacecraft propulsion system) and their description mathematically.

3.2 Modelling Orbital Motion

A body moving through space needs six parameters to fully describe its motion. This can be seen by considering three dimensional motion described in a conventional cartesian system. Here three co-ordinates define the position vector while another three define the velocity vector. However, although cartesian co-ordinates can be employed to describe orbital motion, they are not used commonly. This is because other more useful and more tractable co-ordinate systems can be developed which enable the particular problem of describing the orbit of a spacecraft under the effect of gravity and perturbations to be considerably simplified.

3.2.1 The Classical Orbital Elements

The standard co-ordinates for describing the motion of a satellite are the classical orbital elements. These take the orbit of a satellite to be an ellipse around which the satellite moves with time. Given a stable, unperturbed orbit the motion of a satellite about the Earth can be completely described using five constants which describe the size, shape and orientation in space of the orbit and a variable which changes with time and specifies the position of the satellite on the orbit relative to a defined epoch.

These parameters are:

a	the semi-major axis of the ellipse.
e	the eccentricity of the ellipse.
Ω	right ascension or longitude of the ascending node measured from the First Point of Aries.
i	the inclination of the orbit measured with respect to the equatorial plane.
ω	the argument of perigee measured from the line of nodes of the orbit.
θ	the true anomaly of the satellite measured from the perigee point.

On occasion various of these elements may be replaced by others for the convenience of calculations. The semi-latus rectum, p, of the ellipse may be used instead of the semi-major axis, and the mean anomaly, M, the eccentric anomaly, E, or the time since perigee passage, τ, may all be used instead of the true anomaly.

The relationship between eccentricity, semi-major axis and semi-latus rectum are shown in Figure 3.1 (overleaf), while that between true anomaly, eccentric anomaly and mean anomaly is shown in Figure 3.2 (overleaf), and the respective meaning of inclination, argument of perigee and right ascension of the ascending node in Figure 3.3 (two pages on).

3.2.2 Perturbed Orbits

As described in the previous section, if a satellite is in a Keplerian orbit then only the true anomaly or its equivalent will change with time and this may be modelled quite simply. In reality, however, the orbits of satellites are perturbed by a variety of forces which include, amongst others, atmospheric drag and differential gravitational attraction due to the asphericity of the Earth. All these perturbations act to alter the orbit of the spacecraft in some manner and consequently change the orbital elements and will be discussed in more detail later.

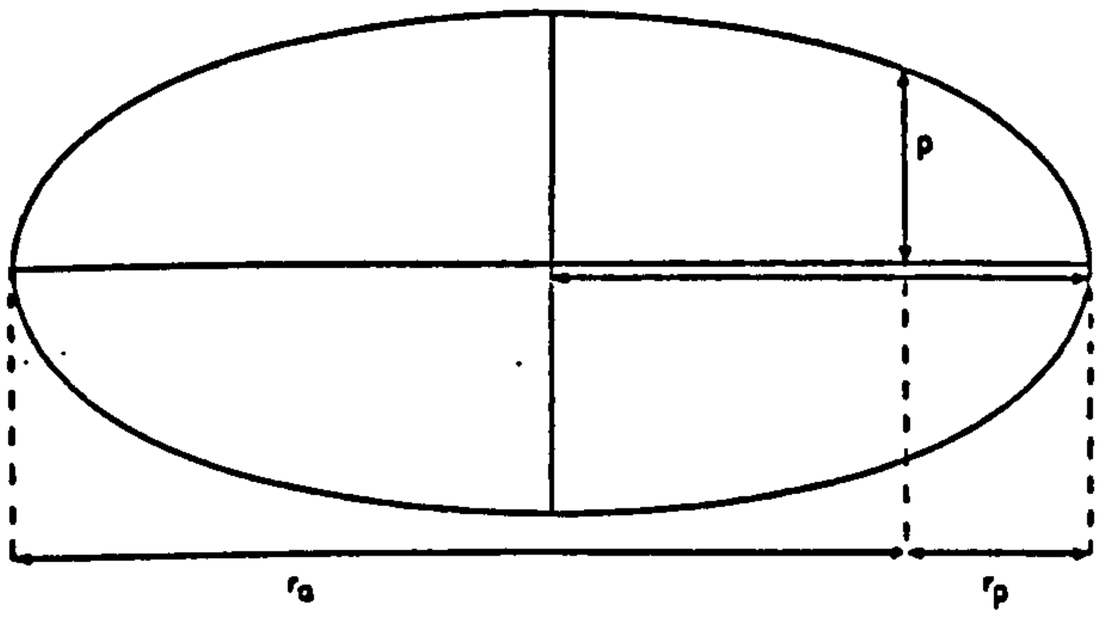

Figure 3.1 Relation between eccentricity, semi-major axis and semi-latus rectum.

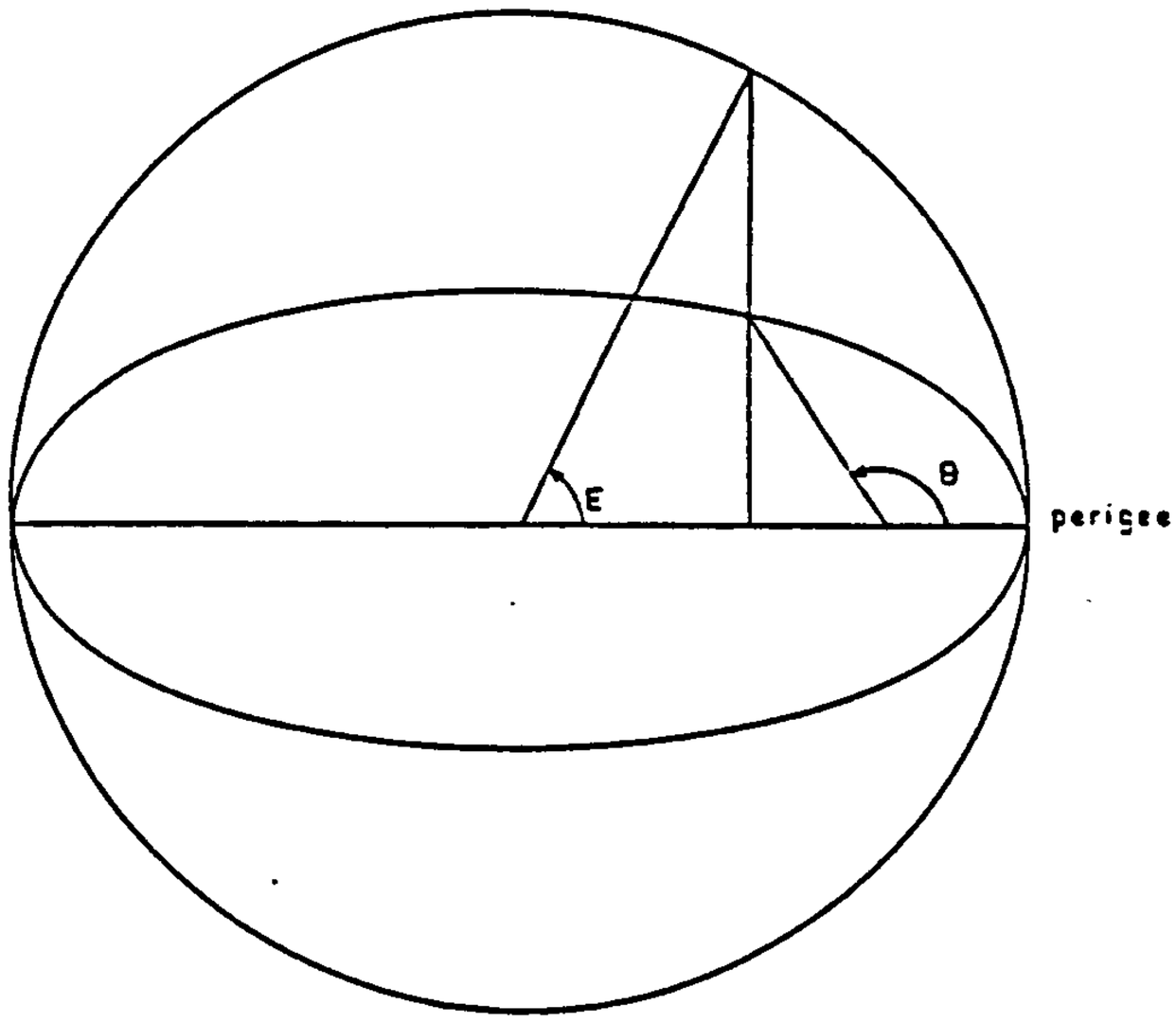

Figure 3.2 Relation between true, eccentric and mean anomaly

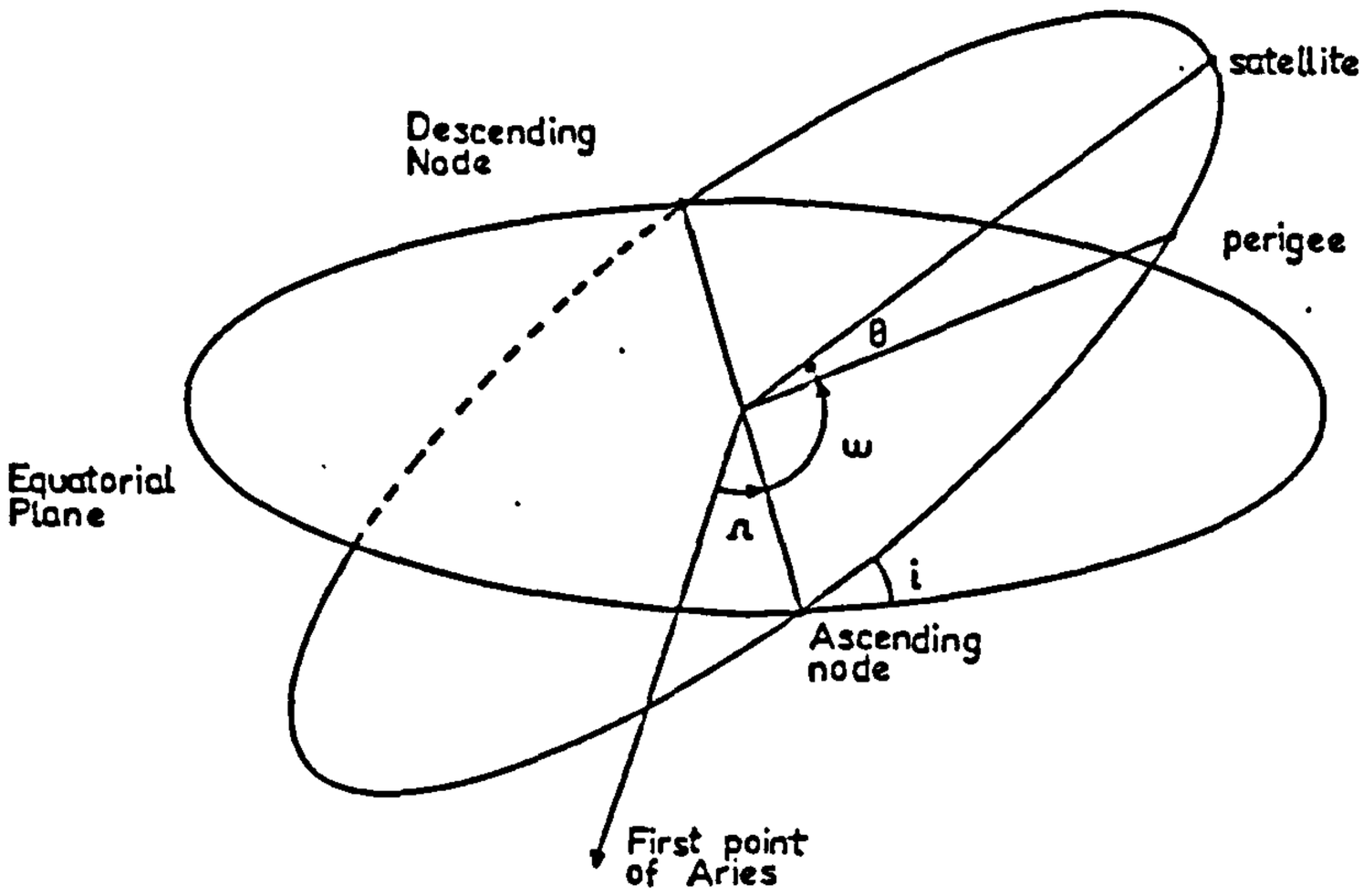

Figure 3.3 Inclination, argument of perigee and right ascension of the ascending node.

Methods of solving the equations of motion of a perturbed spacecraft can be generally considered within the following framework. A general equation of motion for a spacecraft can be written as

$$\frac{d^2\vec{r}}{dt^2} + \frac{\mu\vec{r}}{r^3} = -\nabla U_g + \vec{a}' \qquad \text{Eq. 3.1}$$

where the terms on the right hand side of the equation express the perturbing accelerations. These are of two types; those which may be expressed in a potential form (i.e. gravitation), where U_g is the potential function, and those which cannot be written in such a form (e.g. atmospheric drag).

This equation cannot usually be solved by analytical methods and so either approximate analytical techniques, known as general perturbations, or numerical techniques, known as special perturbations, must be used instead. The primary applications of general perturbations are to planetary orbital mechanics and the analysis of the source of perturbations from orbital data. For orbit modelling and prediction special perturbations are used since they can cope with any form of disturbing force and are amenable to numeric modelling by computer. It is these that will be dealt with here.

3.2.3 Special Perturbations

Special perturbations are techniques that calculate the path of a satellite from equations of motion given its state at epoch. The orbit is found via a numerical step-by-step process. There are many ways of doing this. In general, however, the various schemes are classified according to the manner in which the equations have been formulated. The three most common classical special perturbation methods are Cowell's method, Encke's method and the method of variation of parameters. These are well described by Battin [40] and Cornelisse et al. [41].

Cowell's method is by far the simplest. It directly integrates numerically the equations of motion and, as long as the values of perturbing accelerations remain approximately constant over an orbit, is comparatively easy to implement. Unfortunately this is not usually the case and so the integration step size must be kept small and the number of significant figures must be kept high in order to maintain the

accuracy of the calculations. Furthermore, it cannot be used to analyse orbital data to provide insight into the relative effects of different perturbations.

Encke's method uses a conic section to approximate the orbit. This is used as a reference orbit and the deviations from this are numerically integrated. Although each of the steps can be larger than in Cowell's method each one needs more calculation. As long as the deviations from the reference conic are small this technique gives good results. If the deviations increase to too large a size, however, then the reference orbit must be rectified (i.e. replaced with a new one) which adds to the complexity of implementing this method.

The most common computational technique for modelling the perturbed orbit of a spacecraft is the method of variation of parameters. This method defines a reference orbit but this changes continuously as the integration proceeds from step to step. This constantly changing reference orbit is called the osculating orbit and, hence, the orbital elements that define it are called osculating orbital elements and they also change continuously. The motion of a spacecraft may be described, therefore, in terms of the rate of change of these orbital elements under the effect of the perturbing forces. These equations may be derived in terms of Lagrange's planetary equations and may be written in the Gaussian form (Roth [42]).

$$\frac{da}{dt} = \frac{2a^2}{\sqrt{\mu p}}\left(a_r' e \sin\theta + a_t'(1 + e\cos\theta)\right) \qquad \text{Eq. 3.2}$$

$$\frac{de}{dt} = \sqrt{\frac{p}{\mu}}\left(a_r' \sin\theta + a_t' \frac{e + 2\cos\theta + e\cos^2\theta}{1 + e\cos\theta}\right) \qquad \text{Eq. 3.3}$$

$$\frac{di}{dt} = \frac{r}{\sqrt{\mu p}} a_n' \cos u \qquad \text{Eq. 3.4}$$

$$\frac{d\Omega}{dt} = \frac{r}{\sqrt{\mu p}} a_n' \frac{\sin u}{\sin i} \qquad \text{Eq. 3.5}$$

$$\frac{d\omega}{dt} = \sqrt{\frac{p}{\mu}} \frac{1}{e}\left(-a_r' \cos\theta + a_t' \sin\theta \frac{2 + e\cos\theta}{1 + e\cos\theta}\right) - \cos i \frac{d\Omega}{dt} \qquad \text{Eq. 3.6}$$

$$\frac{d\theta}{dt} = \frac{\sqrt{\mu p}}{r^2} + \sqrt{\frac{p}{\mu}} \frac{1}{e}\left(a_r' \cos\theta - a_t' \sin\theta \frac{2 + e\cos\theta}{1 + e\cos\theta}\right) \qquad \text{Eq. 3.7}$$

where a_r, a_t, and a_n are the components of the perturbing acceleration in the radial, transverse and normal directions respectively. See Figure 3.4 overleaf

Although this scheme is generally useful for modelling orbital motion and serves as the basis of many systems for so doing, it suffers from the disadvantage that as the eccentricity tends to zero (i.e. as the orbit becomes circular) the argument of perigee becomes indeterminate and as the inclination tends to zero the right ascension of the ascending node does likewise. To combat this problem a number of other schemes have been developed ranging from transformations of the classical elements to the definition of alternative sets of elements. In particular, Brouke and Cefola [43], [44] have defined the so-called equinoctial orbital elements. These are nonsingular for all orbits except the rectilinear orbit h' = 0 and for orbits of inclination 90^0. Even this latter singularity can be removed by introducing an auxiliary set of retrograde equinoctial orbital elements. These will not be considered here, however.

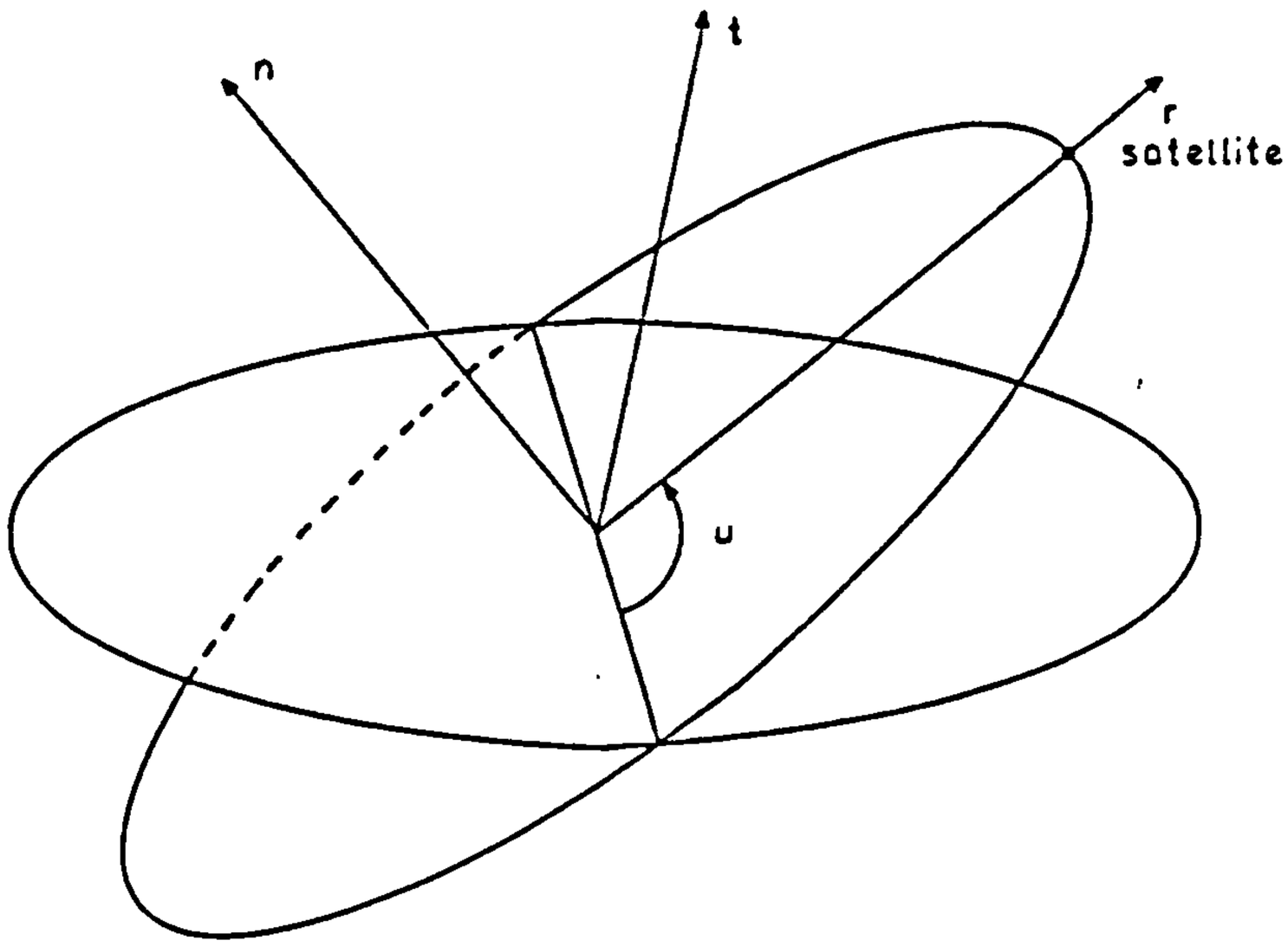

Figure 3.4 Perturbation acceleration components in spacecraft frame.

3.2.4 The Equinoctial Orbital Elements

A set of the equinoctial orbital elements can be associated with the classical orbital elements through the relations (Walker et al. [45])

$$p = a(1 - e^2) \qquad \text{Eq. 3.8}$$

$$f = e\cos(\omega + \Omega) \qquad \text{Eq. 3.9}$$

$$g = e\sin(\omega + \Omega) \qquad \text{Eq. 3.10}$$

$$h = \tan\frac{i}{2}\cos\Omega \qquad \text{Eq. 3.11}$$

$$k = \tan\frac{i}{2}\sin\Omega \qquad \text{Eq. 3.12}$$

$$L = \Omega + \omega + \theta \qquad \text{Eq. 3.13}$$

where p is the classical semi-latus rectum, and L is the true longitude. Defining the additional relationship $u = \theta + \omega$, the inverse relations may be given as

$$e = \sqrt{f^2 + g^2} \qquad \text{Eq. 3.14}$$

$$\Omega = \tan^{-1}\left(\frac{k}{h}\right) \qquad \text{Eq 3.15}$$

$$\theta = \tan^{-1}\left(\frac{f\sin L - g\cos L}{f\cos L + k\sin L}\right) \qquad \text{Eq. 3.16}$$

$$u = \tan^{-1}\left(\frac{h\sin L - k\cos L}{h\cos L + k\sin L}\right) \qquad \text{Eq. 3.17}$$

$$\omega = u - \theta \qquad \text{Eq. 3.18}$$

$$i = \tan^{-1}\left(\frac{2\sqrt{h^2 + k^2}}{1 - h^2 - k^2}\right) \qquad \text{Eq. 3.19}$$

The equinoctial reference frame is defined by the unit vectors f, g, and w where f points towards that place on the satellite orbit Ω behind the ascending node, w is normal to the orbit plane and g completes the orthogonal system of axes such that g = w x f. The relationship between the axes and the equatorial frame of reference is shown in Figure 3.5 (overleaf). The equatorial frame is related to the equinoctial frame by the matrix

$$M' = \frac{1}{1 + h_e^2 + k_e^2} \begin{pmatrix} 1 + h_e^2 + k_e^2 & 2h_e k_e & 2k_e \\ 2h_e k_e & 1 - h_e^2 + k_e^2 & -2h_e \\ -2k_e & 2h_e & 1 - h_e^2 - k_e^2 \end{pmatrix} \qquad \text{Eq. 3.20}$$

and the equinoctial frame to the spacecraft frame by the matrix

$$N' = \begin{pmatrix} \cos L & -\sin L & 0 \\ \sin L & \cos L & 0 \\ 0 & 0 & 1 \end{pmatrix} \qquad \text{Eq. 3.21}$$

Additionally, the position and velocity of a body in the equinoctial frame can be found from it equinoctial elements by

$$\vec{r} = F_e \vec{f}_e + G_e \vec{g}_e + W_e \vec{w}_e \qquad \text{Eq. 3.22}$$

where

$$F_e = \frac{p \cos L}{1 + f_e \cos L + g_e \sin L} \qquad \text{Eq. 3.23}$$

$$G_e = \frac{p \sin L}{1 + f_e \cos L + g_e \sin L} \qquad \text{Eq. 3.24}$$

$$W_e = 0 \qquad \text{Eq. 3.25}$$

and

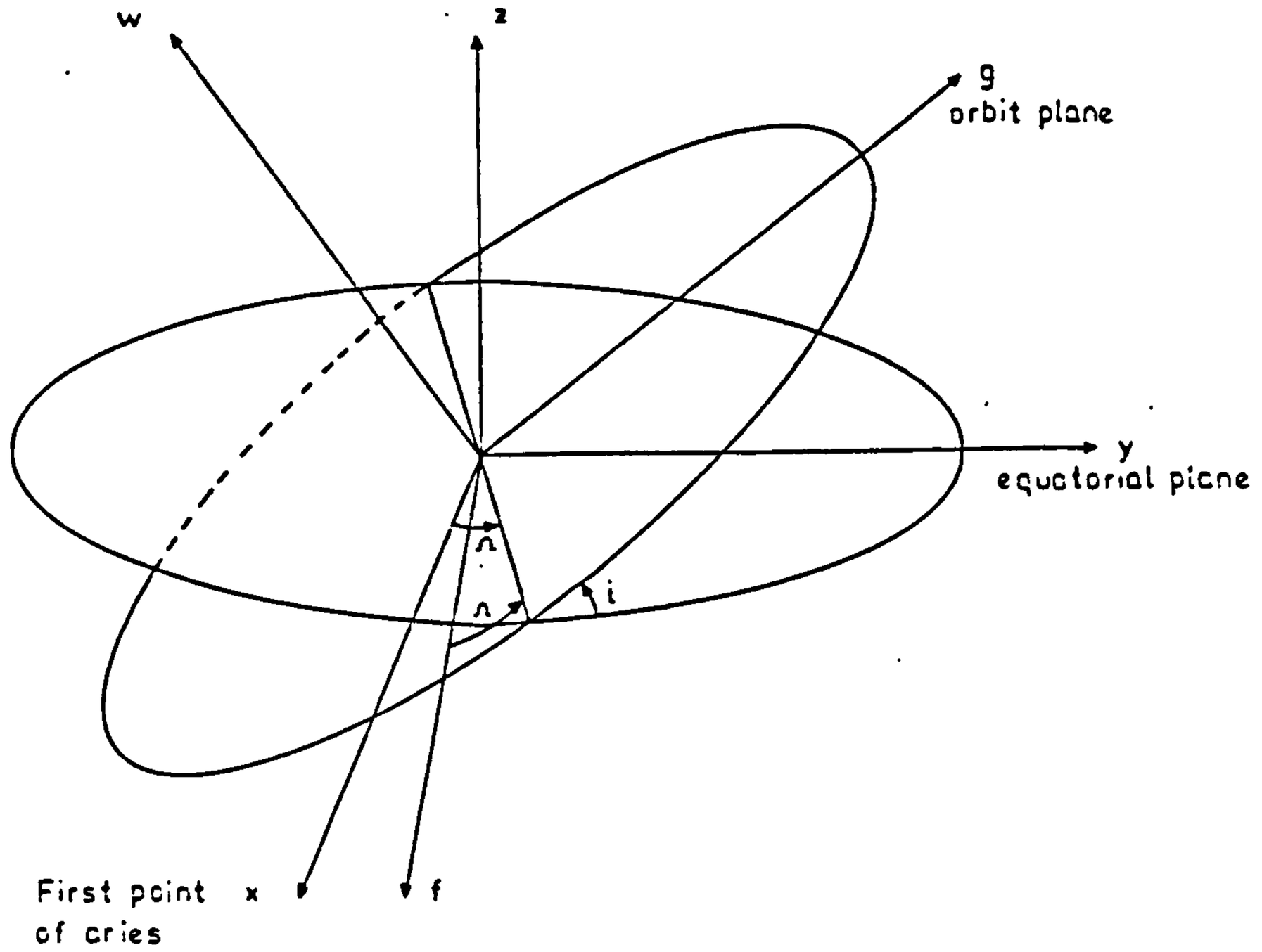

Figure 3.5 Relation between equatorial frame (x,y,z) and equinoctial frame (f,g,w).

$$\vec{v} = \dot{F}_e \vec{f}_e + \dot{G}_e \vec{g}_e + \dot{W}_e \vec{w}_e \qquad \text{Eq 3.26}$$

where

$$\dot{F}_e = -\sqrt{\frac{\mu}{p}}\,(g_e + f_e \sin L) \qquad \text{Eq. 3.27}$$

$$\dot{G}_e = \sqrt{\frac{\mu}{p}}\,(f_e + g_e \cos L) \qquad \text{Eq. 3.28}$$

$$\dot{W}_e = 0 \qquad \text{Eq. 3.29}$$

For Keplerian orbits only the w components of position and velocity are always zero because both the position and velocity vectors always lie in the plane of the orbit.

The Gaussian form of Lagrange's planetary equations can then be given in the form (Roth)

$$\frac{dp}{dt} = \sqrt{\frac{p^3}{\mu}}\,\frac{2}{W}\,a_t' \qquad \text{Eq. 3.30}$$

$$\frac{df}{dt} = \sqrt{\frac{p}{\mu}}\,\frac{1}{W}\left(a_r' W \sin L + a_t' A(L) - a_n' g_e (h_e \sin L - k_e \cos L)\right) \qquad \text{Eq. 3.31}$$

$$\frac{dg}{dt} = \sqrt{\frac{p}{\mu}}\,\frac{1}{W}\left(-a_r' W \cos L + a_t' B(L) + a_n' f_e (h_e \sin L + k_e \cos L)\right) \qquad \text{Eq. 3.32}$$

$$\frac{dh}{dt} = \sqrt{\frac{p}{\mu}}\,\frac{X}{2W}\,a_n' \cos L \qquad \text{Eq. 3.33}$$

$$\frac{dk}{dt} = \sqrt{\frac{p}{\mu}}\,\frac{X}{2W}\,a_n' \sin L \qquad \text{Eq. 3.34}$$

where

$$\frac{dL}{dt} = \sqrt{\frac{\mu}{p^3}}\,W^2 + \sqrt{\frac{p}{\mu}}\,\frac{1}{W}\,a_n(h\sin L - k\cos L) \qquad \text{Eq. 3.35}$$

$$X = 1 + h^2 + k^2 \qquad \text{Eq. 3.36}$$

$$W = 1 + f\cos L + g\sin L \qquad \text{Eq. 3.37}$$

$$A(L) = f + \cos L\,(1 + W) \qquad \text{Eq. 3.38}$$

$$B(L) = g + \sin L\,(1 + W) \qquad \text{Eq. 3.39}$$

Given the magnitude and direction of the various perturbing accelerations at any given instant, therefore, these equation may be evaluated by a special perturbation technique to describe the motion of the spacecraft over a wide range of orbital conditions. Walker et al. have made a numerical study of the perturbations on a highly eccentric orbit (a = 244 km, e = 0.726) by an axially-symmetric Earth using independent formulations in the equinoctial elements and Cowell's method. They report a difference of no more than 3×10^{-6} in the classical orbital elements derived by each method after four and half orbits, while the total specific energy was found to be constant to 10 significant figures and the polar component of angular momentum to be constant to 14 significant figures.

3.3 Modelling orbit perturbations

Given a general technique for modelling the perturbed motion of a spacecraft, it is now necessary to identify the perturbations to be included in the model and to establish the basis for modelling them mathematically. The major perturbations that can affect the orbit of a spacecraft about the Earth include; those that occur because of the gravitational attraction of other bodies; those due to the non-spherical nature of the Earth, those resulting from the drag of the atmosphere; those arising from interaction with solar radiation; and those caused by the action of the spacecraft propulsion system.

All these perturbations cause variations in elements of the orbit affected. These effects are usually classified as one of three types: secular, short-period, or long-period. Secular variations represent a continuous monotonic change with time in the element. Short-period variations are cyclical changes in the elements with a period less than or equal to the period of the orbit. Long-period variations are the same as short-period ones, with the exception that their periods are greater than the orbital period. It is apparent that secular variations are the most important category, since the orbital elements affected increase or decrease constantly.

The relative importance of these sources of perturbations to the modelling of orbits depends in the first instance on their magnitude and this is chiefly dependent on the operational location of the spacecraft. By way of illustration, the magnitudes of the perturbing accelerations in a typical low earth orbit and a geostationary orbit repectively are given overleaf in Table 3.1.

It can be seen that in both orbits the J_2 zonal harmonic component of the Earth's gravitational field is the largest and that this is by a factor of approximately 1000 in the lower orbits and approximately 10 in the higher one. Both the atmospheric drag and the solar radiation pressure acceleration are dependent on the area-to-mass ratio of the spacecraft. A primary factor influencing this is the presence or otherwise of solar arrays or large planar radio antennae (e.g synthetic aperture radars) on the spacecraft. A typical value of $A/M = 0.01$ for a vehicle gives acceleration levels broadly similar to that caused by the Sun's gravity

Table 3.1 - Magnitude of perturbing accelerations acting on a spacecraft of area-to-mass ration A/M

Source of perturbation	Acceleration ($m.s^{-2}$)	
	500 km	Geostationary orbit
J_2 zonal gravity	2.15×10^{-3}	5.66×10^{-5}
J_3 zonal gravity	7.4×10^{-6}	1.95×10^{-7}
Atmospheric drag	6×10^{-5} A/M	1.8×10^{-13} A/M
Solar radiation pressure	4.7×10^{-5} A/M	4.7×10^{-5} A/M
Sun's gravity (mean)	5.6×10^{-7}	3.5×10^{-6}
Moon's gravity (mean)	1.2×10^{-6}	7.3×10^{-6}

in the lower orbit. In the geostationary orbit the same is true with the exception that atmospheric drag has reduced to a level where it has negligible effect compared to the others. This latter demonstrates the extreme variability of atmospheric drag effects. At altitudes lower than 500 km atmospheric drag starts to predominate and eventually becomes the major perturbation to the satellite orbit. At altitudes higher than about 800 km solar radiation pressure has a greater effect than atmospheric drag.

It is apparent, then, that both the J_2 and the atmospheric drag should be included when modelling perturbations in lower orbits, but that the latter may be ignored in higher orbits. Radiation pressure is unimportant in lower orbits, but can have effects at medium altitudes close to upper operational altitudes for polar platforms and should therefore be included for the sake of completness.

The choice of which other perturbations should be included in the model is more complex. The zonal and tesseral harmonics beyond and additional to J_2 have small effects on lower orbits, but become increasingly important at higher altitudes, particularly at those close to the co-rotation radius where their effect is amplified. Although separate models could be used for each of the altitude regimes NASA recommend a combined model sufficient to account for both Earth oblateness and triaxiality (see next section) and this is the one that has been adopted in this work.

Looking at third body forces, the significant factor is more the nature of the effect that the perturbing acceleration has, in particular whether it causes a mainly periodic or a mainly secular change in the orbital elements, rather than the acceleration level per se.

The two third bodies that have the greatest influence on Earth-orbiting spacecraft are the Moon and the Sun (the perturbations caused by them are sometimes referred to jointly as luni-solar perturbations) The magnitude of these luni-solar perturbations is strongly dependent on the radius of the orbit. The mechanism involved is such that the major perturbation caused by these effects all the orbital elements, but is periodic in nature. The only elements effected by secular changes are the inclination, the right ascension of the ascending node and the argument of periapsis. The rate of change of these elements is given for the 500 km and the geostationary orbit in Table 3.2 below. Where these changes are dependent on inclination the maximum value has been quoted. The change in right ascension and argument of periapsis due to the J_2 component has also been quoted for the two orbits for the sake of comparison.

Table 3.2 - Magnitude of secular changes acting on affected orbital elements

Source of perturbation	Variation ($deg.day^{-1}$)	
	500 km	Geostationary orbit
Luni-solar		
Inclination	4.76×10^{-5}	7.50×10^{-4}
Right ascension	3.23×10^{-4}	5.92×10^{-3}
Argument of perigee	5.07×10^{-5}	7.53×10^{-3}
J_2		
Right ascension	7.65	1.33×10^{-2}
Argument of perigee	15.30	2.67×10^{-2}

It can be seen that in the low orbit the J_2 dominates the variation in right ascension and argument

of perigee by at least three to four orders of magnitude and, unless accuracies better than this are required, luni-solar effects may be ignored. For satellites at geostationary altitudes the J_2 effects are reduced and the luni-solar ones increased so that there is only one order of magnitude between them. In order to preserve accuracy in this milieu, therefore, luni-solar perturbations must be included. The same arguments changes in luni-solar changes to inclination and those caused by the rotation of the atmosphere in low orbits.

In addition to the major perturbations given above there are a number of minor perturbations which may also, under rare circumstances, affect the orbit of a spacecraft. These include such things as the impact of solid matter (either artificial debris or micrometeoroids) and interactions between a charged spacecraft and the geomagnetic field. However, because of their uncommon nature, the difficulties inherent in modelling some cases and their minimal effect on general orbit behaviour, they have not been considered further here.

Given the aforementioned considerations, and allowing for the fact that polar platforms and the servicing operations connected occur in near-Earth space, only earth asphericity, atmospheric drag and radiation pressure are modelled here. Obviously, the effects of a propulsion system must be included wherever the spacecraft operates. Given this, the accuracy of the model is of the order of 0.1%. Higher accuracies may be obtained by including the luni-solar perturbations, though this would also require a more sophisticated atmospheric density model than that presented (see 3.3.2.1) capable of accepting the $F_{10.7}$ solar flux level and geomagnetic activity index as inputs. Additional improvements in accuracy would also require a more detailed geopotential model.

3.3.1 Asphericity of the Earth

The Earth can be modelled as an oblate spheroid with its geopotential expanded in terms of harmonics which each represent a different deviation of the geoid from a perfect sphere. For space vehicle design studies NASA recommends the following approximation to the geopotential field [46].

$$U_g = \frac{GM_e}{r}\left(\begin{array}{l} 1 - \frac{J_2}{2}\left(\frac{r_e}{r}\right)^2 (3\sin^2\phi - 1) \\ \quad - \frac{J_3}{2}\left(\frac{r_e}{r}\right)^3 (5\sin^3\phi - 3\sin\phi) \\ \quad - \frac{J_4}{8}\left(\frac{r_e}{r}\right)^4 (35\sin^4\phi - 30\sin^2\phi + 3) \\ \quad + 3\left(\frac{r_e}{r}\right)^2 (C_{22}\cos 2\lambda_g + S_{22}\sin 2\lambda_g)\cos^2\phi \end{array}\right) \qquad \text{Eq. 3.40}$$

where

r	=	radius from centre of earth
ϕ	=	geographic latitude
λ_g	=	geographic longitude
r_e	=	equatorial radius of earth
J_2, J_3, J_4	=	first three zonal harmonic coefficients
C_{22}, S_{22}	=	first two tesseral harmonic coefficients

The harmonics describe the deviation of the potential field from a pure Newtonian one. The zonal harmonics specify this deviation in the north-south direction, while the tesseral harmonics do likewise for the deviations in the east-west direction. The respective magnitudes of the harmonic coefficients are

J_2	=	1082.7×10^{-6}
J_3	=	-2.56×10^{-6}
J_4	=	-1.528×10^{-6}
C_{22}	=	1.57×10^{-6}
S_{22}	=	-0.897×10^{-6}

It can be seen that J_2 is the dominant harmonic, being between approximately four hundred to one thousand times larger than the others.

Isolating the disturbing potential, Q, and formulating in the geographic co-latitude ϕ' (where $\phi' = 90° - \phi$) gives the components of the disturbing acceleration as

$$\frac{\partial Q}{\partial r} = GM_e \left(\begin{array}{l} \frac{3}{2} J_2 \frac{r_e^2}{r^4} (3\cos^2\phi' - 1) \\ + 2 J_3 \frac{r_e^3}{r^5} (5\cos^3\phi' - 3\cos\phi') \\ + \frac{5}{8} J_4 \frac{r_e^4}{r^6} (35\cos^4\phi' - 30\cos^2\phi' + 3) \\ - 9\sin^2\phi' \frac{r_e^2}{r^4} (C_{22}\cos 2\lambda_g + S_{22}\sin 2\lambda_g) \end{array} \right) \quad \text{Eq 3.41}$$

$$\frac{1}{r}\frac{\partial Q}{\partial \phi'} = GM_e \left(\begin{array}{l} 3 J_2 \frac{r_e^2}{r^4} \sin\phi'\cos\phi' \\ - \frac{J_3}{2} \frac{r_e^3}{r^5} (15\sin\phi'\cos^2\phi' - 3\sin\phi') \\ - \frac{J_4}{8} \frac{r_e^4}{r^6} (140\sin\phi'\cos^3\phi' - 60\sin\phi'\cos\phi') \\ + 6\sin\phi'\cos\phi' \frac{r_e^2}{r^4} (C_{22}\cos 2\lambda_g + S_{22}\sin 2\lambda_g) \end{array} \right) \quad \text{Eq 3.42}$$

$$\frac{1}{r\sin\phi'}\frac{\partial Q}{\partial \lambda_g} = GM_e \left(6\sin\phi' \frac{r_e^2}{r^4} (S_{22}\cos 2\lambda_g - C_{22}\sin 2\lambda_g) \right) \quad \text{Eq 3.43}$$

These accelerations can then be transformed into the spacecraft frame for application to the equations of motion.

The asphericity of the Earth causes perturbations in all the orbital elements. However, low-orbiting spacecraft with short orbital periods are insensitive to the periodic variations sectoral terms as these tend to cancel out. Secular perturbations, though, are very much in evidence, being caused by the oblateness of the planet (described by the J_2 term). This has two main effects on an orbit. The first of these is to cause a precession in the line of nodes in the equatorial plane so that Ω decreases with time

for orbits with inclination less than 90° and increases for orbits with inclination greater than 90° (. as already mentioned in Chapter 2) and is given approximately by

$$\frac{d\Omega}{dt} = \frac{-9.975}{(1 - e^2)^2}\left(\frac{r_e}{a}\right)\cos i \quad °/day \qquad \text{Eq. 3.44}$$

which we have already seen as Equation 2.3.

The second effect is to cause a precession of the line of apsides in the orbit plane. The precession is positive if the inclination is less than 63.4° and negative if it is greater, and is given by

$$\frac{d\omega}{dt} = \frac{4.982}{(1 - e^2)^2}\left(\frac{r_e}{a}\right)^2 (5\cos^2 i - 1) \quad °/day \qquad \text{Eq 3.45}$$

The second largest asphericity perturbation is caused by the earth's triaxiality, i.e by the ellipticity of the equator. The effect of this is really only of significance to geostationary satellites, since the ellipticity will exert a force which pulls the spacecraft towards one of the stable potential minima on the minor axis of the ellipse. For spacecraft in lower orbits the affects of the earth's triaxiality are limited to the aforementioned short periodic variations in the orbital elements.

3.3.2 Atmospheric Drag

The effect of the atmosphere on spacecraft in orbit near the Earth is significant. In general two acceleration components are produced; drag along the direction of travel and lift perpendicular to it. In many cases the lift generated is negligible and is can be ignored in comparison to the drag. The effect of the drag component on spacecraft in near-Earth orbits is to make them re-enter the atmosphere eventually unless steps are taken to reboost them. The approximately exponential nature of the atmospheric density profile (to be discussed in more detail in the next section) means that the re-entry process becomes increasingly rapid as altitude decreases. For practical purposes it can be assumed that any spacecraft with an altitude less than 100 km will re-enter within a few days.

Because the atmosphere rotates with approximately the same angular velocity as the Earth, any spacecraft with an inclined orbit will experience a third, out-of-plane acceleration component. King-Hele [47] gives the magnitudes of the three perturbing accelerations as

$$a_n' = -\frac{\rho v \delta}{2\sqrt{F'}} r\omega' \sin i \cos u \qquad \text{Eq. 3.46}$$

$$a_r' = -\frac{\rho v \delta}{2}\sqrt{\frac{\mu}{pF'}}\, e \sin\theta \qquad \text{Eq. 3.47}$$

$$a_t' = -\frac{\rho v \delta}{2}\sqrt{\frac{\mu}{pF'}}\left(1 + e\cos\theta - r\omega'\sqrt{\frac{p}{\mu}}\cos i\right) \qquad \text{Eq. 3.48}$$

where

$$F' = \left(1 - \frac{r_p \omega'}{v_p}\cos i\right)^2 \qquad \text{Eq. 3.49}$$

$$\delta = \frac{F' S C_d}{m} \qquad \text{Eq. 3.50}$$

and

ρ	=	ambient atmospheric density
v	=	satellite velocity
r	=	radial distance of satellite
ω'	=	angular velocity of atmosphere (taken to be ang. vel. of planet)
r_p	=	radius of perigee
v_p	=	velocity at perigee
S	=	reference area of satellite
C_d	=	drag coefficient
m_s	=	mass of satellite

These can be reformulated in the equinoctial elements to give

$$a_n' = -\frac{\rho v \delta}{2}\frac{p\omega'}{\sqrt{F'}\,W}\frac{(h_e \cos L + k_e \sin L)}{1 + h_e^2 + k_e^2} \qquad \text{Eq. 3.51}$$

$$a_r' = -\frac{\rho v \delta}{2}\sqrt{\frac{\mu}{p F'}}\,(f_e \sin L + g_e \cos L) \qquad \text{Eq. 3.52}$$

$$a_t' = -\frac{\rho v \delta}{2}\sqrt{\frac{\mu}{p F'}}\left(1 + f_e \cos L + g_e \sin L - \frac{\omega'}{W}\sqrt{\frac{p^3}{\mu}}\,\frac{1 - (h_e^2 + k_e^2)}{1 + (h_e^2 + k_e^2)}\right) \qquad \text{Eq. 3.53}$$

where

$$F' = \left(1 - \omega' \frac{1 - (h_e^2 + k_e^2)}{(1 + f_e^2 + g_e^2)(1 + h_e^2 + k_e^2)}\right)^2 \qquad \text{Eq. 3.54}$$

Since atmospheric drag acts in the direction opposite to the motion of the spacecraft its main effect is to remove kinetic energy, particularly at the perigee of elliptical orbits since this is where the atmosphere is densest. The cumulative effect is to reduce the radius of apogee (the perigee is also affected to a lesser extent) and hence the semi-major axis and eccentricity of the orbit, while the out-of-plane acceleration causes an alteration in the inclination, and the orientations of the lines of nodes and apsides.

3.3.2.1 Atmospheric Density

In order to calculate the perturbation due to atmospheric drag at any point the atmospheric density at the spacecraft must be found. Although its gross behaviour is well established, accurate estimation and prediction is very difficult since it depends on a number of external factors such as solar radiation flux and the Earth's geomagnetic activity, leading to errors of about 10% of the remaining lifetime for spacecraft approaching re-entry. However, standard models for the variation of a wide range of physical properties with altitude under mean conditions do exist. One such is the 1976 US Standard Atmosphere [48] which contains tables covering the range 0 to 1000 km with step sizes between 1 and 10 km. This is not a particularly useful form for computational analysis, however Lazari [49] has reduced the density data array in this to the density equation

$$\rho = \rho_0 \left(1 + b_0 (h - h_0)^2\right) e^{\left(\frac{-(h - h_0)}{H_0}\right)} \qquad \text{Eq. 3.55}$$

where

ρ	=	atmospheric density
ρ_o	=	atmospheric density at a reference altitude
h	=	altitude
h_o	=	reference altitude
H_o	=	density scale height at reference altitude
b_o	=	arbitrary constant to give zero error for calculated density

Using this equation with reference values of ρ_o, h_o, H_o and b_o updated every 50 km between 150 km and 1000 km allows the atmospheric density to be calculated to give a maximum mid-interval deviation of 0.3% from the reference atmospheric density.

In order to obtain a more accurate estimate of the atmospheric density the oblate nature of the atmosphere must be taken into account. This effect can be simply modelled by calculating the altitude of the satellite by subtracting the radius of the Earth at the sub-satellite point from its distance from the centre of the Earth (i.e. by assuming that the layers of equal atmospheric density are congruent with the surface of the earth). The deviation of the surface of the Earth from a perfect sphere with radius equal to the mean equatorial radius, r_e can be found from the equation given by Wagner [50]

$$r = r_e \left(\begin{array}{l} 1 - \frac{J_2}{2} (3\sin^2\phi - 1) \\ \quad - \frac{J_3}{2} (5\sin^3\phi - 3\sin\phi) \\ \quad - \frac{J_4}{8} (35\sin^4\phi - 30\sin^2\phi + 3) \\ \quad + 3 (C_{22}\cos 2\lambda_g + S_{22}\sin 2\lambda_g)\cos^2\phi \end{array} \right) \qquad \text{Eq 3.56}$$

An additional variation in atmospheric density is caused by solar heating. This causes a diurnal bulge in the atmosphere which lags some 30° behind the sub-solar point. Relative to the equatorial geocentric celestial co-ordinate system the position of the diurnal bulge changes only slowly with time. The right ascension, α, and declination, δ, of the maximum of the diurnal bulge can be given by

$$\alpha = \alpha_0 + t\dot{\alpha} \qquad \text{Eq. 3.57}$$

$$\delta = \tan^{-1}(\sin\alpha \tan\epsilon) \qquad \text{Eq 3.58}$$

where

α_o	=	right ascension of diurnal bulge at epoch
t	=	time since epoch
α	=	mean angular velocity of earth about sun
ϵ	=	angle between equatorial and ecliptic planes

King-Hele [51] states that a simple sinusoidal variation in atmospheric density with angular distance, ϕ, from the centre of the bulge is an effective model, so that

$$\rho = \bar{\rho}(1 + F_a \cos\phi) \qquad \text{Eq. 3.59}$$

where

ρ	=	mean atmospheric density over the diurnal period
F_a	=	density amplitude fluctuation

Ladner and Ragsdale [52] give an equation for F based on the nighttime density profiles. This can be redefined for the mean density profile to give

$$F_a = 0.095\left(e^{5.5 \times 10^{-6}} - 1.9\right) \qquad \text{Eq. 3.60}$$

3.3.2.2 Drag Coefficient

The drag coefficient, C_D, is a function of the shape and orientation of the satellite, the flow regime of the atmosphere and the thermal and momentum accommodation coefficients.

The flow regime is determined by the altitude. Above a certain height conventional aerodynamics cease and free molecular flow occurs. This is usually considered to be at the point when the mean free path of the molecules becomes greater than twice the maximum dimension of the spacecraft. For the size of the spacecraft under consideration here free molecular flow can be considered to occur above 150 km.

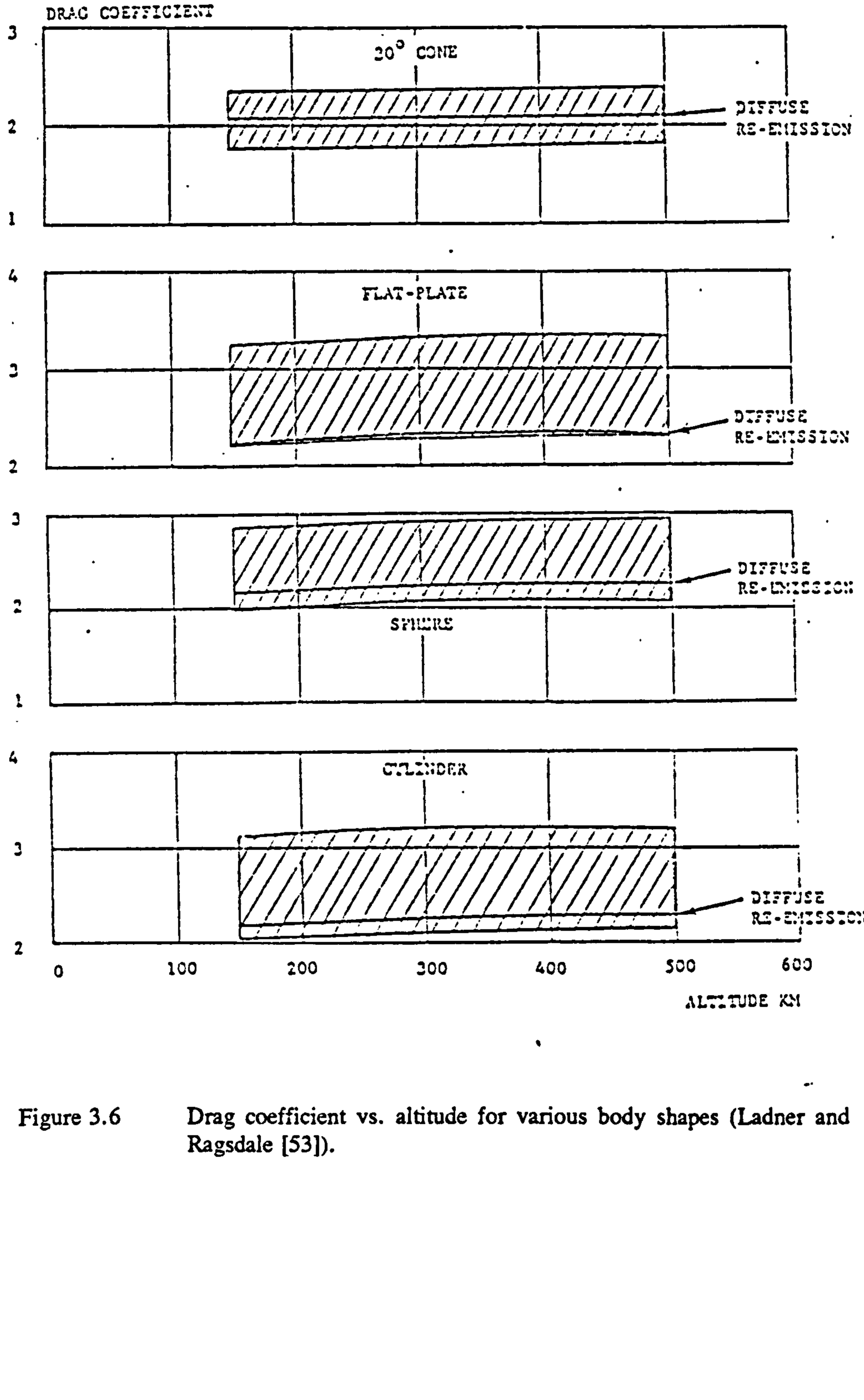

Figure 3.6 Drag coefficient vs. altitude for various body shapes (Ladner and Ragsdale [53]).

This is at the extreme lower end of the altitude range examined. Since any spacecraft at this altitude is likely to re-enter the atmosphere within a very short time it has been assumed that only free molecular flow occurs.

Under free molecular flow molecules may be absorbed onto the surface of the spacecraft and then re-emitted with a different thermal energy and in a diffuse manner. This factor is taken into account by use of thermal and momentum accommodation coefficients, α and σ respectively. Ladner and Ragsdale have further defined two subsidiary momentum accommodation coefficients, σ_n and σ_t, to account for both a normal and a tangential momentum flux. They have calculated and plotted C_D versus altitude for a number of shapes with $0<\alpha<1$, and assuming values of approximately 0.85 and 1.0 for σ_n and σ_t. The results for this can be seen in Figure 3.6 (previous page). The spacecraft can be considered to be a (very approximate) cylinder with the solar arrays represented by flat plates. Consideration of the two relevant graphs indicates a considerable area of overlap between the two shapes. A C_D of 2.25 has been selected as being a representative figure for the purposes of calculation.

3.3.2.3 Reference area

In order to calculate the perturbation due to atmospheric drag at any point the reference area of the spacecraft must be found. This is the projected area of the spacecraft normal to the velocity vector and can be considered as being comprised of two components; that due to the body of the spacecraft and that due to the solar arrays.

The spacecraft is assumed to be three-axis stabilised so it can be assumed to maintain the same orientation with respect to its velocity vector. The solar arrays, however, track the Sun and will present a different reference area at different times. The reference area can then be given by

$$S = S_{front} + | S_{array} \cos\sigma | \qquad \text{Eq. 3.61}$$

where

S_{front}	=	frontal area of spacecraft body
S_{array}	=	area of solar arrays
σ	=	angle between velocity vector and sun vector

3.3.3 Solar Radiation Pressure

Solar radiation pressure is an almost constant 4.6×10^{-6} N.m^{-2} in near-Earth orbit, and exerts comparatively large forces on spacecraft with large area-to-mass ratios. It can cause variation (depending on orientation) in all elements though for many orbits the resulting effects average zero. The main effect of solar radiation pressure is to decelerate the spacecraft as it moves sunwards and to accelerate it as moves away from the Sun. This tends to extend the semi-major axis of the orbit and so increase the eccentricity.

Ignoring parallax effects then the acceleration due to solar radiation pressure can be given by

$$a_q' = \frac{S}{m} k_r q_o \qquad \text{Eq. 3.62}$$

where

S	=	effective area of spacecraft.		
m	=	mass of spacecraft.		
k_r	=	reflection factor	$k_r = 1$	perfect reflection (specular).
			$k_r = 1.44$	diffuse reflection.
q_o	=	solar radiation pressure at 1 AU	(4.6×10^{-6} N.m^{-2}).	

For part of each orbit the spacecraft is eclipsed by the Earth. During this period the radiation pressure cannot affect the orbit. The satellite can be considered to be in eclipse if the following condition is fulfilled

$$\alpha_s > 90^\circ + \cos^{-1}\left(\frac{r_e}{r}\right) \qquad \text{Eq. 3.63}$$

where

α_s	=	angle between earth-spacecraft and earth-sun vectors (0°-180°).
r_e	=	radius of Earth.
r	=	radial distance of spacecraft from centre of earth.

3.3.3.1 Effective area

The calculation of the effective area of the platform exposed to solar radiation is necessary to find the perturbation due to radiation pressure and is similar to that for the reference area for atmospheric drag. In this case, however, the solar array area is fixed (since it always points at the Sun) and it is the projected area of the spacecraft that changes with time. In addition to this the spacecraft has a non-zero thickness, so that even when $\sigma = 0°$ it will present and area of S_{front} to the Sun. The effective area can be given by the equation

$$S = S_{Array} + S_{front} + | (S_{side} - S_{front}) \cos\sigma | \qquad \text{Eq. 3.64}$$

where

S_{side}	=	side area of spacecraft

3.4 Modelling the thrust vector

The spacecraft thrust vector is modelled quite easily and breaks down into two parts; the direction of the vector and the magnitude of the vector. Both of these may either stay constant or vary with time.

The direction of the thrust vector is specified using two angles, ψ_1 and ψ_2. ψ_1 describes the angle between the projection of the thrust vector on the orbit plane and transverse direction, while ψ_2 describes the angle between the thrust vector and orbit plane. The magnitude of the thrust vector, T, is defined as the scalar value of thrust produced by the spacecraft propulsion unit. Given these three parameters and the mass of the spacecraft the perturbing components of the acceleration due to the spacecraft propulsion system can be calculated for direct use with the Gaussian form of the planetary equation (i.e equations 3.30 through 3.35).

Chapter 4 - The computer programs

4.1 Introduction

This chapter first describes the structure and operation of the computer program ORBIT_CALC developed to implement the mathematical model described in Chapter 3. It then outlines two other programs, PROFILE_FIT and ORBIT_GRAF used in conjunction with ORBIT_CALC chapter, before summarising some computations performed to investigate aspects of ORBIT_CALC when used to simulate electrically-propelled servicing-missions.

4.2 Program descriptions

Three computer programs have been written in the course of the work. These are ORBIT_CALC, the general orbital simulation program, PROFILE_FIT, a utility program used to generate thrust vector profiles for input to ORBIT_CALC, and ORBIT_GRAF, a graphical post-processor for use on the data produced by ORBIT_CALC. These are described in more detail hereafter.

4.2.1 ORBIT_CALC

The mathematical model of the perturbed orbital motion and the necessary associated calculations have been coded in double precision FORTRAN 77 and together make up the ORBIT_CALC computer program. The underlying design philosophy for the program has been to structure it in such a way as to make it very flexible so that as wide a number of missions, spacecraft and propulsion systems as possible may be simulated. ORBIT_CALC has currently been implemented on a number of platforms under different operating systems; a variety of DEC VAX machines running under VAX/VMS, a SUN SparcServer 760 and a CONVEX 220 supercomputer both running under variants of UNIX.

The data input and output to and from the program is shown overleaf in Figure 4.1. Input to the program is contained in up to eight different data files. These are as follows;

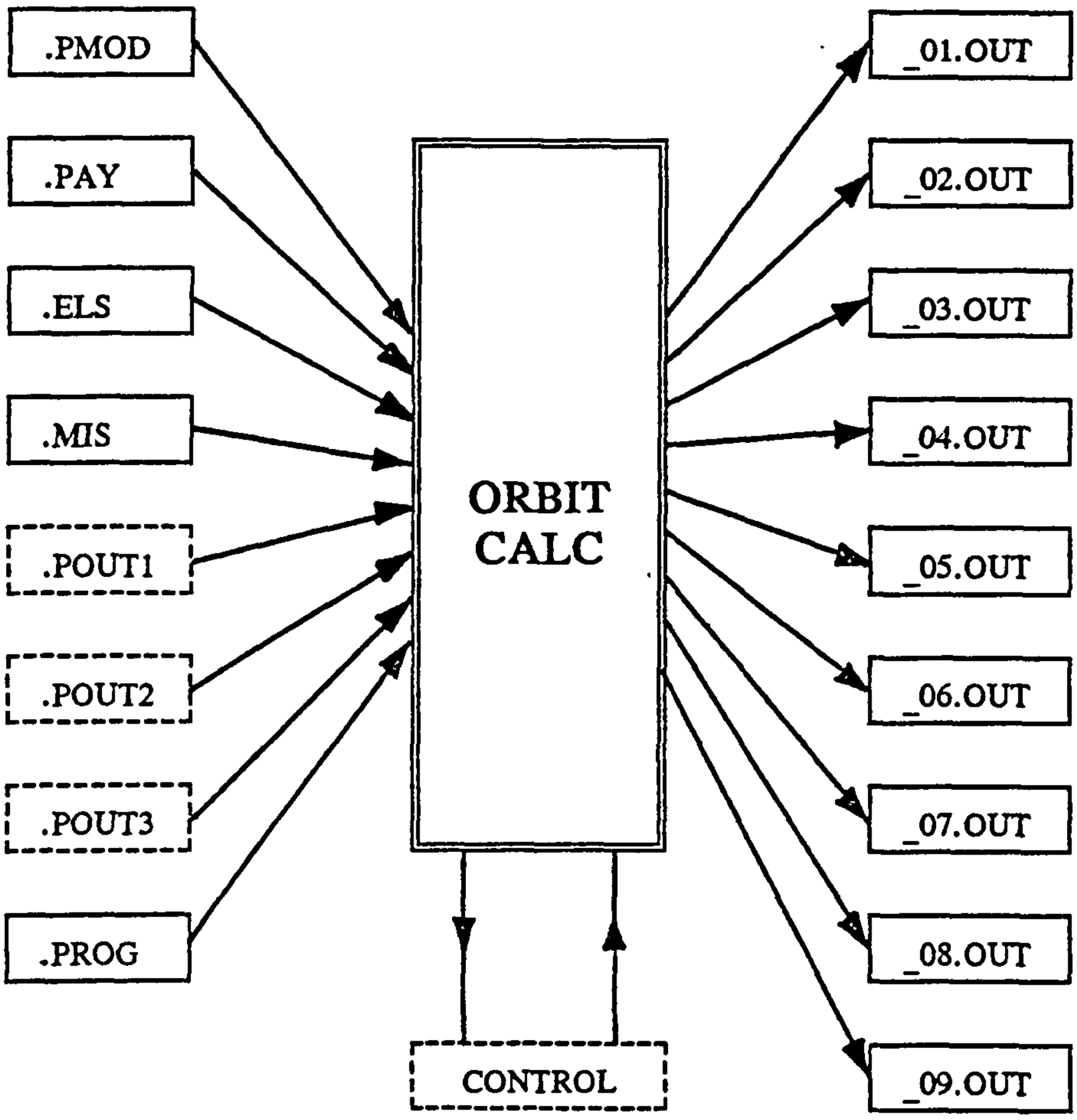

Figure 4.1 ORBIT_CALC datafile input and output

The .PMOD file contains propulsion module data which includes various module dimensions, engine, tankage and structural masses, maximum propellant load, exhaust velocity and impulse, as well as details of manufacturer, propellant type and formulation where appropriate. The latter data are included for completeness and so as to provide for the possibility of using .PMOD files as the basis for a propulsion system computerised database to be accessed by a putative program written for this purpose.

The .PAY file contains payload data, where payload is deemed to include all that part of the spacecraft that is not the propulsion system. This consists primarily of payload dimensions and masses. This split between propulsion module and payload was implemented so as to allow for the easy modelling of modular spacecraft.

The .ELS file contains the initial state of the spacecraft. Although the program performs its calculations using the equinoctial elements described in Chapter 3, the initial state is defined in terms of the classical orbital elements since these are more easily comprehended by most users.

The .MIS contains mission-related parameters and defines the start and end time of the simulation, the propellant load, the drag coefficient, the year angle of the Sun and the hour angle of the Earth at epoch, a number of switches for turning various aspects of the program on and off, most importantly, the various perturbations effects and the type of thrust vector control. This file also contains any comments relevant to a particular mission simulation. Additionally, the prefix for the .MIS file acts as a unique identifier for a particular program run and is used as the prefix for the output data files and graphical files produced by ORBIT_GRAF.

The .POUT1, .POUT2 and .POUT3 files contain thrust vector control data. They are output files generated by the program PROFILE_FIT and contain the information necessary to define the magnitude and direction of thrust at a given time if no control law is to be used to control these. This is typically the case when a solid propellant motor with a predefined thrust versus time profile is being used. When

thrust vector control requires feedback from the state of the spacecraft then the program uses a subroutine, here generically named CONTROL, in a user-defined library external to ORBIT_CALC.

The .PROG file contains parameters that define the size of the time-steps and output intervals as well as a number of switches that enable or disable output to particular files.

There are nine possible ORBIT_CALC output files and these are named by taking the .MIS file prefix and appending _01.OUT through _09.OUT. File _01 is a two-page summary file. It is made up of a standard header page that forms the top of every output file listing run time, comments, input and output filenames, and a second page that gives mission, mass, program parameter information along with the initial and final values of the classical and equinoctial orbital elements and a number of other orbital parameters (radius and velocity of periapsis and apoapsis, orbital period and similar).

Files _02 to _09 are of variable length and contain different sets of program output (with respect to time) as follows;

File _02	Classical orbital elements
File _03	Other orbital parameters
File _04	Thrust vector parameters
File _05	Equinoctial elements
File _06	Polar and cartesian co-ordinates
File _07	Atmospheric drag parameters
File _08	Asphericity perturbation and impulse parameters
File _09	Radiation pressure parameters and user-definable output

The broad structure and process of the ORBIT_CALC program is shown overleaf in Figure 4.2.

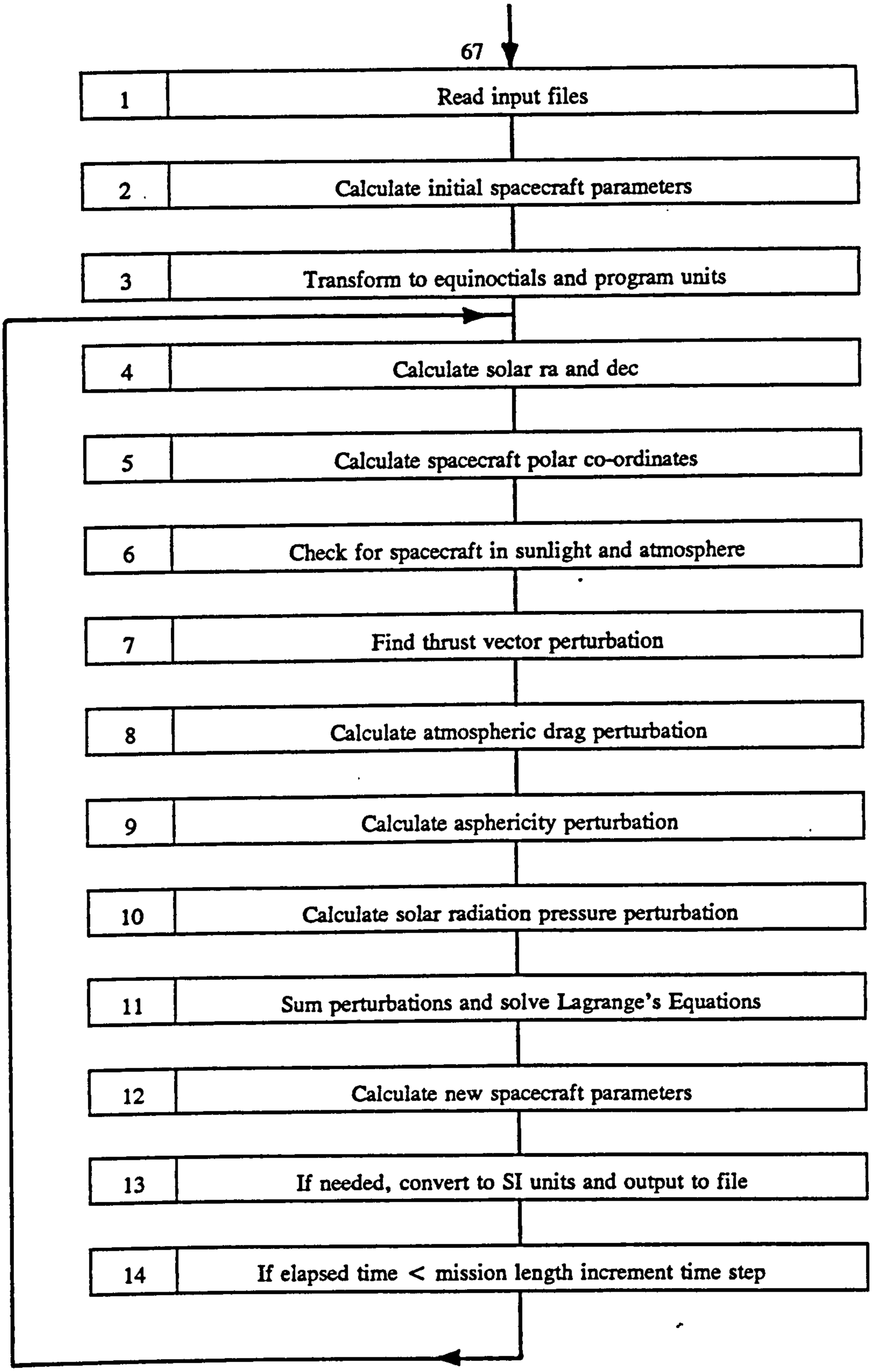

Figure 4.2 Functional schematic of ORBIT_CALC

Initially the input files are read. If the thrust vector profile is predefined this includes the .POUT series. The initial spacecraft parameters (e.g. total mass, array areas and similar) are then calculated, the initial classical orbital elements converted to equinoctial ones for use by the program. In order to increase program stability Lagrange's equations have been formulated in a non-dimensional form. To accomodate this, quantities in the SI system are first converted to 'program units' before calculation proceeds.

The position of the Sun, the spacecraft polar co-ordinates and the solar vector are then found and checks performed to find if the spacecraft is in sunlight or in eclipse, and inside the atmosphere limits. If the altitude is less than 150 km then the spacecraft is deemed to have re-entered and the program terminates. If the altitude is greater than 1000 km the spacecraft is deemed to be outside the atmopshere.

The thrust vector is determined, either by reference to the information contained in the .POUT files or by reference to the external subroutine CONTROL. The former contain details of the parameter profile with respect to time in the form of either a Chebyshev-derived polynomial or simple linear spline fit (see the section following on PROFILE_FIT). The latter contains the mathematical formulation of whichever control laws have been selected for a particular run.

If the location of the spacecraft makes it appropriate (i.e if in sunlight for solar radiation pressure, and if in the atmosphere for drag) the environmental perturbations to the orbit are then calculated before being summed with the effects of the propulsion system. These are then input to Lagrange's Equations which are integrated across the time step using a fourth-order Runge-Kutta method.

At the end of the time step, the spacecraft parameters are updated and, if required, data output to the appropriate files. As long as the total elapsed time is smaller than the mission length the program returns to point 4. The program continues, stepping in time, until end conditions are met. The simulation can be split into two phases, thrusting and non-thrusting, to enable two different time step regimes to be defined where this is appropriate.

When running on a VAX computer, the type of machine used for nearly all of the work, ORBIT_CALC takes approximately 100 minutes of cpu time to simulate one day of mission time. This can lead to very long run times, particularly for low-thrust missions. However, this unfortunate factor is being increasingly mollified by newer computer architectures and more 'user-friendly' run times should be available in the near future.

The computational structures used in ORBIT_CALC were designed to provide a computational accuracy at least in excess of that offered by the perturbed orbit model used in it (0.1%). This required the control of both round-off and truncation errors such that the combined total error was less than the required accuracy at the end of a simulation.

Round-off errors, which are a function of the number of digits available to describe a number in the computer memory, were found to be adequately controlled by performing all calculations in double precision, i.e to sixteen decimal places. Truncation errors, which are a function of the numerical technique used, were controlled by selection of an appropriate method. This choice was also influenced by the aforementioned desire to keep program design as general as possible. Because of this, the Runge-Kutte integration procedure was selected as a stable technique offering small truncation errors, requiring no start-up procedure and providing scope for easily alterable step sizes (albeit at the expense of speed of computation). Variability of step size is important in Runge-Kutte techniques as the truncation error cannot be calculated in advance in any simple manner. In general it is easier to investigate truncation errors experimentally using various time-steps and select one small enough to give the desired accurcacy. For ORBIT_CALC this process is described later in the chapter (Section 4.3.2). A timestep of 0.1 seconds was found to give the required computational accuracy.

The overall accuracy of ORBIT_CALC was assessed by comparison with the Ephemeris Generation and Coverage Module of Cygnus Engineering's Orbital Workbench package (Cygnus Engineering [53]). This package does not cater for the simulation of spacecraft propulsion systems so that

ORBIT_CALC can only be checked against it with thrust level set to zero. This is a realistic check, however, as changes due to perturbing forces are verified.

Over a twenty-day simulation of asphericity and solar radiation pressure effects, the maximum r.m.s. difference in any of the orbital elements was found to be 0.005%. This was not the case for a simulation of atmospheric drag effects which showed larger variations depending on initial altitude and right ascension of the ascending node. These were shown to be a result of the difference in atmospheric density models used in the two programs and primarily due to the inclusion of the diurnal density variation in ORBIT_CALC which is not included in Orbital Workbench. Calculations show that if the diurnal bulge effects are ignored the magnitude of the difference between the results from the two programs is reduced towards the 0.005% quoted above. As an additional check on the atmospheric drag model, a number of lifetime simulations were performed and compared with general predictions made by Ladner and Ragsdale [52]. The results of this comparison are shown overleaf in Figure 4.3, where it can be seen that there is good general agreement.

Given these error levels, the ORBIT_CALC program is very accurate over short periods and, in the context of the low-thrust propulsion missions discussed later, maintains its target design accuracy of 0.1% for simulation periods of up to around one year. If higher accuracy than this is required then more a more sophisticated multi-step numerical technique will be needed to replace the Runge-Kutte.

4.2.2 PROFILE_FIT

PROFILE_FIT is a program designed to generate thrust vector profiles in a form usable by ORBIT_CALC. In particular the ability to simulate thrust versus time curves for non-throttleable propulsion systems was deemed particularly important. Input to PROFILE_FIT takes the form of digitised data in files with suffix .PIN1, .PIN2 or .PIN3 (describing thrust level and two angles). PROFILE_FIT then generates either a linear spline or Chebyshev polynomial fit to the data (user-selectable at run-time) and plots the results graphically on the screen for acceptance or rejection by the user. In the case of a

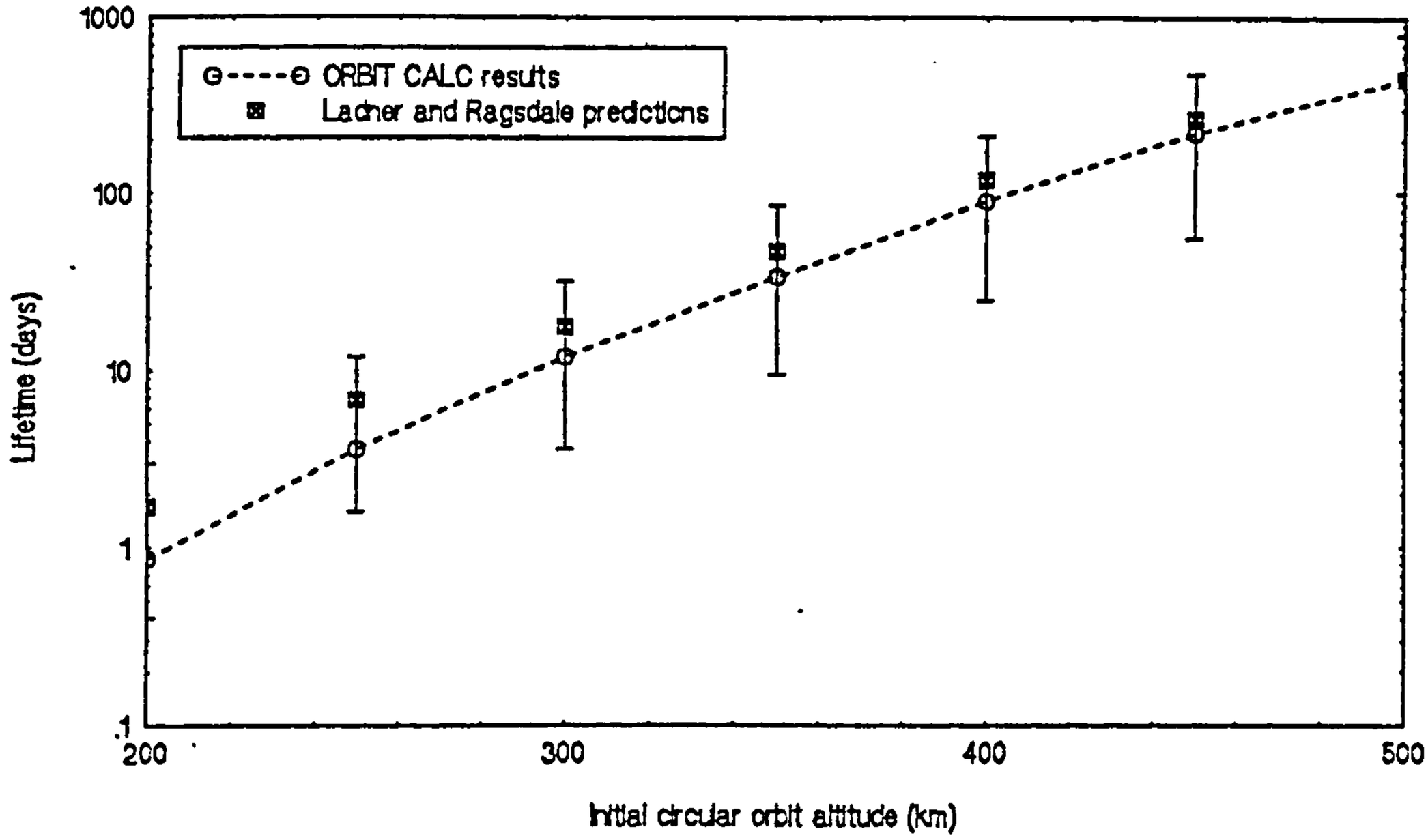

Figure 4.3 Comparison of orbital lifetime for ORBIT_CALC and Ladner and Ragsdale [52].

thrust profile it also finds the burn-out time, the maximum thrust and the total impulse.

If accepted, the profile data is written to the appropriate .POUT file and the graph saved in a file with the extension .PUPI1, .PUPI2 or .PUPI3 (where UPI stands for Unipict Image, the graphical image format for saving images generated by the McDonnell-Douglas UNIRAS family of software packages used here.) Overleaf in Figure 4.4 is an example of PROFILE_FIT graphical output showing the thrust versus time profile for the first stage of the Boeing Aerospace Inertial Upper Stage.

4.2.3 ORBIT_GRAF

The data written to output files by ORBIT_CALC can be viewed using ORBIT_GRAF, a graphics program designed to convert the data into a graphical form for easier analysis and process it for hard-copy output when wanted. Like PROFILE_FIT, ORBIT_GRAF uses the UNIRAS run-time graphics library of subroutines to do this. ORBIT_GRAF is interactive in use and, when prompted with the appropriate .MIS prefix (i.e. the unique program run identifier), locates all the relevant output files and indicates which parameters are available for analysis. Any parameter can be plotted against any other one under a variety of user-controllable conditions. Plots are displayed on the screen and may be saved to a file with .MIS prefix and the suffix .GUPI. An example of ORBIT_GRAF output is given overleaf in Figure 4.5.

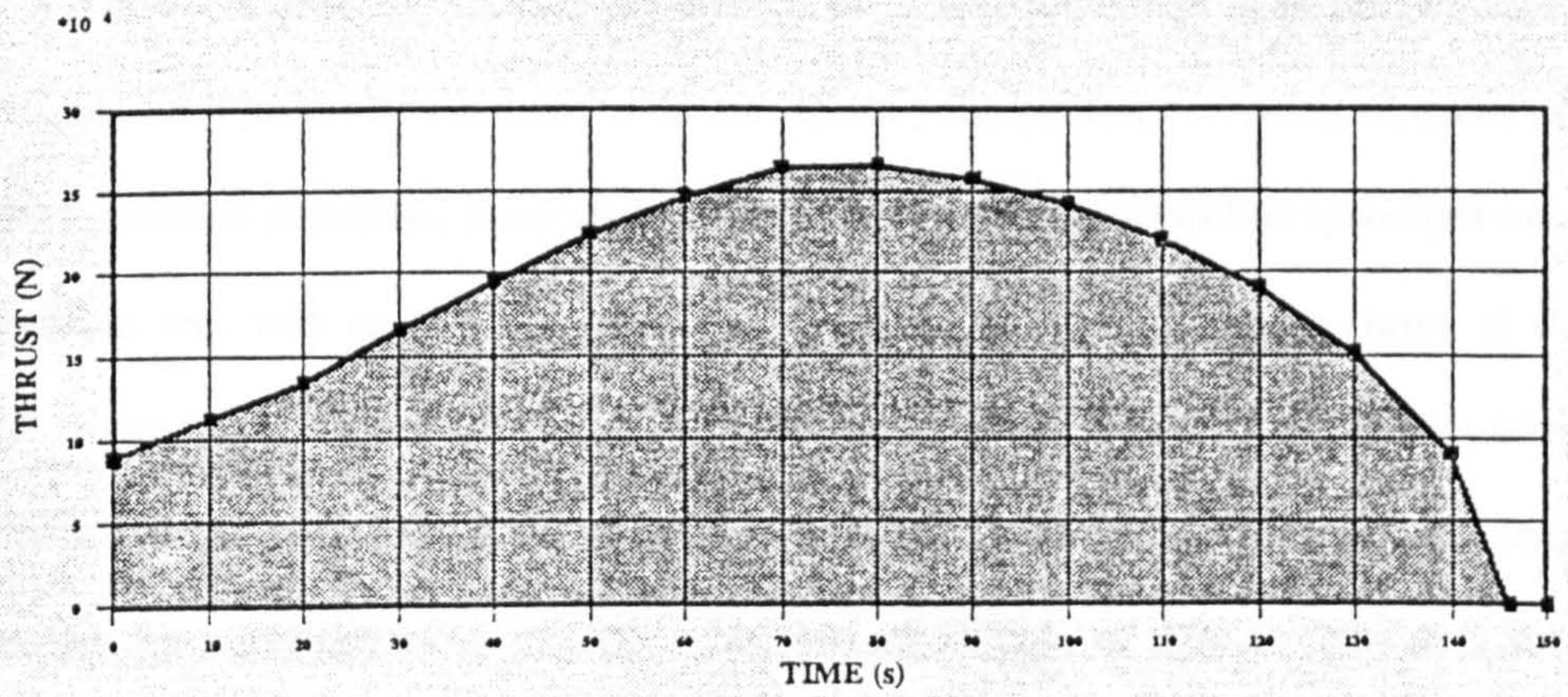

Burnout time (s) = 1.46000E+02
Total impulse (Ns) = 2.79584E+07
Maximum thrust (N) = 2.66640E+05

Input file : IUS1.PIN1
Output file : IUS1.POUT1
P FIT Runtime : 17-JUN-1988 16:08:13.15

This plot stored as segment no. 2
in UNIPICT datafile IUS1.PUPI1

THRUST VECTOR MAGNITUDE PROFILE

Figure 4.4 IUS first stage thrust-time profile produced by PROFILE_FIT.

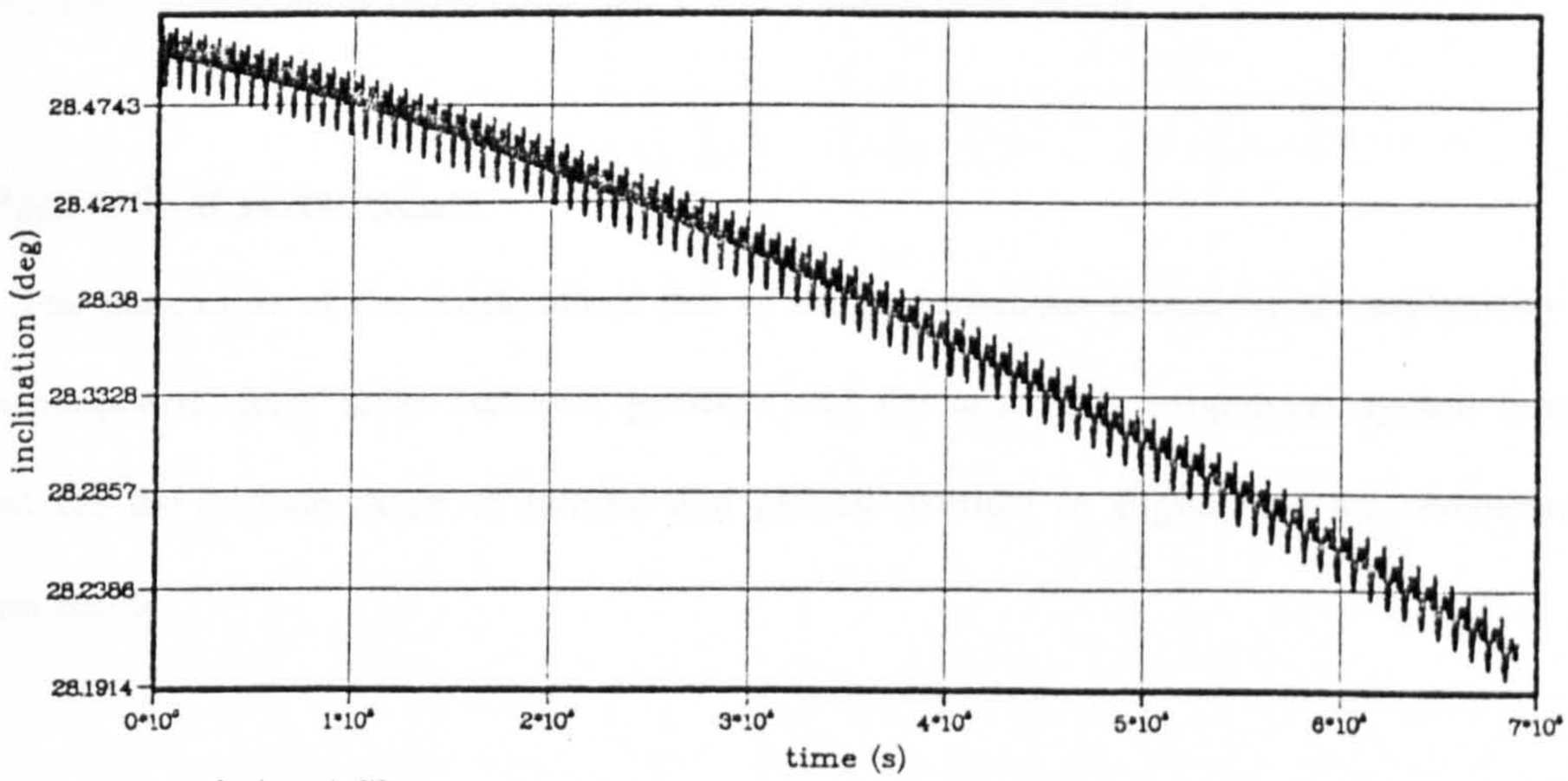

o calc input files

propulsion module : nothrust.pmod
payload : test.pay
orbital elements : ecc-1.eis
mission data : test4.mis
thrust profile : nothrust.pout1
angle 1 profile : nothrust.pout2
angle 2 profile : nothrust.pout3
program control : nothrust3.prog

o calc runtime : 13-SEP-1990 20:23:29
o graf runtime : 14-SEP-1990 07:58:06.86

segment no. 3
unipict datafile test4.upi

Figure 4.5 Example of ORBIT_GRAF output.

4.3 Program investigation

A number of program runs and calculations have been performed to investigate various aspects of the program with particular reference to the low-thrust polar platform servicing missions to be carried out. Unless specified otherwise, these are based upon an electrically propelled spacecraft using a xenon ion propulsion unit with an exhaust velocity of 57.4 $km.s^{-1}$ and providing a thrust of 0.6 N. The spacecraft has an all-up mass of 6400 kg and a maximum projected area of 88 m^2. This is taken from the characteristics of the gamma servicing vehicle configuration described in Chapter 8. The standard orbit used has the same inclination as an EOS orbit, but an altitude of 326 km (the drift orbit altitude calculated for the spacecraft, also in Chapter 8) and has the following orbital elements

a	6378 km
e	0
i	98.7°
Ω	0°
ω	0°
θ	0°

The epoch for calculations is 0000 GMT Jan 1 2020, Julian date 2458818.5.

4.3.1 Magnitude of perturbations

The magnitude of the accelerations due to the perturbations caused by the asphericity of the Earth, atmospheric drag, solar radiation pressure and the spacecraft propulsion system have been calculated for the altitude range of interest and plotted overleaf in Figure 4.6 for comparison and discussion below.

4.3.1.1 Earth asphericity

The perturbative effects due to the asphericity of the Earth are dominated by those due to the oblateness. This is because, as shown in Chapter 3, the J_2 zonal harmonic is over one thousand times larger than any of the other harmonics. The accelerations that result are the largest of all the 'natural'

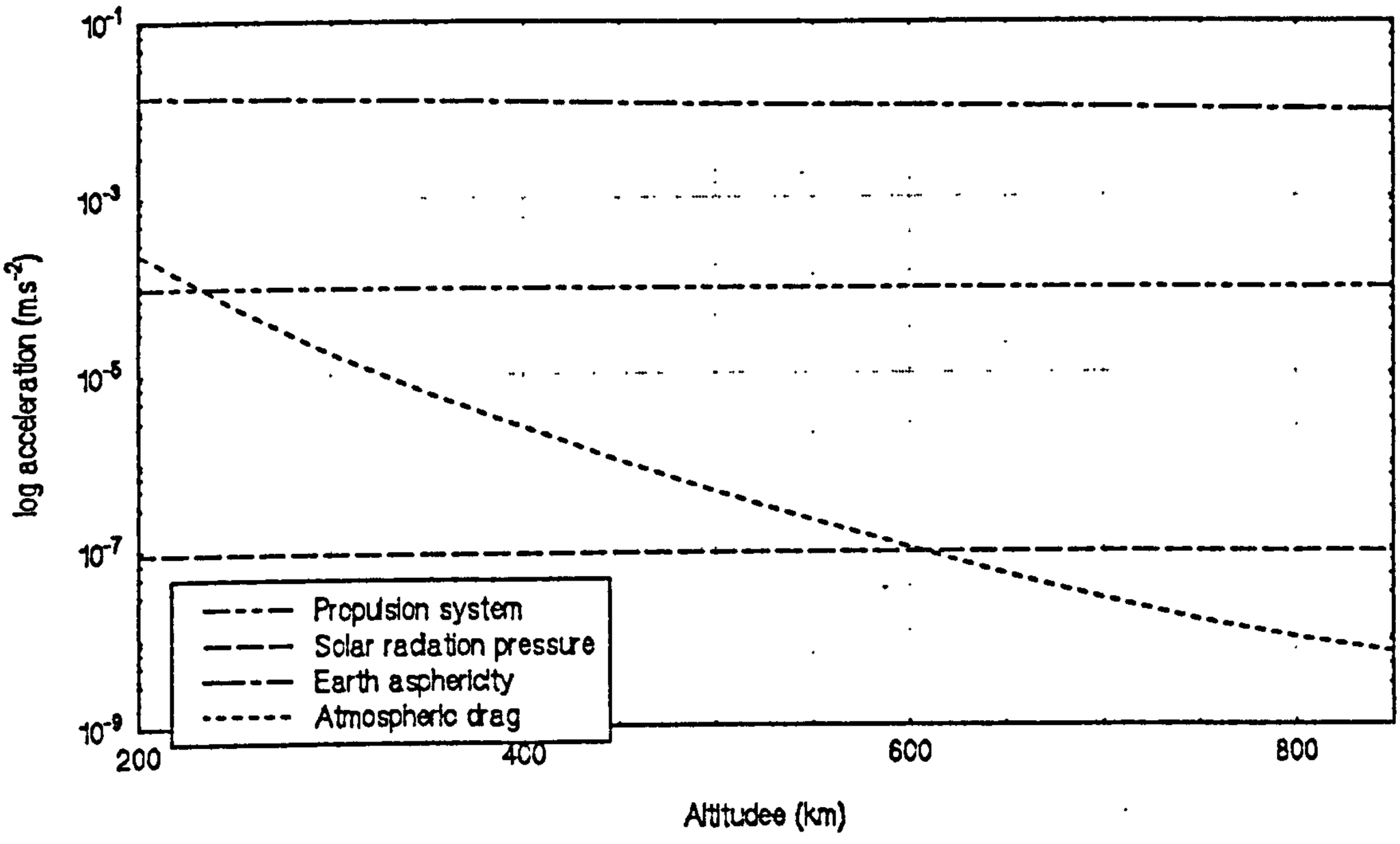

Figure 4.6 Log of different perturbing accelerations vs. orbit altitude

perturbations acting on the spacecraft and, in this case, larger than the perturbation caused by the spacecraft propulsion system itself. It should be noted, however, that Earth asphericity effects are conservative in action and neither add nor remove energy from the orbit. The perturbing acceleration level falls off with altitude but does so comparatively slowly over the given altitude range.

The primary effect of Earth asphericity on an orbit is the precession/regression of the ascending node and the argument of periapsis. These have been outlined in Chapter 3 and equations 3.44 and 3.55 give the rates at which these alter. For orbits close to circular (i.e quasi-circular low-thrust transfer orbits typical of those used by the reference vehicle), the two factors which have most effect on these are inclination and altitude. Figures 4.7 and 4.8 (overleaf) show the rates of change for different altitudes and inclinations. For the reference spacecraft in the reference orbit, the nodal precession rate is approximately 1.44 degrees per day, and the argument of perigee rate is -4.02 degrees per day, although for a circular orbit the latter does not have a real significance.

4.3.1.2 Atmospheric drag

The effect of atmospheric drag on a spacecraft depends on the atmospheric density, the orbital velocity, the effective area of the spacecraft and the drag coefficient. The drag force is given by

$$F_d = \frac{1}{2}\rho S C_d v^2 \qquad 4.1$$

The magnitude of the atmospheric density decreases from around 10^{-9} kg.m^{-3} at 150 km altitude to 10^{-15} kg.m^{-3} at 1000 km although, as already mentioned in Chapter 2, this may vary by several orders of magnitude with diurnal effects and solar activity. It can bee seen in Figure 4.1 that the acceleration due

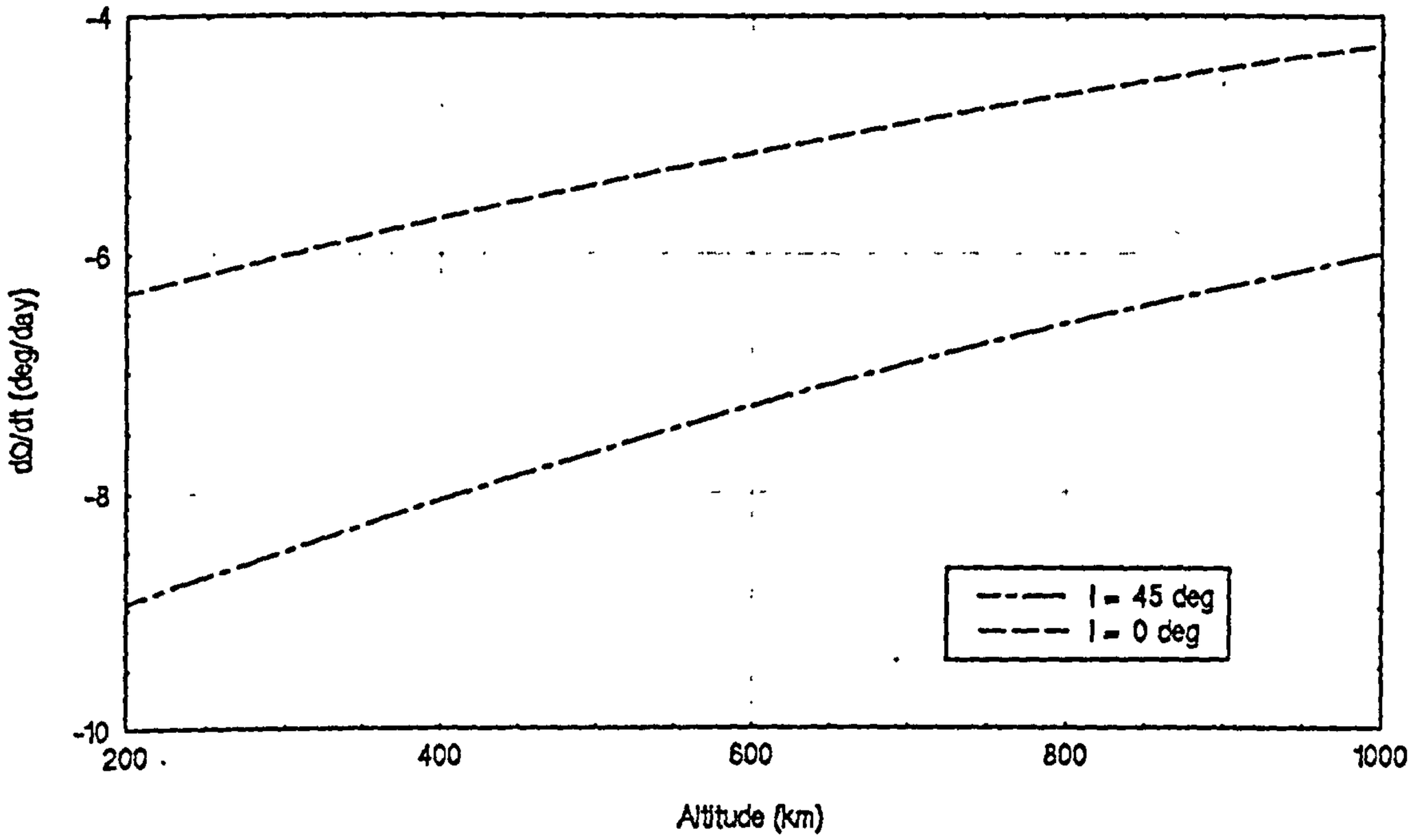

Figure 4.7 Nodal precession rate vs. altitude

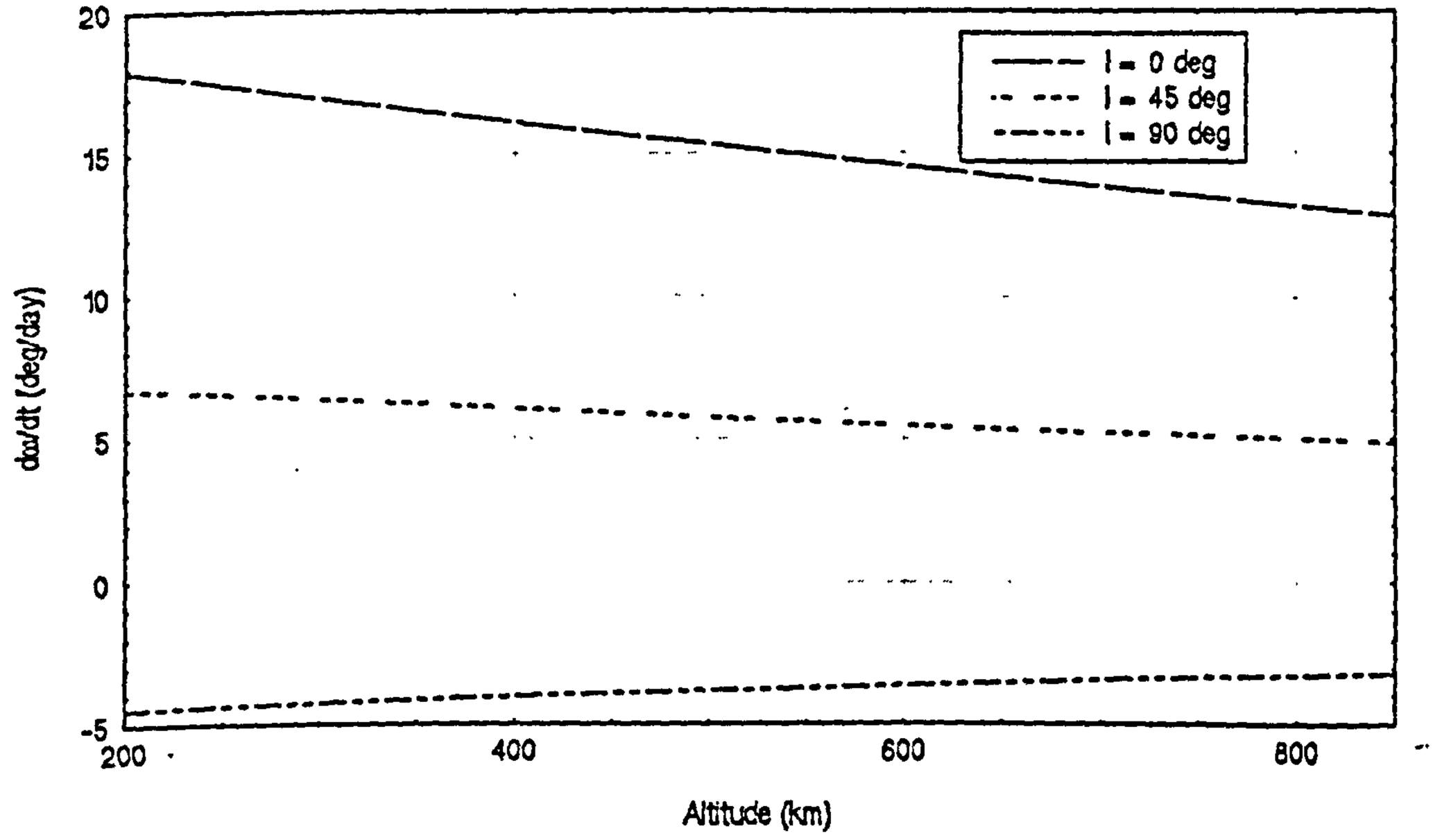

Figure 4.8 Argument of perigee precession rate vs. altitude

to drag (which is a dissipative effect and removes energy from the orbit) falls off with altitude much more that the others. At 850 km the drag acceleration represents a perturbing acceleration of approximately 0.01% of the thrust, while at low altitudes the converse becomes true. The break even point occurs at around 230 km for the reference spacecraft. Below this altitude the propulsion system can no longer provide drag-make up and the spacecraft will re-enter.

4.3.1.3 Solar radiation pressure

The acceleration due to solar radiation pressure depends on the reference area of the spacecraft, the reflective nature of the spacecraft and the actual value of the solar radiation pressure. This latter varies with distance from the the Sun and so may be considered to be constant in the vicinity of the Earth. The acceleration is given by equation 3.62. Taking a reflection factor of 1.44, then the force acting on the is approximately 9×10^{-8} m.s^{-2}. This is approximately equal to the perturbative acceleration due to atmopsheric drag at an altitude of 600 km. Below this altitude drag is the dominant of the two, above this radiation pressure.

The scope for solar radiation pressure to effect the orbit depends in part on the proportion of each orbit for which the spacecraft is eclipsed bu the Earth. This can vary between continual illumination in a dawn-dusk orbit ($U = 1$) down to some minimum value ($1 > U > 0.5$), dependent on the orbital altitude and orientation, for a midday-midnight orbit. This minimum, U_{min}, has been found for the altitude range of interest and is plotted in Figure 4.9 overleaf. It can be seen that it varies from 0.58 at 200 km to 0.66 at 850 km so that, for the most severe case, the spacecraft may be eclipsed for just over 40% of its orbit.

4.3.1.4 Spacecraft propulsion unit

The perturbing accleration due to the spacecraft propulsion unit depends on the spacecraft configurartion and, hence, on the overall mission design. For a higher thrust, shorter burn time propulsion unit the acceleration level could vary substantially depending on the thrust profile. However,

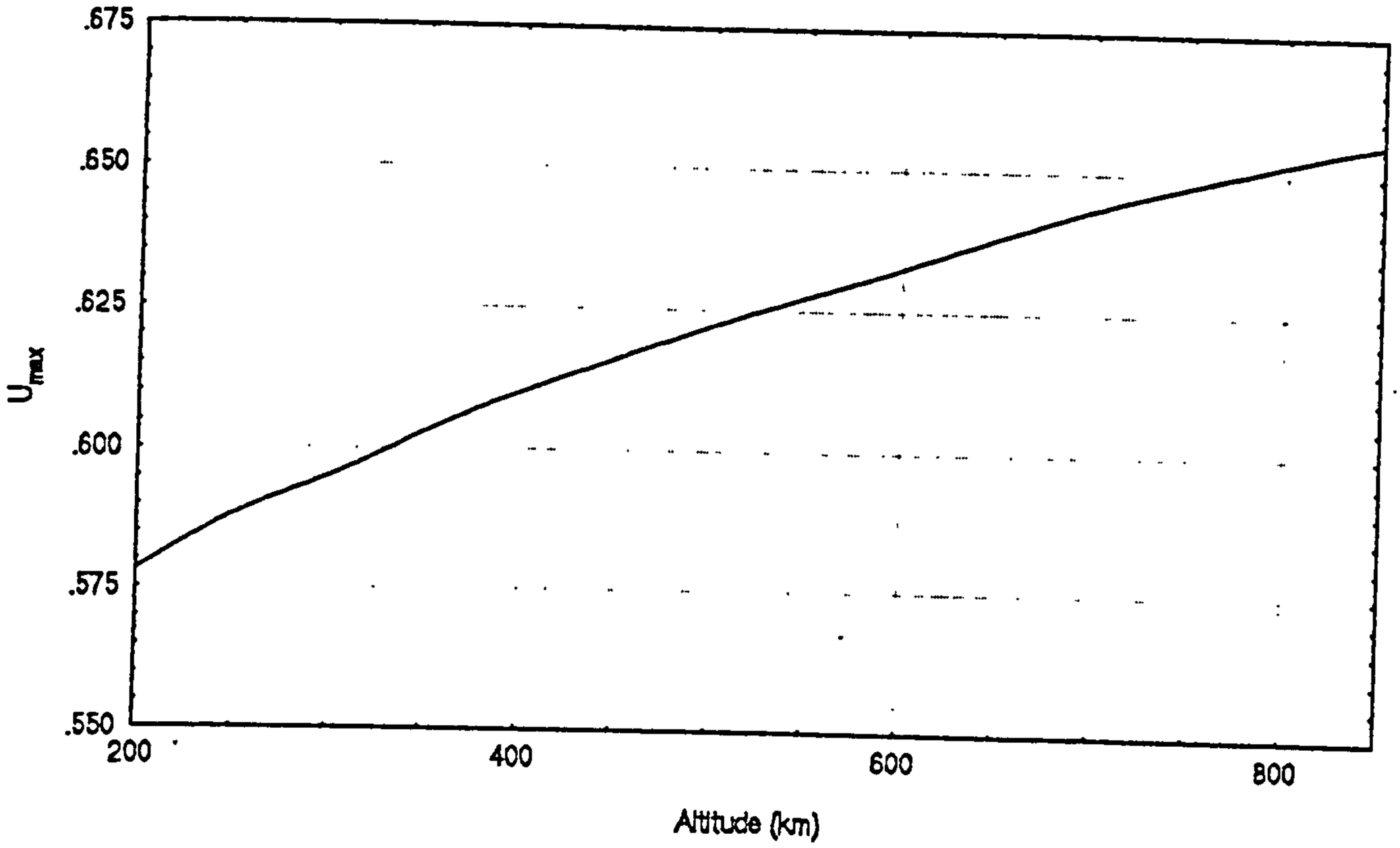

Figure 4.9 Minimum illumination factor vs. altitude.

for the reference vehicle, the thrust and acceleration can be considered, at least to a first degree approximation, to be constant. This gives an accleration level due to the spacecraft propulsion system in this case of approximately 9.5 x 10^{-4} $m.s^{-2}$. The effect on the orbit of this acceleration depends on the programming of the thrust direction which is discussed in more detail in Chapter 6.

4.3.2 Step length

The size of the time step used in the numerical integration process is not fixed and may be adjusted. It is desirable to have as large a time step as possible in order to reduce program run time. This desire is offset, however, by the wish to maintain accuracy. If larger time steps are used then errors in computation will arise and these will propagate through run time making the output increasingly in error. In general a compromise between a required level of accuracy and a practicable run time is achieved.

The time step related performance of the program was mapped under perturbation accelerations over the range 10^{3} - 10^{-9} $m.s^{-2}$. For each acceleration level the program was run a number of times with identical initial conditions, but with different time steps. The output of each successive run was then compared to indentify convergence in results. For all but the extreme top end of the acceleration scale (i.e. accelerations in excess of 100 $m.s^{-2}$) the time step necessary to provide accurate answers was found to be 0.1 seconds. This time step gives convergence to at least fourteen out of sixteen decimal places when compared with results obtained using a time step of 0.01 seconds.

This result, although acceptable for high-thrust, short burn time propulsion systems is somewhat less so for low-thrust propulsion systems where it predicates very long program run times. However, it is also inevitably concomittant with the aim of the program (to provide a uniform, high-accuracy simulation platform for a wide range of mission/propulsion studies) that it never be as 'efficient' in any one area as a program designed for that area alone.

Chapter 5 - Electric propulsion systems

5.1 Introduction

The type of propulsion system used by a spacecraft has a major effect both on the type orbital manoeuvres it can perform and hence overall mission design. In particular, there are significant differences between the ways in which high and low thrust systems may be applied. This chapter examines briefly the differences between the two sorts of propulsion system and, because of the relevance of low-thrust systems to this work (See Chapter 6), then examines the types and properties of electric propulsion systems available, the possible energy sources for these systems and some of the restrictions on their usage.

5.2 Comparison of chemical and electric propulsion systems

Space propulsion systems differ from those used on Earth in that they must carry all their propellant with them. Thrust is developed by imparting energy and momentum to the propellant and expelling it from the engine. The energy for this process can come from one of a number of sources such as a chemical or nuclear reaction or solar generated electricity. The energy transfer process may be a thermal one or use electrostatic or electromagnetic forces.

For a spacecraft of initial mass m_o which ejects a mass of propellant m_p over some period to end at a final mass m_f the mass ratio, R, of the rocket can be given by

$$R = \left(\frac{m_o}{m_o - m_p}\right) = \left(\frac{m_o}{m_f}\right) \qquad \text{Eq. 5.1}$$

and it is well-known that Tsiolkowsky's equation states that the change in velocity of the spacecraft in field-free space, Δv, is then given by

$$\Delta v = v_e \ln R \qquad \text{Eq 5.2}$$

where v_e is the exhaust velocity of the propellant. It can be seen, therefore, that the fraction of the original mass that can be accelerated through a given Δv is given by

$$\frac{m_f}{m_o} = e^{-\left(\frac{\Delta v}{v_e}\right)} \qquad \text{Eq. 5.3}$$

and that for a given Δv this is made large by choosing as high an exhaust velocity as possible.

In chemical propulsion systems thrust comes from the kinetic energy given to a propellant heated by its own chemical reaction which is then expanded through a nozzle. The exhaust velocity of such systems is limited by the amount of energy released by the reaction and the efficiency with which it can be transferred to the exhaust gases. Compared to electrical propulsion systems the resulting powers are high, but can only be sustained over short periods of time. Chemical systems are classified as *energy-limited* propulsion systems. Table 5.1 gives examples of typical exhaust velocities for chemical propulsion systems.

Table 5.1 - Characteristics of chemical propulsion systems

Propulsion system	Exhaust velocity ($m.s^{-1}$)
Cold gas jet	650
Liquid monopropellant	1700 - 2900
Solid propellant	2100 - 3200
Liquid bipropellant	2900 - 4500

Electric propulsion systems use energy provided from a source which is independent of the expellant. Depending on spacecraft configuration, this power source may be dedicated purely to supplying electricity to the thrusters or may also supply power to rest of the spacecraft. Whichever is the case, however, the additional mass of the power system required to this must be included in the overall mass calculations. In general, the greater the power system mass, the greater the power and hence the greater

the exhaust velocity. However, although the amount of energy which can be supplied to the propulsion system over the thrust period may be quite large, the rate at which it can be supplied by the power source is restricted. For this reason electric propulsion systems are described as being *power-limited.*

There are three main classes of electric propulsion; electrothermal propulsion, electrostatic propulsion and electrodynamic propulsion. These are described in section 5.4. Typical exhaust velocities for the three categories are given in Table 5.2.

Table 5.2 Characteristics of electric propulsion systems

Propulsion system	Exhaust velocity ($m.s^{-1}$)
Electrothermal	1500 - 15000
Electrostatic	20000 - 60000
Electrodynamic	15000 - 60000

The variation of 1/R with both exhaust velocity and the Δv required is shown in Figure 5.1 overleaf. The higher the required Δv the more important a high exhaust velocity is, and for a given Δv more payload can be delivered if the exhaust velocity is increased. For example, if the mission Δv is 5000 $m.s^{-1}$ then an exhaust velocity of 5000 $m.s^{-1}$ will deliver 0.4 of the initial mass, while an exhaust velocity of 10000 $m.s^{-1}$ will increase this to 0.6 (both points indicated by arrows). This highlights the potential benefit of electric propulsion, namely to increase the amount of useful payload delivered for a given initial mass or to deliver a given payload while minimising the initial (i.e launch) mass. Notwithstanding this, electric propulsion does have some limitations. These are discussed in the next section.

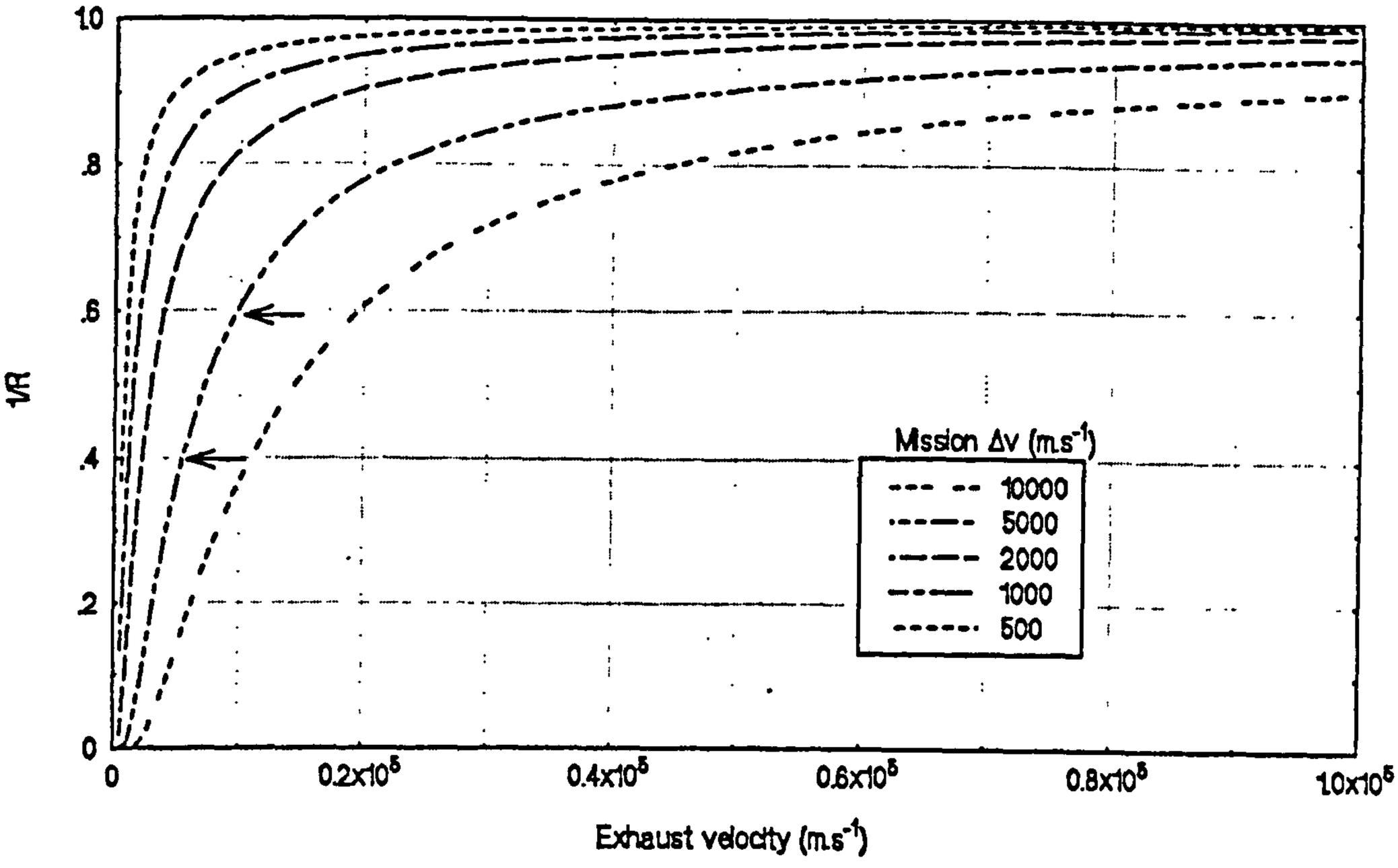

Figure 5.1 Fraction of initial mass delivered vs. exhaust velocity for different Δv's.

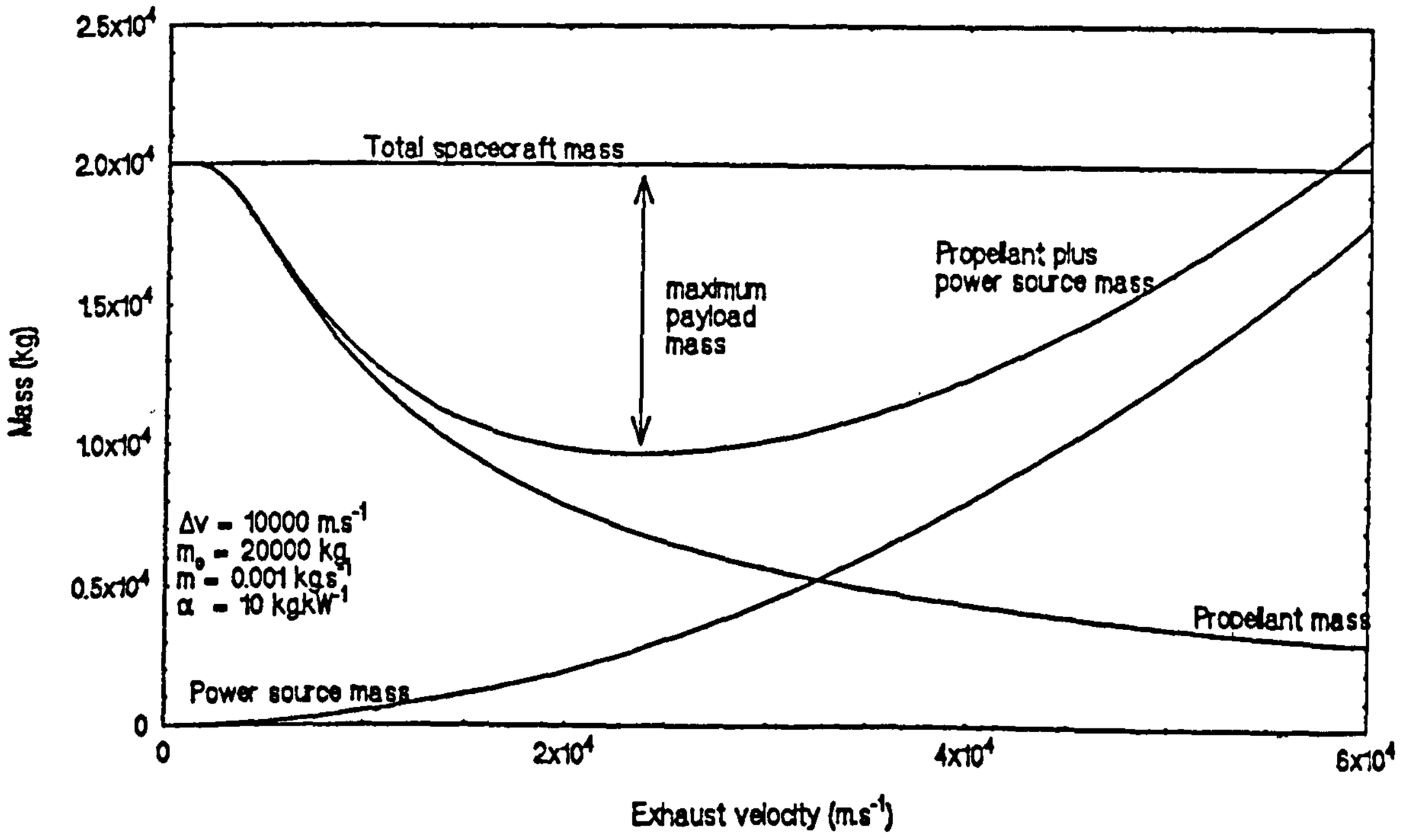

Figure 5.2 Effect of power source mass on optimum exhaust velocity for an electrically propelled mission.

5.3 Limitations of electric propulsion systems

The primary disadvantage of electric propulsion systems is the mass penalty that must be paid because of their need for a power source. This mass penalty detracts directly from payload capability and, ideally, should be minimised. Because of this, quantitative evaluation of power sources is required. The inverse specific power of the power source, α_{ps} (sometimes also known as the specific mass) is used to do this and is defined as the mass required to produce one kilowatt. If an efficiency of 100% is assumed then the beam power, P_b, of the exhaust is given by

$$P_b = \frac{\dot{m} v_e^2}{2} \qquad \text{Eq. 5.4}$$

and the mass of the power source by

$$m_{ps} = \alpha_{ps} P_b \qquad \text{Eq. 5.5}$$

This mass drives the selection of exhaust velocity for electric propulsion missions. Although for a given Δv the propellant mass decreases with increasing exhaust velocity additional power is needed to achieve this. Eventually the exponential decrease in the former with increasing exhaust velocity becomes negligible in comparison with the power plant mass which increases as the square. The optimum choice of exhaust velocity, known as the characteristic velocity, v_{ch}, is given by

$$v_{ch} = \sqrt{\frac{2t_b}{\alpha_{ps}}} \qquad \text{Eq. 5.6}$$

where t_b is burn time.

This behaviour is illustrated in Figure 5.2 on the previous page. A spacecraft of total mass of 20000 kg, propellant consumption rate of 0.001 $kg.s^{-1}$ and a power source with an inverse specific power of 10 $kg.kW^{-1}$ is to be used to perform a mission that requires a Δv of 10000 $m.s^{-1}$. The payload mass is given by the difference between combined mass of the propellant and power source.

It can be seen that for the example cited above the characteristic velocity is approximately 24000 $m.s^{-1}$, that the maximum payload mass is of the order of 10000 kg, and that the mass of propellant required is about 7000 kg. Assuming a value of 20 $kg.kW^{-1}$ for α_{ps} (typical of present light-weight solar arrays), we get a burn time of seventy days and a mean acceleration level of 4×10^{-4} $m.s^{-2}$. By way of comparison a cryogenic chemical propulsion system would require at least 74000 kg of propellant to give the same payload the same Δv but could achieve this in several minutes at much higher acceleration levels. Obviously, electric propulsion is confined to use in-space on missions that are not time-critical. However, on such missions, it offers significant mass savings. A typical example of such a mission is given in section 6.3.

5.4 Electric propulsion

Electric propulsion uses electric power to accelerate propellant. Compared to chemical propulsion it is characterised by high exhaust velocities, low thrust levels, low propellant consumption and long burn times and offers considerable benefits it term of payload capability.

There are three main types of electric propulsion. These are:

- Electrothermal propulsion, where a propellant is heated electrically and then expanded through a nozzle in a manner similar to that of chemical propulsion system.
- Electrostatic propulsion, where a charged or ionised propellant is accelerated by the application of an electric field.
- Electrodynamic propulsion, where a conducting propellant is accelerated by the interaction of crossed electric and magnetic fields.

5.4.1 Electrothermal Propulsion

Electrothermal propulsion uses electrical energy to increase the enthalpy of the propellant. The heated propellant is then allowed to expand through a nozzle, converting its thermal energy into kinetic energy. There are two basic types of electrothermal thruster, classified according to the method by which

the propellant is heated. Resistojets pass the propellant over heated elements, while arcjets pass it through an arc discharge.

For either sort of electrothermal propulsion, however, if one dimensional flow, constant specific heat, c_p, and adiabatic expansion are assumed then, given a chamber temperature T_c and an exit temperature T_e, the exhaust velocity can be found from the equation

$$v_e = 2\sqrt{c_p(T_c - T_e)} \qquad \text{Eq. 5.7}$$

5.4.1.1 Resistojets

The resistojet is the simplest form of electric propulsion and is shown schematically in Fig 5.4a overleaf. Propellant gas enters the thrust chamber where it is passed over, around or through resistively heated elements. The gas is then expanded through a supersonic nozzle. Since the exit temperature is effectively zero, Eq. 5.7 gives that the exhaust velocity is a function of the chamber temperature and the specific heat of the propellant. If hydrogen is used as a propellant (giving the highest specific heat) and a maximum realistic chamber temperature of 3000 K is taken (constrained by material properties of heating elements and chamber) then exhaust velocities must be less than 9000 $m.s^{-1}$. Hydrogen is not a particularly practical propellant for long term applications, however, as it must be stored cryogenically.

Unfortunately, resistojets do not conform to the one dimensional model. In addition to frozen flow losses (i.e. those losses caused by the failure of an expanding flow to remain in chemical equilibrium) they also suffer from losses due to viscous effects during propellant expansion through the nozzle and radiative cooling and heat transfer losses. Each of these is typified by the efficiency factors, η_f, η_n and η_h respectively. These combine to give an overall efficiency

$$\eta = \eta_h \eta_n \eta_f \qquad \text{Eq. 5.8}$$

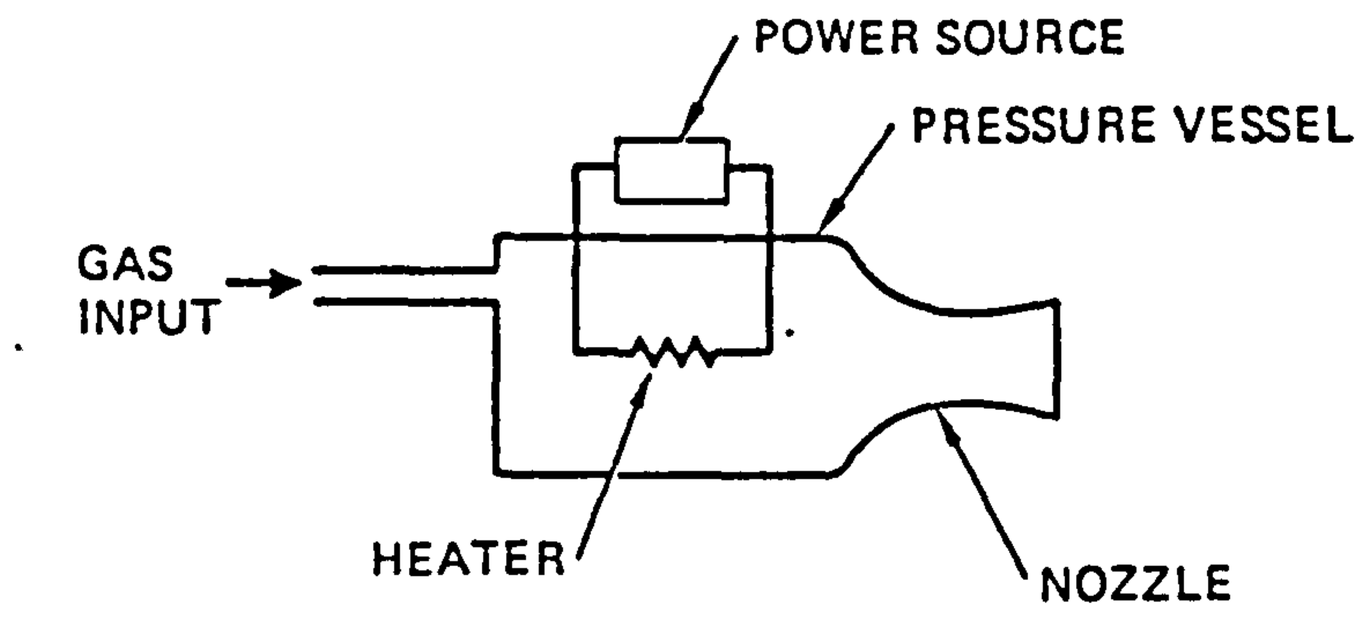

Figure 5.3a Schematic drawing of a resistojet (Poeschel & Hyman, [54])

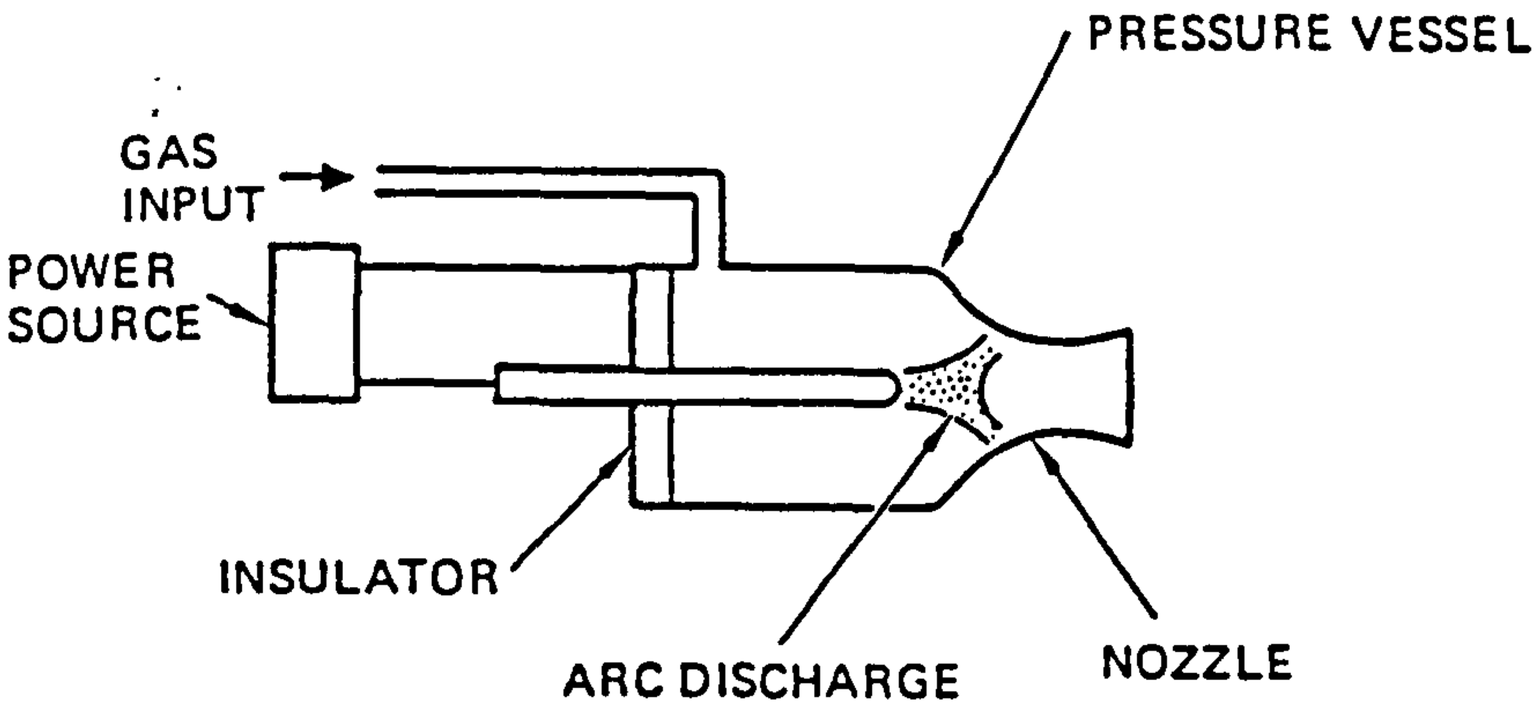

Figure 5.3b Schematic drawing of arcjet (Poeschel & Hyman, [54])

Practical examples of resistojets use nitrogen, ammonia and hydrazine as propellants. Although these have lower specific heats than hydrogen they are more easily stored and do not suffer from frozen flow losses to the same degree. They provide exhaust velocities in the range 1500 - 7000 $m.s^{-1}$ and thrusts in the range 0.005-0.5 N for powers between 0.01 and 3 kW with overall efficiencies better than 80.6. (Poeschel & Hyman [54], Jones [55]).

5.4.1.2 Arcjets

Arcjets attempt to improve upon the exhaust velocities obtainable in resistojets by using higher temperatures. This is achieved by setting up an arc discharge in the propellant. The self magnetic field of the current in the arc tends to constrict the current channel thus making the temperature of the propellant flow higher towards the centre of the flow than it is at the walls.

An arcjet is shown in Fig 5.4b (previous page). The propellant is heated and accelerated by collisions between the gas molecules and the ions that make up the plasma and then expanded through a supersonic nozzle. The higher temperatures obtainable in the arc lead to higher exhaust velocities, but only at the expense of lower efficiencies. This is unavoidable because energy used in maintaining the arc can only be recovered partially and the additional thermal energy transferred to the thruster must be removed.

Arcjets use ammonia, hydrazine and hydrogen (though still with the same limitations as for resistojets). They typically have powers in the region 1 - 30 kW and produce exhaust velocities between 5000 and 15000 $m.s^{-1}$ and thrusts of 0.05 - 5 N. Their lower efficiencies, usually of the order of 0.3, mean they have high power levels, typically 1 - 30 kW (DeVincenzi et al. [56], Cassady [57]).

5.4.2 Electrostatic propulsion

Electrostatic propulsion uses electric fields to directly accelerate a propellant. This propellant has the form of charged particles, usually atomic ions, but sometimes also molecular ions or charged droplets of liquid. A schematic of an electrostatic thruster is shown overleaf in Figure 5.4.

There are four basic stages to electrostatic propulsion, each involving the propellant ions. These stages are; production, extraction (i.e. separation of ions from the electrons), acceleration and neutralisation (i.e. the recombination of the ions and electrons to prevent spacecraft charging).

The generation of the ions can be done in a number of ways. The most common, however, is electron bombardment. An axially mounted thermionic cathode injects electrons into an ionisation chamber with a concentric, cylindrical anode and containing a weak magnetic field. This field causes the electrons to spiral around within the chamber where they ultimately strike and ionise a propellant atom. An alternative technique is radio frequency ionisation which uses a self-sustaining, electrodeless discharge to produce ions. The discharge chamber is a cylinder of insulating material placed within a set of coils through which a radio frequency electric current is passed. This produces an axial magnetic field which induces an azimuthal electric field which accelerates discharge electrons until they have enough energy to cause propellant ionisation. Since these electrons result from previous collisions a small thermionic initiator is also needed. A number of other ionisation techniques also exist although they will not be detailed here.

After the ions have been produced they are extracted. The exact technique used depends on the method of production, but in general it is achieved by making the exit end of the chamber negative relative to the anode. This can be done either with a specific extraction cathode or by giving the chamber a suitable geometry. Once the ions have been extracted they are then accelerated by one or more perforated acceleration electrodes. Once they have been ejected from the thruster the ion beam has electrons injected into it. This maintains the neutral charge of the thruster/spacecraft.

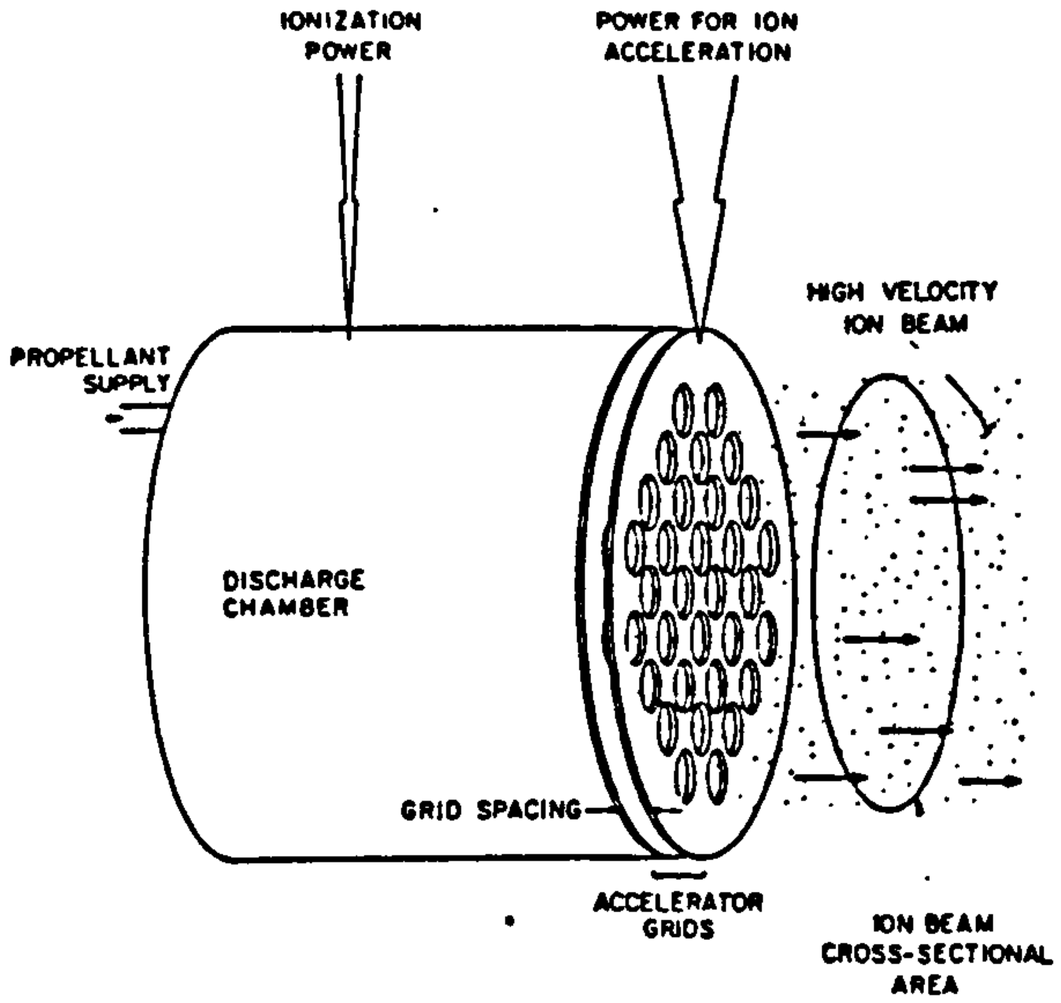

Figure 5.4 Schematic of an electrostatic thruster (Wilbur [58])

A particle of mass m and charge q will gain kinetic energy when it passes through a potential difference V_a. If its initial velocity is zero its final exhaust velocity is given by

$$v_e = \sqrt{\frac{2V_a q}{m}} \qquad \text{Eq. 5.9}$$

the beam power is given by

$$P_b = \frac{\dot{m}v_e^2}{2} = \frac{Fv_e}{2} \qquad \text{Eq 5.10}$$

so that the thrust is given by

$$F = \frac{2P_b}{v_e} = P_b\sqrt{\frac{2m}{v_o q}} \qquad \text{Eq. 5.11}$$

It is apparent from equations 5.9 and 5.11 that the charge-to-mass ratio, q/m, of the propellant particles effects both the exhaust velocity and the thrust. A high q/m gives a high exhaust velocity and a low thrust, while a small q/m has the opposite effect. The charge-to-mass ratio also determines whether the thruster is a high voltage, low current device (q/m small) or a low voltage, high current device (q/m large). The former arrangement is preferred (since it leads to lighter ion sources and chambers) and so electrostatic propellants tend to be charged, heavy molecules such as mercury, caesium (both less popular now for environmental reasons), xenon, krypton, and argon.

Ion thrusters have exhaust velocities in the range 20000 to 60000 $m.s^{-1}$ and develop thrusts between 5×10^{-3} and 0.5 N for powers of between 0.125 and 10 kW. Their efficiencies are given by

$$\eta = \eta_e \eta_m \qquad \text{Eq. 5.12}$$

where η_e is the electrical efficiency, i.e. the ratio of the directed energy to the input energy, and η_m is the mass utilisation efficiency which is the proportion of the propellant which is usefully employed in producing thrust. The total efficiency is high, 0.6 to 0.8. (Poeschel & Hyman [54], Jones [55]).

5.4.3 Electrodynamic propulsion

Electrodynamic thrusters use the interaction of electric and magnetic fields in a conducting propellant to generate a force to accelerate it. Either of the two fields may be externally generated or induced.

An electrodynamic thruster may be modelled in one dimension as follows. A flow of ionised gas of scalar conductivity σ_c is subjected to an electric field E and a magnetic field B which are perpendicular to each other and the gas flow velocity v. This causes a current of density

$$\vec{j} = \sigma_c(\vec{E} + \vec{v} \times \vec{B}) \qquad \text{Eq. 5.13}$$

to flow through the gas parallel to E. This will interact with B to cause a force

$$\vec{f}_B = \vec{j} \times \vec{B} \qquad \text{Eq. 5.14}$$

which is distributed throughout the gas and acts in direction of flow, hence accelerating the propellant.

5.4.3.1 MPD Arcjet

One form of electrodynamic thruster is the magnetoplasmadynamic (MPD) arcjet. This has evolved from experiments combining electrothermal arcjets with magnetogasdynamic channel flow. A schematic of an MPD arcjet is shown overleaf in Figure 5.6.

In the MPD arcjet the arc discharge not only ionises and heats the propellant but also accelerates it electrodynamically. At low power levels (in the kilowatts) the heating of the plasma is the predominant acceleration mechanism. As the power levels rise to 100 kW and above, the electrodynamic forces increase in effect. This occurs because the arc discharge at the cathode is compressed by its own azimuthal magnetic field. This field then interacts with the radial current component to produce a body force in the propellant. This effect can be enhanced by use of an externally applied magnetic field, though this tends to be most effective at the lower power levels. At higher power levels continuous operation is no longer possible and pulsed, quasi-steady-state, modes with pulse rates of the order of 20

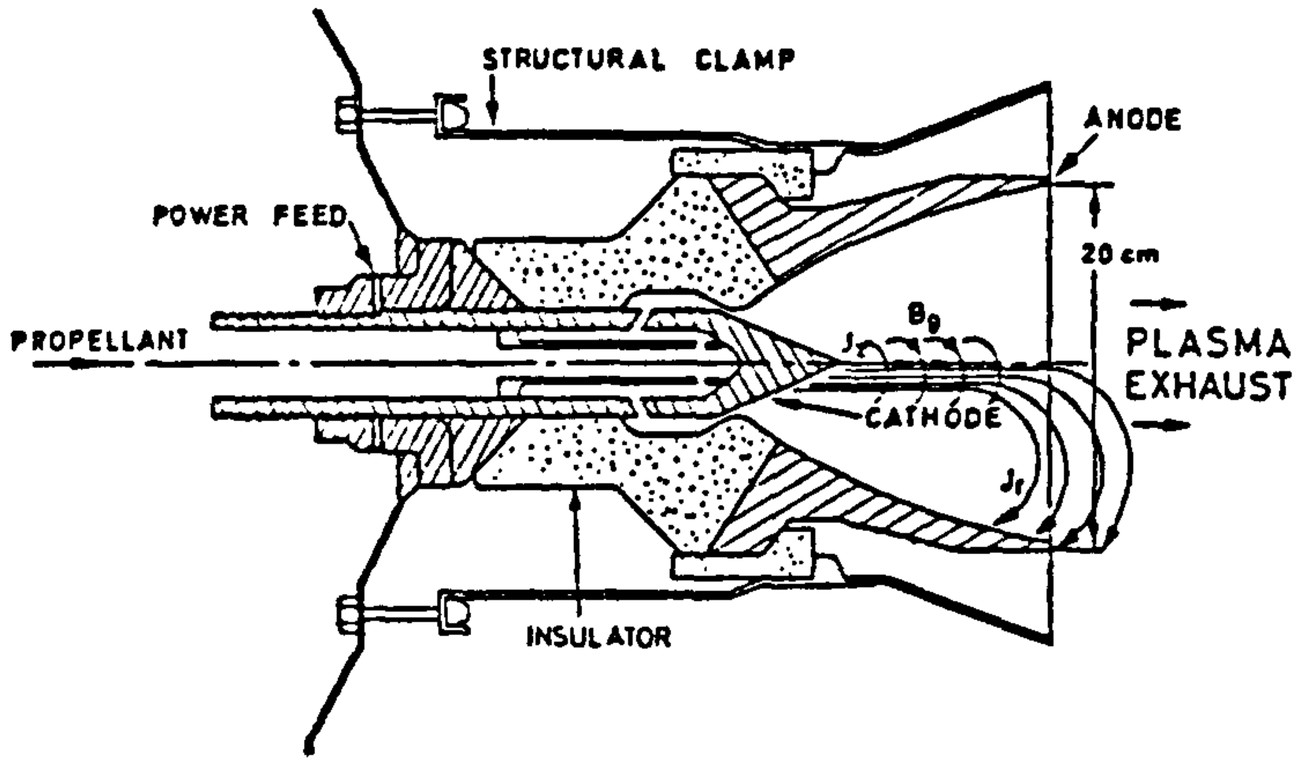

Figure 5.5 Schematic of multimegawatt MPD thruster
(Fearn and Wallace [31])

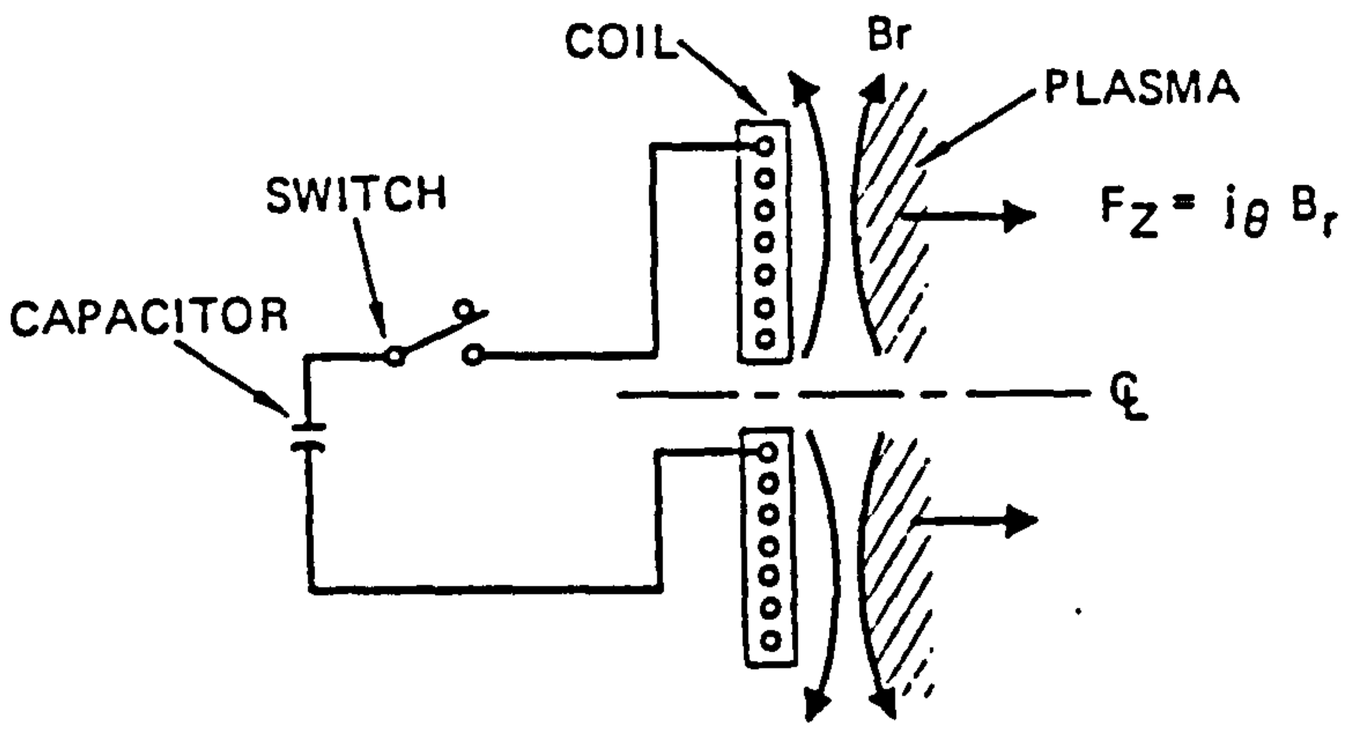

Figure 5.6 Schematic of a pulsed inductive plasma thruster
(Poeschel and Hyman, [54])

Hz are used instead.

The main propellants used in MPD arcjets are those used in electrothermal arcjets, i.e. hydrogen, ammonia and similar, and argon is also popular. Typical exhaust velocities are greater than 20000 $m.s^{-1}$, though greater than three times this has been achieved. MPD arcjets are also capable of producing substantial levels of thrust from fractions of a newton up to several hundred. Unfortunately they are not very efficient and suffer badly from thermal losses. They have η in the range of 0.1 - 0.15 at low power but fortunately this increases with power to around 0.35 at the megawatt levels envisaged for space applications (Seikel et al. [59]). The high powers and temperatures typical of this sort of operation tend to cause accelerated erosion of the electrodes, however, posing possible lifetime limitations. Nevertheless, these devices show considerable promise.

5.4.3.2 Pulsed inductive thruster

In the pulsed inductive thruster gas is delivered in bursts to the rear surface of a flat coil which is then energised. The current in the coil induces a voltage in the propellant which ionises it. The current in the resulting plasma interacts with the magnetic field of the coil to produce a body force which accelerates the plasma away from the coil. A schematic of a pulsed inductive thruster is shown in Figure 5.6 on the previous page. The main advantage that the pulsed inductive thruster offers is that the plasma discharge is electrodeless and so erosion of thruster surfaces is much reduced over that in arcjets.

Thrusts in the range 2 to 200 N have been achieved using pulsed inductive thrusters, at exhaust velocities of 15000 - 25000 $m.s^{-1}$. The most common propellants are argon and ammonia. Although the power conversion efficiency of pulsed inductive thrusters is around 0.8 the low efficiency of the actual engine means that the total thruster efficiency rarely rises over 0.5. Most of the loss is due to the fact that the energy used to generate the plasma is lost almost immediately. (Poeschel & Hyman [54]).

5.5 Power Sources

Any form of electric propulsion needs a source of electric power. The amount of power required depends on the thrust to be generated by the propulsion system. The various propulsion systems can be characterised in terms of the power they need to produce one newton of thrust. Some typical values given by Poeschel and Hyman are reproduced below in Table 5.3.

Table 5.3 Power/thrust for electric propulsion systems

Propulsion system	Power/thrust ($kW.N^{-1}$)
Resistojet	5
Arcjet	20
Ion thruster	23
MPD arcjet	33
Pulsed inductive plasma thruster	17

Power can, in theory, be provided from a wide number of sources. Figure 5.7 overleaf shows a number of power output-mission duration regimes. It should be noted that the boundaries are by no means well-defined and that there is actually considerable overlap between the various areas. The minimum effective output for a power source for use with electric propulsion is in the vicinity of 100 W, with a minimum output time of around one month. This limits the choice to radioisotope, solar photovoltaic, solar dynamic and nuclear dynamic systems.

Radioisotope generators use the thermoelectric effect to convert heat generated by a decaying radioactive isotope (e.g. Polonium 210 or Plutonium 238) into electricity. They are comparatively inefficient ($\eta \approx 0.1$) and highly expensive in terms of cost per watt. They also have high inverse specific powers. (See Table 5.4 below) This makes them generally unsuitable as power sources for electric propulsion. Their major use is on interplanetary probes unable to use solar photovoltaics.

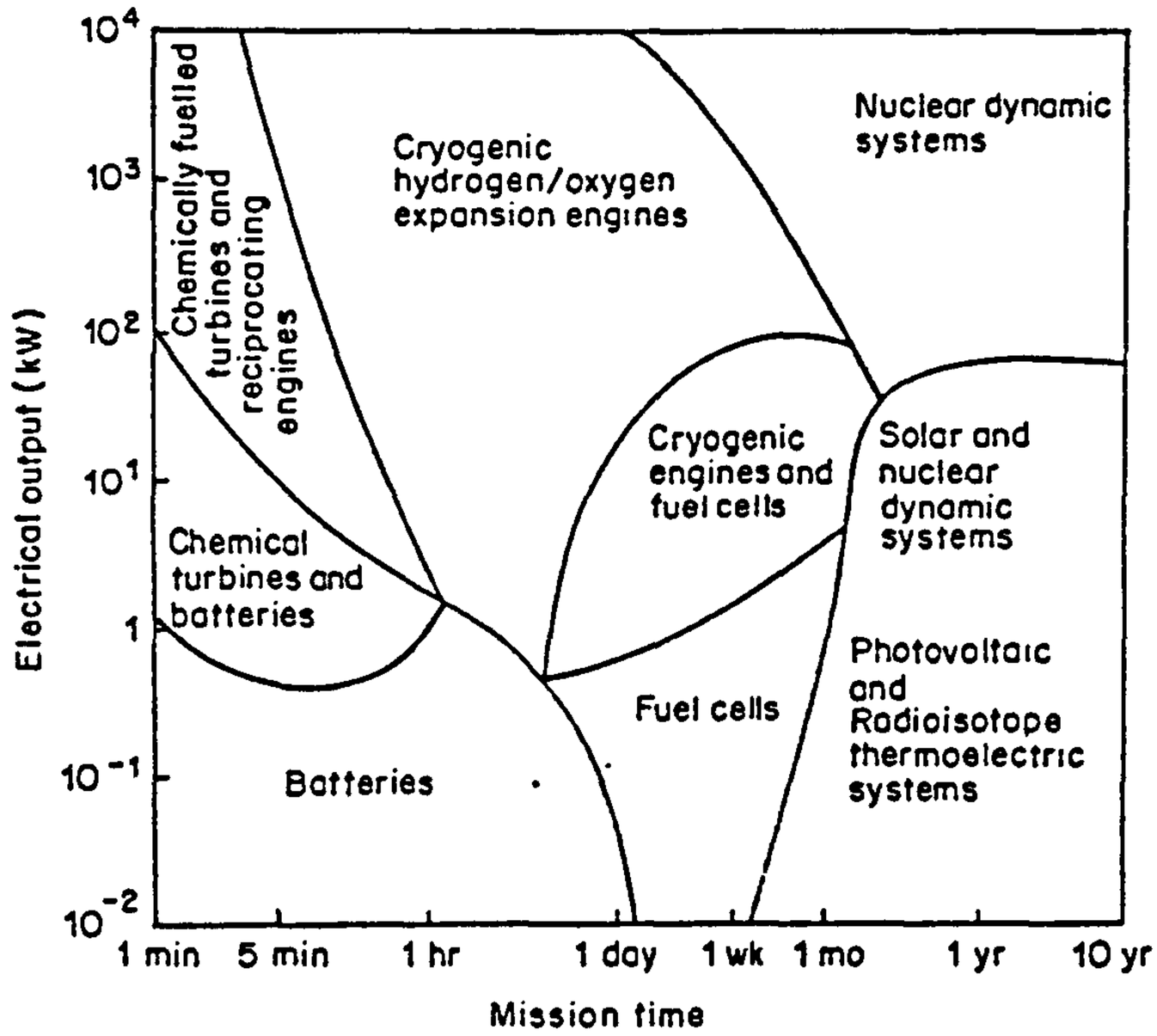

Figure 5.7 Power output - mission duration regimes for various power sources. (Angst, [60])

Solar photovoltaics use semiconductor cells to convert sunlight into electricity via the photoelectric effect. They can provide power over a useful range and have favourable inverse specific powers as their widespread use on satellites has stimulated development, although they are not particularly efficient. At high power levels, however, they become very expensive and the large area required can cause significant atmospheric drag problems if used at low altitudes.

Solar dynamic systems concentrate sunlight and use it to heat working fluid which then drives electrical generators. They have conversion efficiencies in excess of five times those of photovoltaics and significantly less surface area, so mitigating drag problems. However, the machinery associated with solar dynamic system means that they have an effective lower size limit so that they are not particularly attractive below power levels of approximately 100 kW.

Nuclear dynamic systems use a nuclear reactor to provide the heat for the working fluid. They offer very high power in a compact package for a long duration at a comparatively low cost. They do, however, require heavy shielding since electronics cannot withstand the radiation they emit and this tends to make them rather large.

Table 5.4 below summarises power range and inverse specific power for each of these four power sources.

Table 5.4 - Characteristics of Space Power Sources

Parameter	Radio-isotope	Solar Photovoltaic	Solar Thermal Dynamic	Nuclear Reactor
Power range (kW)	0.2 - 10	0.2 - 25	1 - 300	40 +
Inverse specific power ($kg.kW^{-1}$)	100 - 500	10 - 50	70 - 110	20 - 70

It can be seen that all but the radioisotope source are possible power sources. However nuclear power sources (both RTG and reactor) are used in near earth orbit only for military applications and are not as yet considered acceptable as energy sources for civilian spacecraft. This leaves only solar photovoltaic and solar dynamic power sources for consideration. Leaving aside the relative immaturity of solar dynamic power systems, the choice of power system then appears to be solar photovoltaics for applications up to around 100 kW and solar dynamic power above this. The majority of electrically propelled spacecraft contemplated to date have been powered by solar photovoltaics. These technologies will, therefore, be considered further in the next section.

5.5.1 Solar photovoltaic power

Solar photovoltaic cells are semiconductor devices that convert solar radiation into electricity. The most common form of cell is made from silicon doped with boron which then has phosphorus diffused into the top surface to make a semiconductor p/n junction across the cell. Irrespective of the material used the current generation mechanism is the same. Solar photons striking the cell liberate excess electrons from the top layer and their movement to the electron deficient lower layer results in a current flow. The required current and voltage can be then be obtained by combining cells in series and parallel.

5.5.1.1 Effect of temperature on cell performance

Figure 5.8 overleaf shows a typical current-voltage plot for a cell. A change in the operating temperature of the cell causes three changes in this curve; a scaling of the curve along the I axis, a translation of the curve along the V axis and a change in the shape of the curve in the area where it goes from horizontal to vertical. The operational effect of these changes is to decrease the efficiency of a cell as the temperature increases above its nominal operating temperature as the random motion of the electrons and holes starts to swamp the current generated by the solar radiation. The temperature coefficient depends on the type of semiconductor used, its output characteristics, operating temperature etc. For a silicon cell the temperature coefficient is $0.5\%.^{\circ}C^{-1}$ relative to an efficiency of approximately 18% at 28 °C.

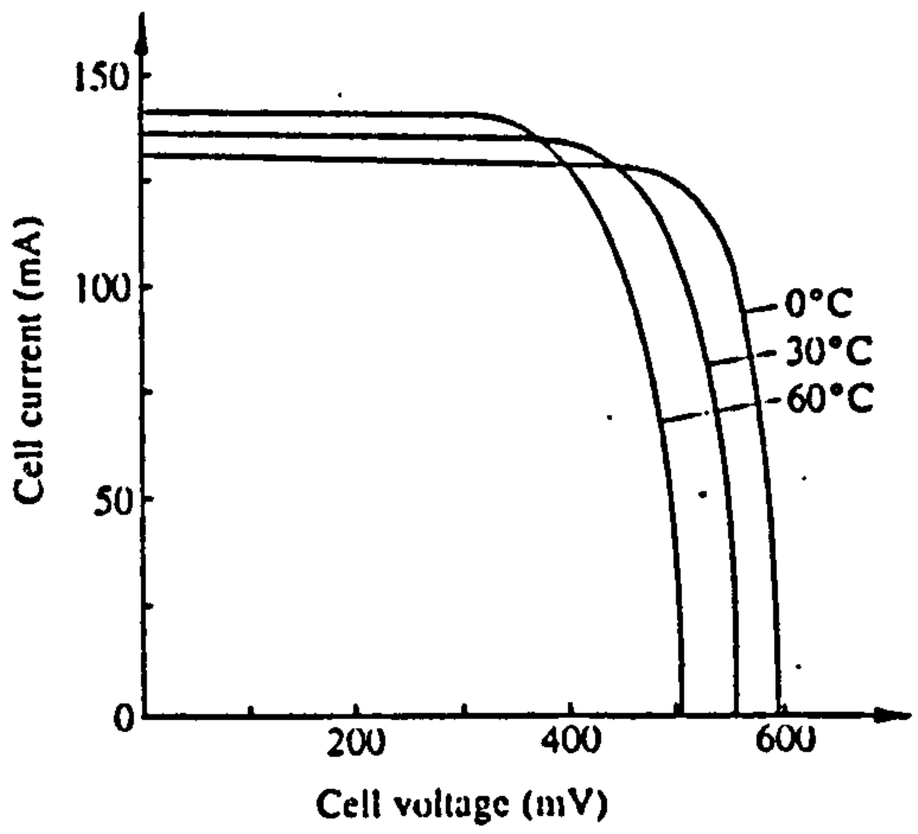

Figure 5.8 Current-Voltage curve of a solar cell (Berlin [61]).

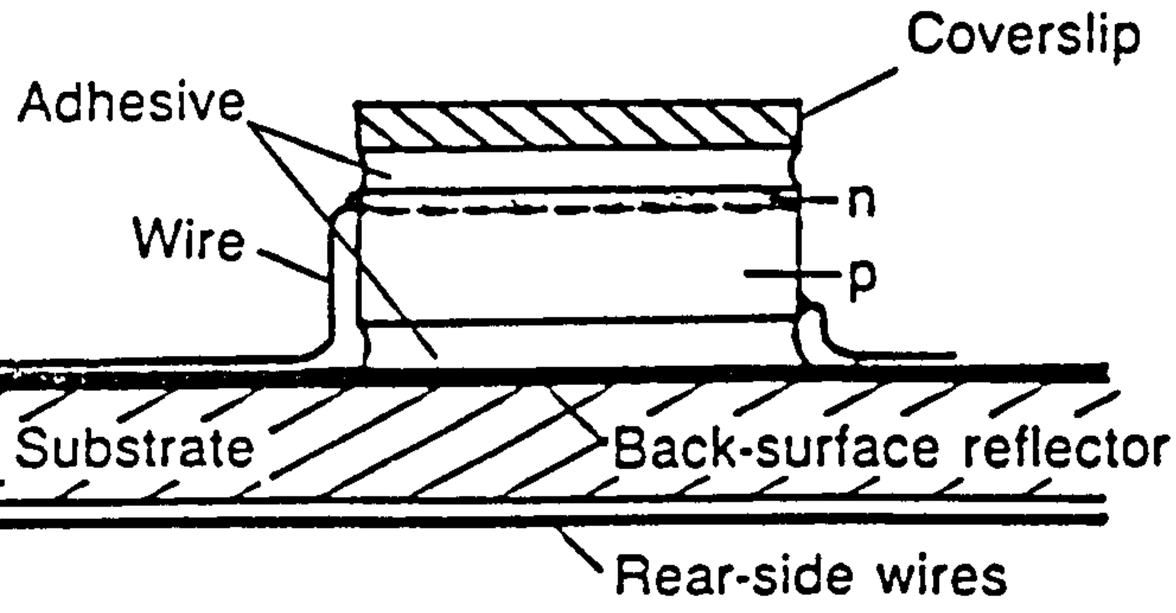

Figure 5.9 A semiconductor photovoltaic cell (Williamson [62])

Operating temperature, and its control, are key issues in solar cell and array design. This should aim to provide good emission characteristics in the infra-red while maximising absorption in the relevant portion of the solar spectrum and minimising it elsewhere. This is achieved by use of coverslips bonded on top of the cells, which filter out short wavelength ultra-violet and infra-red wavelengths and provide better thermal emission than the semiconductor (They also provide protection from radiation - see next section). Additionally, back-surface reflectors, which direct incident solar radiation back through the cell again, and optical coatings, which are reflective and non-reflective at the appropriate wavelengths, may also be used.

5.5.1.2 Effect of radiation damage on cell performance

Solar photovoltaic cells are susceptible to damage by energetic electrons and protons which damage the crystal lattice and cause a loss of performance, higher internal resistance and increased temperature dependence. This is of particular relevance to spacecraft which have orbits that intersect the Van Allen trapped radiation belts. The inner belt extends from approximately 1500 km to 5600 km in the equatorial plane containing predominantly protons with energies greater than 30 MeV and is densest within about 35° of the geomagnetic equator. The outer belt extends from 13000 to 19000 km, contains mostly electrons with energies in the range 50 keV - 5 MeV and low energy protons with energies less than 1 MeV, and spreading between 55°-70° north and south of the geomagnetic equator.

The wide range of energies possessed by particles in the space environment has necessitated some standard technique for describing their effects in terms of conditions that can be reproduced in the laboratory. The base marker for such work is the damage caused to cells by a 1 MeV fluence under test conditions. The damage caused by particles of other energies is then related to this by damage coefficients. This is illustrated overleaf in Figure 5.10 for a particular cell configuration. It can be seen that energetic protons have significantly more effect than electrons and that this effect is heavily dependent on the altitude of the orbit and less so on the inclination.

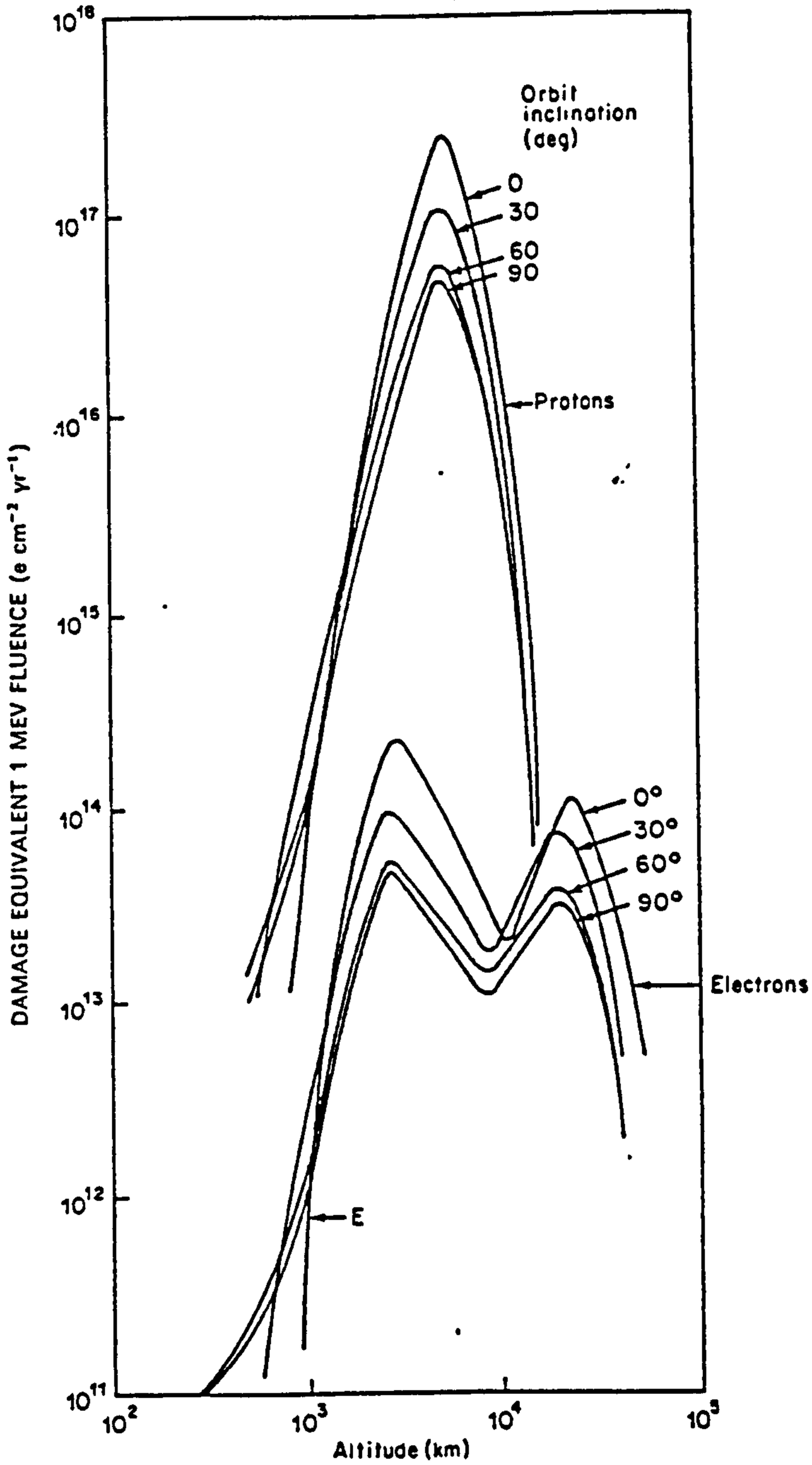

Figure 5.10 Damage equivalent 1 MeV fluence caused by electrons and protons due to trapped particles, to silicon cells protected by 150 μm fused silica covers and infinitely thick rear shielding (Rauschenback [63])

Although radiation damage can be minimised by cell and array design, there is a cumulative degradation in performance with time. This forces solar array sizing to be based on the power required at the end-of-life (EOL) of the mission with the result that the array is oversized for the power required at the beginning of life (BOL). For a typical silicon array this degradation is approximately 15% over five years in a low earth orbit.

5.5.1.3 Solar photovoltaic developments

Although only typical silicon photovoltaic cells have been mentioned so far, development of advanced cells and arrays is taking place with the aim of providing higher efficiencies, better radiation resistance and lower inverse specific powers. The best of present arrays in-orbit (again almost all silicon based) have inverse specific powers of between 15 to 30 $kg.kW^{-1}$ (Stark [64]), while values as low as 15 $kg.kW^{-1}$ have been demonstrated on experimental flights (NASA [65]).

Beyond this, NASA's Advanced Photovoltaic Solar Array (APSA) programme has as its aim the development of a high-performance solar array with an inverse specific power of 3 $kg.kW^{-1}$ at BOL power levels of 25 kW by the turn of the century. Construction of arrays expected to give an inverse specific power of 8 kg. kW^{-1} and an area-to-power ratio of 7.4 $m^2.kW^{-1}$ at 10 kW BOL has commenced using thin silicon cells (Kurland and Stella [66]). Although these represent considerable progress in some areas, no increase in resistance to radiation damage is reported.

For this reason research is also taking place into alternatives to silicon as the semiconductor, concentrating chiefly on the substances gallium arsenide (GaAs) and indium phosphide (InP) (Flood, [67]). The former provides the possibility of efficiencies in excess of 25% (compared to around 18% for silicon) or higher if used in conjunction with a concentrator system which collects sunlight over a large area and either reflects or refracts it onto the array proper. Such concentrator array may also be able to provide some degree of shielding against radiation damage. InP cells have efficiencies only fractionally lower than those GaAS cells, typically around 23%, but are at least a factor of ten more radiation

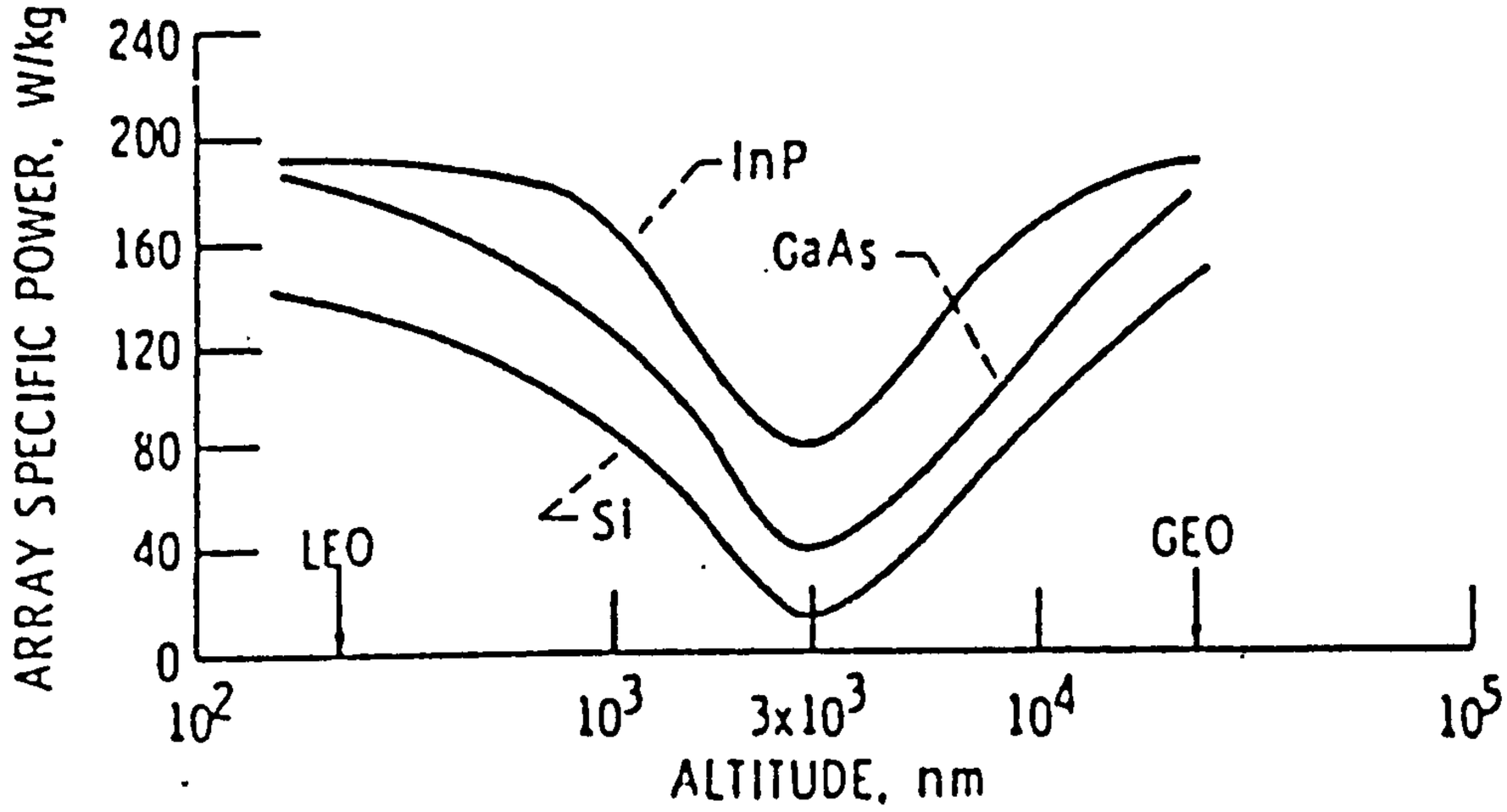

Figure 5.11 Comparison of solar array calculated output as a function of orbit altitude, based on 1 MeV electron equivalent fluences. Time in orbit = 7 years, circular orbit, 30° inclination, T = 60°C.
(Weinberg and Brinker, [68])

resistant. This means that although they have a slightly worse inverse specific power at BOL they are significantly better at EOL. This is demonstrated in Figure 5.11 on the previous page where they are compared to both GaAs and Si cells. The innate radiation resistance of InP may be able to be amplified by use of a concentrator array designed to keep the photovoltaic cells operating at temperatures just over 100 °C. Beyond this temperature complete thermal annealing of radiation damage has been observed. This presents the possibility of high efficiency, high inverse specific power and radiation immune solar arrays. Projected inverse specific powers and area-to-power ratios for such arrays are as good as 10 $kg.kW^{-1}$ and 3 $m^2.kW^{-1}$ and would prove very attractive for use on missions having either a high radiation environment or long duration.

Chapter 6 - Orbital manoeuvres using low-thrust propulsion

6.1 Introduction

This chapter describes the controlled alteration of a spacecraft's orbital elements using low-thrust propulsion. It starts with a general consideration of the problem based upon Lagrange's equations and then examines its reduction to address the quasi-circular orbits appropriate to satellite emplacement. Following this the chapter describes the optimisation of low-thrust manoeuvres and extends this to show that constant thrust angle techniques may be used to obtain near optimum wedge angle and radius alterations. The alteration of ascending node is then addressed in particular showing how the node may be altered by combined changes to inclination and altitude. This is illustrated by considering an optimum transfer between two Earth Observing System platforms.

6.2 The orbit mechanics of low-thrust spacecraft

Lagrange's planetary equations (equations 3-2 to 3-7) describe the motion of an orbiting body under the effect of perturbations to the orbit. They can be used to describe the motion of a low-thrust spacecraft by treating the thrust produced by the propulsion system as another perturbation and then examining the resulting secular changes in the orbital elements. A full coverage of this topic is given by Burt [69] and Edelbaum [70]. A less complex but useful summary is also supplied by Ennix et al. [71].

The effects of constant low level accelerations may be summarised as follows. A radial acceleration induces a rotation of the orbital plane and only affects the argument of perigee. A tangential acceleration changes the energy of the orbit and alters the eccentricity and semimajor axis. A normal acceleration has a short period effect on the inclination and right ascension of the ascending node, but no long term one.

To provide significant adjustment to the orbital elements it becomes necessary to modulate the direction of the accelerations, altering the sign at a particular point on the orbit so as to cause the small periodic variations to become additive. Burt summarises these manoeuvres as follows, using a tilde to signify secular changes;

A constant tangential acceleration causes a secular change in semimajor axis and eccentricity.

$$\frac{d\tilde{a}}{dt} = 2a\left(\frac{p}{\mu}\right)^{0.5} a_t' \qquad \text{Eq. 6.1}$$

$$\frac{d\tilde{e}}{dt} = -\frac{3}{2}\left(\frac{p}{\mu}\right)^{0.5} e\, a_t' 7762 \qquad \text{Eq. 6.2}$$

A constant tangential acceleration reversed at each crossing of the minor axis causes a secular change in eccentricity.

$$\frac{d\tilde{e}}{dt} = (sgn\ a_t)_{E=0}\ \frac{4}{\pi}\left(\frac{p}{\mu}\right)^{0.5} |a_t'| \qquad \text{Eq. 6.3}$$

A constant tangential acceleration reversed at each crossing of the major apside causes a secular change in the argument of perigee.

$$\frac{d\tilde{\omega}}{dt} = (sgn\ a_t)_{E=\frac{\pi}{2}}\ \frac{2}{\pi}\left(\frac{a}{\mu}\right)^{0.5}\ \frac{(2-e^2)}{e}\ |a_t'| \qquad \text{Eq. 6.4}$$

A constant normal acceleration reversed at each orbit apex causes a secular change in inclination.

$$\frac{d\tilde{i}}{dt} = (sgn\ a_n)_{\theta+\omega=0}\ \frac{1}{\pi}\left(\frac{a}{\mu}\right)^{0.5}\ \phi\ |a_n'| \qquad \text{Eq. 6.5}$$

A constant normal acceleration reversed at each orbit node causes a secular change in argument

of perigee and right ascension of the ascending node.

$$\frac{d\tilde{\omega}}{dt} = -(sgn\ a_n')_{\theta+\omega=\frac{\pi}{2}}\ \frac{1}{\pi}\left(\frac{a}{\mu}\right)^{0.5}\ \phi\ \cot i\ |a_n'| \qquad \text{Eq. 6.6}$$

$$\frac{d\tilde{\Omega}}{dt} = (sgn\ a_n')_{\theta+\omega=\frac{\pi}{2}}\ \frac{1}{\pi}\left(\frac{a}{\mu}\right)^{0.5}\ \frac{\phi}{\sin i}\ |a_n'| \qquad \text{Eq. 6.7}$$

where

$$\phi = \frac{2 - e\,2(5\sin^2\omega - 1) + e^4\sin^2\omega\,(3\sin^2\omega - 1)}{(1 - e^2\sin^2\omega)^2} - \frac{3e\cos\omega}{2\,(1 - e^2)^{0.5}}\ \tan^{-1}\left(\frac{2e\,(1 - e^2)^{0.5}\cos\omega}{e^2\,(1 + \cos^2\omega) - 1}\right) \qquad \text{Eq. 6.8}$$

In each case the secular change in the other orbital elements is zero. Evidently, then, to alter several elements at one time will require a combination of normal and tangential thrust together with a time-varying programme to control them.

6.3 Quasi-circular low thrust transfers

To date the main area of interest in low-thrust dynamics has been that of orbit raising, most commonly from low earth to high earth orbits usually with an inclination change included. By far the most common sort of mission studied is that of geostationary satellite emplacement (See Holdaway [72], Sarnecki [73], Edelbaum and Sackett [74]). Some other types of orbit-raising mission have also been studied and the work of Sponable and Penn [75] on the placement of global positioning system (GPS) satellites is summarised below as being a typical application.

Sponable and Penn have attempted to assess the viability and cost of using electric propulsion to transfer future GPS satellites from shuttle orbits into their operational orbits ($r = 26000$ km, $i = 55°$). They have investigated the use of a modular electric orbital transfer vehicle (EOTV) propelled by either ammonia arcjet or xenon ion thrusters. They anticipate returning the propulsion module of the EOTV to Earth between flights while leaving the main structure and power bus in orbit. In addition they also investigate the use of an ion EOTV launched by an expendable launch vehicle (ELV).

Taking deployment time as a requirement defined by the user they have established that there is an exponential dependence of both mission cost and solar array power on this factor. This is shown overleaf in Figure 6.1a. The near congruence of the curves emphasises the importance of power supply inverse specific powers in controlling mission capability. They also identify the thruster as the other key technology. Figure 6.1b illustrates the existence of a broad, relatively insensitive 'optimum' specific impulse that minimises mission cost.

Figure 6.2 (overleaf) shows the savings (compared to the same mission performed with a PAM-DII class system) that they predict. The same figures for geosynchronous emplacement are also included.

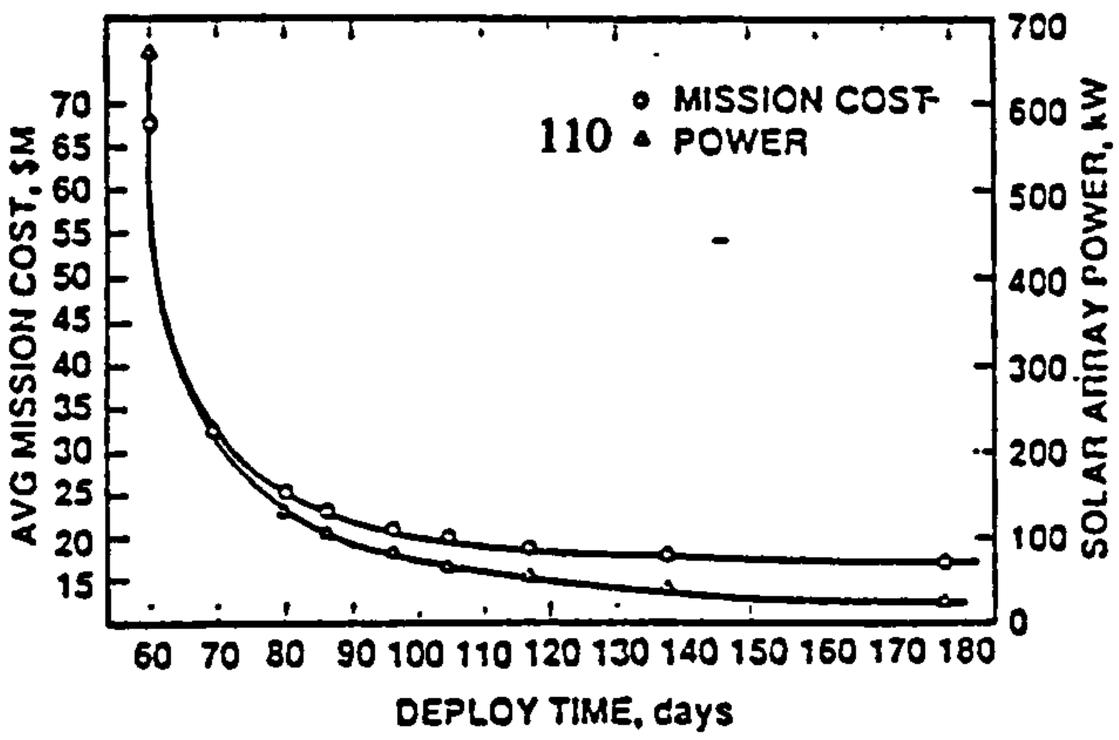

Figure 6.1
a) Average mission cost and BOL power requirement vs. deployment time.
b) Average mission cost and deployment time vs. specific impulse.

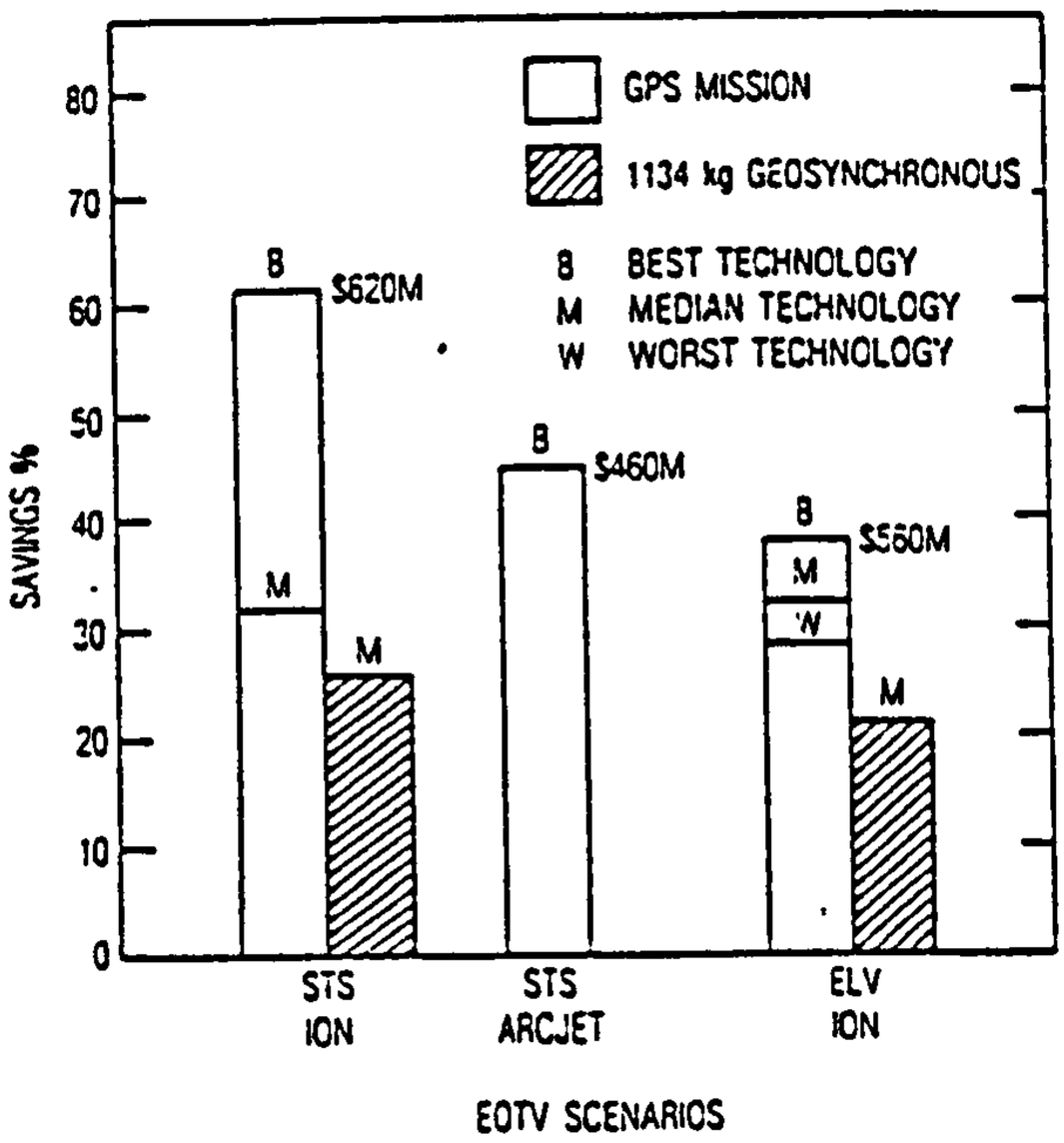

Figure 6.2 Electric orbit transfer vehicle savings comparison

The analysis of such missions, in which both both initial and final orbits are circular, is significantly simpler than that for general elliptical orbits since the radius/semimajor axis changes so slowly that the spacecraft can be considered to be in a quasi-circular orbit at all times. Under these conditions equation 6.8 becomes

$$\phi = 2 \qquad \text{Eq. 6.9}$$

and equations 6.1 to 6.7 are replaced by 6.10 to 6.14, given below.

$$\frac{d\tilde{r}}{dt} = 2\left(\frac{r^3}{\mu}\right)^{0.5} a_t' \qquad \text{Eq. 6.10}$$

$$\frac{d\tilde{e}}{dt} = 0 \qquad \text{Eq. 6.11}$$

$$\frac{d\tilde{\omega}}{dt} = \textit{undefined} \qquad \text{Eq. 6.12}$$

$$\frac{d\tilde{i}}{dt} = (sgn\ a_n')_{\theta+\omega=0}\ \frac{2}{\pi}\left(\frac{r}{\mu}\right)^{0.5} |\, a_n' \,| \qquad \text{Eq. 6.13}$$

$$\frac{d\tilde{\Omega}}{dt} = (sgn\ a_n')_{\theta+\omega=\frac{\pi}{2}}\ \frac{2}{\pi}\left(\frac{r}{\mu}\right)^{0.5} \frac{1}{\sin i} |\, a_n' \,| \qquad \text{Eq. 6.14}$$

Even though the dynamics are now much simpler, it is not possible, generally, to alter the inclination without also altering the right ascension of the ascending node and vice versa. As before, though, by modulating the thrust for the manoeuvres defined by equations 6.13 and 6.14 (and represented diagrammatically in Figure 6.3, overleaf) the change in one of the elements can be made periodic and the other secular, giving a net change in the latter over multiple orbits.

For changes in the orbit elements now of interest (i.e. radius, inclination and ascending node) the Δv's for the manoeuvres defined by equations 6.10, 6.13 and 6.14) are given by

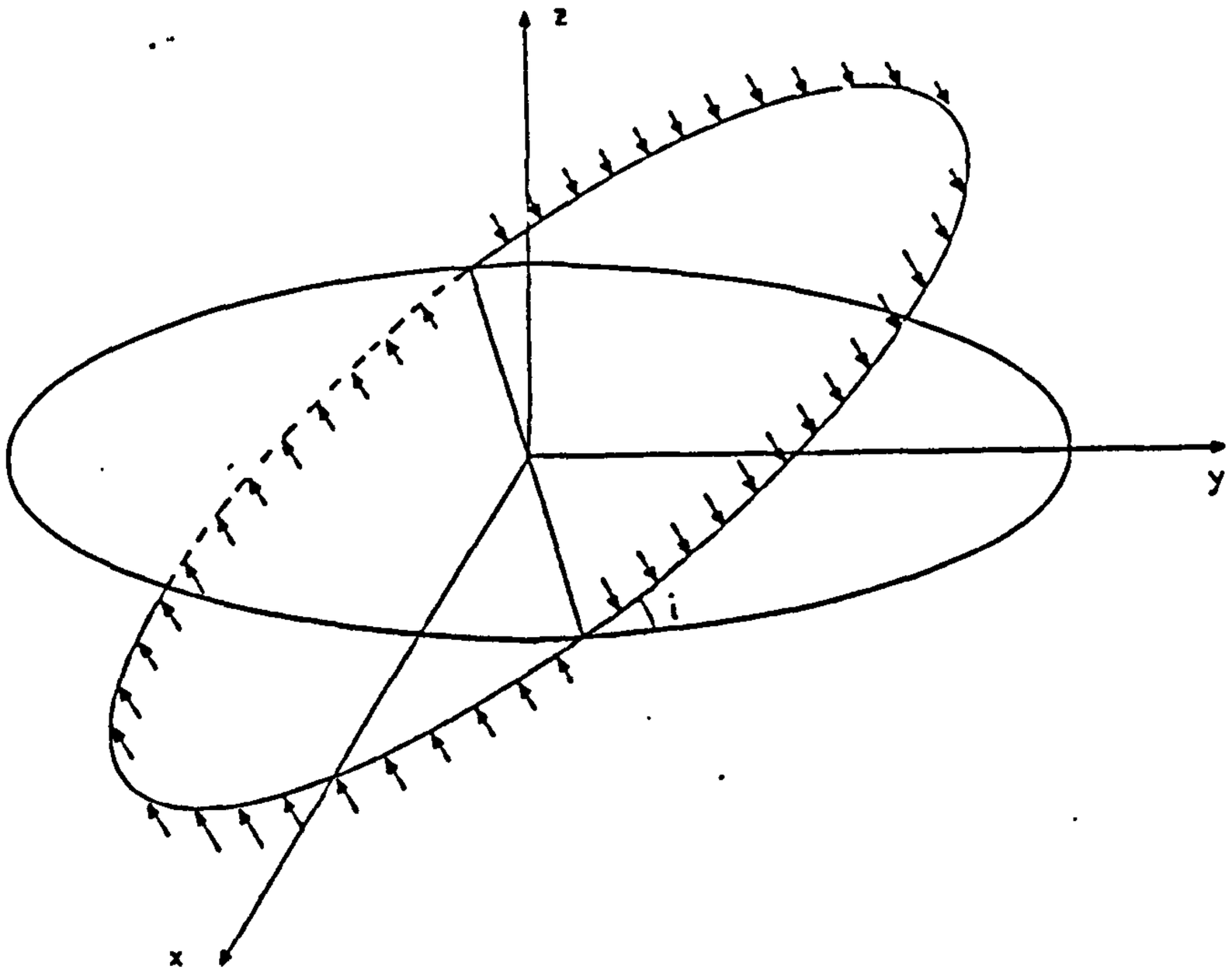

Figure 6.3a Thrust modulation for obtaining secular changes in inclination.

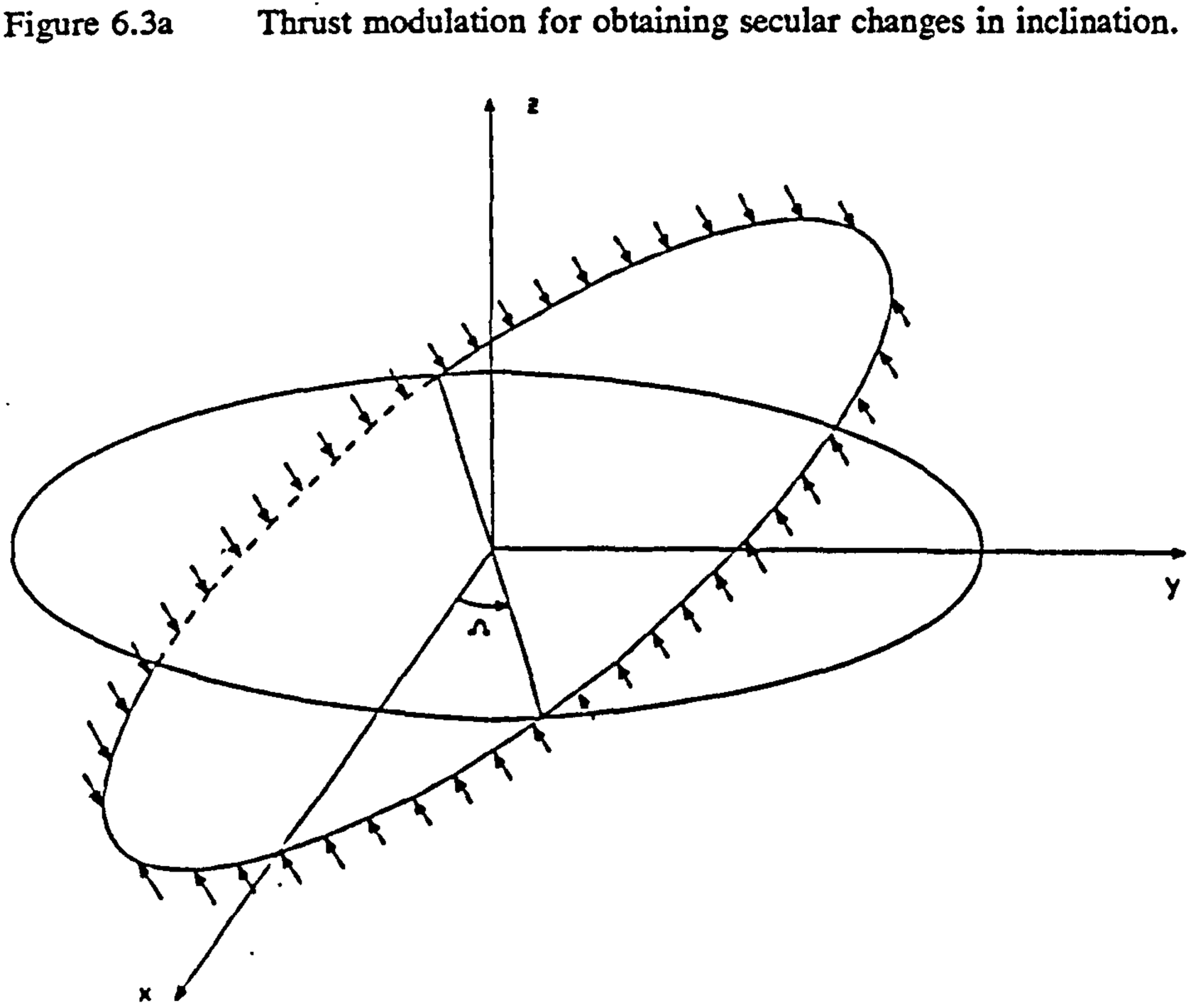

Figure 6.3b Thrust modulation for obtaining secular changes in node.

$$\Delta v(r_1,r_2) = \left(\frac{\mu}{r_1}\right)^{0.5} - \left(\frac{\mu}{r_2}\right)^{0.5} \qquad \text{Eq. 6.15}$$

$$\Delta v(i_1,i_2) = \frac{\pi}{2} v\,(i_2 - i_1) \qquad \text{Eq. 6.16}$$

$$\Delta v(\Omega_1,\Omega_2) = \frac{\pi}{2} v \sin i\,(\Omega_1 - \Omega_2) \qquad \text{Eq. 6.17}$$

where v is the circular orbital velocity.

From equation 6.17 we can now calculate the Δv necessary to perform direct low-thrust alterations of right ascension of the ascending node. For a single servicing cycle (i.e alteration of the ascending node by 360°) at EOS altitude, this is approximately 73 $km.s^{-1}$. This is a very high figure, even for electrically-propelled vehicles and, taken at face value, would appear to limit their applications. This is discussed further in section 6.5.

6.4 Optimisation of low thrust manoeuvres

It is apparent that the Δv of a low thrust transfer is governed by the manoeuvre selected to perform the transfer, which is controlled by the thrust angle control programme selected. It follows that the selection of optimal control programmes is of great importance to low-thrust missions, particularly those where two or more orbital elements are to be altered simultaneously.

Edelbaum [70] conducted much of the early work in this field, concentrating chiefly on defining optimal manoeuvres for altering semimajor axis, eccentricity and inclination at the same time (a typical LEO-GEO transfer). He showed that for small changes in the orbital elements the optimum steering angles were given by

$$\tan \alpha'_{opt} = \frac{\lambda_1 \sin\theta}{2(1 + \lambda_1 \cos\theta)} \qquad \text{Eq. 6.18}$$

$$\tan \beta'_{opt} = \frac{\lambda_2 \cos(\omega + \theta)}{\sqrt{(4 + \lambda_1 \cos\theta)^2 + \lambda_2 \sin\theta}} \qquad \text{Eq. 6.19}$$

where α' is the angle between the velocity vector and the in-plane thrust component and β' is the angle between the thrust vector and the orbit plane. (For quasi-circular orbits these are equivalent to the thrust angles ψ_1 and ψ_2 defined in Chapter 3). λ_1 and λ_2 are Lagrangian multipliers that make the partial derivatives of the first derivatives of the elements equal to zero.

For in-plane manoeuvres the thrust line always lies in the orbit plane so that λ_2 and β both become zero. For a planar change in orbit radius only, the thrust vector should always be tangential to the orbit so that

$$\tan \alpha'_{opt} = 0 \qquad \text{Eq. 6.20}$$

$$\tan \beta'_{opt} = 0 \qquad \text{Eq. 6.21}$$

Non-planar changes can also be considered. For manoeuvres where the eccentricity is to remain fixed, equations 6.18 and 6.19 become

$$\tan \alpha'_{opt} = 0 \qquad \text{Eq. 6.22}$$

$$\tan \beta'_{opt} = \frac{\lambda_2}{2} \cos(\omega + \theta) \qquad \text{Eq. 6.23}$$

Edelbaum reformulates these latter two equations using the auxiliary parameters k and k′ so that

$$\tan \beta'_{opt} = k' \cos \theta \qquad \text{Eq. 6.24}$$

$$k = \frac{k'}{\sqrt{1 - k'}} \qquad \text{Eq. 6.25}$$

For a change only in inclination k is set to one, for a change only in radius/semimajor axis k is set to zero. Using this formulation Edelbaum has calculated the Δv requirements for a number of optimum transfers. Figure 6.4 (overleaf) shows the results for combined inclination/semimajor axis change manoeuvres. Also plotted is the effect of selecting a constant value of β to effect a change in inclination. It can be seen that the difference between the optimised case and the non-optimised case is very small. This has important implications for the steering programmess of low-thrust spacecraft; a fully optimised transfer requires analysis in terms of elliptic integrals, while the constant angle approach, which provides results almost as good, requires analysis simply in terms of trigonometry. It may seen, therefore, that in terms of general mission analysis the latter approach is significantly more useful, with the full optimisation only being appropriate for detailed mission design.

The optimisation of combined semimajor axis and right ascension of the ascending node manoeuvres can be extended from the previous results very simply, since the basic difference between inclination change and node change manoeuvres is the location of the normal thrust component reversal

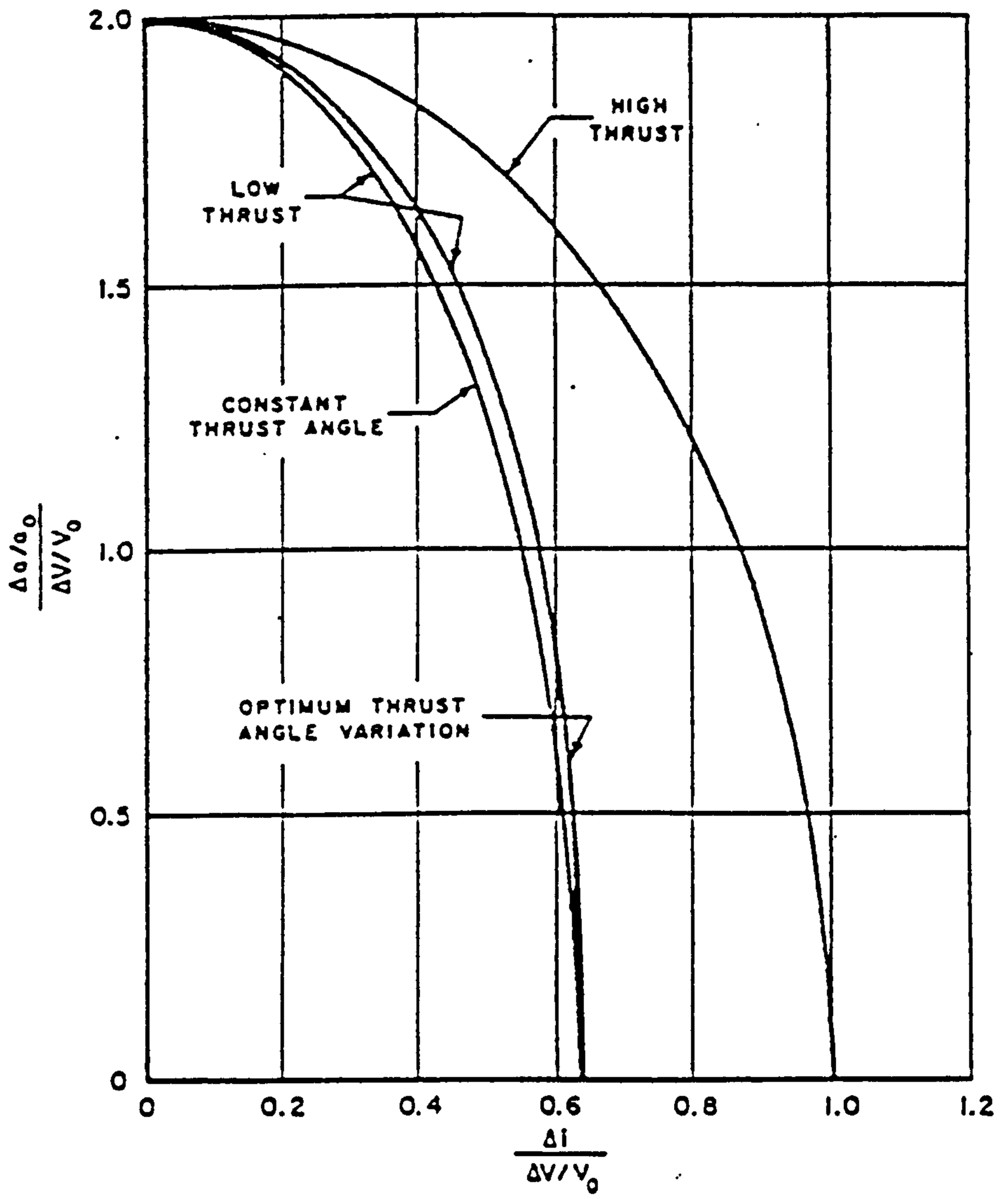

Figure 6.4 Characteristic velocity requirements for changes in semimajor axis and inclination.

points. For this manoeuvre, then, the optimum thrust angles are given by

$$\tan \alpha'_{opt} = 0 \qquad \text{Eq. 6.26}$$

$$\tan \beta'_{opt} = \frac{\lambda_2}{2} \cos(\omega + \theta + \frac{\pi}{2}) \qquad \text{Eq. 6.27}$$

Furthermore, the relation between the effectiveness of an optimally controlled transfer and one using a fixed thrust angle will also hold true. We can, therefore, alter radius together with either inclination or ascending node in a near-optimal manner using very simple controls.

Since we have already seen that both inclination and ascending node are effected by accelerations normal to the orbit plane, it should be possible to establish a manoeuvre that will allow the simultaneous alteration of i and Ω. This has been done using an approach similar to that developed by O'Connor and Korsemeyer [76] and outlined below.

For two orbit planes with ascending nodes and inclinations Ω_1, i_1 and Ω_2, i_2 respectively the planes will intersect with the wedge angle, β, already defined by equation 2.5 (see Figure 6.5 overleaf). A transfer from one orbital plane to the other involves making the wedge angle become zero. This manoeuvre can be analyzed more easily by defining a new geocentric reference plane based on the target orbit plane. The x-axis of this plane lies along the intersection of the two orbits and the z-axis in the direction of the angular momentum vector of the target plane. In this system, shown in Figure 6.6 overleaf, the wedge angle is now equivalent to the inclination in the normal geocentric system. This means that it may be adjusted by a normal acceleration reversed at each apex of the spacecraft orbit. This point can be found with reference to the angle u_s measured around the initial orbit in the normal co-ordinate system, where

$$\sin u_\beta = \frac{\sin i_2 \sin(\Omega_2 - \Omega_1)}{\sin \beta} \qquad \text{Eq. 6.28}$$

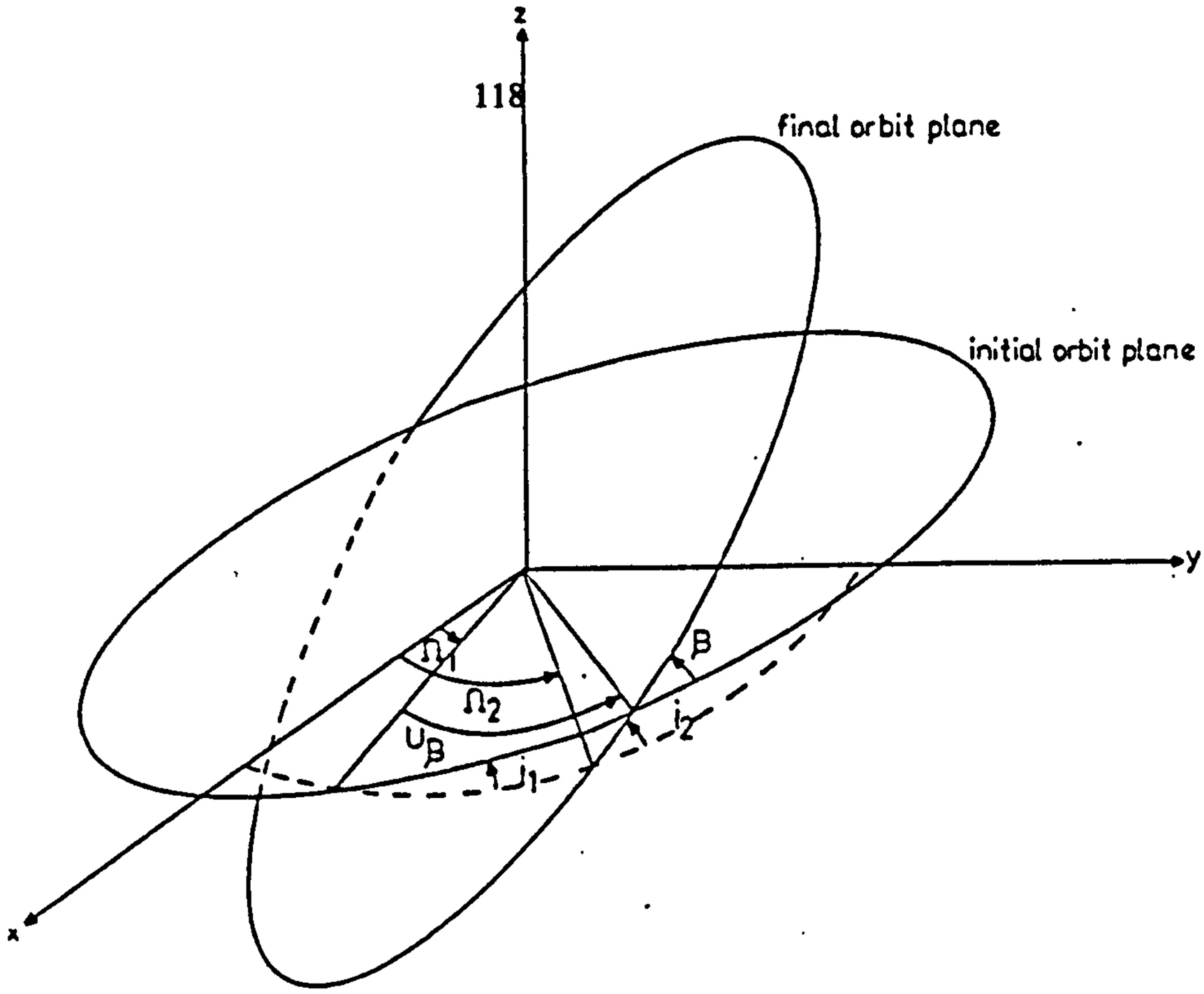

Figure 6.5 Wedge angle for intersecting orbit planes of different inclinations and nodes.

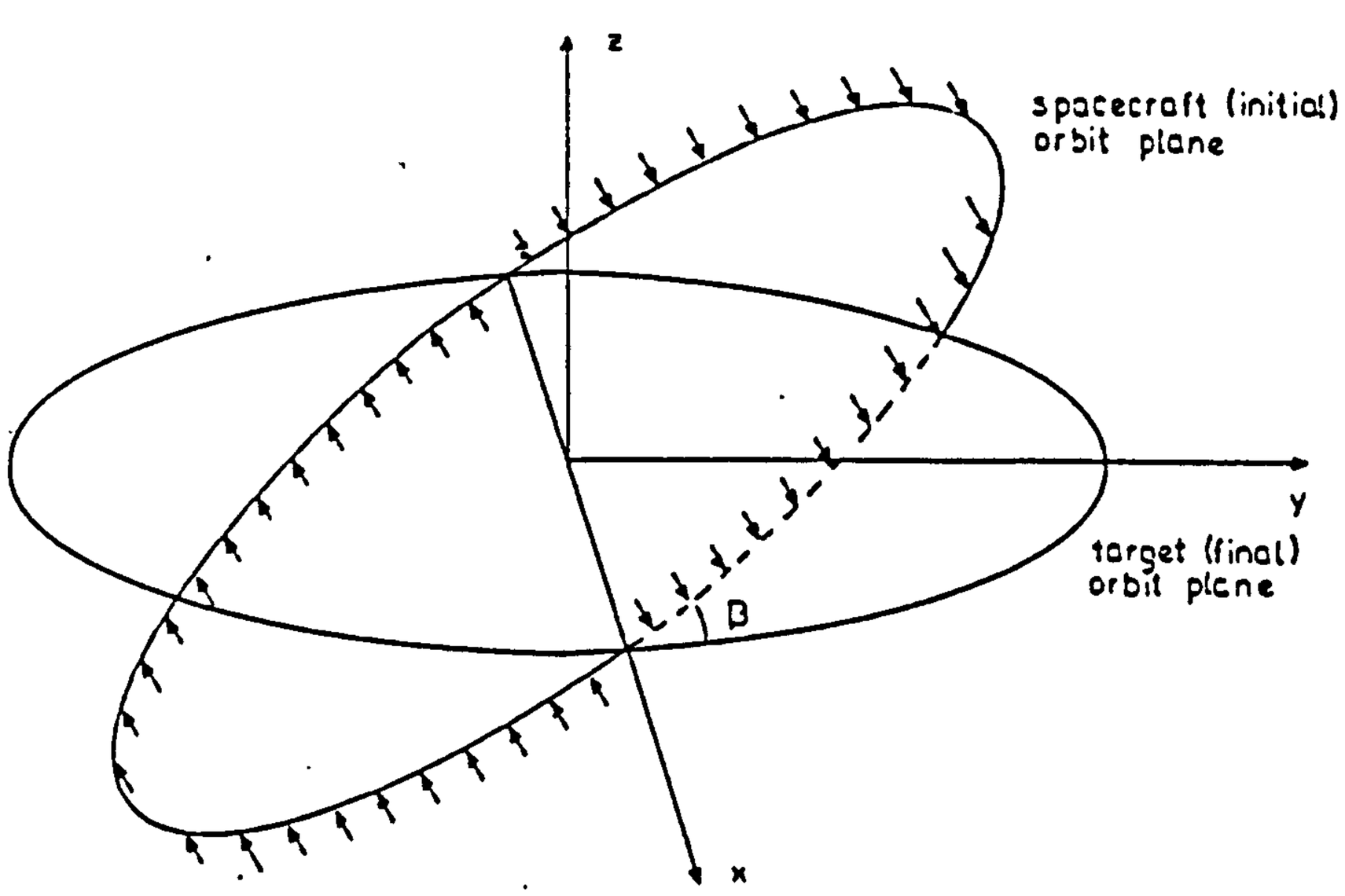

Figure 6.6 Wedge angle in geocentric reference plane based on target orbit.

$$\cos u_\beta = \frac{-\cos i_2 + \cos i_1 \cos \beta}{\sin i_1 \sin \beta} \qquad \text{Eq. 6.29}$$

The secular change of wedge angle can then be found to be

$$\frac{d\tilde{\beta}}{dt} = (sgn\ a_n')_{\theta + \omega = u_\beta} \frac{1}{\pi} \left(\frac{a}{\mu}\right)^{0.5} \phi\ |a_n'| \qquad \text{Eq. 6.30}$$

or for quasi-circular orbits

$$\frac{d\tilde{\beta}}{dt} = (sgn\ a_n')_{\theta + \omega = u_\beta} \frac{2}{\pi} \left(\frac{r}{\mu}\right)^{0.5} |a_n'| \qquad \text{Eq. 6.31}$$

and the Δv needed to reduce the wedge angle to zero is given by

$$\Delta v(\beta) = \frac{\pi}{2} v_c \beta \qquad \text{Eq. 6.32}$$

The equivalence between wedge angle and inclination indicates that Edelbaum's results may be applied to alteration of wedge angle and radius at the same time. O'Connor and Korsemeyer have used their approach to perform simultaneous alterations of radius/semimajor axis, inclination and ascending node and have achieved near-optimal results.

It is apparent, therefore, that for quasi-circular orbits the complex process of optimising thrust direction control to achieve the best results can be replaced with considerably simpler thrust programmes involving only trigonometric calculations to be performed with only a fractional decrease in performance.

6.5 Nodal transfers using low thrust propulsion

The previous section dealt with optimising the changing of r, i, and Ω in general and concluded that fixed thrust angles could be used to give near optimum results. The servicing of polar platforms using a low-thrust, differential nodal drift-assisted vehicle requires a particular application of these results.

The underlying mission constraint is to perform the servicing using the minimum propellant mass. This aim is modified by the necessary servicing schedule of the platforms. In manoeuvre terms what is being sought is the optimum orbital transfer, constrained by the final values of Ω and t. This alteration can be achieved by directly changing Ω, by altering either or both of the orbital radius and inclination to cause differential nodal drift, or a combination of both techniques.

To discuss the fundamentals of nodal alteration transfers we shall use the upcoming Earth Observation System (EOS) as a baseline platform configuration (Scolese, [77]). This has four satellites in three orbits, each with inclination of 98.7° and altitude 824 km. The orbits have ascending nodes of 150°, 202.5°, and 322.5° respectively. Although EOS is not designed to be replenished it is representative of a possible future system and has been used for this purpose in other studies (Graves et al. [36]). Since the EOS is not replenishable, no total system service period has yet been defined. Here, after Graves, one of three years has been assumed. If a constant nodal alteration rate is also assumed then a mean nodal rate of 0.329 degrees per day is needed to perform this. Taking the first nodal transfer, this move then requires a change of 52.5° to be effected over 160 days.

As mentioned earlier, this transfer can be performed by direct alteration of the ascending node. In general, however, such transfers are not particularly attractive. The Δv required to perform this manoeuvre by low thrust can be shown to be 10.6 $km.s^{-1}$. Although not beyond the capability of electric propulsion, it is sufficiently high to make this form of transfer unappealing if other, more efficient, techniques exist.

A more useful approach, mentioned in Chapter 2, is to alter either or both the orbital inclination and radius so altering the nodal drift rate and causing a differential nodal drift to occur between the initial and final orbit. Using this technique, a whole nodal transfer requires a manoeuvre out to some orbit (the drift orbit), a period in this orbit (the drift time) over which the differential nodal drift changes the node of the orbit, and then a manoeuvre back, to restore the original value of radius and inclination with the target value of the node for the end of the transfer period. This process is shown schematically in Figure 6.7 overleaf where the differential nodal drift rate is shown against time. The total alteration in node is given by the area under the graph.

Given that fixed thrust angles are being used it is possible to plot contours of constant manoeuvre velocities for combined altitude and inclination changes. This is done in Figure 6.8 overleaf for the Δv range 0 to 400 $m.s^{-1}$ for an EOS orbit. Each point on a particular contour is obtained by using a different thrust angle. The contour plot is not symmetrical about the zero altitude change line. This is because change in altitude is not linearly related to change in orbital velocity.

Combined changes in orbit radius and inclination are achieved by using an appropriate value of ψ_2 (modulated as necessary) to give the required tangential and normal acceleration components. Orbit radius increases for $90^\circ < \psi_2 < 270^\circ$ and decreases for $90^\circ > \psi_2 > 270^\circ$, while inclination increases for $0^\circ < \psi_2 < 180^\circ$ and decreases for $360^\circ > \psi_2 > 180^\circ$.

For independent alterations of radius and inclination, the evolution of the parameters with repsect to time can be found from equations 6.10 and 6.13. The first result (i.e that for radius) is also valid for combined radius and inclination manoeuvres and, noting that the accleration components are described by, $a_t = a \cos \psi_2$ and $a_n = a \sin \psi_2$, is given by

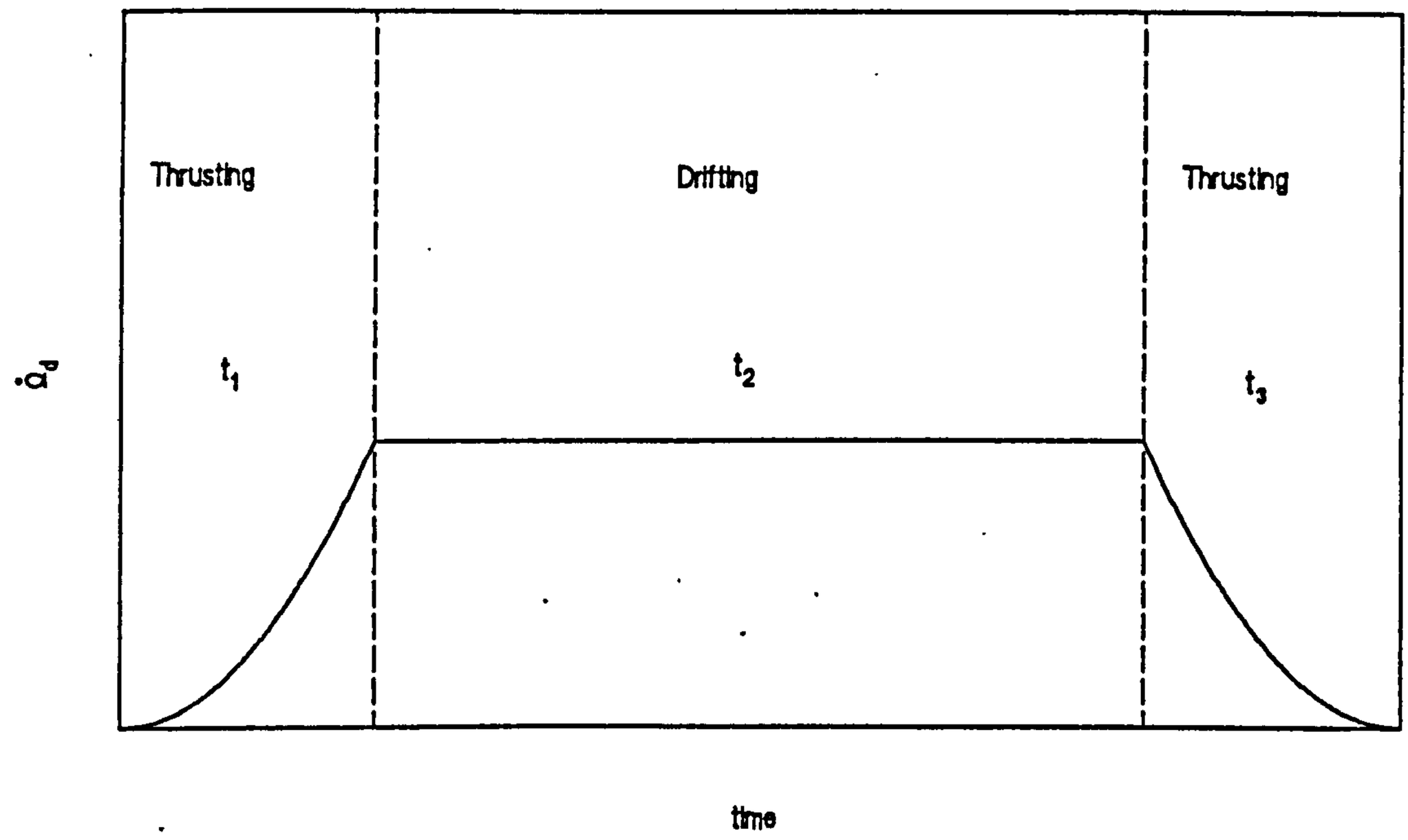

Figure 6.7 Change of node by enhanced nodal drift manoeuvre showing outward manoeuvre, drift and return manoeuvre periods.

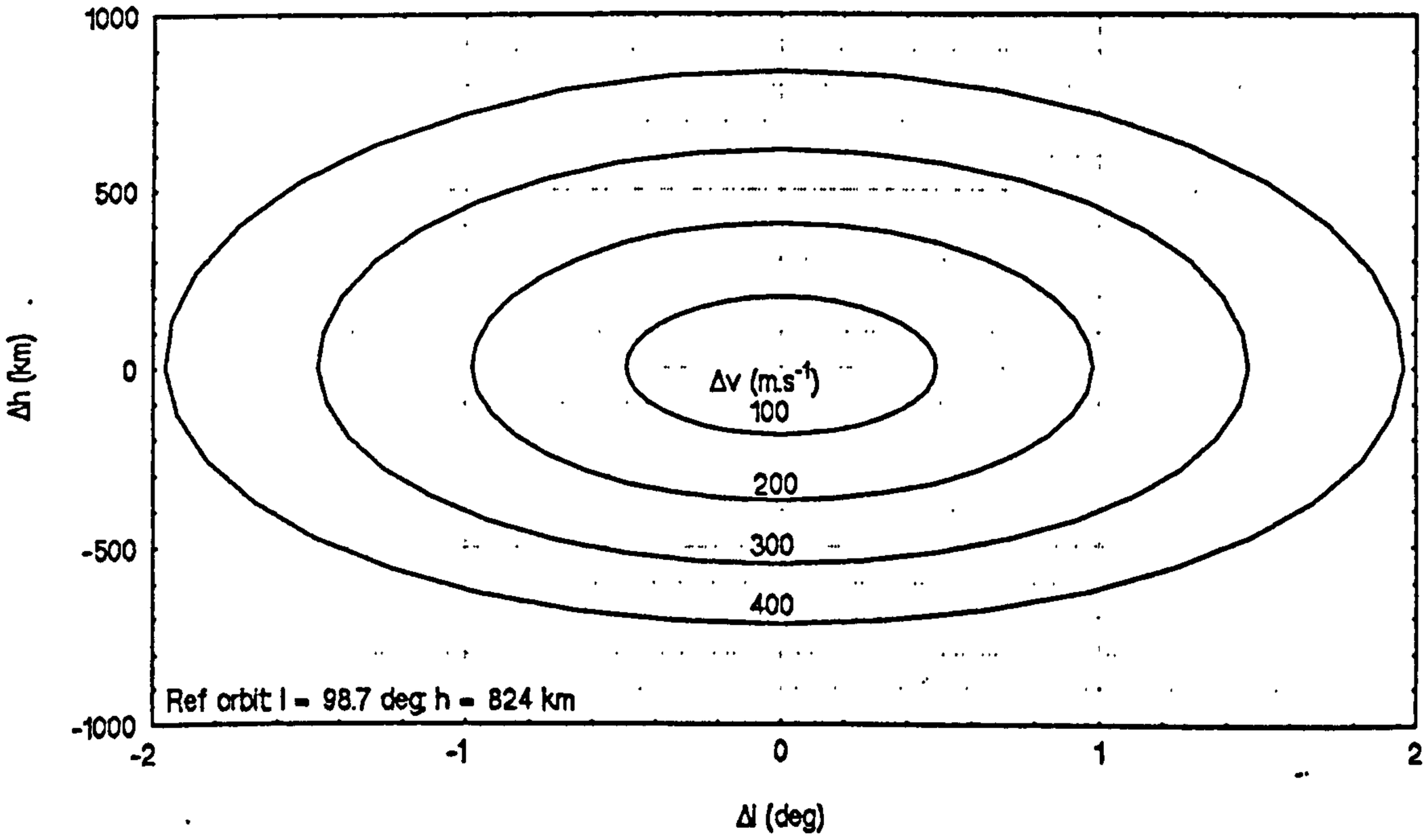

Figure 6.8 Contours of constant manoeuvre velocities for combined altitude and inclination changes.

$$r(t) = \frac{r_0}{\left(1 + \frac{t\,a' \cos\psi_2}{v_0}\right)^2} \qquad \text{Eq. 6.33}$$

A different equation must be derived for for the evolution of inclination, however. This is obtained by substituting equation 6.33 into 6.13 and proceeding as before. This gives

$$i(t) = i_0 + \frac{2}{\pi}\tan\psi_2 + \ln\left(1 + \frac{t\,a' \cos\psi_2}{v_0}\right) \qquad \text{Eq. 6.34}$$

(where a is the acceleration and inclination is in radians). The tan term in Equation 6.34 leads to unstable behaviour when ψ_2 is close to 90° or 270°. For computational purposes it is advantageous to replace the natural log term with its equivalent Maclaurin's series since this enables a cancellation of cos ψ_2 to be performed, allowing the tan to be supplanted by a sin. This gives i(t) as

$$i(t) = i_0 + \frac{2\,t\,a' \sin\psi_2}{\pi\, v_o}\left(1 - \frac{\beta}{2} + \frac{\beta^2}{3} - \frac{\beta^3}{4} + \frac{\beta^4}{5} \ldots.\right) \qquad \text{Eq. 6.35}$$

where

$$\beta = \frac{t\,a' \cos\psi_2}{v_0} \qquad \text{Eq. 6.36}$$

When $\psi_2 = 90°$ the series becomes equal to one and Equation 6.35 can be transformed into Equation 6.16 which gives the Δv necessary to perform an inclination change at constant radius.

Now, the differential nodal drift rate between a reference orbit, A, and another orbit, B, is given by the difference between their drift rates so that

$$\dot{\Omega}_d = \dot{\Omega}_B - \dot{\Omega}_A \qquad \text{Eq. 6.37}$$

We already have an expression for the drift rate of an orbit (see Equations 2.2, 2.3) so that the differential drift rate is given by

$$\dot{\Omega}_d = A\left(\frac{\cos i_B}{r_B^{3.5}} - \frac{\cos i_A}{r_A^{3.5}}\right) \qquad \text{Eq. 6.38}$$

where A = 1.31895 x 10^{18} for an answer in radians per second and A = 6.5293 x 10^{24} for an answer in degrees per day.

By substituting Equations 6.33 and 6.34 or 6.35 into 6.38 we can obtain the differential nodal drift rate relative to the reference orbit as a function of vehicle time, vehicle acceleration level and out-of-plane thrust angle. It is then possible to choose a particular value of ψ_2 which maximises this differential drift for a particular manoeuvre Δv, i.e the product of the acceleration and time (though the equations resulting from differentiation of the expression for $\dot{\Omega}_d(\psi_2)$ are intractable analytically, so this process is best performed numerically). As may be deduced from the form of Equation 6.38, the value of $\psi_{2,opt}$ is very sensitive to the inclination of the reference orbit and highly insensitive to the orbit altitude. This demonstrated overleaf in Figures 6.9 and 6.10. The first shows the variation in $\psi_{2,opt}$ with i for an 824 km (i.e typical EOS altitude) orbit. The second shows the variation in Ω_d with ψ_2 for orbits of three different altitudes, but common inclination of 98.7° (i.e. typical EOS inclination). It can be seen from the latter that Ω_d is maximised by a value for ψ of approximately 32°. $\psi_{2,opt}$ is also unaffected by the manoeuvre Δv, as shown in Figure 6.11, two pages on.

Ideally, we wish to optimise the total change in node for a given Δv. To do this it is convenient to define a new parameter, the mean differential nodal drift rate $\dot{\Omega}_{md}$, the mean change in node over the duration of the manoeuvre. Using this parameter, contours of constant manoeuvre velocities against changes in altitude and changes in inclination can be plotted. These are given, again for the EOS orbit, in Figures 6.12 and 6.13 two and three pages on, respectively. The increase in $\dot{\Omega}_{md}$ with decrease in altitude and increase in inclination is apparent and the locus of the optima for $\dot{\Omega}_{md}$ manoeuvres can be clearly seen on each of these. On Figure 6.13 lines of change in altitude have also been plotted.

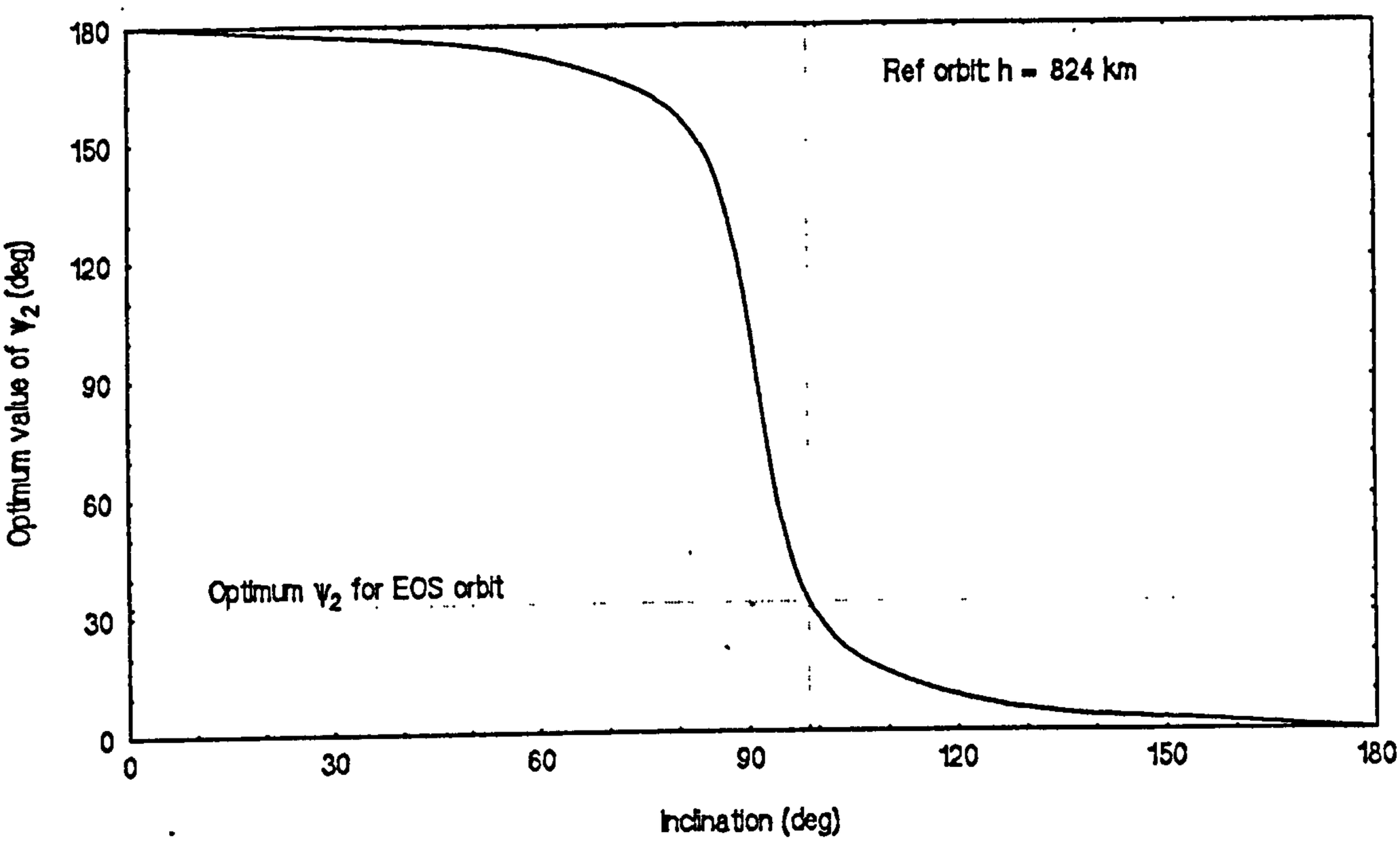

Figure 6.9 Variation in $\psi_{2,opt}$ with orbital inclination for EOS altitude.

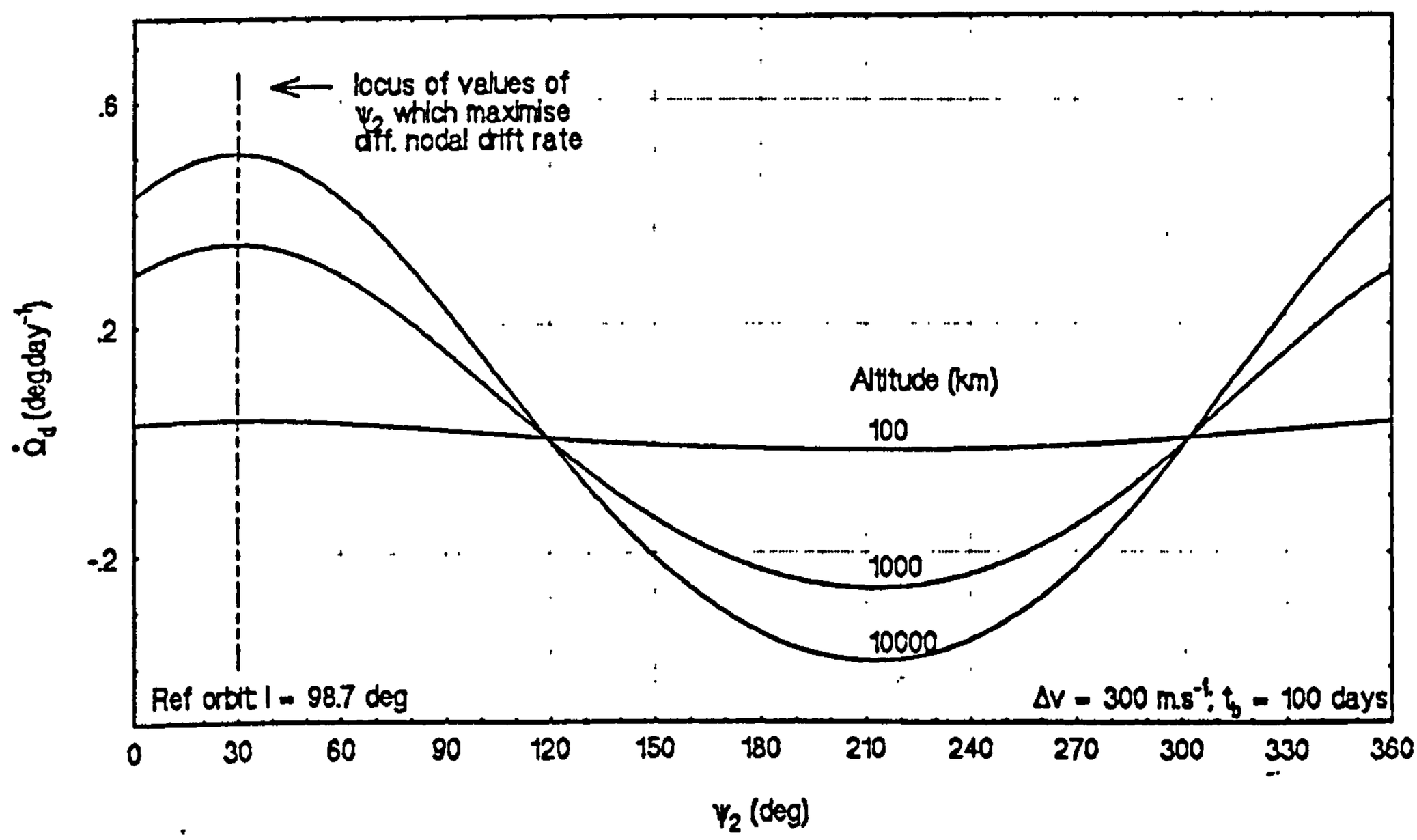

Figure 6.10 Variation in differential nodal drift rate with ψ_2 for different altitudes and EOS orbital inclination.

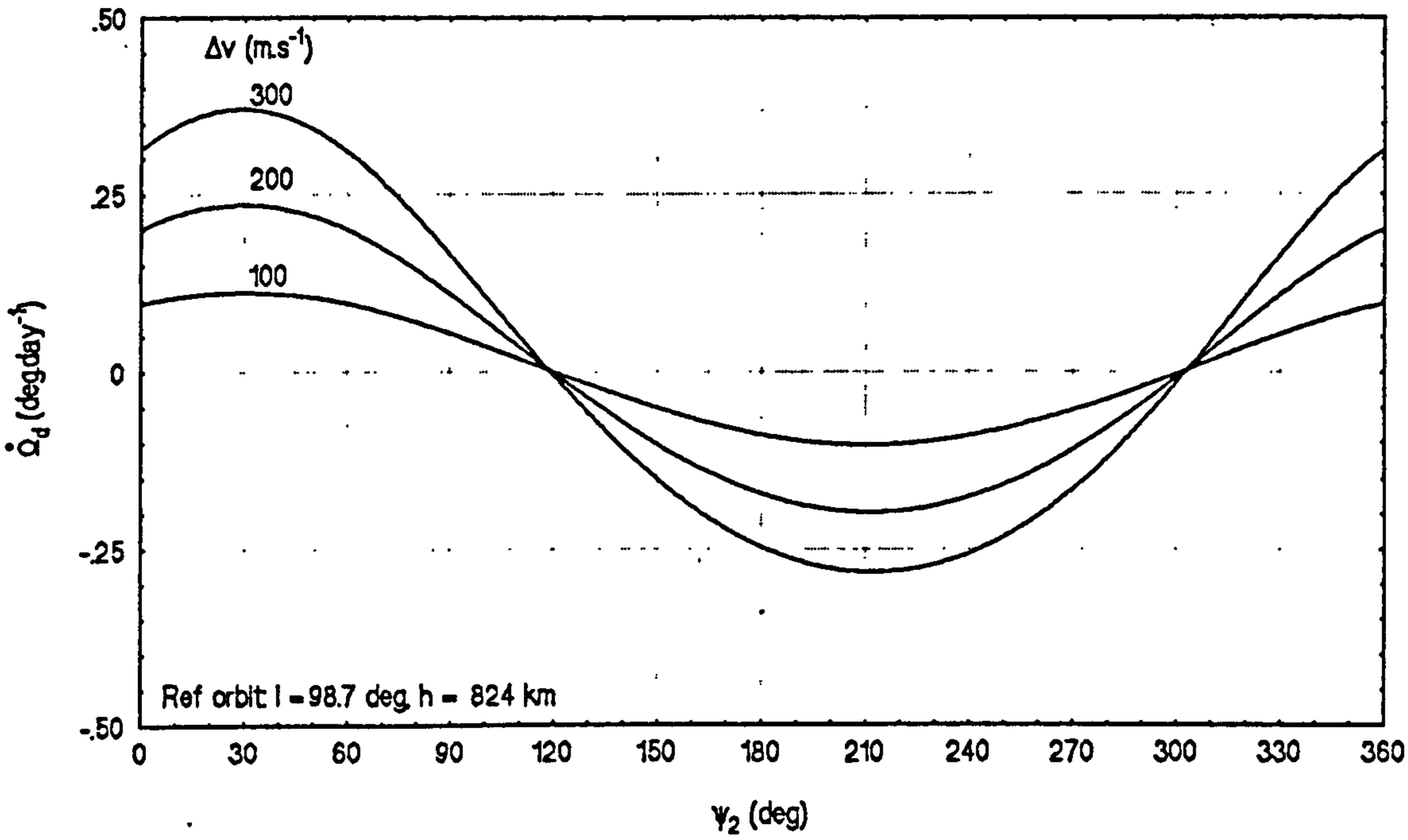

Figure 6.11 Variation in differential nodal drift rate with ψ_2 for different Δv manoeuvres about an EOS orbit.

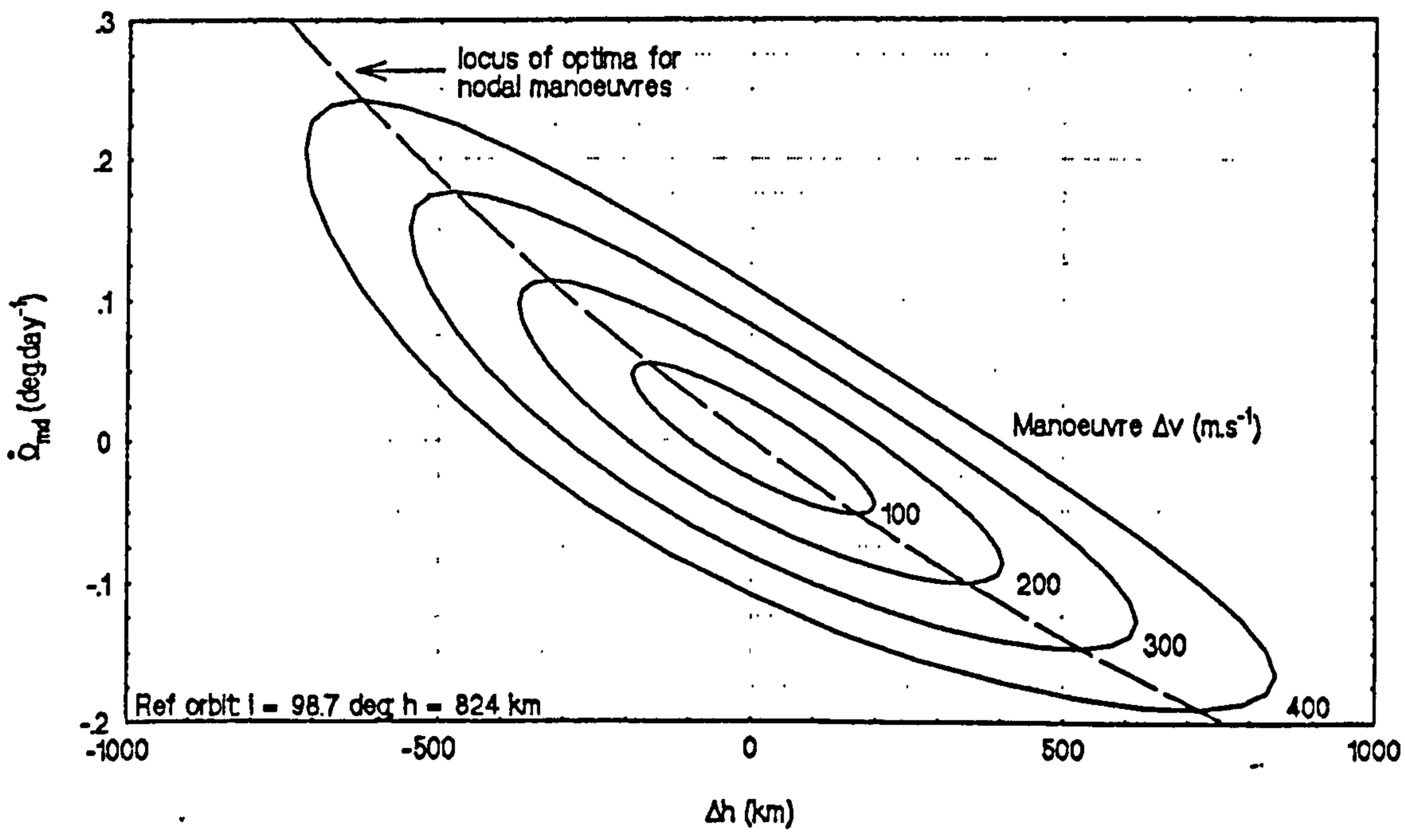

Figure 6.12 Contours of constant manoeuvre velocities for combined altitude and inclination changes about EOS orbit showing $\dot{\Omega}_{md}$ vs. $\Delta h1$.

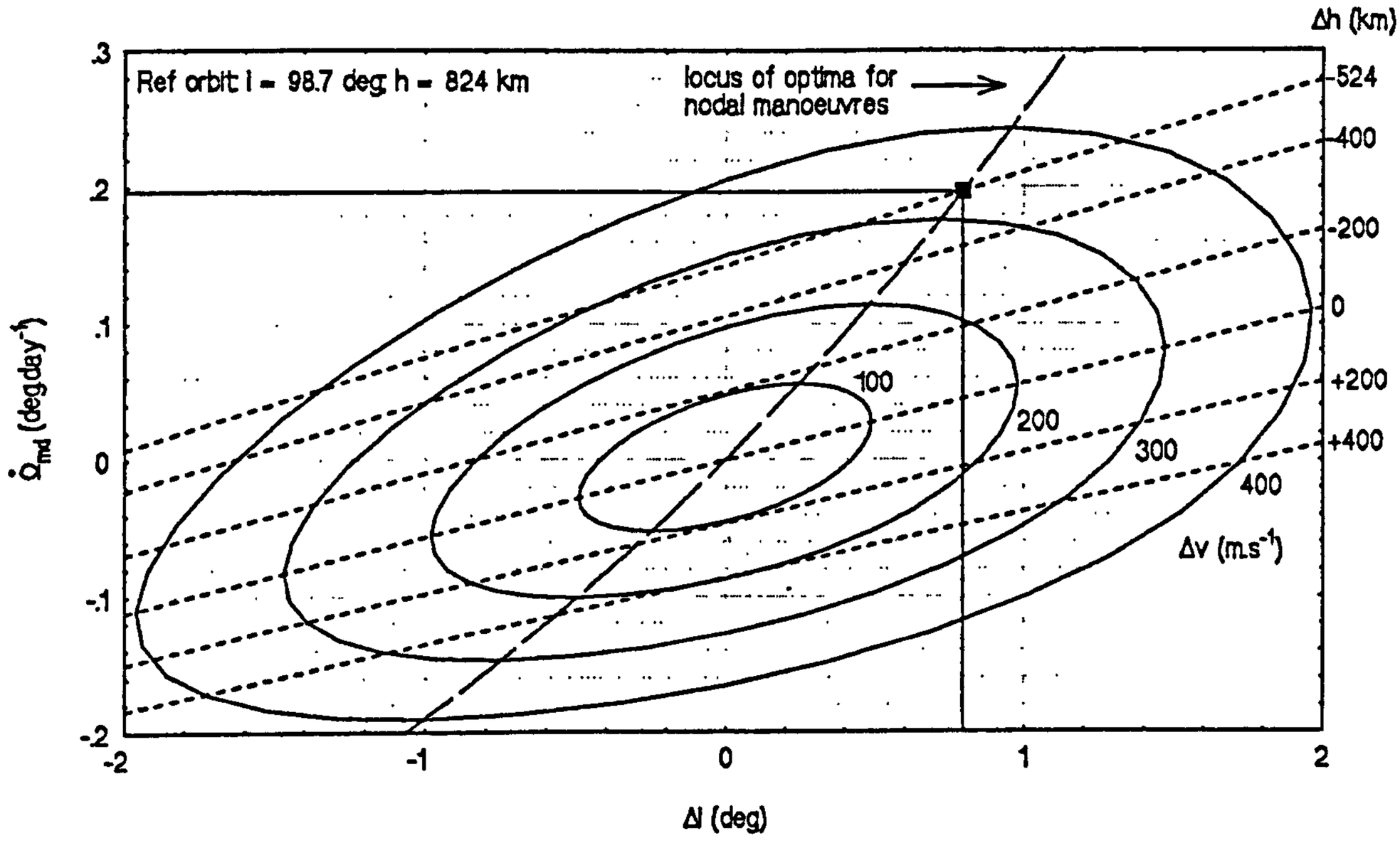

Figure 6.13 Contours of constant manoeuvre velocities for combined altitude and inclination changes about EOS orbit showing $\dot{\Omega}_{md}$ vs. Δi with lines of Δh marked.

It is possible, then, to identify a class of manoeuvres which give a maximum value of Ω_{md} for a particular value of Δv. These will also maximise the differential nodal drift rate of the drift orbit and hence will be characterised by the same value of $\psi_{2,opt}$. Although, in theory, these manoeuvres may be used to increase Ω_{md} to some maximum value over a time equal to half the nodal transfer period (i.e. with no drift period) for eastward transfers there is a practical limitation on this. This is the minimum altitude to which the spacecraft may be taken without the onset of unfeasibly large atmospheric drag effects. For westward transfers this limitation does not exist, although such transfers are less efficient in terms of propellant, and would also require the spacecraft to spend long periods of time in the enhanced radiation environment of the Van Allen belts.

Considering the limitations imposed by atmospheric drag, and still using the EOS example, if an altitude lower limit of 300 km is chosen (as discussed in Chapter 2) then a mean differential nodal drift value of around 0.2 deg.day^{-1} is the maximum that can be obtained for an eastwards transfer. This uses a Δv of approximately 330 m.s^{-1} to decrease the altitude by 524 km and increase the inclination by 0.8°. The resulting orbit has a differential nodal drift rate of 0.41 deg.day^{-1}. This manoeuvre is indicated on Figure 6.13 by the black square.

A westward manoeuvre using the same Δv (and $\psi_2 = 210°$) gives a mean differential nodal drift value of -0.16 deg.day^{-1}, decreases the inclination by 0.82°, increases the altitude by 587 km and places the spacecraft in a drift orbit with a differential nodal drift rate of -0.31 deg.day^{-1}. Although less efficient in terms of direct transfer propellant mass utilisation than eastwards transfer, westward servicing means that the drift orbit, with an altitude in excess of 1000 km, is scarcely affected by atmospheric drag. A service vehicle in a 300 km orbit will also need to carry additional drag make-up propellant, increasing the upload mass. Conversely, the drift period spent in the lower of the two Van Allen radiation belts would lead to increased array degradation. To offset this would require either a larger BOL array size, so imposing a mass penalty, or the use of an advanced, radiation-immune array such as the indium phosphide type described in Chapter 5. Additionally, the prospect of engineering all the platform supplies

and payloads to be radiation-resistant is singularly unattractive and, if nothing else, would serve to decrease the effective efficiency of westward transfers still further. Assuming a larger BOL array is selected, then an altitude upper limit of 1500 km is selected, equivalent to a manoeuvre Δv of 375 $m.s^{-1}$. Similar sets of contours can be plotted for the manoeuvre returning from the drift orbit. The return manoeuvre is also an optimal one, producing the same $\dot{\Omega}_{md}$ for the opposite change in altitude and inclination.

The results for the EOS manoeuvre indicate that this entire nodal transfer may be performed for a Δv of approximately 660 $m.s^{-1}$. For this particular pair of manoeuvres, whether or not the transfer can be performed in the time required is a function of the spacecraft acceleration level. The higher the acceleration level, the shorter the thrust periods at each end of the transfer and the longer spent in the drift orbit. If constant acceleration levels are assumed for the two thrust periods then the duration of the two thrust periods will be the same and the drift period will the difference between the sum of these and the required transfer time. This is examined in more detail in Chapter 8.

It should be noted that this discussion has assumed that continuous thrust is available. Although this is possible for a continuous source of power, such as a nuclear reactor, if the low-thrust propulsion used for the nodal alteration has a solar array as its primary power source then this will not be possible unless the vehicle carries substantial amounts of power storage. The amount of time that the servicing vehicle is eclipsed during an orbit depends on its orientation to the earth-sun vector. This will change completely during one complete servicing cycle. During those periods when the vehicle is eclipsed the mean differential nodal rate will be lessened and there will be a tendency for eccentricity to build up unless cancelled out.

Chapter 7 - Servicing vehicle role and background

7.1 Introduction

The use of servicing vehicles to resupply polar platforms has already been discussed in Chapter 2. When considering the use of such vehicles in more detail, however, it is apparent that their role cannot be defined in isolation, but must rather be considered as part of a wider scheme of future space operations which includes both the nature and size of the platforms to be serviced, the capabilities of launch systems to place payloads in the appropriate orbits, and the scope of the in-orbit infrastructure in the time period of interest. Although all these will have evolved from their current positions, the detailed nature of the changes that will have occurred is beyond the scope of this study, or, indeed, any others, to speculate. Nevertheless, since the definition of the servicing vehicle role requires this information, certain general predictions and extrapolations must be made. This chapter addresses the definition of a future space infrastructure against which a baseline platform configuration, and hence the role of the servicing vehicle, can be defined. It then discusses a number of possible roles/operating scenarios before identifying four basic mission scenarios to be used as the basis for servicing vehicle design

7.2 Infrastructure and technology

As has been discussed in Chapter 2 the polar orbiting component of the Earth Observing System was to have consisted of a constellation of four modular polar platforms (2 American, 1 European, 1 Japanese) serviced at regular intervals in low orbit by the space shuttle, giving the system a fifteen year lifespan. However, the withdrawal of Shuttle launches from Vandenburg made such servicing an impossibility. The US component has evolved into six large (15000 kg) non-serviced platforms with design lifetimes of five years. (Abramson [78]). These are to be orbited in pairs starting in 1997-98. By using disposable satellites in this way the overall fifteen year system lifetime can still be obtained.

There is, however, the possibility that the US contribution to EOS may change again. NASA

and the external EOS Engineering Review Panel disagree on optimum satellite sizing in the face of a shrinking budget (Isbell [79]) with NASA maintaining that larger platforms offer a smaller overall cost. They also point out that contracts have already been placed for the first group of satellites and any further change of plan is likely to delay the program by at least two years.

European and Japanese plans are more stable and involve smaller families of satellites. The 5200 kg Columbus polar platform (POEM-1) due to be launched in 1997 will represent the European contribution. This will also have a design life of five years and need replacing on this timescale.

Given the escalating importance of Earth-orientated remote sensing it is anticipated that, after the EOS programme is complete (in the period 2010 to 2015), a replacement will be required. This new system, hereafter referred to as EOS2, is likely to be more mature and possibly of an even more international nature. The original arguments in favour of a serviceable system will still apply so it may be anticipated that EOS2 will be designed not only to take advantage of the benefits offered by a serviceable system but to provide even longer term, and more permanent and continuous, access to sun-synchronous orbits. As such, it appears very likely that EOS2 would resemble the original modular design for EOS. This would render resupply and replacement of platform payloads necessary at regular intervals, though the requirement for two platforms in one of the orbital slots is obviated by the larger payload capability that EOS2 platforms would offer.

Both the size and design of the platforms and support mechanisms for EOS2 platforms and service mechanisms will be heavily influenced by the space infrastructure and technology extant at the start of the system operational period. As outlined at the start of the thesis, those areas of infrastructure and technology of particular relevance are transportation systems, in-orbit assets and teleoperations.

7.2.1 Launch vehicles and capabilities

The United States has recently decided not to enlarge the current Shuttle fleet but to concentrate on upgrading current expendable launch systems and developing new ones (Lawler [80]) to provide a National Launch System (NLS). Although America is also developing a National Aerospace Plane (NASP) the future of this is uncertain since it requires numerous new technologies to be developed. Furthermore, NASP is to be a technology demonstrator rather than a practical payload delivery system. Given these factors, the lack of Shuttle launch pad at Vandenburg and the need for the Shuttles to support Space Station Freedom it appears that Shuttle launches into polar orbits are unlikely ever to take place. This limits near and mid-term access to polar orbits to that provided by unmanned expendable launch vehicles. Currently the US has three families of launchers which provide the capability to launch significant payloads into polar orbits. These are the Martin-Marietta Titan IV (which was to have been used to launch the original American EOS satellites), the McDonnell Douglas Delta series and, since a recent decision to refurbish a launch pad at Vandenburg (Isbell [81]), the General Dynamics Atlas 2 series (which is likely to be used to launch the new 'down-sized' American EOS satellites). These three launch systems will provide the United States with a launch capability of up to around fourteen tonnes into a 200 km polar orbit.

Looking forward to the NLS it is anticipated that it will consist of a low-cost, reliable core (powered by cryogenic Space Transportation Main Engines (STMEs) that are already under development), a number of solid, liquid or hybrid rocket boosters and a high performance cryogenic upper stage (Gunn [82]). The baseline NLS configuration is expected to be able to deliver in excess of 20 tonnes to LEO. Through an ascending series of goals it is anticipated that this baseline will be developed until the larger NLS configurations are capable of lifting payloads of over 100 tonnes. Once these greater capabilities have been developed it is anticipated that a man-rated NLS crew carrier and a crew-only ascent/descent vehicle (CADV) may be developed and that a complementary space tug/OTV may also be built.

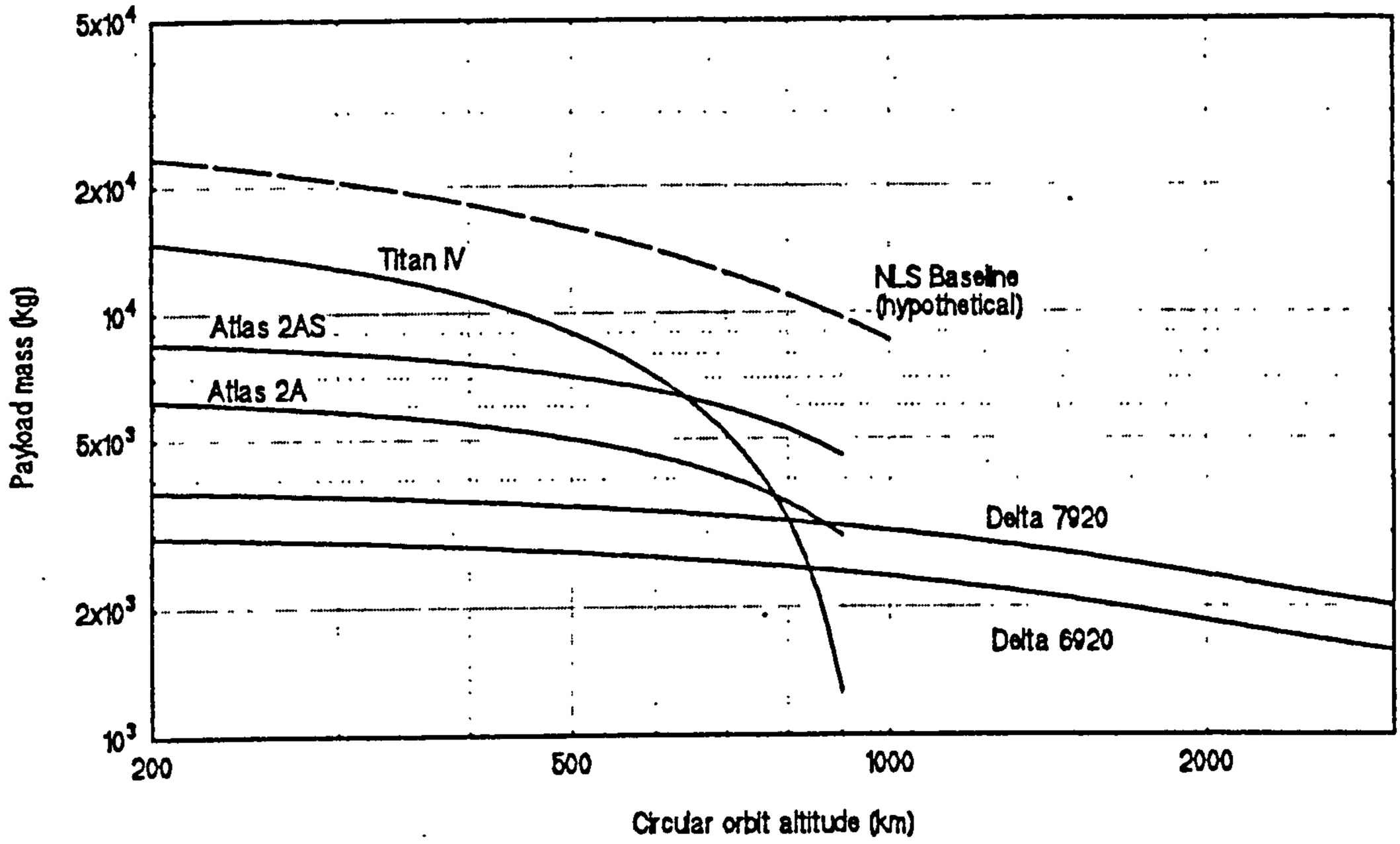

Figure 7.1 Payload capability of US launch systems into polar orbits

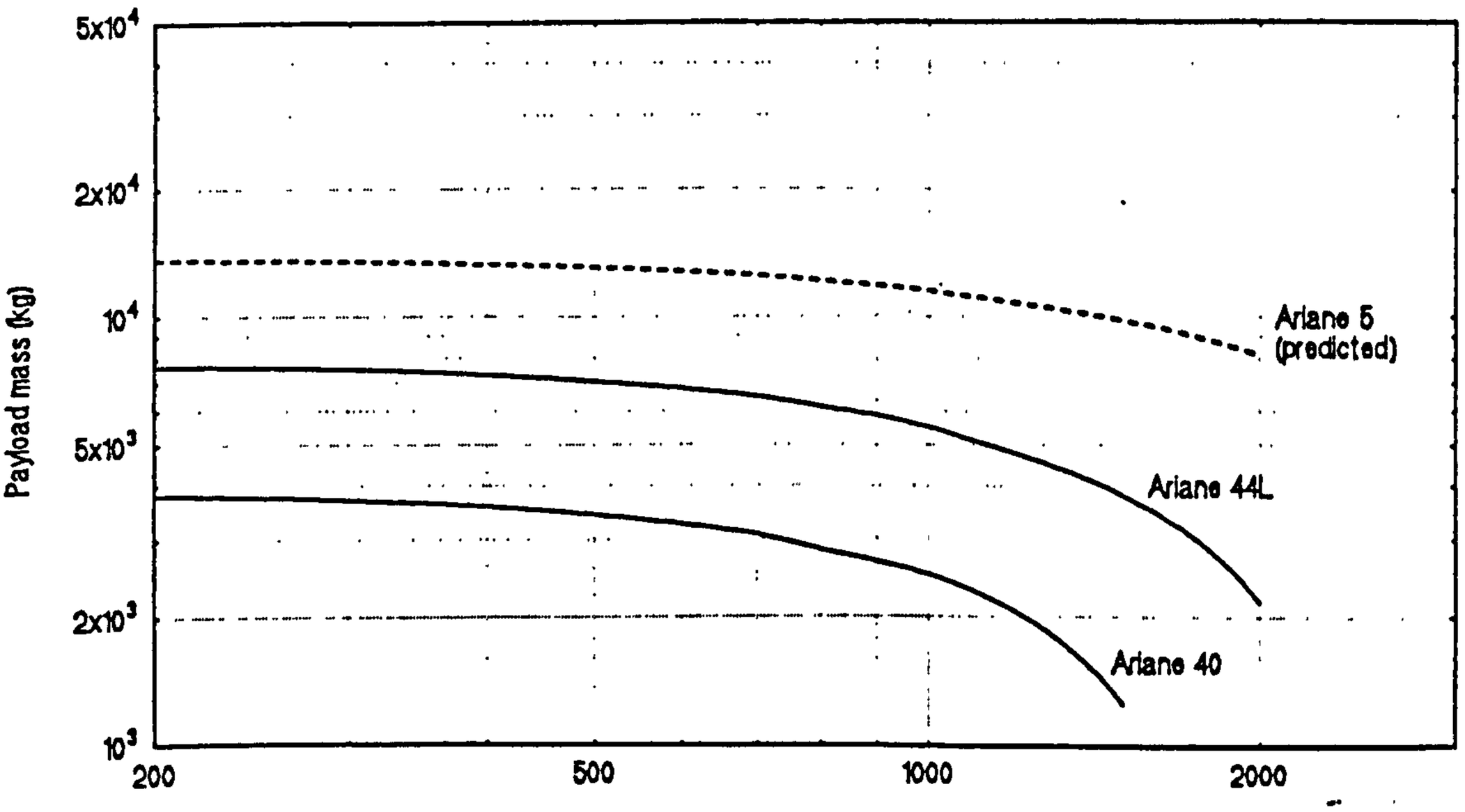

Figure 7.2 Payload capability of European launch systems into polar orbits

It is hoped to start NLS development in the mid to late 1990's with an initial launch sometime in the first five years of the next century. If no programme slippage occurs then it appears that the NLS basic configuration and some of the earlier extended versions should be available at around the same times as EOS2 is being placed in orbit. If this is not the case then the existing US launchers will still be available. The capabilities of these launchers plus a hypothetical curve representing baseline NLS performance are shown on the preceding page in Figure 7.1. Although manned vehicle launch to polar orbits maybe possible in the timeframe of interest, a significant payload will be unable to accompany the vehicle.

Over the last ten years Europe has developed the Ariane launch system, culminating in the Ariane 4. Either or both solid and liquid strap-on boosters may be added to the basic Ariane 40 to give six different versions topped-off by the Ariane 44L. The former is capable of placing approximately 3000 kg into an EOS orbit, the latter 6500 kg (Arianespace [83]). Of more interest is the Ariane 5 launch vehicle, currently under development. Although the main purpose of Ariane 5 is the launch of commercial payloads into geostationary orbit it is also being designed to launch elements of the Columbus system, including the European polar platform component of EOS, and the European spaceplane Hermes (Hergott [84]). Payload capabilities versus circular orbit altitude for the Ariane family are shown in Figure 7.2 on the previous page.

The first launch of Ariane 5 is due 1995, with the system expected to completely replace Ariane 4 by 1999 (Vedrenne [85]). Like the earlier Ariane launchers, Ariane 5 is viewed as the first in an evolutionary series and it is expected that further development will occur to give greater capabilities and flexibility. It is anticipated that the Vulcain cryogenic engine will be upgraded or that the single engine be replaced with two. Additional or modified boosters are also an option (Fuestel-Buechl et al. [86]). Evolution into a partially reusable launcher has also been discussed with the suggestion that the system's solid boosters could be replaced by winged liquid boosters with 'fly-back' capability.

Beyond Ariane 5, ESA has expected that some form of reusable aerospace plane/rocket would be developed sometime after 2000 with first flights taking place in the period 2010 plus. The main use envisaged for such a vehicle would be crew delivery and recovery. As yet no programme has been initiated and current funding difficulties being experienced for existing projects may lead to this being postponed indefinitely.

From consideration of the information it appears likely, therefore, that in the period 2010-2015 a payload capability of 15000 kg to EOS orbit will be available as a matter of routine, using either presently existing or new expendable launch systems. There is a high likelihood that 20000 kg could be placed in an EOS orbit. Although manned vehicles may be able to achieve the same orbit is is very unlikely that significant (if any) payload could be carried by these manned vehicles so that servicing, if performed by direct launch into polar orbits, will have either have to be effected remotely using unmanned vehicles or performed using two launches, one for the human servicing team and one for the supplies.

7.2.2 In-orbit infrastructure

The servicing of polar orbiting platforms is also driven by in-orbit infrastructure. Depending on the amount, location and sophistication of this infrastructure the servicing process may either be made easier or more difficult. In particular, the elements of in-orbit infrastructure that are important for servicing are transportation nodes and systems and communication systems since these effect both physical presence at, and remote monitoring of, the servicing process.

The prime in-orbit space transportation node in the 2010-2015 period will almost certainly be the Freedom space station. Although considerably descoped from its original configuration it is still likely to be the main in-orbit destination for human beings and will act as the main base for a variety of orbital operations. If Freedom should be cancelled in the interim, there is the possibility that other plans may be adopted by Europe (such as those based around use of a common orbital module to be launched by

Ariane 5, as suggested by Hempsell [87]), though these would inevitably be of smaller scale than those current at present. However, both Freedom and the alternate concepts are planned to occupy a low inclination orbits. Given an inclination of 28° the Δv needed to transfer from the Freedom orbit to the EOS orbit is the vicinity of 9 $km.s^{-1}$, far beyond the capability of the in-orbit transportation systems that have been considered for the servicing of space station co-orbiting platforms and similar. As a result, it is generally accepted that second generation space stations such as Freedom will not be able to play a significant role in polar platform servicing (Reinhartz [88]). Third generation space stations placed in high inclination orbits would obviously mitigate this limitation. However, optimistic estimates of these have suggested that the earliest date possible for the introduction of such a space station to be 2025 (Qualls and Ferebee [39]). This makes it suitable for the support of a putative EOS3 (assuming a 15 year life time for EOS2) support role, but not for EOS2.

In-orbit transportation systems for the period 2010-2015 are somewhat difficult to assess as there are no firm plans to develop them any further at present. As described in Chapter 2, NASA and ESA both originally considered developing Orbit Transfer or Orbit Manoeuvring Vehicles in conjunction with Freedom/Columbus but have since decided not to proceed further with these programmes. Although it may be expected that similar programmes will be recommenced at some stage, as part of the NLS development programme for instance. If this is the case then development might be envisaged to start only when the NLS programme was reasonably mature, say around 2010. In any event, these systems, like their planned predecessors, are very unlikely to have the capability to transfer from Freedom to EOS orbit, making their possible contribution to polar platform servicing very limited.

It has been seen that in the period 2010-2015 manned access to polar platform orbits, either from the ground or from orbit, will either be impossible or difficult to achieve, certainly if any useful level of payload is to accompany the astronauts. It appears that if platform servicing is to be accomplished this will have to be performed remotely. This is discussed in more detail in the next section. However, if such remote servicing is to be achieved, then an adequate space communications infrastructure will also have

to exist in order to support the high data-rate, real-time monitoring that would be needed. Fortunately the existence of any EOS-type constellation can be presupposed to include such a system since the data flow generated by the platforms when operating (expected to be in excess of 10^{12} bytes per day for EOS, (Colucci [89])) cannot be handled without such a system. NASA already has its Tracking and Data Relay Satellite System (TRDSS) system in orbit and ESA is planning two European Data Relay Satellites (EDRS) for launch in 1998. Based on these factors, the provision of a suitable space communications is one of the few parts of a future infrastructure that can be predicted with some degree of certainty.

7.2.3 Teleoperations

Rendezvous, docking and orbital servicing are complex operations. Active inclusion of a human intelligence in orbital operations is at a premium when the operation requires significant versatility. Even when human intelligence cannot be replaced, a human operator can be supported or augmented by automation. It follows from this that three levels of human mediation in orbital operations can be defined;

* Direct mediation by humans at the operational location
* Indirect mediation by humans at another location via remote control (teleoperations)
* Zero mediation by humans with all operations performed by autonomous robots

As far as on-orbit servicing of EOS2 is concerned, the first option requires delivery of humans and servicing equipment and supplies to the individual platforms. As has already been seen, the delivery of a manned craft to operational polar orbits is unlikely to be possible in the period 2010-2015, either by direct launch from the ground or from the Freedom space station. To perform servicing then requires either the second or third options to be adopted.

Beyond the concern with the level of human mediation in the servicing process, there are also different techniques for accomplishing the servicing. As outlined by Scolese [77] there are two basic categories; add-on servicing and exchange servicing. In the former a servicing vehicle carrying a pallet

or module bearing the appropriate new and replacement equipment is docked with the platform. The old equipment is taken out of service but remains on the platform in its original position. Depending on system requirements the servicing vehicle may also remain attached or may be detached and proceed onwards to other servicing operations.

In exchange servicing the old or failed equipment is removed from its location and replaced by the new. Old equipment may then be left attached to the platform but mounted on the new equipment carrier or removed from the platform. In the latter case it may become part of the servicing vehicle payload or be disposed of by de-orbiting to atmospheric re-entry using a small rocket motor or high drag device.

Add-on servicing is technically easier to perform but less mass-efficient in terms of platform design and operations, especially if items such as solar arrays are to be replaced. Exchange servicing is considered the better option, providing it is technically viable.

The United States, Europe and Japan all have forward-looking programmes in this area. The various key enabling technologies have been identified and are under active development. These include such topics as robot arms, dextrous manipulators, the design of satellites to be compatible with automatic servicing, space qualified robotic-systems, robot vision, knowledge-based data systems and autonomous docking techniques (a good coverage of these fields is given in the fifty-plus papers in [90]).

The dextrous manipulator is of particular importance since, whether teleoperated or autonomous servicing is performed, it is necessary to be able to handle supplies with a fine degree of control. Considerable work has already been performed in this area. Advanced dextrous manipulators are expected to be available by the mid 1990's for inclusion on space station Freedom. Original predictions expected most major milestones in robotic servicing to have been accomplished by the year 2000 (Meissinger [91]). Funding limitations have reduced the rate of progress somewhat, although rapid development is to be

expected once Freedom becomes operational. Even if the necessary technology for fully autonomous servicing is delayed then the lesser task of telerobotic servicing should be easily accomplishable. Given this it is anticipated that a teleoperated remote manipulator system (TRMS) will be developed capable of being used on a wide range of space vehicles and structures to give teleoperations capability and hence allow exchange servicing on EOS2.

7.3 Mission scenarios

Based on the information already given it is apparent that in the 2010-2015 timeframe manned servicing of the polar platforms in operational orbit be extremely unlikely. However, technology will have advanced enough for remote telerobotic, or possibly autonomous, servicing to be performed by service vehicles placed into EOS orbit by expendable launchers. The capabilities of these launch systems also define the possible size of platforms placed into the EOS orbit. Given future development plans, it is thought that 15000 kg can be taken as a representative platform mass, though this could actually be as high as 20000 kg. In order to establish the servicing requirements of such a platform it now becomes necessary to address the likely configuration and mass breakdown of such a platform.

7.3.1 Baseline polar platform configuration

It is assumed that the mass of the EOS2 platforms will be 15000 kg and that the same orbit selection drivers will hold so that the orbit configuration will be identical to that for EOS. The baseline EOS2 platform configuration can then be extrapolated from the original EOS configuration, allowances being made for likely improvements in technology.

On the serviceable Columbus polar platform for EOS those systems dealing with power supply and conditioning, data management, guidance navigation and control and similar were to have been placed in standard Orbital Replacement Units (ORUs). These ORUs are modular units of size 1m x 1m x 0.75m with standard mechanical, power, data and manipulator interfaces for easy removal and attachment. The solar arrays, the communications antenna, and the propulsion module were also ORUs,

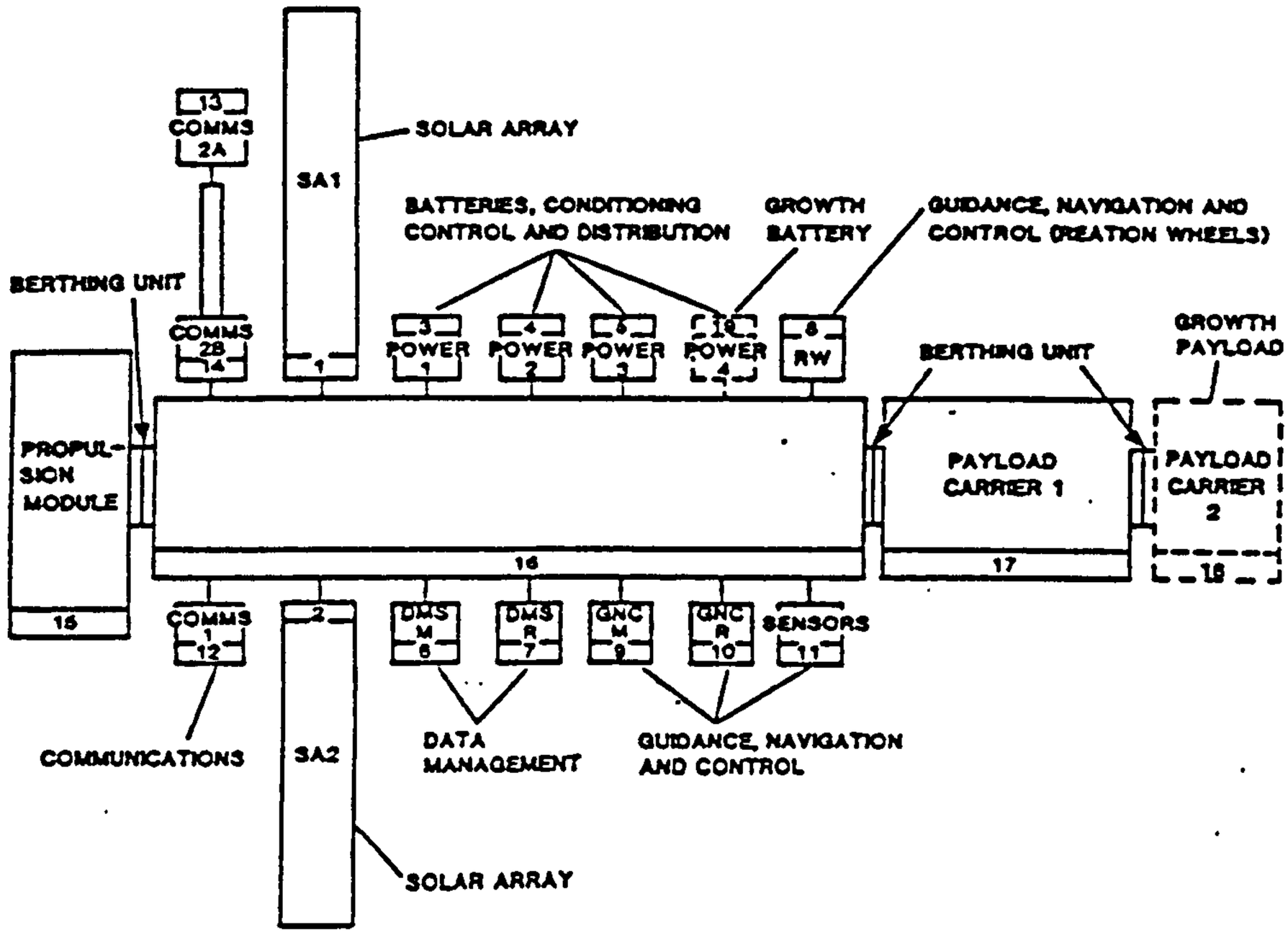

Figure 7.3 Serviceable platform utility ORU definition (Sawdon et al. [25]).

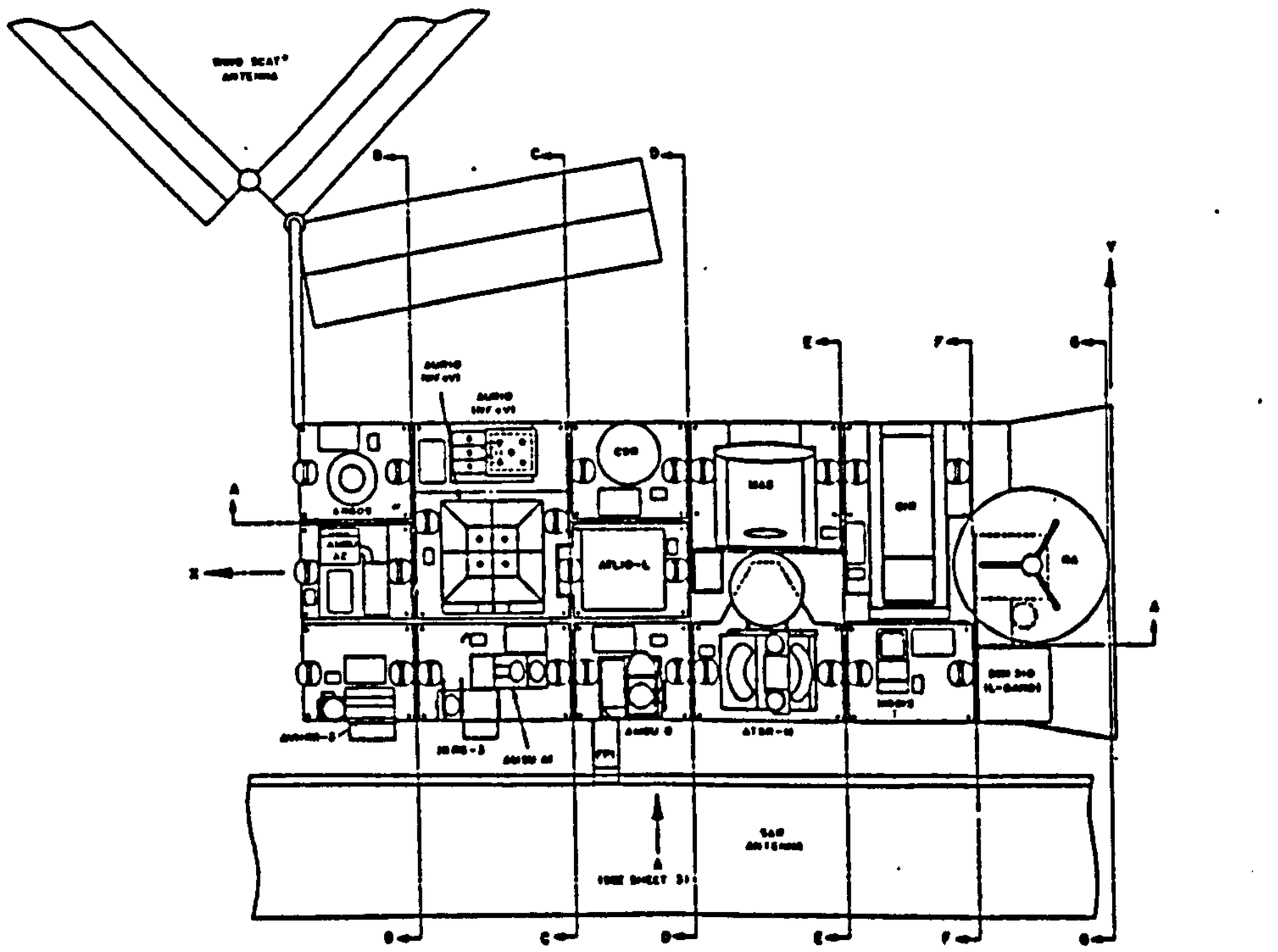

Figure 7.4 Serviceable platform payload accommodation layout (Conchie and Windsor [92]).

though of a non-standard type. (Sawdon et al [25]). A platform ORU definition for this concept is shown in Figure 7.3. on the preceding page. Payload accommodation was to have been achieved by mounting instruments on a standard plate bearing the same standard interfaces as the ORUs. These plates would then have been attached on an instrument grid on the underside of the platform. (Conchie & Windsor [92]). This is shown in Figure 7.4 on the preceding page. Small instruments could be fitted several to a plate, large ones on plates occupying several sites. Figure 7.3 shows separate utilities and payload modules. This is a configuration for Shuttle launch. For ELV launch these two modules were to have been merged with the ORUs on the top surface and the payload on the bottom. ORU masses lie in the 200 to 300 kg range while experiments are much more variable, with masses from 10 kg to beyond 1000 kg. The propulsion unit is the single most massive ORU (though of a non-standard type). In order to perform the necessary orbit lowering and raising to and from the shuttle servicing orbit the original EOS platform propulsion module was to carry 4800 kg of propellant, giving it a fully-fuelled mass of 5200 kg. This was to have been replaced at every servicing.

It is anticipated that any EOS2 platform will follow this modular construction very closely. However, a higher percentage of the platform all-up mass will be available for payload primarily because the need for orbit raising/lowering propellant will be obviated and also because of the expected improvements in photovoltaic power system mass efficiency (as discussed in Chapter 5). ORU sizing will be expected to follow that for the EOS concept while payload designers will be expected to have developed this approach to allow larger instruments to be built up from smaller component units also. As well as enabling easier payload servicing and replacement this latter approach, suggested by Hathaway [93], allows payload ORUs to be classed (according to their likely reliability) as long and short-life units and for servicing strategies to reflect this.

A berthing node for servicing vehicle docking/ORU carrier attachment is located on one end of the platform. The platform could also carry a TRMS (as assumed by Graves and Rosen [35]) but the best location for it, i.e. on either the platform or the service vehicle, depends on numerous factors. Whichever

of these the TRMS is placed on it reduces the amount of useful payload that can be carried. However, placing the TRMS on the platform allows continuous visual monitoring of the spacecraft throughout its lifetime and the replacement of failed ORUs between service intervals from a stock of on-board spares. For this reason this option has been selected for the baseline EOS2 platform configuration.

Placing the TRMS on the platform makes the TRMS a critical component. It the TRMS fails then no servicing can take place. It is assumed, therefore, that the TRMS itself will comply with the ORU design philosophy and, in the event of complete, irretrievable breakdown, be capable of being replaced by a dedicated servicing mission equipped with TRMS capability.

Power system sizing follows, in the main, both the reasoning and data and applied by Hermel et al. [94] to the design of a power system for an electrically-propelled vehicle suggested for the emplacement of future NAVSTAR/GPS satellites. A GaAs concentrator solar array is used as the primary power source and provides an inverse specific power of 12 $kg.kW^{-1}$ and an operational lifetime of ten years. The value for the array area-to-power ratio used by Hermel et al. was felt to be too optimistic, even given a "focused development effort" and was approximately doubled from 1.7 $m^2.kW^{-1}$ to 3.3 $m^2.kW^{-1}$ to match more conservative assessments of future developments in this technology (e.g. Flood, [67]). Energy storage is performed using advanced NiH cells with an energy density of 60 $W.hr.kg^{-1}$. During the operational lifetime of the platform, it is anticipated that both of these power system components may be updated with more efficient and durable units. In the initial configuration, however, and given a baseline servicing interval of three years, the array will be replaced every third servicing and the batteries every servicing.

On-platform spares consist of ORUs for those payload, utility and TRMS components defined as short-life units. Based on an analysis of ORU design considerations in other modular spacecraft (Falkenhayn [95] the mass of these has been taken as one sixth of the above systems. The platform propulsion is provided by an arcjet thruster ORU which is also replaced every servicing. This is based

on a similar idea by Boriello et al. [28] sized to provide the necessary Δv for this platform.

Having defined a model for the platform a spreadsheet was used to derive the final mass and power breakdowns. These are summarised below in Table 7.1.

Table 7.1 - EOS2 platform baseline configuration

Structure mass	2250 kg	Solar array EOL power	23 kW
Payload mass	4650 kg	Solar array area	95 m^2
Utilities mass	3825 kg	Solar array mass	345 kg
TRMS mass	1200 kg	Solar array life	10 years
Spares mass	1410 kg	Annual degradation	2%
Power system mass	1355 kg	Battery mass	345 kg
Propulsion system mass	310 kg		

The standard mass that must be supplied to the platform at servicing can now be calculated. It is assumed that all the in-use, low-reliability ORUs on board the platform have been replaced by the on-board spares in the period before servicing, and that a full set of new spares are delivered. To this must be added the mass of the battery and propulsion ORUs and the mass of those payload and utility ORUs to be replaced anyway. In addition a new solar array must be delivered every third servicing. This makes the maximum normal servicing mass delivery approximately 3800 kg. Assuming the payload carried has structure fraction approximately equal to that of the platform then the carrier has a mass of 600 kg which gives the single service payload mass as approximately 4500 kg.

7.3.2 Possible mission scenarios

The servicing of the EOS2 constellation involves the delivery of new ORUs to the platforms in some manner. There are a number of ways in which the servicing mission can be configured in order to to achieve this.

The first set of alternatives deals with the placing of the service vehicle and ORU sets into orbit. In theory, it is possible for the service vehicle to be put into orbit on the same launcher as a platform, and that it may carry either no, one, or more ORU sets. However, the first of these options seems most unlikely, particularly because of the mass limitation this would place on the platform and the fact that this might well leave the service vehicle in orbit for a substantial period before it was needed. Assuming, then that the service vehicle has a dedicated launch, there remains the decision on the number of ORU sets to be carried along with it. Unless there is a severe constraint on the mass that can be uploaded at a single time it is likely that simple economics would predicate the launch of a service vehicle and a single ORU set on separate launchers. The question of whether multiple ORU sets should be launched at one time (either with or without a service vehicle) is likely to be decided by a trade-off between economics and convenience. It is again cheaper to launch multiple ORU sets on a single launcher than to launch them individually. However, this means that significant upload flexibility is lost. Although the impact of this on platform operations is offset by the stock of low-reliability unit ORUs on the platform, it constrains decisions on general payload and equipment changes to be taken on a three-year basis and also requires a servicing vehicle of generally greater capability to be used to carry the additional mass.

A second set of servicing mission alternatives revolves around the lifetime of the service vehicle. At its simplest, this becomes a question of whether the service vehicle is single or multiple use. The first of these is very unlikely since it would require thirty-six servicing vehicles over the constellation's lifetime. Given the emphasis on extended life through modular design of the platform, it is much more likely that a similar approach is adopted for the servicing vehicle. There is no reason, a priori, why the platform mounted TRMS cannot be used to replace service vehicle ORUs as well as platform ones so

extending service vehicle lifetime indefinitely at the cost of additional ORU upload.

As outlined earlier in the chapter, either add-on servicing or exchange servicing might be used. In the former case and possibly in the latter case old ORUs may remain on the platform, either in their original position or on the newly-arrived carrier. Alternatively, exchange servicing also admits of the possible removal of the old ORUs on the new carrier. The first of these appears somewhat impractical since it would require the platform to grow by around 4500 kg at every servicing. Over a 30 year lifetime this would require the platform to grow from 15000 kg to 60000 kg.

If the second option is pursued the old ORUs may be taken away by the servicing vehicle and either remain with it throughout the rest of its mission or be disposed of either by de-orbiting propulsively direct from EOS orbit or by being released at a lower orbit and using some form of drag-enhancer to initiate re-entry. The propulsive re-entry requires a Δv of approximately 130 $m.s^{-1}$ to be applied to the carrier. Using a simple bipropellant motor to perform this task would add approximately 300 kg to the mass of each carrier. Alternatively, for multiple ORU sets, the service vehicle itself can be used to de-orbit them, but this means that a new servicing vehicle is then required.

If the drag-enhanced disposal is made use of then a large, lightweight deployable structure would need to be built into the ORU carrier. Calculations show that, assuming the carrier is taken to 300 km by the service vehicle before being released, a drag enhancer area of around 1000 m^2 (equivalent to a disc of radius 18 m) would be needed to ensure re-entry within one month. Before this option could be adopted it would have to be ascertained that there was minimal likelihood of the carrier surviving re-entry. If this was not the case, each re-entry would require monitoring from the ground, adding considerably to the cost of the exercise. This option appears very attractive, otherwise.

It is apparent that there are numerous possible scenarios for EOS constellation servicing and that it is inevitable that overall design of the servicing vehicle will depend on the scenario selected. Considering the options discussed above, however, two broad categories of mission can be defined corresponding to the number of ORU sets that are uploaded at one time - either one for a single platform servicing or three for an entire constellation servicing and whether the service vehicle is designed to be used for a single servicing cycle or multiple cycles. Against this background four mission scenarios have been defined, designated alpha, beta, gamma and delta.

The alpha scenario features a 'small' service vehicle sized and fuelled to be able to carry a single ORU through a single servicing cycle. The mission would proceed as follows;

i) Service vehicle (SV) + one ORU set launched on expendable launch vehicle (ELV)

ii) SV rendezvous with first platform. ORU set exchanged.

iii) SV starts transfer to second platform. At lowest point of transfer old ORU set released and re-enters using passive drag enhancer.

iv) New ORU set launched by ELV and retrieved by SV. SV continues transfer to second platform.

v) i) to iv) repeated for third platform.

vi) SV and one old ORU de-orbited.

This scenario requires one combined service vehicle and single ORU set launch and two single ORU set launches per servicing cycle.

The beta scenario features a 'large' service vehicle sized and fuelled to carry three ORU sets through a single servicing cycle. The mission would proceed as follows.

i) SV and three ORU sets launched on ELV.

ii) SV rendezvous with first platform. One ORU set exchanged.

iii) SV transfers to second platform.

v) i) to iii) repeated for second and third platforms.

vi) SV and three old ORU sets de-orbited.

This scenario requires one combined service vehicle and three ORU sets launch per servicing cycle.

The gamma scenario features a 'small' service vehicle sized and fuelled to carry a single ORU set through three servicing cycles (this period is chosen because it is the time over which the array will degrade to approximately 75% of its BOL power). The mission proceeds in the same way as the alpha scenario except that nine, rather than three, servicings would be carried out and that two fewer service vehicles are required.

The delta scenario features a 'large' service vehicle sized and fuelled to carry three ORU sets through three servicing cycles. Propulsively this represents an over-capability for the baseline delta mission since the old ORU units may be de-orbited during each transfer. It does, however, provide for the redistribution of certain ORU set components between EOS2 platforms and offers additional operational flexibility given that new ORUs would typically be uploaded every three years. This scenario would proceed as follows;

i) SV and three ORU sets launched on ELV.

ii) SV rendezvous with platform. ORU set exchanged.

iii) SV starts transfer to next platform. At lowest point of transfer old ORU set released and re-enters using passive drag enhancer.

iv) ii) to iii) repeated for platforms two and three.

v) After last old ORU set de-orbited three new ORU sets uploaded by ELV.

vi) ii) to v) repeated for second and third servicing cycle.

vii) At the end of third servicing cycle SV de-orbited.

This scenario requires one servicing vehicle + three ORU set launch and two three ORU set only launches over nine years. The upload patterns for the four scenarios are shown overleaf in Figure 7.5.

The design of the service vehicle for the four configurations cannot be be performed until more detailed calculations on mission Δvs have been carried out. These two topics form the basis of the next chapter.

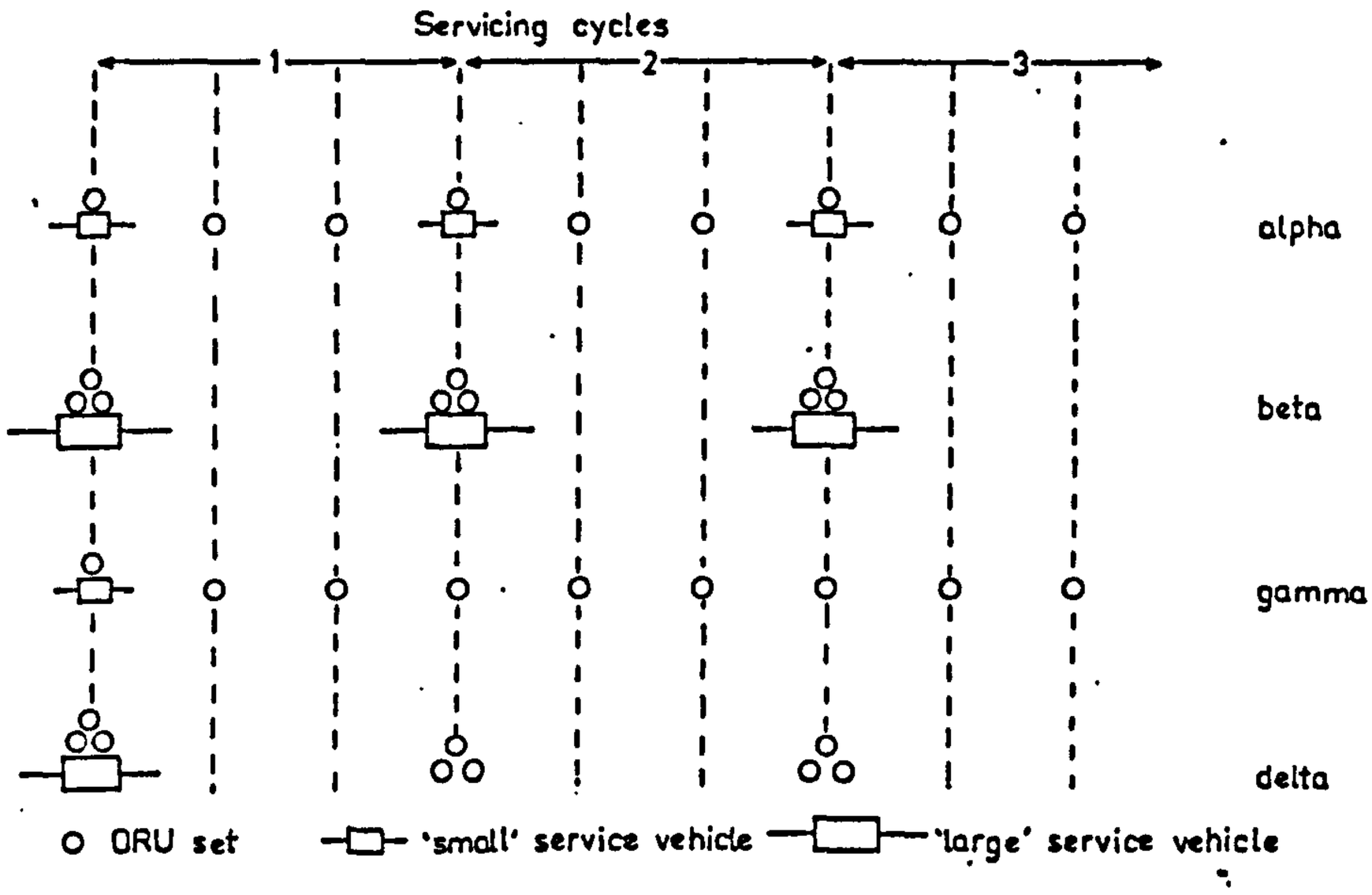

Figure 7.5 Upload sequences for four service mission scenarios

Chapter 8 - Servicing vehicle definition

8.1 Introduction

This chapter defines the spacecraft to be used for the EOS2 servicing mission. It starts by defining the parameters and mathematical model used to simulate the service vehicle. It then discusses the characterisation of the various electric propulsion systems under consideration and defines the baseline values of the various parameters to be used as input to the model. The propulsive requirements of the servicing mission scenarios are then investigated and the required Δv and acceleration levels established. The suitability of the different propulsion systems for the four service vehicle configurations is then analyzed and a xenon ion system established as the best in each case. Two mission scenarios/service vehicle configurations, designated as the beta and the gamma, are then selected for further investigation.

8.2 Modelling the service vehicle

As already stated in the last chapter, it is anticipated that the servicing vehicle will be constructed along modular lines similar to the polar platform. This approach is well demonstrated in the spacecraft described by DeVincenzi et al. [56], Sponable and Penn [75] and Hermel et al. [94] and, as well as making on-orbit assembly possible (if appropriate) and maintenance/repair easier, would allow other electrically-propelled vehicles to be constructed for other missions elsewhere in the space infrastructure.

Here the service vehicle has been modelled as eight separate parts. These are the power supply, the power processor, the thermal control system, the thrusters, the propellant tankage, the close manoeuvring system, the TT&C/GN&C system, and the structure. The overall mass of the service vehicle is given by

$$m_{sv} = m_{ps} + m_{pp} + m_{tc} + m_t + m_{tk} + m_{ms} + m_{ttc} + m_s \qquad \text{Eq. 8.1}$$

Each component is modelled as outlined below. The values of the various input parameters for the servicing vehicle are given in Table 8.1, nine pages on.

The power supply is assumed to be an advanced gallium arsenide concentrator photovoltaic array with a cell efficiency approaching 30% (the same as that used on the EOS2 platform design outlined in Chapter 5). The concentrators provide shielding and a high-temperature operating environment for the cells which continuously thermally anneals them and repairs radiation damage, so minimising power output degradation. The concentrator array can be pointed independently of the service vehicle attitude so that its output power can be controlled to provide the propulsion system nominal input power over its lifetime. Should this two degree of freedom control prove impossible to perform for any reason, then the arrays can be pointed by giving them one degree of freedom and rolling the vehicle. This saves somewhat on mass but, in order to relax the necessity for comparatively rapid rolls at certain times, requires a certain off-pointing of the array to be allowed, thereby increasing its mass.

To account for the drop in performance due to radiation damage an annual degradation factor, f_{dg}, is assigned so that then the end of life power, after a mission time t_m in years, is given by

$$P_{eol} = P_{bol} (1 - f_{dg})^{t_m} \qquad \text{Eq 8.2}$$

The array can be typified by inverse specific power α_{ps} and an area-to-power ratio, β_{ps}, so that its mass and area are given by

$$m_{ps} = \alpha_{ps} P_{bol} \qquad \text{Eq. 8.3}$$

$$a_{ps} = \beta_{ps} P_{bol} \qquad \text{Eq. 8.4}$$

The values of f_{dg}, α_{ps} and β_{ps} used are the same as those used for the EOS2 platform definition, since the arrays are expected to be of the same type.

The power supplied by the array (which is typically between 5 and 50 kW for an electrically propelled spacecraft) is then processed and conditioned to provide the current and voltage required by the thruster. This conditioning is performed with an efficiency η_{pp} so that the power supplied to the thrusters is given by

$$P_t = \eta_{pp} P_{eol} \qquad \text{Eq. 8.5}$$

while the remainder is rejected as heat to the thermal control system and is given by

$$P_{tc} = (1 - \eta_{pp}) P_{eol} \qquad \text{Eq. 8.6}$$

The mass of the power processing sub-system is then given by

$$m_{pp} = \alpha_{pp} P_{eol} \qquad \text{Eq. 8.7}$$

η_{pp} is generally fairly high, typically 0.9 for ion thrusters and higher for arcjet systems. The power processor inverse specific power, α_{pp}, varies much more with the type of propulsion system. Arcjets operate typically at voltages of the order of 100 volts and currrents in the 10-100 amp range while MPD arcjets use even higher amperages. Ion thrusters, however, use operating voltages measured in kilovolts and have beam currents of only a few amps.

It is likely that the power processing unit would be implemented as a number of units in parallel since, in the wider context of operating multiple electrically propelled vehicle configurations, this allows the unit to be sized to the mission power without the need for a specialised design. It also increases reliability since the failure of a single module would only reduce the power available rather than make it zero.

The thermal control system is required to remove the excess heat produced during the power processing and will probably take the form of a base plate on which the power supplies are mounted, cooled by heat pipes which transfer the heat to a radiator plate. Ideally, this plate is orientated so that its larger surface it is normal to the direction of the Sun. The thermal control system can be characterised

by an inverse specific power α_{tc}, typically in the range 10 to 15 kg.kW^{-1}, so the mass of the power processing system is given by

$$m_{tc} = \alpha_{tc} P_{tc} \qquad \text{Eq. 8.8}$$

The thrusters are used for both primary propulsion and attitude control, a feature of several electric OTV designs (Zafran et al. [96], Hermel et al.[94]), which requires them to be gimballed. Attitude control is performed during periods when the service vehicle is in sunlight. During eclipse the vehicle attitude is allowed to drift uncontrolled. On emergence from eclipse the solar array reacquires the sun vector independently of the service vehicle attitude control which ensures power will be available. The correction of attitude control errors is done so at the expense of some propellant in excess of that required for the main propulsion. Irrespective of the actual type of propulsion selected, the thrusters can be characterised by an inverse specific power, an efficiency and an exhaust velocity, α_t, η_t and v_e, respectively. These vary considerably depending on the type of thruster and its operating conditions and are described in more detail in the next section. The beam power is given by

$$P_b = \eta_t P_t \qquad \text{Eq. 8.9}$$

while thrust developed is given by

$$F = \frac{2 P_{eol} \eta_{pp} \eta_t}{v_e} \qquad \text{Eq. 8.10}$$

The mass of the thrusters is

$$m_t = \alpha_t P_t \; int\left(\frac{t_b}{l_t} + 0.5\right) \qquad \text{Eq. 8.11}$$

where l_t is the lifetime of the thrusters and the int term accounts for the number of thruster sets needed to give the necessary burn time. The propellant mass flow rate is given by

$$\dot{m}_p = \frac{2\,P_b}{v_e^2} \qquad \text{Eq. 8.12}$$

The tanks contain the propellant used by the thrusters, the mass of which is a function of the payload, mission Δv, and thruster exhaust velocity. The mass of the tankage is defined by a tankage fraction, f_{tk}, which varies between 0.01 and 0.16 depending on the propellant being used (Jones [55] and Manvi and Fujita [97]). Hence, the tankage mass is given by

$$m_{tk} = f_{tk}\, m_p \qquad \text{Eq. 8.13}$$

Although the thrusters can be used for service vehicle attitude control during nodal transfer, they are not sufficient on their own since fine control is necessary as the vehicle approaches and docks with the polar platform. An additional close-quarters manoeuvring system is needed, therefore, for performing the approach over the last five hundred metres. The first stage of the docking (five hundred metres to twenty metres) is assumed to be performed by storable bipropellant propulsion. A water electrolysis system using electricity to produce hydrogen and oxygen was also considered but the mass penalty incurred because of the extra tankage and the electrolysis make this unattractive (as demonstrated by Feconda and Rauscher [30]). The final stage of docking, from twenty to zero metres, must be performed using a cold gas system to prevent plume impingement. Assuming that the approach is made along the +/- v bar (i.e.along the orbit track) and that the whole docking must be performed in half the maximum sunlit period of this orbit (approximately 40 minutes) as suggested by Blais et al. [98] then the Δv required is approximately 0.25 $m.s^{-1}$ for the first stage and 0.01 $m.s^{-1}$ for the second. The final velocity at contact should be below 1 $cm.s^{-1}$ with the acceleration level not exceeding 1 $cm.s^{-2}$ to minimise placing excessive manoeuvring or contact loads on either spacecraft.

The total mass of either the bipropellant or cold gas system is given by the sum of the thrusters, the propellant and the tankage.

$$m_{ms} = m_{m.th} + m_{m.prop} + m_{m.tk} \qquad \text{Eq. 8.14}$$

The mass of the thrusters is a function of the mass of the spacecraft, m_{sc}, the maximum acceleration level, a'_{max}, and the specific thrust of the thrusters, $\alpha_{m.th}$. This last usually lies in the range 0.005 - 0.018 $kg.N^{-1}$ for bipropellant thrusters and 0.003 $kg.N^{-1}$ for cold gas systems. Thus,

$$m_{m.th} = N m_{sc} a'_{max} \alpha_{m.th} \qquad \text{Eq. 8.15}$$

where N is the number of thrusters in the network. The mass of propellant needed is given by the rocket equation so that

$$m_{m.prop} = m_{aum}\left(1 - e^{\frac{-\Delta v}{v_e}}\right) \qquad \text{Eq. 8.16}$$

and the tankage is given by Eq. 8.13 applied to this mass using an appropriate tankage factor.

The TT&C mass is a constant as it depends primarily on the amount and rate of data transmission that is needed and this is not affected by changes in the vehicle size. For convenience, the electronics part of the GN&C system has been lumped in with this together with the necessary safe-hold batteries (assumed to be of advanced design, again the same as those used in the EOS2 platform design). The combined mass has been estimated as 200 kg.

The structure which underpins the service vehicle and its sub-systems is defined by a structure factor, f_s, so that the structure mass is given by

$$m_s = f_s m_{sv} \qquad \text{Eq. 8.17}$$

To work out the total wet mass of the vehicle (and also the tankage), it is necessary to know the propellant mass. This can be found from the rocket equation. Defining an attitude control propellant

factor, f_{ac}, the total mass of propellant, m_{pl}. is given by

$$m_p = \frac{(1 + f_{ac})\,(e^{\frac{\Delta v}{v_e}} - 1)\,m_o}{e^{\frac{\Delta v}{v_e}}} \qquad \text{Eq. 8.18}$$

Beyond the actual mass and power modelling of the service vehicle systems there are two major factors that may affect its performance. These are atmospheric drag and eclipsing. The drag will act on the service vehicle, in particular on the arrays. This can be counteracted fairly easily using the propulsion system for drag make-up, but acts so as to decrease the performance the vehicle. This will be dealt with in more detail later.

Depending on the orientation of the orbit, the vehicle may spend up to approximately one third of its orbit eclipsed by the earth and so be unable to generate power and thrust. This will prolong the time taken to perform a given orbital manoeuvre. The effect of this eclipsing can be modelled using an eclipse factor, f_{ec}, equal to the fraction of each orbit that the spacecraft is eclipsed. Including eclipse effects and the propellant used for attitude control, the total trip time is given by

$$t = \frac{m_p\, v_e^2}{2\,(1 - f_{ec})(1 - f_{ac})P_b} \qquad \text{Eq. 8.19}$$

8.3 Propulsion system characterisation

As already discussed in Chapter 5, ion thrusters, arcjets and MPD arcjets are possible choices for the service vehicle propulsion system. In terms of the service vehicle model, these can all be characterised by their respective inverse specific powers and their efficiencies, since these control the mass of thruster needed and the input power to produce a given thrust (and hence size of array needed). Another important factor in selection of propulsion systems is form and quality of the input that they need, both in terms of power and propellant. As outlined in the previous section, if the power from the power source only needs minimal modification then the inverse specific power of the power processor will be low, so reducing overall mass. Similarly, if the propellant is compact and easily storable then it will have a small tankage fraction which again decreases the mass of the service vehicle. A final, but very important factor, is the thruster lifetime since this effectively limits the maximum burn time that may be used on a single mission.

A database containing information on all these factors has been assembled covering all three of the candidate propulsion systems. This was assembled from data given in the following; Kaufman and Robinson's summary of their performance predictions for large inert-gas thrusters [99]; Burton et alia's measurements of MPD thruster performance using argon as the propellant [100]; Poeschel and Hyman's comparison of a wide range of electric propulsion technologies [54]; DeVincenzi et alia's systems level analysis of the USAF Elite vehicle [56]; Manvi and Fujita's comparison of ammonia and hydrogen arcjets and xenon ion thrusters used as part of a nuclear-electric propulsion system (NEP) [97]; Sponable and Penn's case study of GPS satellite emplacement using either xenon ion thrusters or ammonia arcjets [75]; Free's examination of NEP arcjet and ion systems for near-earth operations [100]; Smith and Knowles' study of electric propulsion concepts for near-term applications [101]; Beattie et alia's report on the current status of xenon ion propulsion technology [102]. From this database curves of inverse specific power and efficiency versus exhaust velocity were derived for each thruster type. These are shown overleaf in Figures 8.1 and 8.2.

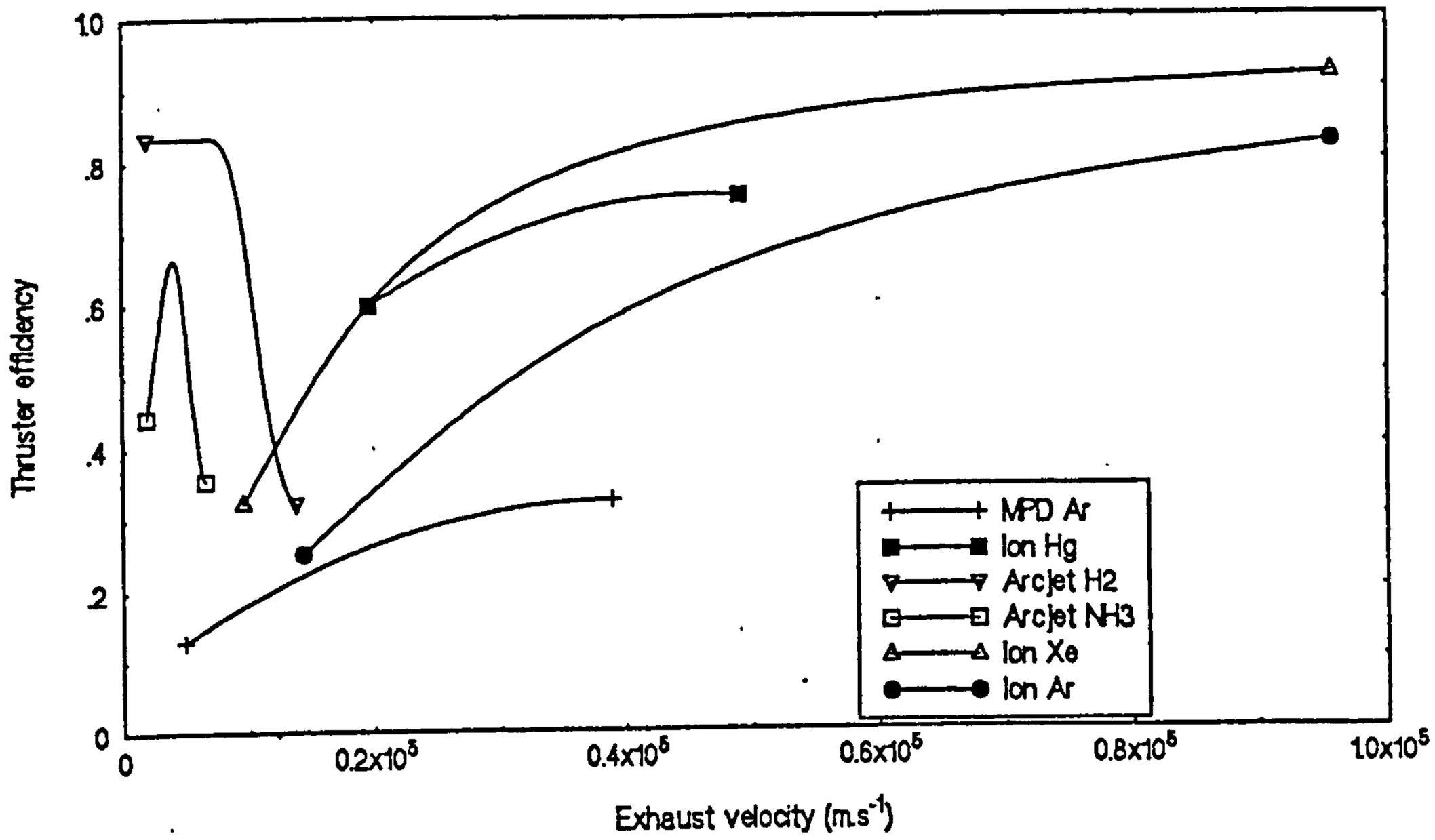

Figure 8.1 Thruster efficiency vs. exhaust velocity

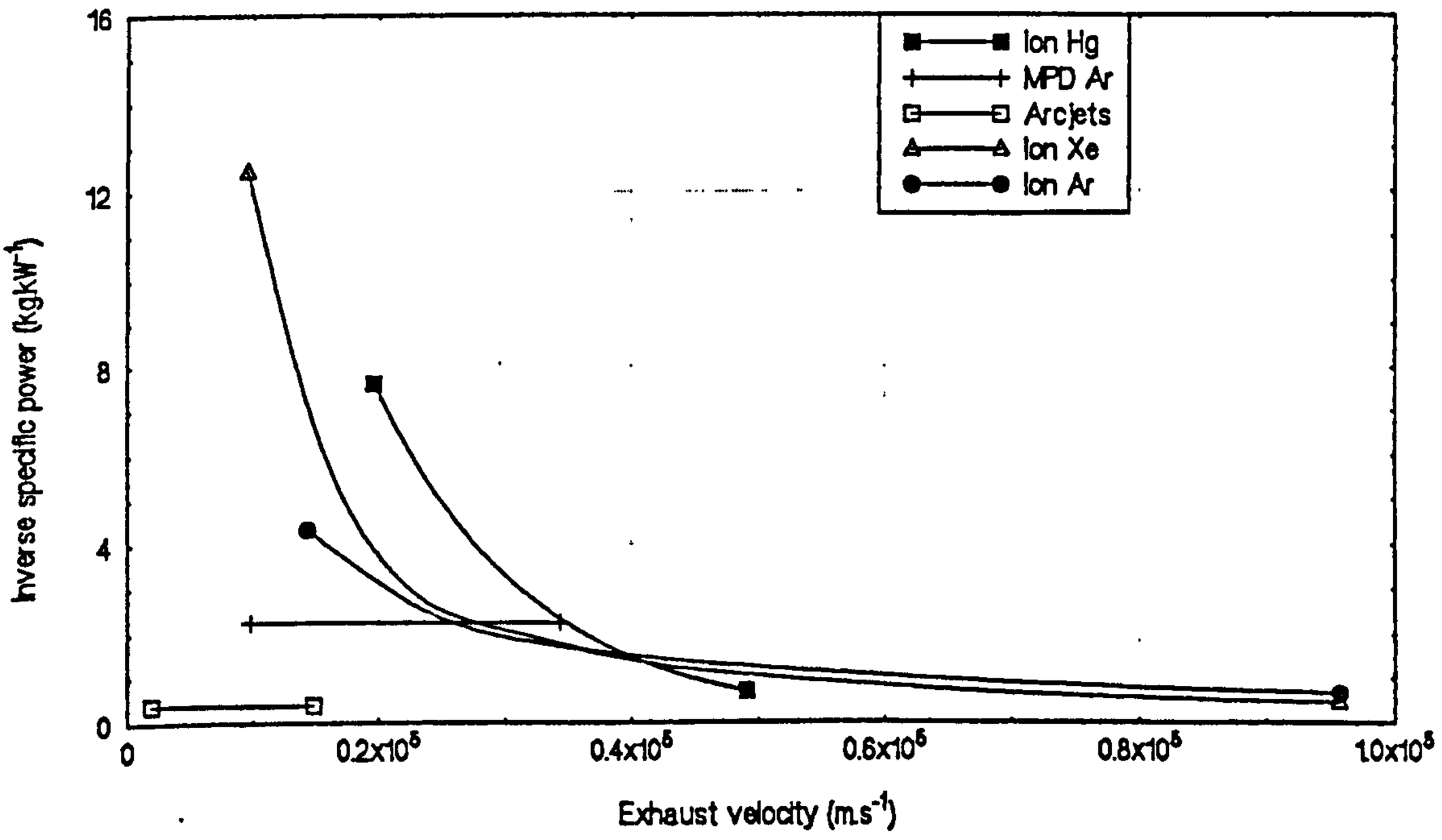

Figure 8.2 Thruster inverse specific power vs. exhaust velocity

As can be seen, ion thrusters have the widest range of exhaust velocities of the three types of propulsion system. Their inverse specific power decreases with increasing exhaust velocity while that of the other two system types is (approximately) constant. The efficiency of ion systems increases with exhaust velocity since this is controlled by the accelerating voltage and the higher this is the more ions are extracted from the plasma. The same increase in efficiency with exhaust velocity holds true for MPD arcjets. This is because the fraction of propellant that can be ionised at a given mass flow increases with increasing power. The efficiencies of thermal arcjet systems are strongly dependent on propellant properties and operating temperature. This means that their performance tends to be maximised over comparatively small exhaust velocity ranges when compared to ion and MPD thrusters.

The various propellants under consideration have different advantages and disadvantages. For the ion systems, mercury is a highly attractive propellant as it has a very small tankage fraction, but environmental considerations probably preclude it from use in near-Earth operations. Xenon is also a good propellant for ion thrusters, though its tankage fraction is over ten times that of mercury. It is also somewhat costly and, at the moment, not necessarily available in large quantities. Argon is a possible propellant for both ion systems and MPD arcjets. It has an average tankage fraction but must be stored cryogenically which may prove a disadvantage for missions with long durations, despite improvement in storage technology. Hydrogen also needs to be stored cryogenically, and its low density means that it has a poor tankage fraction. Lastly, ammonia is comparatively easy to store and has an average tankage fraction. The actual values of tankage fractions used are summarised overleaf in Table 8.1.

Thruster lifetime is also a major concern. Ion thrusters have significantly better lifetimes than arcjets (either MPD or otherwise). At the moment the upper limits are typically around 15,000 hours for the former and 7000 hours for the latter. Future developments should extend these considerably. Lifetimes of the order of 25,000 hours should be achievable for ion thrusters and 12000 hours for arcjets have been predicted by Hermel et al. [94].

8.4 Service vehicle model baseline parameters

The baseline values used as inputs to the service vehicle model are given below in Table 8.1.

Table 8.1 - Baseline service vehicle parameters

Solar array:	Inverse specific power		12.3	$kg.kW^{-1}$
	Area-to-power ratio		3.3	$m^2.kW^{-1}$
	Annual degradation		0.02	yr^{-1}
Power processor:	MPD/arcjet specific mass		0.25	$kg.kW^{-1}$
	Ion specific mass		10	$kg.kW^{-1}$
	Efficiency		0.9	
Thermal control:	Specific mass		11.4	$kg.kW^{-1}$
Thrusters:	Efficiency		From Fig 8.1	
	Specific mass		From Fig 8.2	
	MPD/arcjet lifetime		12,000	hours
	Ion thrusters		25,000	hours
Propellant:	Attitude control fraction		0.04	
Tankage:	Tank. fraction	Mercury	0.01	
		Xenon	0.12	
		Argon	0.1	
		Hydrogen	0.16	
		Ammonia	0.12	
Close man. system:	Max. acceleration		0.01	$m.s^{-2}$
	Tankage fraction		0.1	
	No of thrusters		12	
	Δv		4/0.08[$]	$m.s^{-1}$
	Specific thrust		0.01/0.005*	$kg.N^{-1}$
	Exhaust velocity		3200/750*	$m.s^{-1}$
TT&C/GN&C:	TT&C mass		145	kg
	GN&C mass		40	kg
	Batteries		15	kg
Structure:	Structure fraction		0.1	

* - Figures for: Bipropellant approach system/Cold gas docking system
$ - Per servicing cycle

8.5 Servicing propulsive requirements

Before a service vehicle can be defined using the model described in section 8.2 it is necessary to know what propulsive requirements it will have, namely what Δv it needs to perform a particular baseline scenario and at what acceleration levels. Here this translates into a need to determine the out and back manoeuvres necessary to obtain the required nodal alterations over the required time.

The eastwards differential nodal drift rate of the servicing vehicle is limited by the lowest altitude at which the vehicle can operate. As stated in Chapter 6, Martin and Cresdee [32] have determined 300 km to be a realistic lower altitude limit for electrically propelled vehicles. This limit has been adopted as a baseline here. It is assumed that the EOS2 operational orbits are the same as those for EOS1 and are hence characterised by an altitude of 824 km and an inclination of 98.7°. Given these conditions, for an optimum nodal alteration manoeuvre, the downward Δv may not exceed 330 $m.s^{-1}$ (see Fig. 6.11). The upward manoeuvre necessary to return the service vehicle to the EOS orbit can be shown to have the same Δv needed as for the downward manoeuvre.

The relative arrangement of the lines of nodes of the EOS2 orbits is shown overleaf Figure 8.3, with the orbits denoted A, B and C respectively. The line of nodes of each orbit will precess constantly with time (but maintain uniform separation from the other two) at a rate designed to give constant upward local equatorial crossing times (1000, 1330 and 2130 hours for A, B and C respectively). This uniform separation of the ascending nodes is as follows;

AB	52.5°
BC	120.0°
CA	187.5°

For an eastwards servicing sequence, A-B-C, (since nodal transfers are more efficient in the eastwards direction, as stated earlier) the total mission Δv is the sum of the six transfer Δvs that are

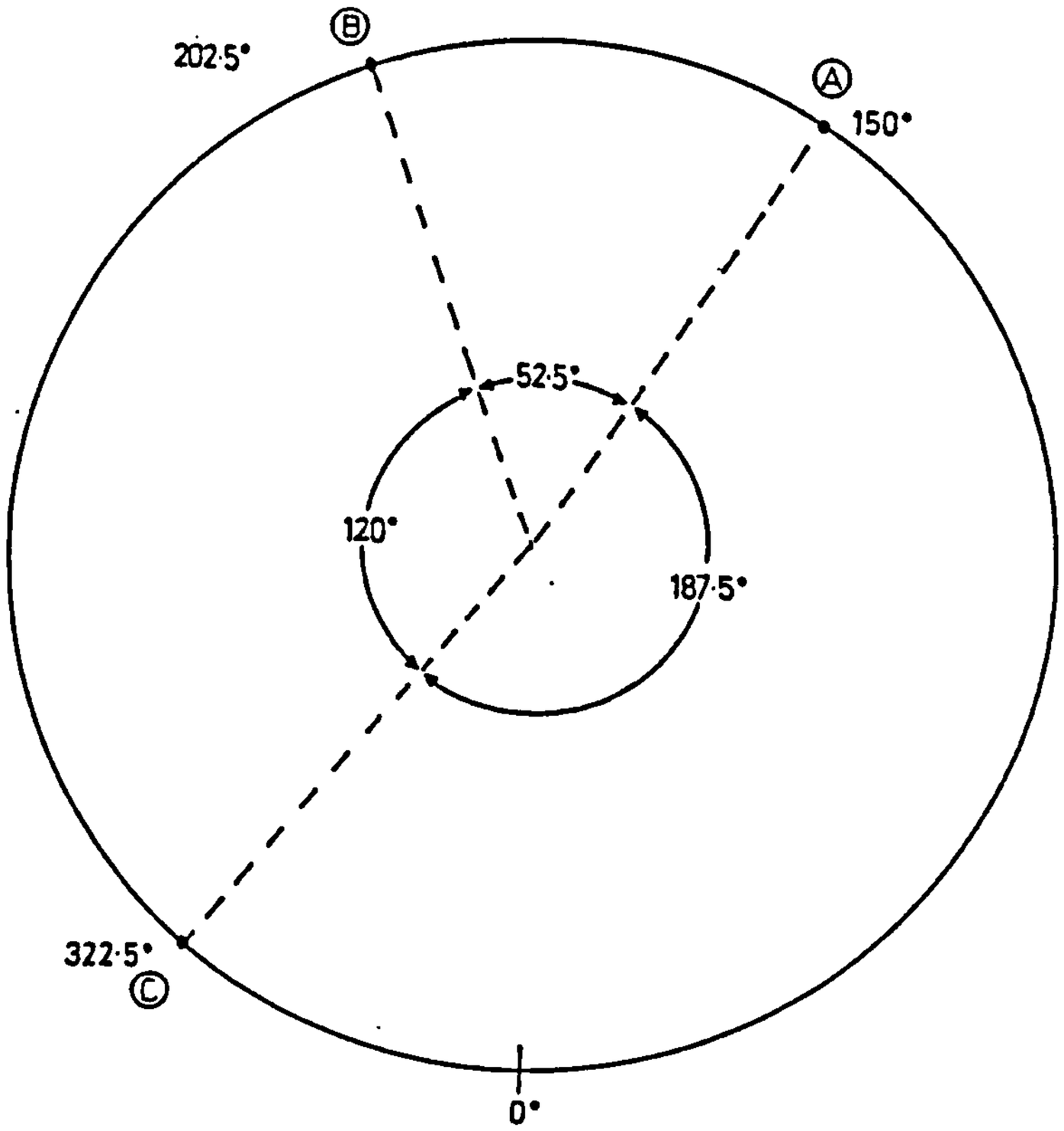

Figure 8.3 Relative orientation of EOS2 lines of nodes

required for three transfers to and back from the drift orbits. The total constellation servicing period is taken to be three years (the same as that for EOS1, given by Scolese [77]). Allowing seven days for each service then the service cycle total transit time is 1075 days.

Each nodal transfer operation can be considered to consist of three periods; two identical burn periods (with the same Δv) at the beginning and end of the transfer and a drift period in the middle. Under these circumstances, the change in ascending node of the servicing vehicle is then given by

$$\Delta\Omega = 2\dot{\Omega}_{dd}\, t_b' + \dot{\Omega}_d\, t_d \qquad \text{Eq. 8.20}$$

with the limits that

$$t_t = 2t_b' + t_d \quad \textit{and} \quad 0 \le t_b' \le \frac{t_t}{2} \qquad \text{Eq. 8.22}$$

We have seen in Chapter 6 that the relation between the drift orbit drift rate, the mean differential nodal rate and other factors is typically somewhat complex. For the purposes of defining mission parameters for this servicing mission it is sufficient to observe that, for optimum nodal manoeuvres over the Δv range of interest, there is an approximately linear relation between both of these and the manoeuvre Δv. This is shown in Figures 8.4 and 8.5 overleaf for both eastward and westward transfers. This linearity allows the Δv necessary for a particular eastwards nodal alteration to be approximated by

$$\Delta v_{east} = \frac{\Delta\Omega}{0.00127\ (t_t - 1.06\, t_b)} \qquad \text{Eq. 8.23}$$

and the Δv for a westwards nodal manoeuvre to be given by

$$\Delta v_{west} = \frac{\Delta\Omega}{0.00090\ (t_t - 1.06\, t_b')} \qquad \text{Eq. 8.24}$$

where Δv is in $m.s^{-1}$, $\Delta\Omega$ is in degrees and t_t, t_b are in days.

Although the equations for westward nodal transfers are also quoted here, such transfers have

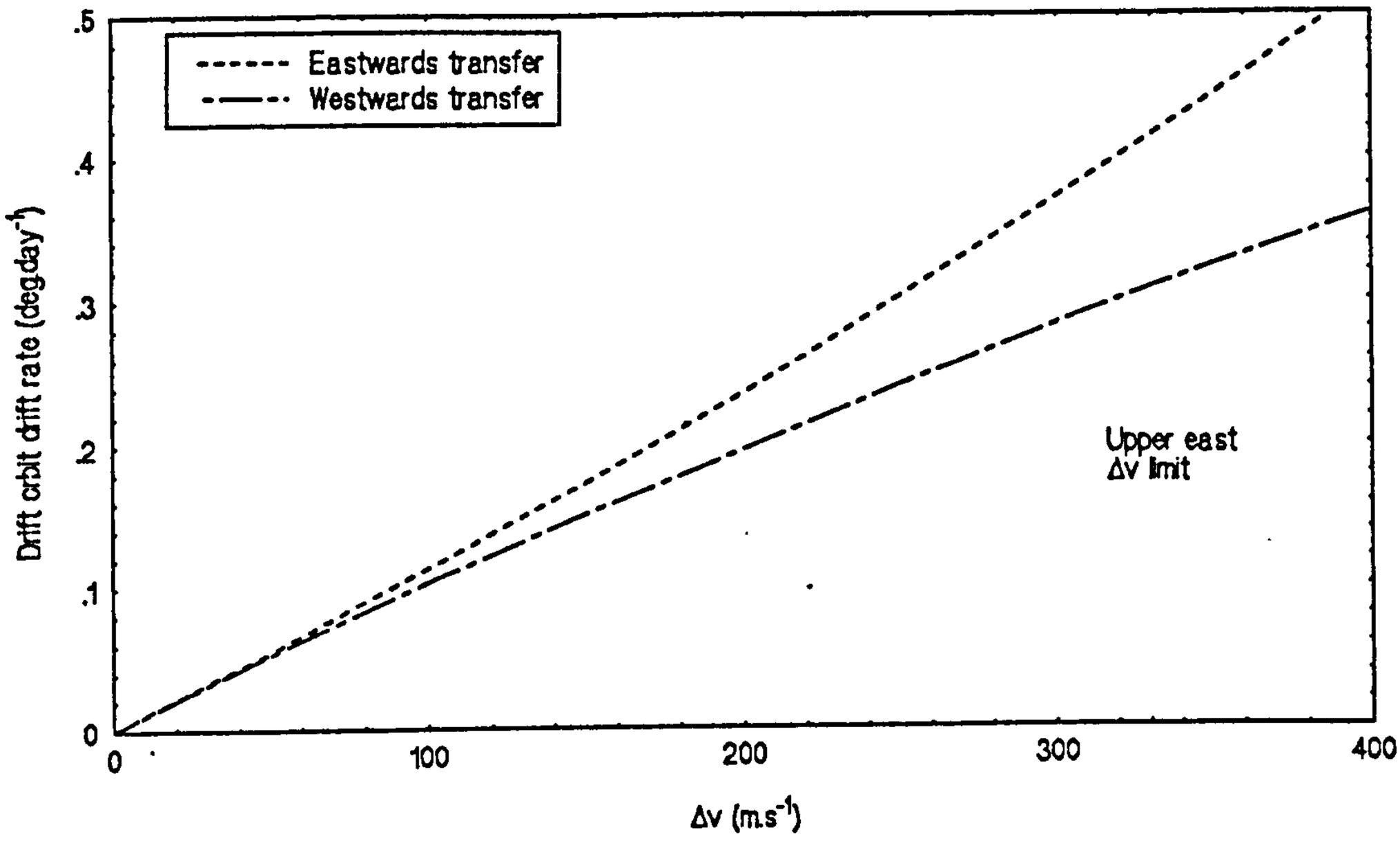

Figure 8.4 Drift orbit drift rate versus Δv for optimal nodal transfers

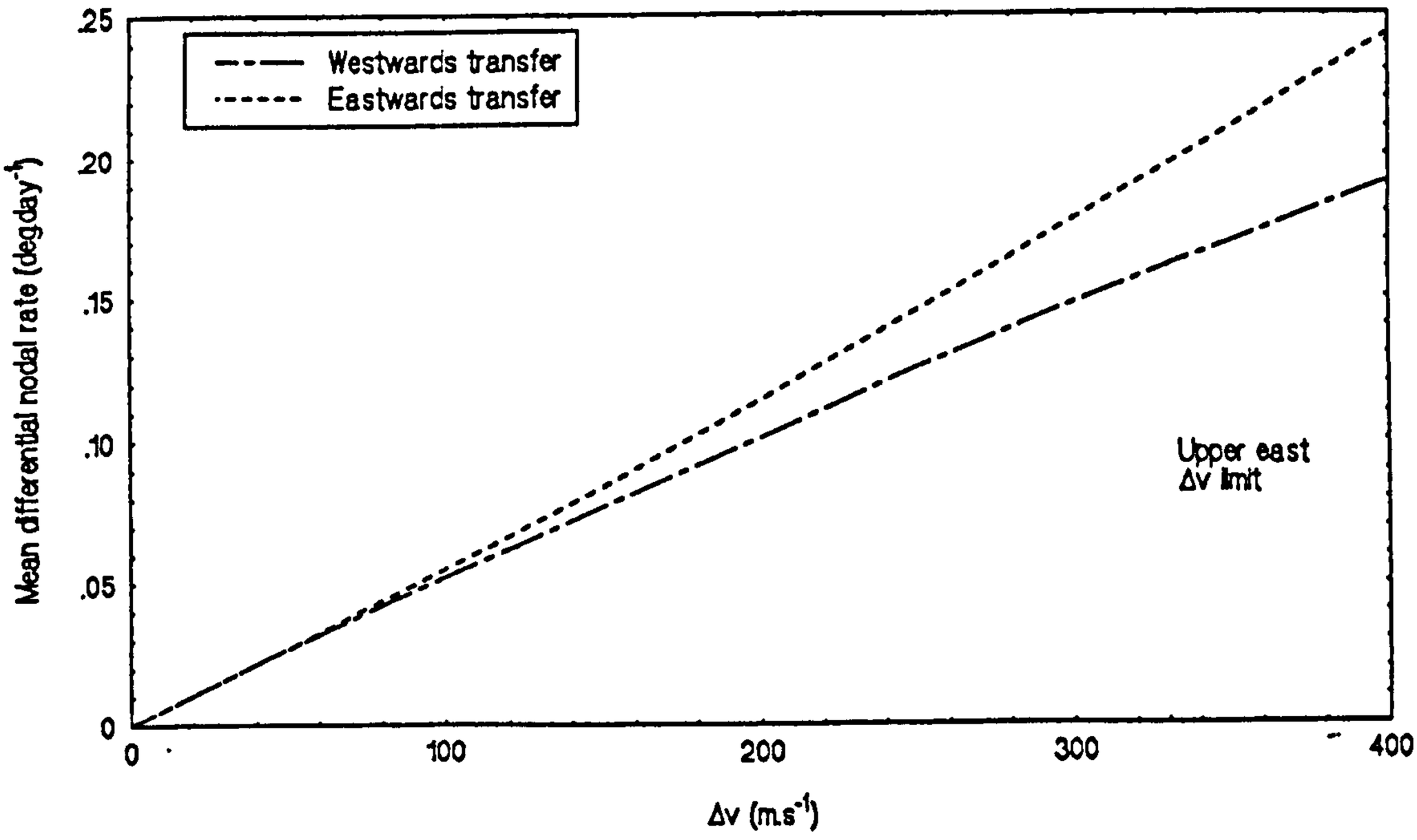

Figure 8.5 Mean differential nodal drift rate versus Δv for optimal nodal transfers

not been investigated. This is because these would require the service vehicle and payload to spend protracted periods within the lower of the two Van Allen belts. As already mentioned in Chapter 5, it is conceivable that solar arrays that are largely immune to radiation damage may be designed. However, the effects of extended exposure (ranging from approximately two to seven years depending on the service scenario) on other service vehicle electronic systems and, in particular, on the payloads are likely to be sufficiently severe to make this option very unattractive.

It can be seen that Δv is minimised by making t_t as large as possible and t_b as small as possible. This is equivalent to an impulsive transfer to a drift orbit where, since a long time is spent on the transfer, only a small differential drift rate is required. Impulsive manoeuvres are the simplest to estimate. They may be calculated by sizing them in same proportions as the angular separation. For eastward transfers this gives the following

	t_t(days)	$d\Omega/dt$ (deg/day)	Min Δv ($m.s^{-1}$)
AB	156 days	0.335	267
BC	358 days	0.335	267
CA	560 days.	0.335	267

There is no reason, a priori, why all transfers need to be performed at the same rate. Graves et al. [36] has shown that, for impulsive manoeuvres, transfers between closer orbits should be performed at lower rates and those between further orbits at higher ones so that the sum of the rates in minimised. In the EOS2 case this gives

	t_t(days)	$d\Omega/dt$ (deg/day)	Min Δv ($m.s^{-1}$)
AB	244	0.215	172
BC	355	0.338	260
CA	461	0.407	325

which offers a 5.5% decrease in mission Δv requirement.

However, although this arrangement gives the minimum Δv mission, the manoeuvres are all impulsive. For electrically propelled spacecraft we are also interested in the acceleration levels. The relation between Δv and acceleration is given by

$$\Delta v = 86400\, a' t_b' \qquad \text{Eq. 8.25}$$

so that the eastwards and westwards acceleration levels are given by

$$a'_{east} = \frac{\Delta\Omega}{107.93\, t_b' (t_t - 1.06\, t_b')} \qquad \text{Eq. 8.26}$$

$$a'_{west} = \frac{\Delta\Omega}{78.02\, t_b' (t_t - 1.06\, t_b')} \qquad \text{Eq. 8.27}$$

For EOS2 constellation servicing by electric propulsion we seek the combination of transfer times, burn times and acceleration levels that allow us to perform the mission in the specified service time. Since we are using an power-limited propulsion system we wish to do this at as low an acceleration level as possible and we approximate this acceleration level as a constant throughout the mission. Considering eastward transfer solely, we can combine equations 8.25 and 8.26 which allows us to plot acceleration level and manoeuvre Δv against manoeuvre time to obtain Figure 8.6, shown overleaf. It can be seen that, as expected, the Δv is minimised by maximising the acceleration level and performing an impulsive transfer between operational and drift orbit. As the manoeuvre time increases so does the Δv required for the manoeuvre. This is because less time is being spent in the drift orbit so that a higher differential drift rate must be obtained for this period. In order to achieve this a drift orbit that is further away in terms of inclination and altitude must be used and so a higher Δv is needed to transfer to and from it.

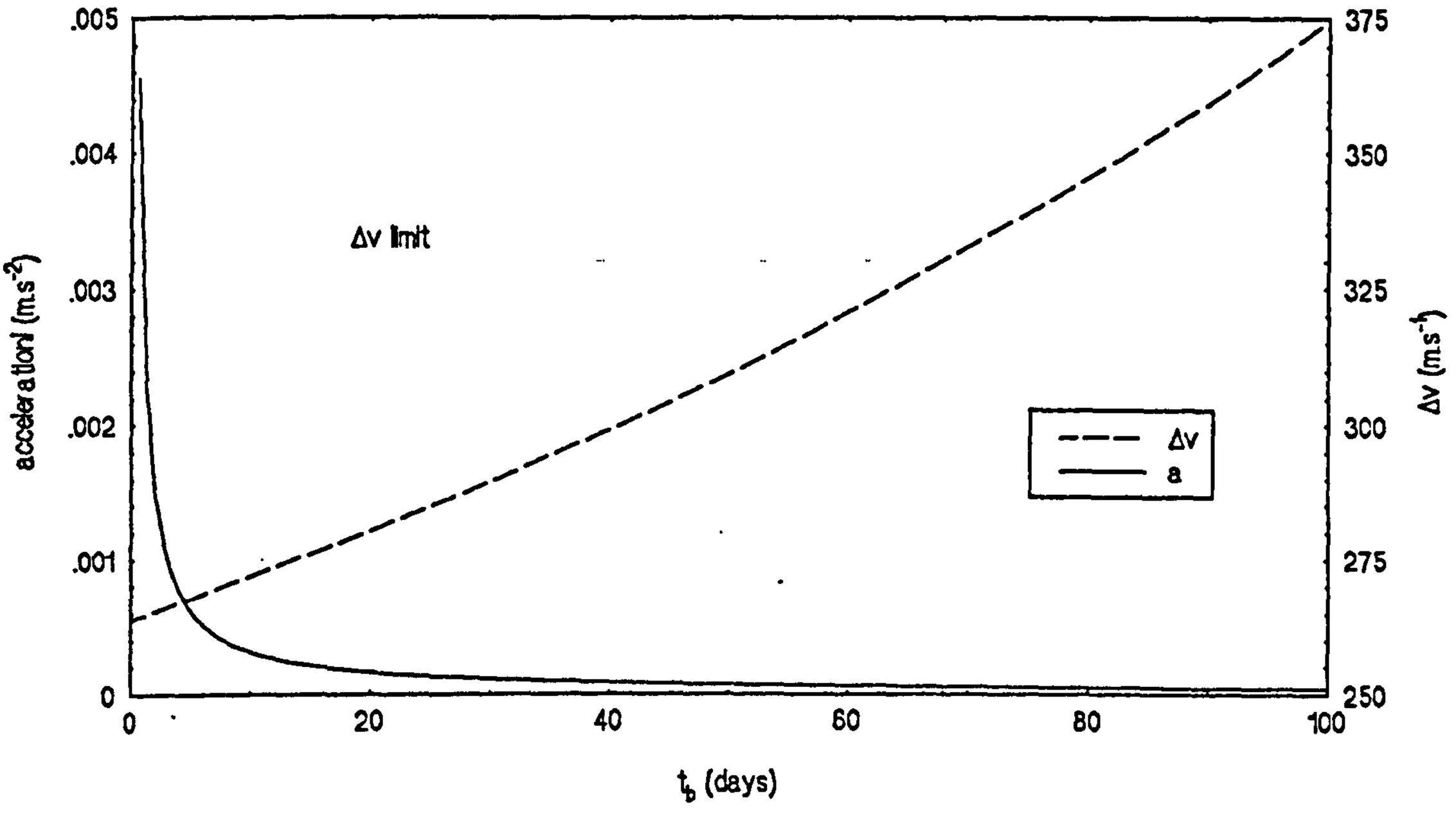

Figure 8.6 Acceleration level and Δv versus manoeuvre time for eastwards nodal transfers.

8.6 Effects of atmospheric drag

The effects of atmospheric drag must now be taken into account, since they effect the propulsive requirements of the service vehicle. These effects exhibit themselves in two distinct phases; firstly, during the manoueuvring between EOS2 orbit and the drift orbit, and secondly during the period spent in the drift orbit. The latter is the dominant of the two effects since the service vehicle spends much longer in the drift orbit than it does manoeuvring, and it is in the drift orbit that the density is the higher.

Given this, it is apparent that, because of the exponential variation of density with altitude, that choosing the lowest propulsively possible drift orbit altitude may not be the best in terms of minimising the all-up mass (fully-fuelled service vehicle plus payload) to be launched by ELV. Since the drag depends on the array area, the mass of the spacecraft and the density of the atmosphere, and that the array area and mass depend, in part, on the drag make-up Δv it can be seen that the service vehicle model and the mission model are interdependent.

For both the manoeuvring phase and the drift phase the drag make-up Δvs were calculated using the following expression for the Δv required per revolution.

$$\Delta v_{drag} = \pi C_d \frac{A}{m_{sc}} \rho r v \qquad \text{Eq. 8.27}$$

The atmospheric density in the drift orbit in $kg.m^{-3}$ is given by

$$\rho = 1.916 \times 10^{-11} e^{\left(\frac{300 - h}{51.18}\right)} \qquad \text{Eq. 8.28}$$

where h is the drift orbit altitude in km. This gives a good approximation to the atmospheric density (under mean solar conditions) over the altitude range of interest. Given optimum nodal manoeuvres, the drift orbit altitude can be found from the manoeuvre Δv by

$$h = 824 - 1.58 \Delta v \quad km \qquad \text{Eq. 8.29}$$

For calculating the manoeuvring drag loss a mean atmospheric density over the change in altitude from the EOS2 orbit to the drift orbit (Δh) is given by the polynomial

$$\begin{aligned}\bar{\rho} = &+ 1.34 \times 10^{-21} \Delta h^4 \\ &- 4.94 \times 10^{-19} \Delta h^3 \\ &+ 7.99 \times 10^{-17} \Delta h^2 \\ &- 3.78 \times 10^{-15} \Delta h \\ &+ 7\ 1.42 \times 10^{-13}\end{aligned} \qquad \text{Eq. 8.30}$$

The equations above, those describing the propulsive requirements for the servicing missions and those defining the model of the service vehicle have all been linked into a single model servicing vehicle and mission model. The calculation of the service vehicle systems mass breakdown and mission characteristics using this model is an iterative process and usually requires several cycles to obtain convergence. In practical terms a given mission and service vehicle configuration were defined and the beginning of life array power manipulated to make the thruster burn time as calculated from the mission requirements and that as calculated from the service vehicle propulsive characteristics became identical.

These results of this procedure are outlined in the next section.

8.7 Performance of propulsion systems

Using the relationships describing the service vehicle, the mission propulsive requirements and those governing the effects of atmospheric drag incorporated them into a single model, the four servicing vehicle configurations may now be evaluated using the baseline data given in section 8.4 to investigate their performance with the different possible propulsion systems. On the first and third pages overleaf Figures 8.7 - 8.10 give the all-up mass against exhaust velocity for the alpha, beta, gamma and delta configurations respectively. In each case the curve is for a propulsion system is that for a mission using a 300 km drift orbit.

In the first case, for the alpha configuration, (payload 4500 kg, 1 servicing cycle) it can be seen that the xenon and mercury ion propulsion systems gives the best performance. Although the latter has a significantly better tankage fraction, this is offset by the elevated efficiencies that xenon thrusters demonstrate at higher exhaust velocities. The argon ion system gives the worst performance of the ion systems since it has a tankage fraction comparable with that of xenon, but does not demonstrate the same level of efficiency. The low mass of argon MPD power processor allows this thruster to better the argon ion system at low exhaust velocities (where the efficiency of both is quite low), but the latter is still capable of giving a smaller all-up mass. Of the two arcjet systems considered only the hydrogen is capable of giving even vaguely comparable performance due to its low thruster inverse specific power and high efficiency. The low efficiency and poor exhaust velocity of the ammonia arcjet make its performance very poor indeed. Only the extreme lower end of its curve is seen on Figure 8.7.

These factors hold true in the analysis of the other service vehicle configurations. The same overall relationship for the performance of the various systems holds for the beta configuration (payload mass = 13500 kg, 1 servicing cycle) as shown in Figure 8.8 overleaf, though the net differences in all-up mass are increased. The ion propulsion systems still give the best performance with the mercury and argon giving roughly equal minimum values for all-up mass. The performance of the MPD and argon ion system is also still roughly comparable. The effectiveness of arcjets has become still further

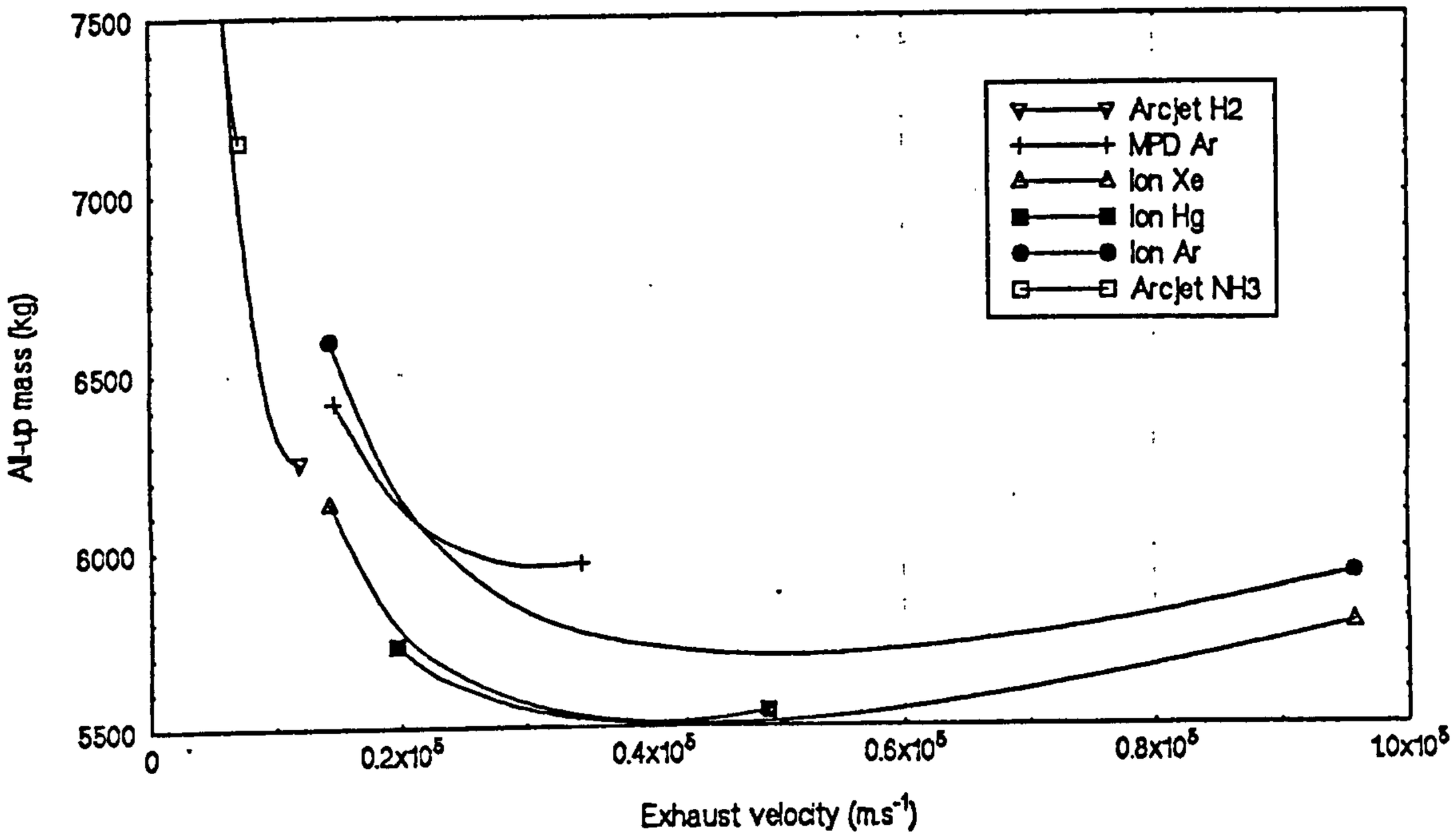

Figure 8.7 All-up mass vs. Exhaust velocity for alpha configuration

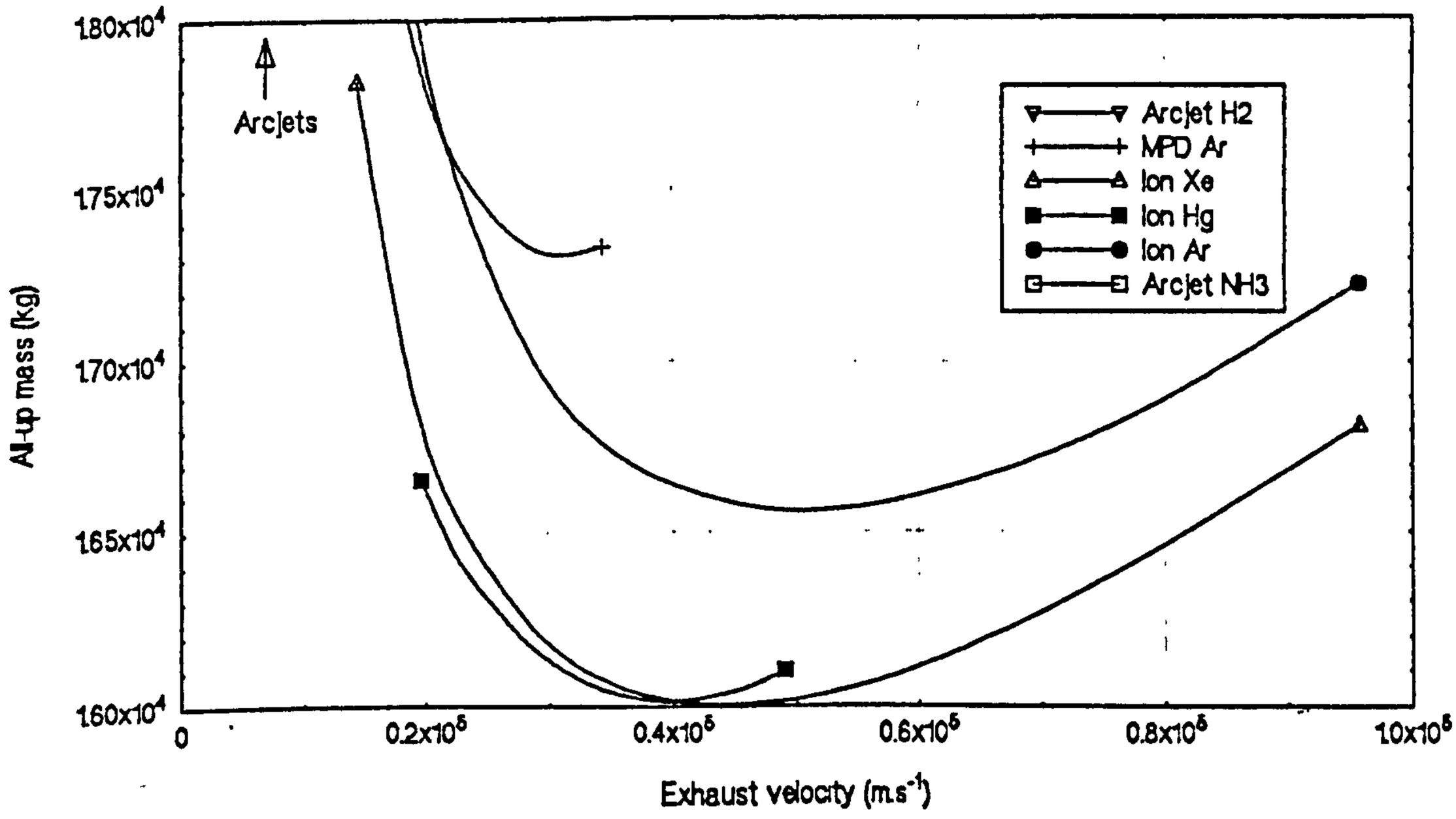

Figure 8.8 All-up mass vs. Exhaust velocity for beta configuration

marginalised with the increase in payload. Although not actually shown on the graph, the hydrogen arcjet gives no advantage over any of the other systems and the ammonia arcjet is worse still.

The arcjets have completely disappeared as meaningful propulsion systems for the gamma configuration (payload mass = 4500 kg, 3 servicing cycles), as shown in Figure 8.8 overleaf. The performance of the argon MPD system relative to the argon ion system remains approximately the same at low exhaust velocities, but neither are as good as the mercury and xenon ion systems. The superior tankage fraction of the mercury system is demonstrated by the fact that the all-up mass of mercury systems is less than that of the xenon system over its whole exhaust velocity range, though the argon system still retains its very slight advantage, again due to to its significantly higher efficiencies at higher exhaust velocities.

For the delta configuration (payload mass = 13500 kg, 3 servicing cycles) only the ion systems remain as worthwhile propulsion systems (See Figure 8.9 overleaf) with the xenon ion system giving the smallest all-up masses.

The above results hold true for servicing missions that use a 300 km drift orbit only, however. By choosing other drift orbit altitudes we may obtain different results. Figures 8.11 to 8.13 on the second and third pages overleaf show, for each mission scenario, the minimum all-up mass obtainable (i.e the lowest point on one of the curves in Figures 8.5 to 8.9) plotted over the drift orbit altitude range 300 to 380 km.

Examining Figure 8.11 we see that the results for the 300 km drift orbit hold true across the whole altitude range, with the mercury and xenon ion systems outperforming the others and the latter being very marginally superior. We also see that, although generally poor in performance, the variation in all-up masses for arcjet propelled service vehicles is much smaller than that for ion and MPD ones. This is because a higher drift orbit altitude means that a smaller Δv is needed to fulfil the servicing

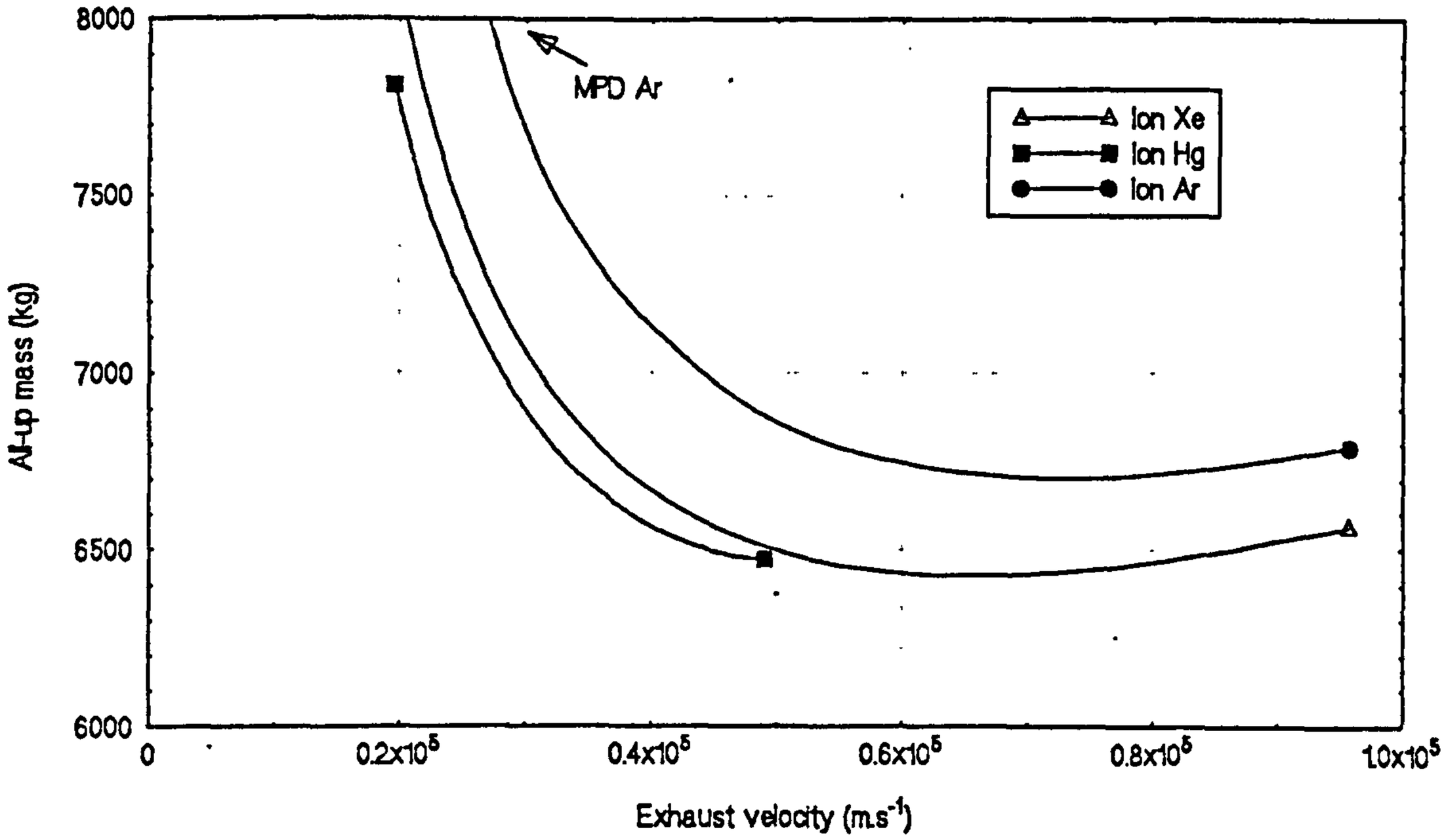

Figure 8.9 All-up mass vs. Exhaust velocity for gamma configuration

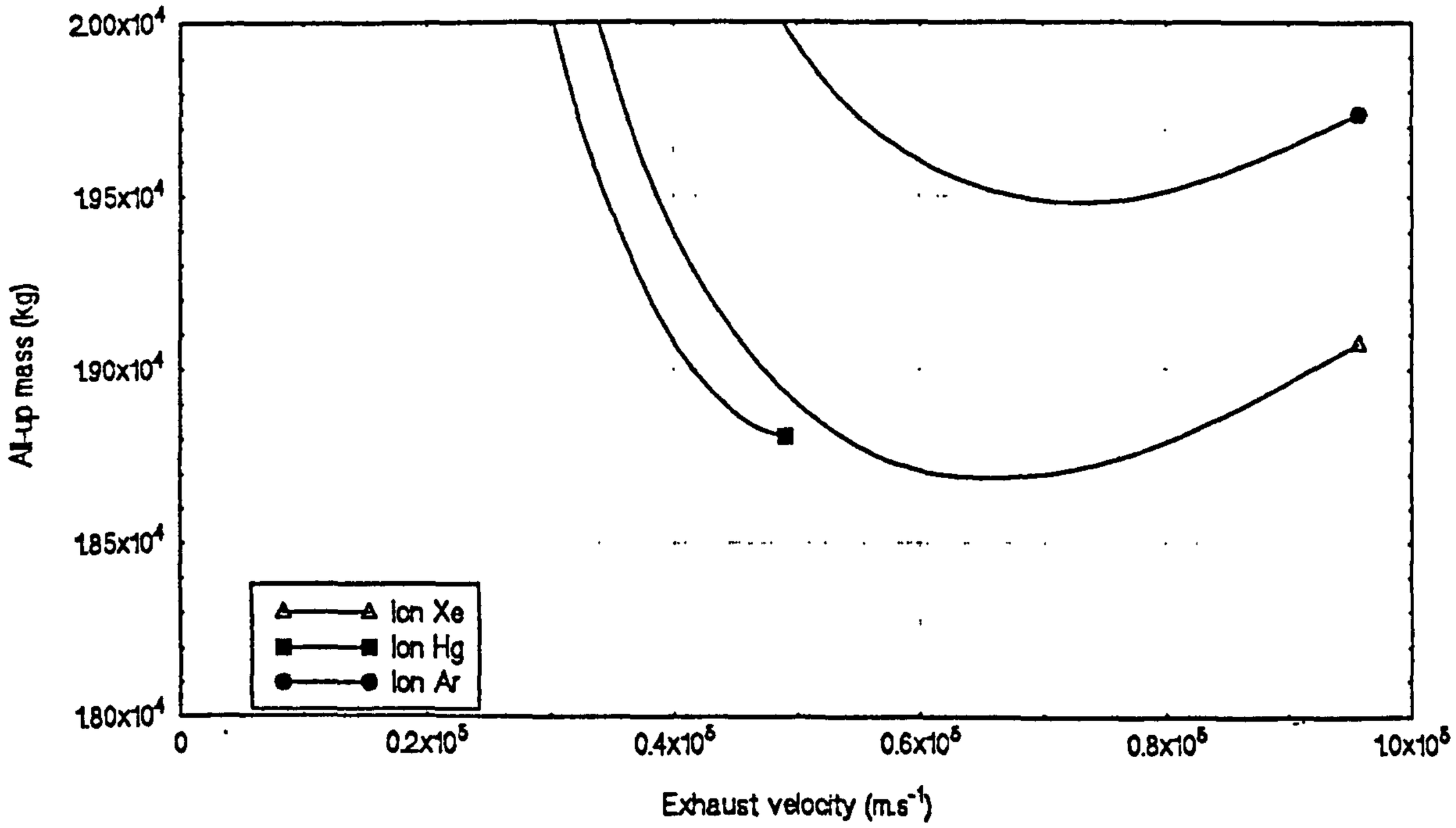

Figure 8.10 All-up mass vs. Exhaust velocity for delta configuration

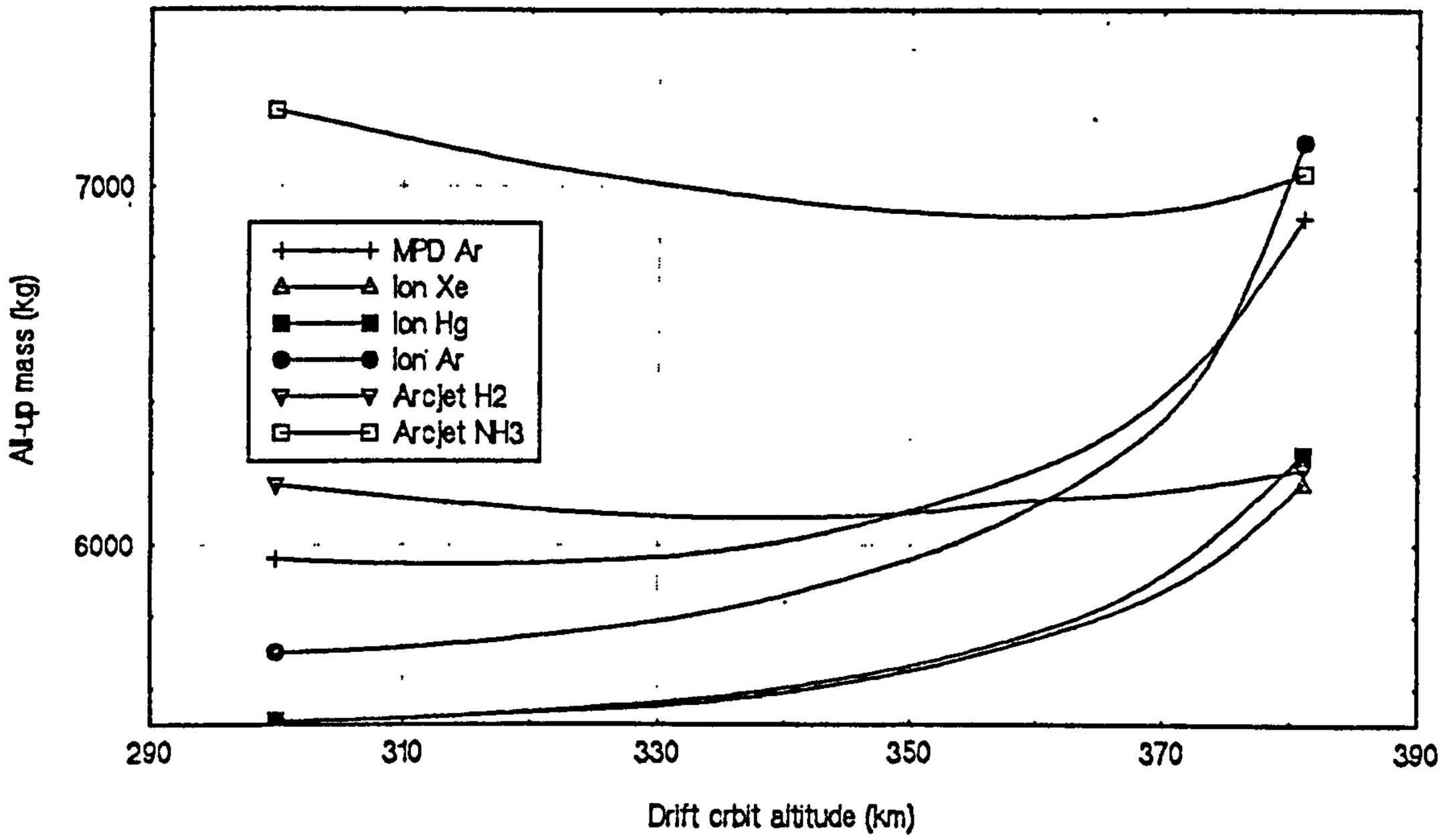

Figure 8.11 Best all-up mass vs. drift orbit altitude for alpha configuration

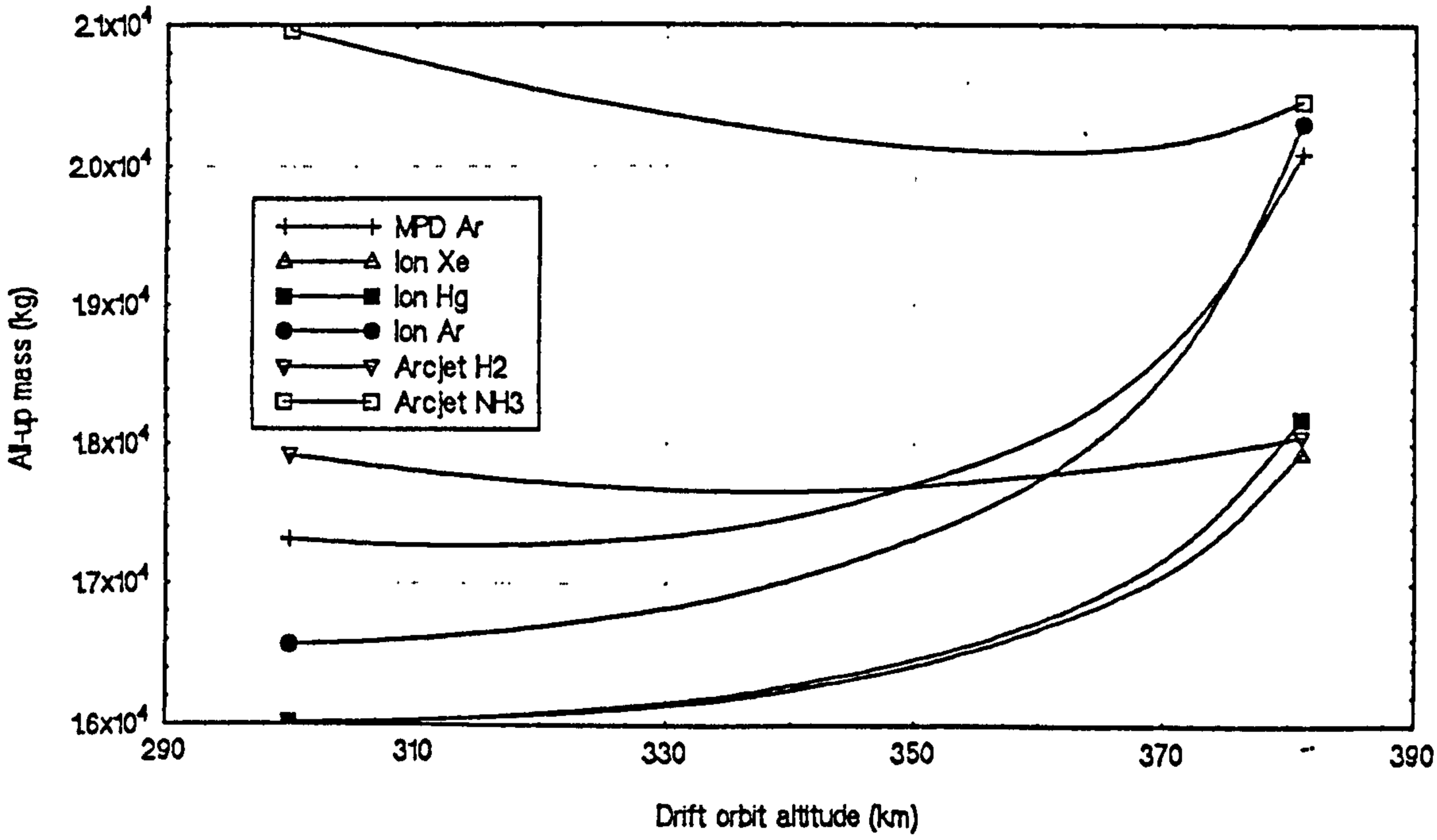

Figure 8.12 Best all-up mass vs. drift orbit altitude for beta configuration

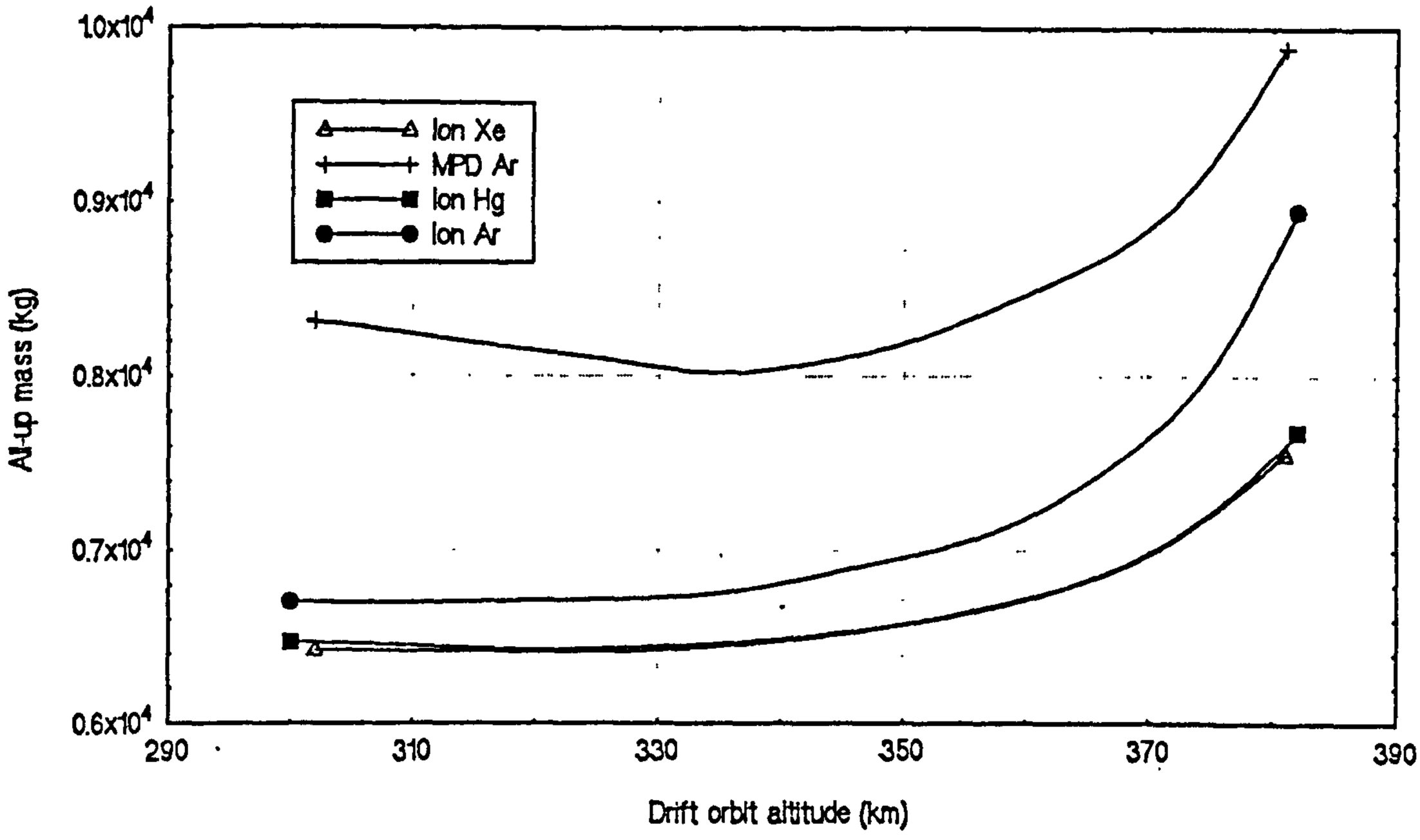

Figure 8.13 Best all-up mass vs. drift orbit altitude for gamma configuration

requirements, but that this must be applied in a much shorter period hence requiring a significantly higher acceleration level. These two factors combined militate against ion systems in particular. They must transfer to lower altitudes which are characterised by higher drag make-up Δvs, but not so much that they cannot be overcome by use of the more highly efficient ion propulsion systems. The MPD arcjet falls between these two cases, generally requiring around 50 to 100% more power than the ion system to counteract its low efficiency. This means that it suffers significantly more drag and cannot descend as far as ion systems without starting to suffer a resulting mass penalty.

Another factor worthy of consideration is the congruency between the results for alpha and beta, and gamma and delta configurations. This can be explained (to a first approximation) as follows. For a given alpha configuration transfer a particular Δv must be applied in a particular time and so is characterised by a particular acceleration level. Increasing the mass by some factor whilst requiring that this acceleration level be maintained requires that the thrust be scaled by the same amount. For a given configuration the thrust and array area are linearly related. This then means that the ballistic coefficient of the spacecraft remains the same, consequently so does the drag make-up Δv, and so does the overall servicing Δv. The net result is that if a particular combination of service vehicle parameters and drift orbit altitude give the minimum all-up mass for the alpha configuration they will also do so for the beta configuration, and will give the same total servicing Δv. The same relationship also holds true for the gamma and delta configurations.

From all of the above, it is apparent that an ion propulsion system should be selected for all configurations of the service vehicle since they offer by far the best all-up masses. Furthermore, the propellant of choice should be xenon since this gives the best performance (marginally) and is more acceptable for use in the near-earth environment than mercury.

The optimum exhaust velocity for the alpha and beta configuration is around 47800 $m.s^{-1}$, while for the gamma and delta configurations this figure rises to 57400 $m.s^{-1}$. Using these figures the four

service vehicle configurations can be established. These are summarised below in Table 8.2

Table 8.2 - Service vehicle configuration breakdown

Configuration	Alpha	Beta	Gamma	Delta
No of servicing cycles	1	1	3	3
ORU sets carried	1	3	1	3
Total Δv ($m.s^{-1}$)	2756	2756	8039	8039
Drift orbit altitude (km)	300	300	326	326
Array BOL power (kW)	15.3	44.5	26.6	77.1
Propulsion system	Ion	Ion	Ion	Ion
Propellant	Xenon	Xenon	Xenon	Xenon
Exhaust velocity ($m.s^{-1}$)	47800	47800	57400	57400
Thrust (N)	0.5	1.3	0.6	1.8
Payload mass (kg)	4500	13500	4500	13500
Propellant mass (kg)	320	933	872	2533
Service vehicle mass (kg)	689	1578	1041	2600
All-up mass (kg)	5509	16011	6413	18633

It can be seen from Table 8.2 that the alpha and gamma all-up masses are well within the baseline mass upload limitation of 15,000 kg into EOS2 orbit. The alpha configuration, however, provides only single servicing cycle capability while the gamma configuration provides three times this for a small (sixteen percent) increase in all-up mass. Unless there are very powerful external reasons for using the alpha mission scenario/service vehicle it appears to be of little further interest.

Both the beta and delta configurations of the service vehicle exceed the 15,000 kg baseline mass limitation. This does not discount their use, however, if the mission scenarios are altered to allow the vehicles to be placed into a lower orbit and then raising themselves to EOS2 orbit before commencing the servicing cycle. This requires an increase of around two percent in both cases. The same relation between beta and delta holds as between alpha and gamma, with the latter (in each case) offering significant improvements in performance for approximately ten percent more mass. Unless the ORUs could not be de-orbited on independently, necessitating the use of the service vehicle for this at the end

of each servicing cycle, there appears to be little benefit in favouring the beta scenario.

Given that the gamma and delta scenarios appear to be the most attractive, these have been selected for further investigation. The final choice between them would most likely be made on economic grounds after performing a trade-off between the greater flexibility in ORU upload given by multiple 'small' ELV launches (i.e one for each platform servicing) and the lower cost of of a single 'large' ELV (i.e one for each servicing cycle).

Chapter 9 - Simulation of orbit transfers

9.1 Introduction

This chapter outlines the results of simulating nodal manoeuvres using the ORBIT_CALC program. The effects of the various perturbations on transfers to and from an EOS orbit using the delta service vehicle are described and the implications for servicing missions discussed.

9.2 Comparison with predicted results

A comparison has been made between the results predicted by the theory developed in Chapters 6 and 8 to describe optimum nodal transfers. These are presented primarily with particular reference to nodal transfer manoeuvres related to the B platform. This is done because the B platform is 'closest' to the diurnal bulge in the atmosphere caused by the solar heating. This reaches its maximum at 1400 hours local time and its minimum 0300 hours local time. The ascending and descending node pass times for the B platform are 1330 and 0130 respectively. Because the EOS2 platform constellation ascending nodes/pass times are locked relative to the sun vector, the B platform passes much closer to the atmospheric density maximum and minimum. It therefore experiences greater variation in drag forces over an orbit than either the A and C platforms, leading more pronounced secular perturbation effects. The same holds true for service vehicles manoeuvring to and from it.

The A and C platforms experience broadly similar atmospheric density variations since their ascending nodes are almost 180° apart. The relative arrangement of the platforms, the sun and the diurnal maximum and minimum in the equatorial plane is shown overleaf in Figure 9.1.

The results of the service vehicle modelling carried out in Chapter 8 indicated that for the delta servicing vehicle a 55 day, 315 $m.s^{-1}$ manoeuvre to a drift orbit with an altitude of 320 km and an inclination of 99.5° would give the required conditions for performing the servicing mission. Figure 9.2

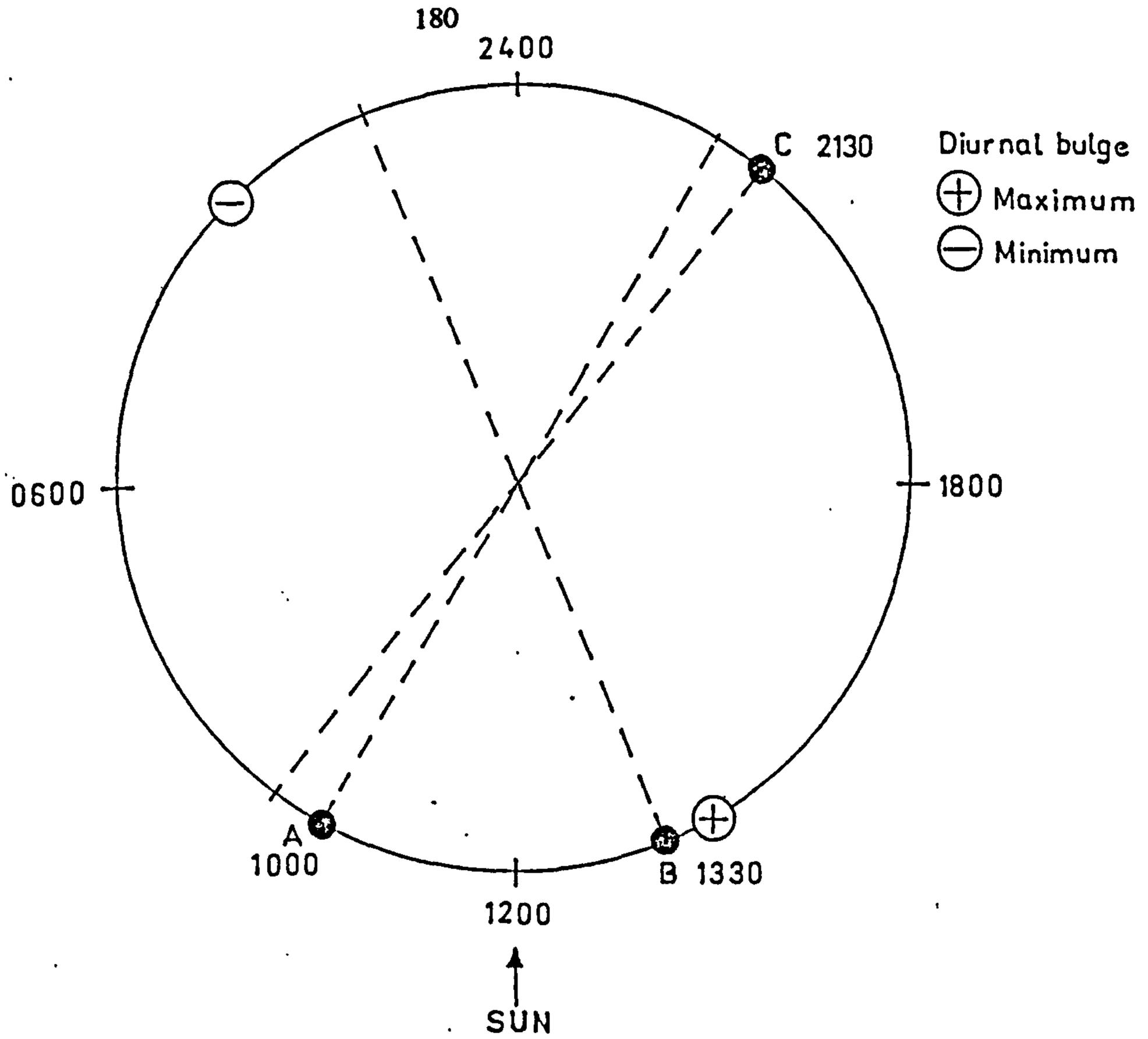

Figure 9.1 Relative positions of platform ascending nodes, Sun, and diurnal bulge.

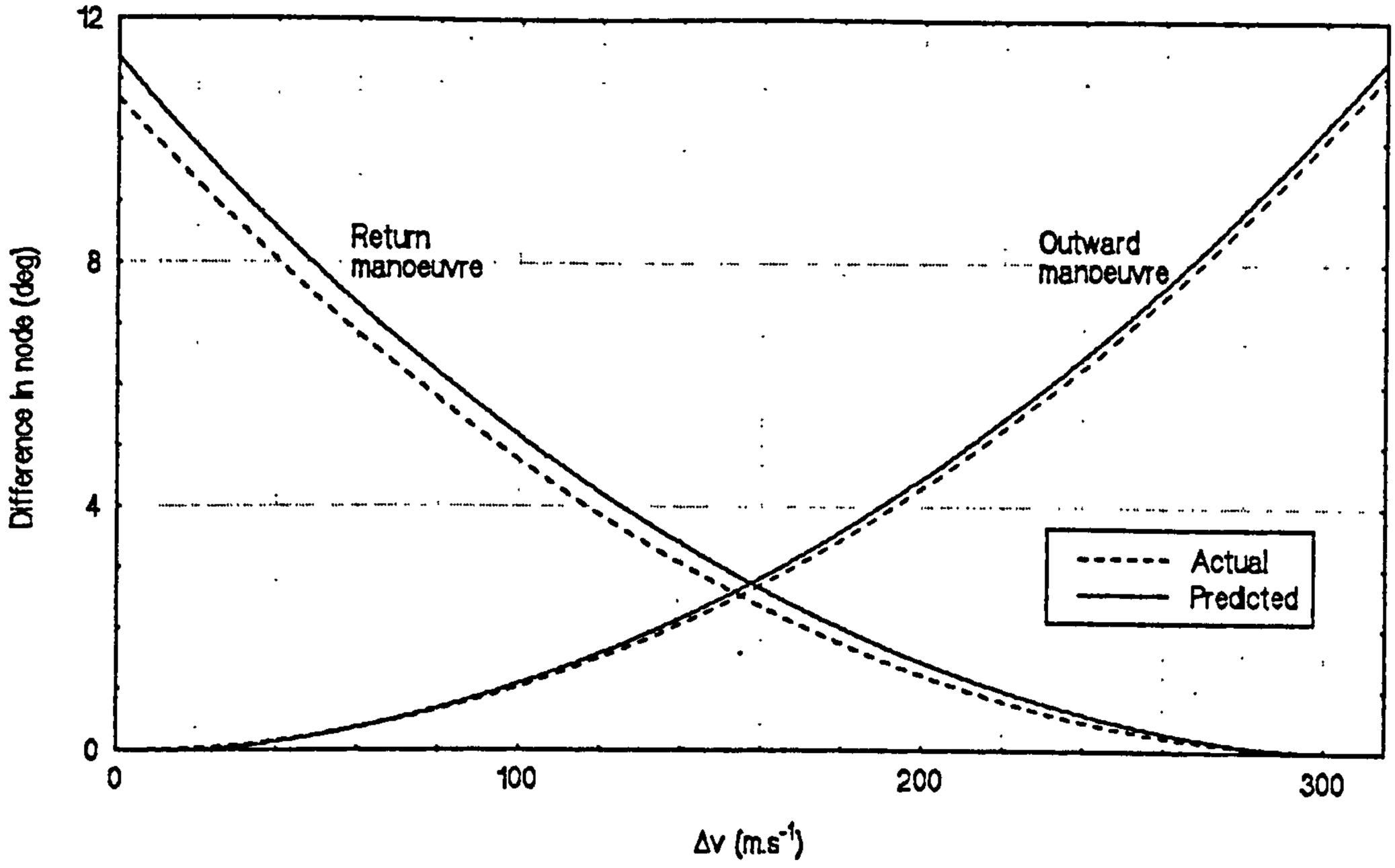

Figure 9.2 Actual and predicted difference between platform and servicing vehicle ascending nodes vs. manoeuvre Δv.

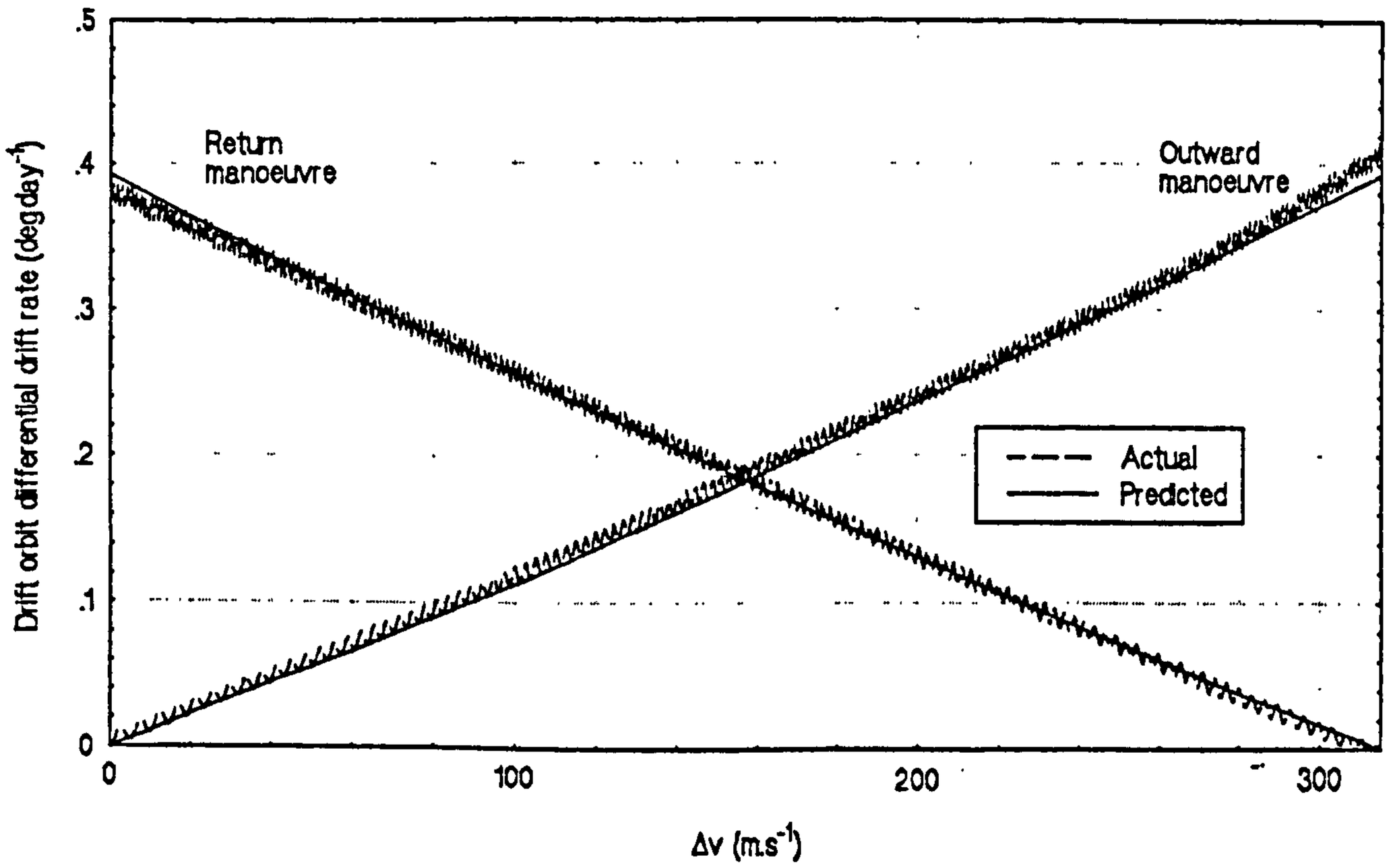

Figure 9.3 Actual and predicted drift orbit differential nodal drift rate vs. manoeuvre Δv.

and Figure 9.3 on the preceding page give comparisons of predicted and actual difference (where predicted means the results given by the simpler model) and actual that given by the ORBIT_CALC simulation) in node (i.e. service vehicle node minus platform node) and drift orbit differential nodal drift rate for both outward and return manoeuvres. In both cases the agreement is very close. Basing calculations on the actual results from these two graphs gives a total single servicing period as be 1065 days. This differs by less that 1% from the target single servicing period of 1075 days.

9.3 Effects of perturbations

Although good agreement has been obtained between the general predictions for the transfer manoeuvres and simulation results the particular effects of each of the perturbations on the transfer manoeuvre have implications for the transfer design. These effects are described below;

9.3.1 Earth asphericity

Earth asphericity has both direct and indirect impact on transfer manoeuvres. The direct interaction of the asphericity with the orbit of the service vehicle is to cause a short term periodic alteration in the orbital elements. The frequency of this oscillation increases as the period of the orbit decreases and can be seen in Figure 9.4 overleaf which plots semimajor axis versus manoeuvre time.

More significantly, the asphericity indirectly affects the eccentricity of the service vehicle. This is shown in Figure 9.5 overleaf where the variation of eccentricity with time is plotted for no natural perturbations and the full set of natural perturbations are acting respectively. It can be seen that in the former case the unequal thrusting caused by the eclipsing of the service vehicle causes a steady build-up in eccentricity. In the latter case, though, the eccentricity reaches a peak value and then starts to decline. Such changes in eccentricity have been described in other electric propulsion missions studies (e.g. Holdaway [72]). They are a function of shadowing and change in the solar vector over the duration of the mission. In this particular case, however, these effects are additionally modified by the regression of the line of apsides caused by the J_2 asphericity component. The high inclination and decreasing semimajor

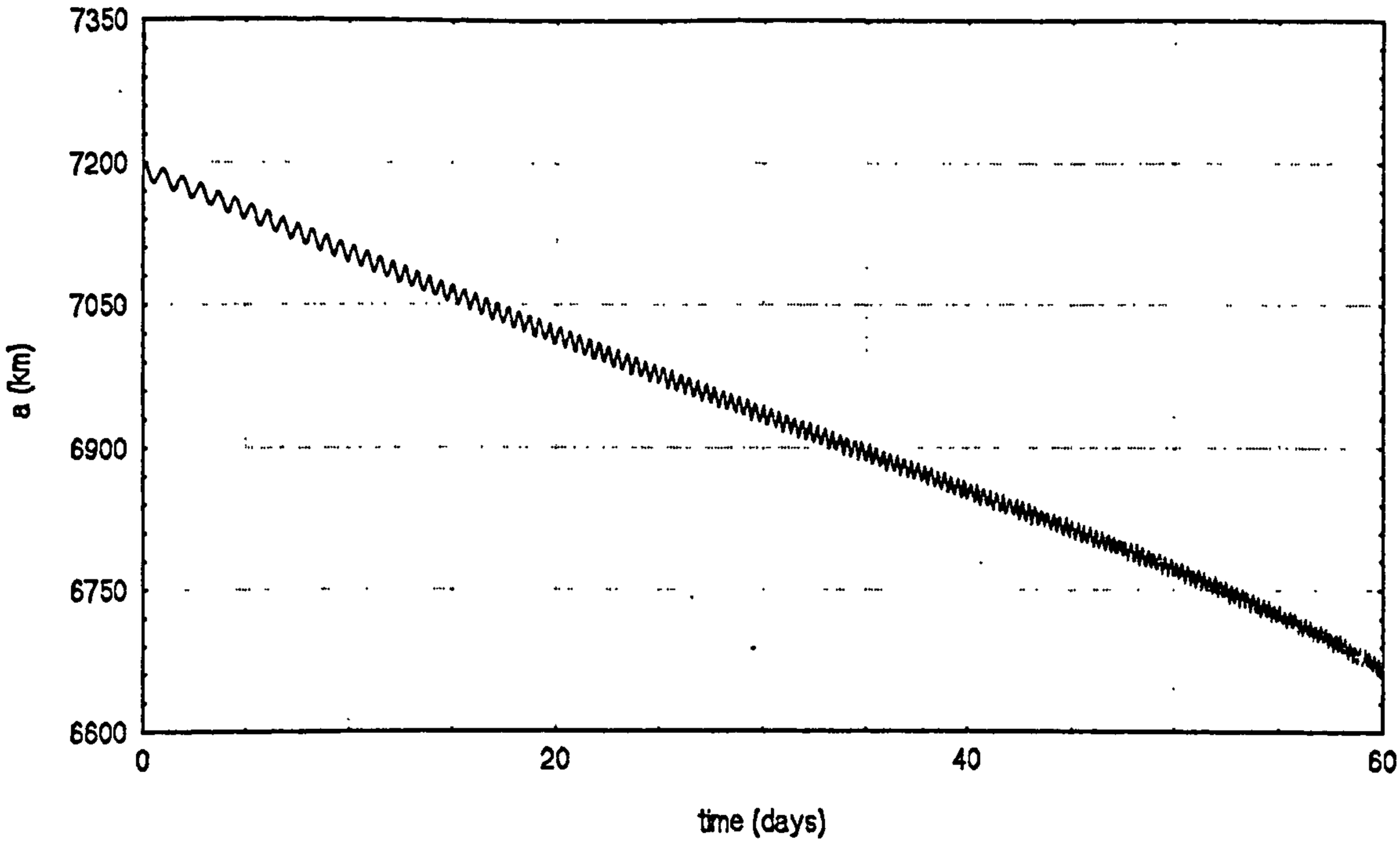

Figure 9.4 Semimajor axis vs. manoeuvre time.

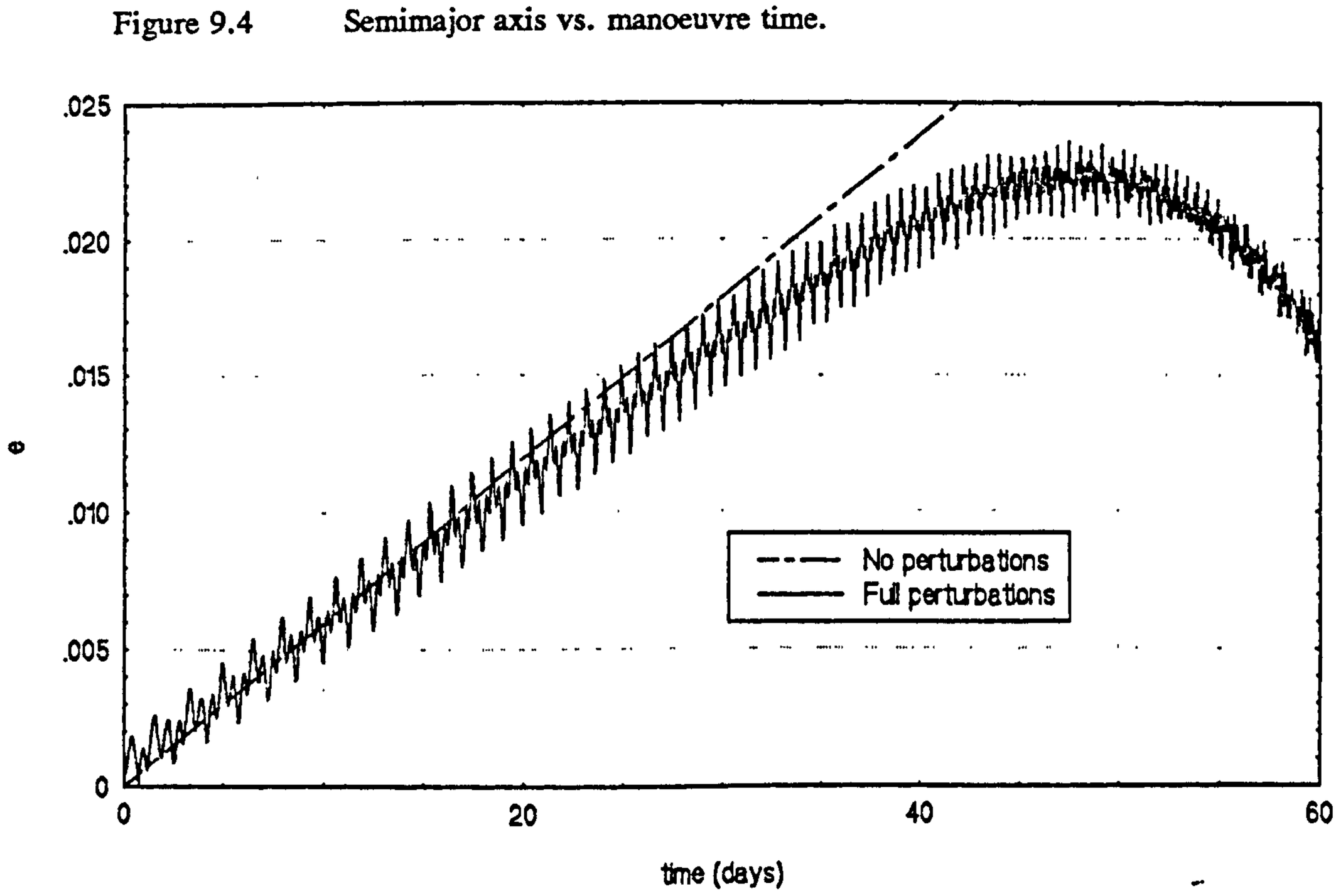

Figure 9.5 Comparison of unperturbed and perturbed eccentricity vs. manoeuvre time.

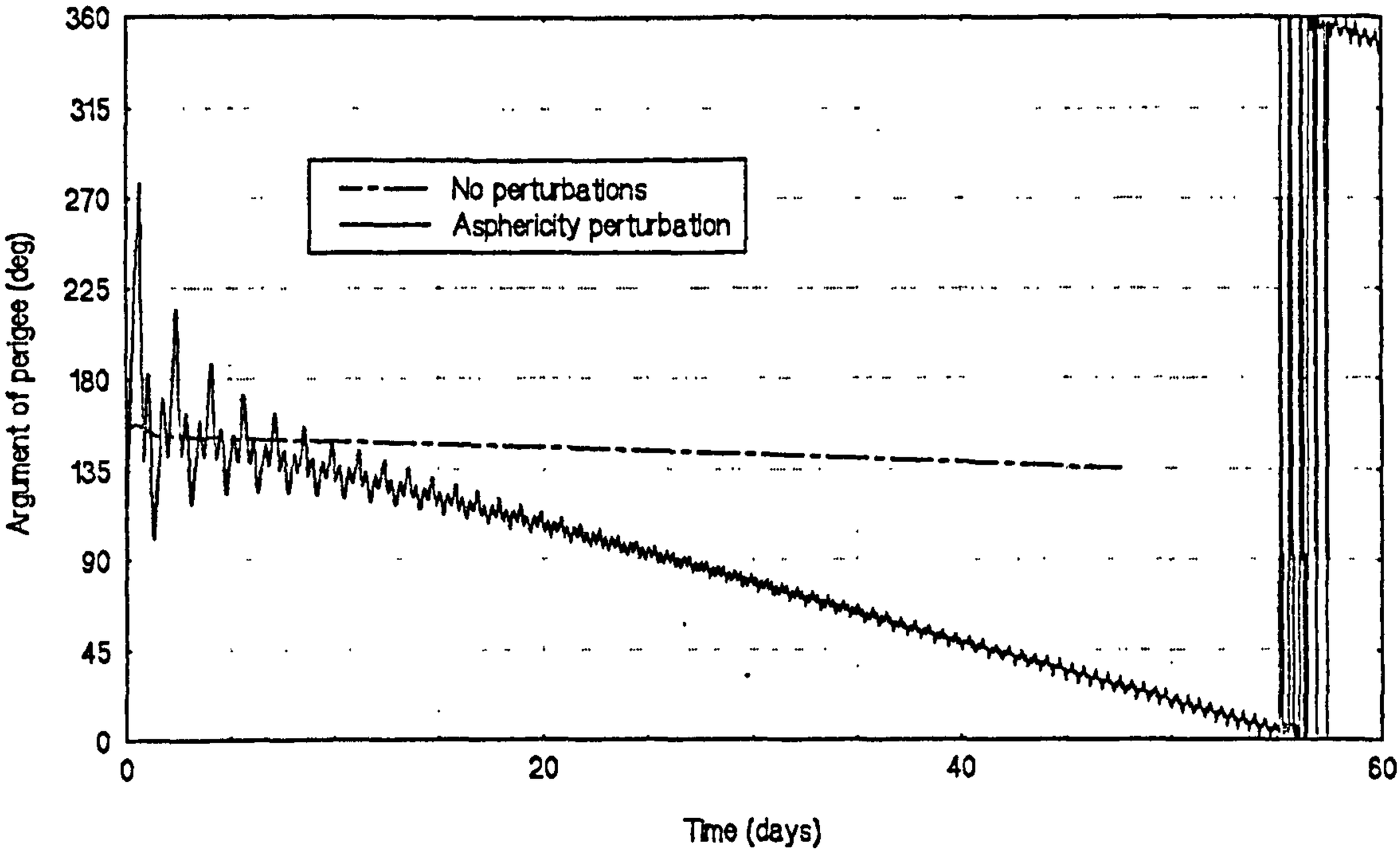

Figure 9.6 Argument of perigee vs. manoeuvre time.

axis of the service vehicle give its orbit a regression rate of between 2.9 and 3.7 degrees per day. Over the course of the transfer manoeuvre this leads to an alteration in argument of perigee of approximately 180 degrees. In this particular case the initial argument of perigee is approximately 180 degrees so that the apogee of the orbit is towards the Sun and changes to approximately 360 degrees over the manoeuvre period so that the orbit ends with the perigee towards the sun. This is shown in Figure 9.6 on the preceding page which also shows the change in the perigee position if the asphericity effects are removed from the simulation. This change in orbit orientation with respect to the eclipse zone initially stimulates and latterly retards eccentricity. In this particular (worst) case the effect is of benefit to the service vehicle. Without it the build-up in eccentricity leads to a perigee altitude of less than 150 km which, in simulation terms, is equivalent to atmospheric entry. For manoeuvres from the A and C platforms this is not so critical as the orbit-Sun geometry does not stimulate quite such a steep increase in eccentricity.

9.3.2 Atmospheric drag

The prime effect of atmospheric drag is to decrease the build-up in eccentricity caused by eclipsing of the solar arrays. This effect can be seen overleaf in Figure 9.7. where the difference in eccentricity for the perturbation-free and the drag-only cases are plotted. The sharp decrease in eccentricity at around 50 days occurs when the perigee of the service vehicle orbit drops below approximately 300 km and into increasingly dense regions of the atmosphere. This tendency of the atmospheric drag to reduce orbital eccentricity also effects the change in eccentricity described in conjunction with earth asphericity effects. This is shown overleaf in Figure 9.8. Again, the drag only starts to have significant effects at altitudes of around 300 km and below.

9.3.3 Solar radiation pressure

We have already seen in Chapter 4 that the acceleration due to solar radiation pressure is much smaller that the other perturbing accelerations over a large part of the service vehicle altitude range. Comparing simulations of the manoeuvre from the B platform to the 320 km drift orbit over 55 days shows that largest error occurs in the true anomaly, approximately 0.38°. All other parameters show

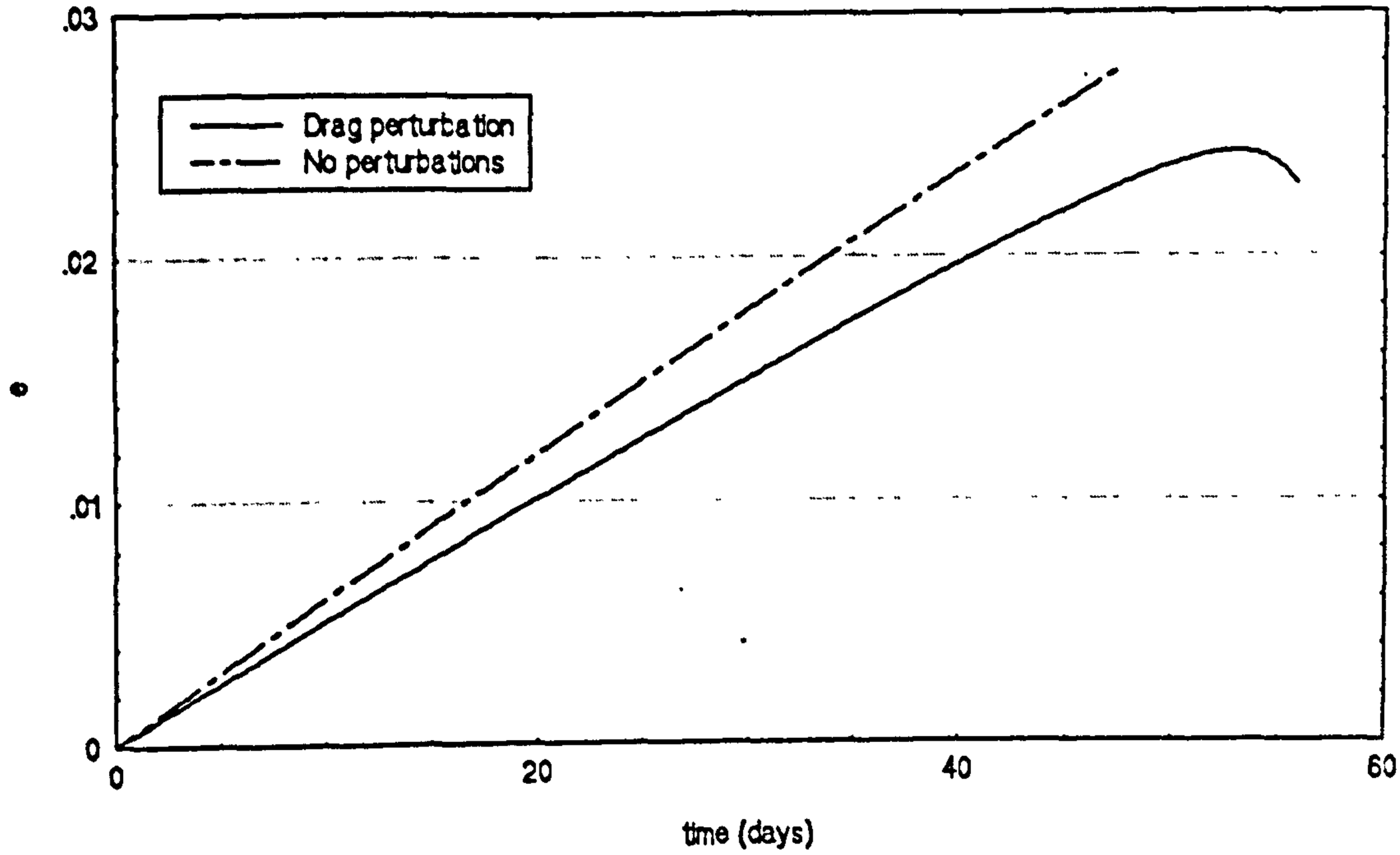

Figure 9.7 Comparison of unperturbed and drag-perturbed eccentricity.

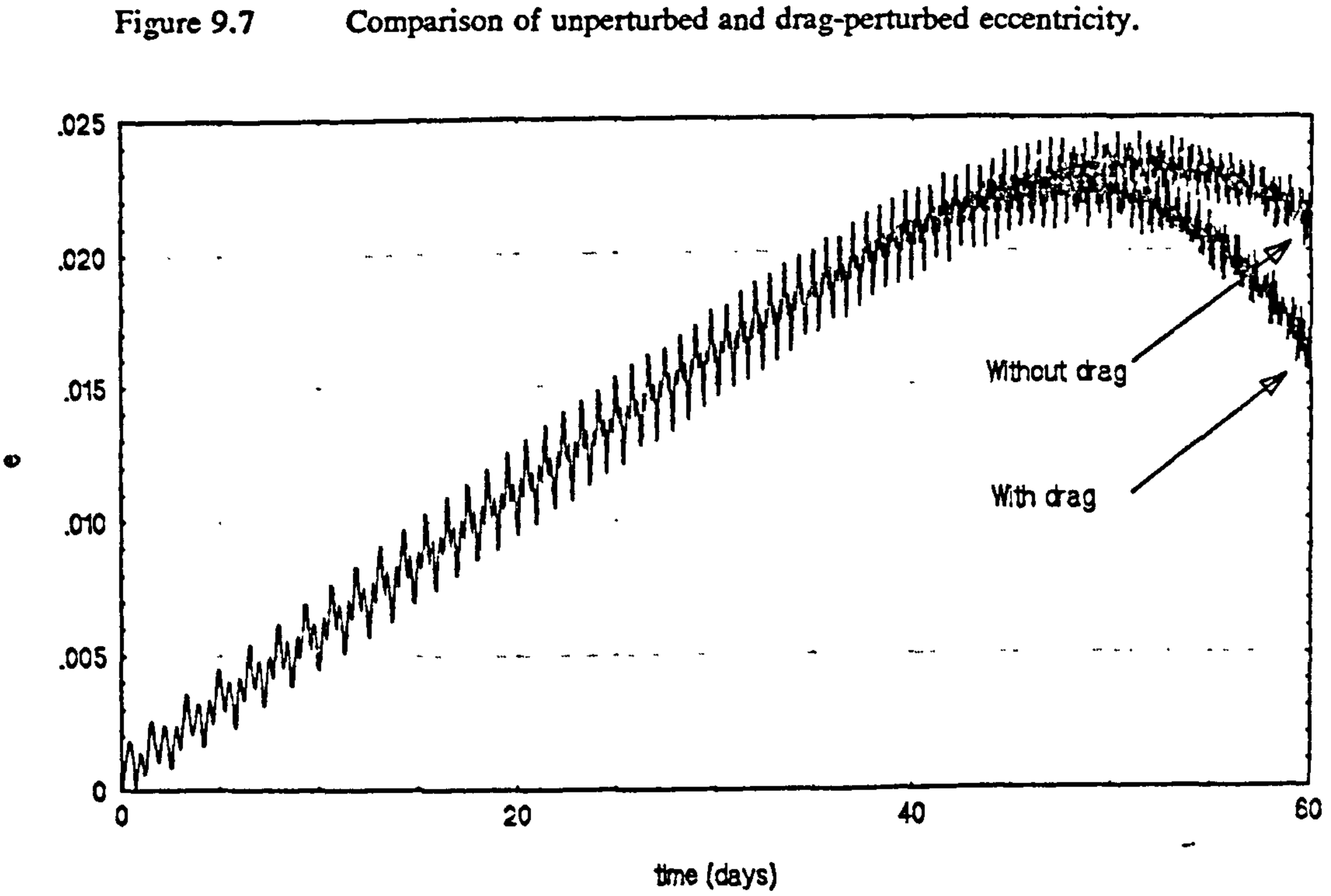

Figure 9.8 Comparison of asphericity-perturbed eccentricity with and without drag perturbations.

agreement to at least four decimal places. These differences are sufficiently small that the effects ofradiation pressure may be ignored for this type of manoeuvre.

9.4 Implications for servicing missions

Although the actual difference in node and drift orbit differential nodal drift rate conform closely to those predicted, it has been seen that the uneven character of the thrusting leads to a build up in eccentricity. This occurs for all manoeuvres and attains a maximum value of approximately 0.025 for the transfer from the B platform orbit to the B-C drift orbit. This level of eccentricity is comparatively small and would not pose particular problems for typical electrically-propelled orbit-raising missions. However, for the manoeuvres under examination here, and in particular those that lower the orbit, the proximity of the Earth means that even small changes in eccentricity can have important effects on the orbit. In such an operational milieu a 300 km difference in perigee and apogee radii can result in an orbit which experiences a variation in atmospheric density of at least three orders of magnitude, leading to further alteration of the orbit.

It can be seen, then, that this build-up in eccentricity will have important implications for servicing missions. Figure 9.9 overleaf shows the variation in apogee and perigee altitudes versus mission time for the manoeuvre from the B platform. It can be seen that after 55 days (i.e. at the end of the planned manoeuvre) that the apogee altitude is 480 km and the perigee altitude is 210 km. Under these circumstances the orbit will circularise much lower in the atmosphere than planned. Although the service vehicle does have drag make-up capability, this, as designed, is incapable of handling the demands that such a low orbit would place on it and the vehicle and payload would consequently re-enter.

To prevent this, the service vehicle could be resized to allow it to operate at such low altitudes. This approach gives rise to spacecraft with an all-up mass in excess of 40,000 kg. Since this would be impossible to launch using the systems expected to exist at the time, this approach may be ruled out and other strategies must be developed.

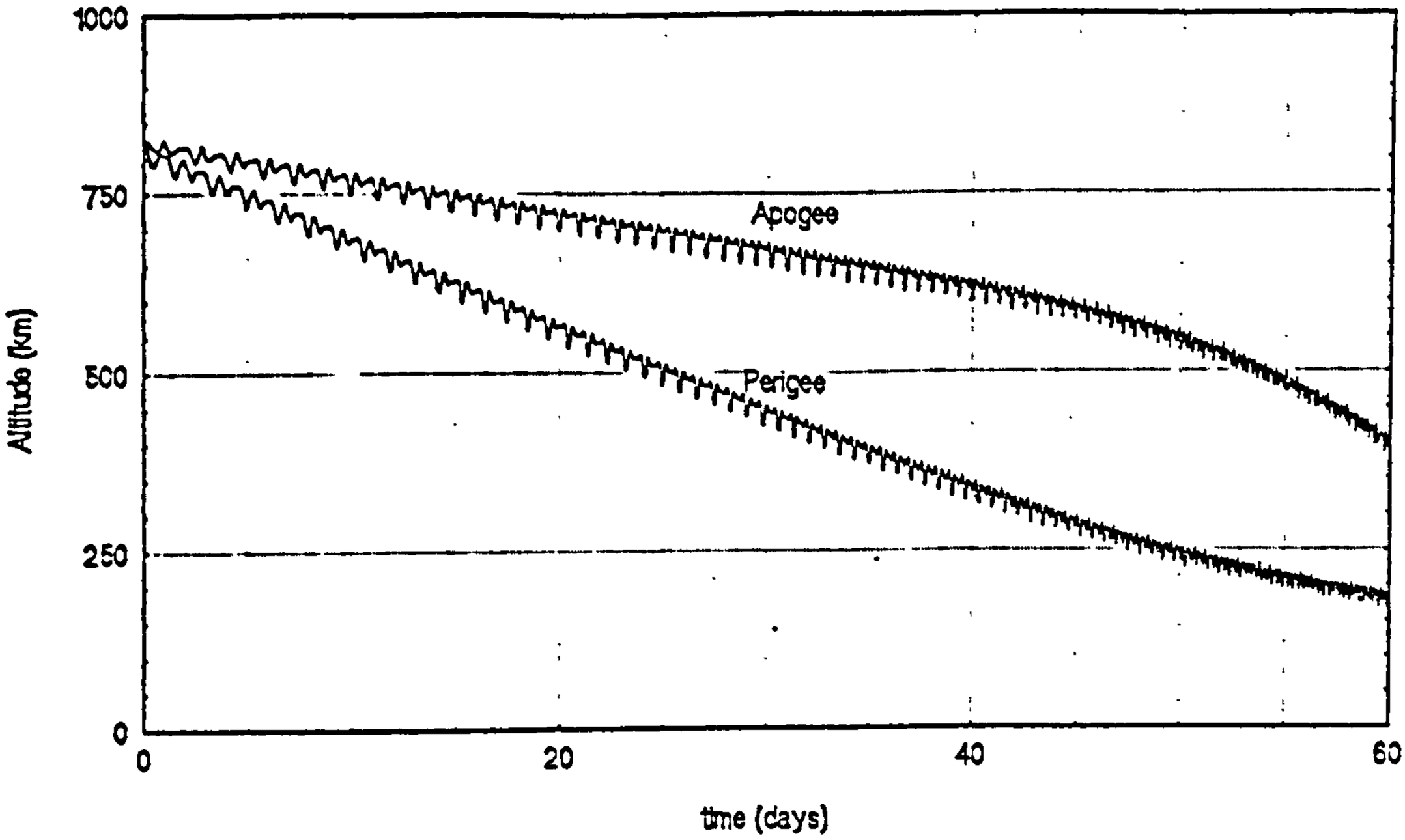

Figure 9.9 Apogee and perigee evolution for manoeuvre from B platform.

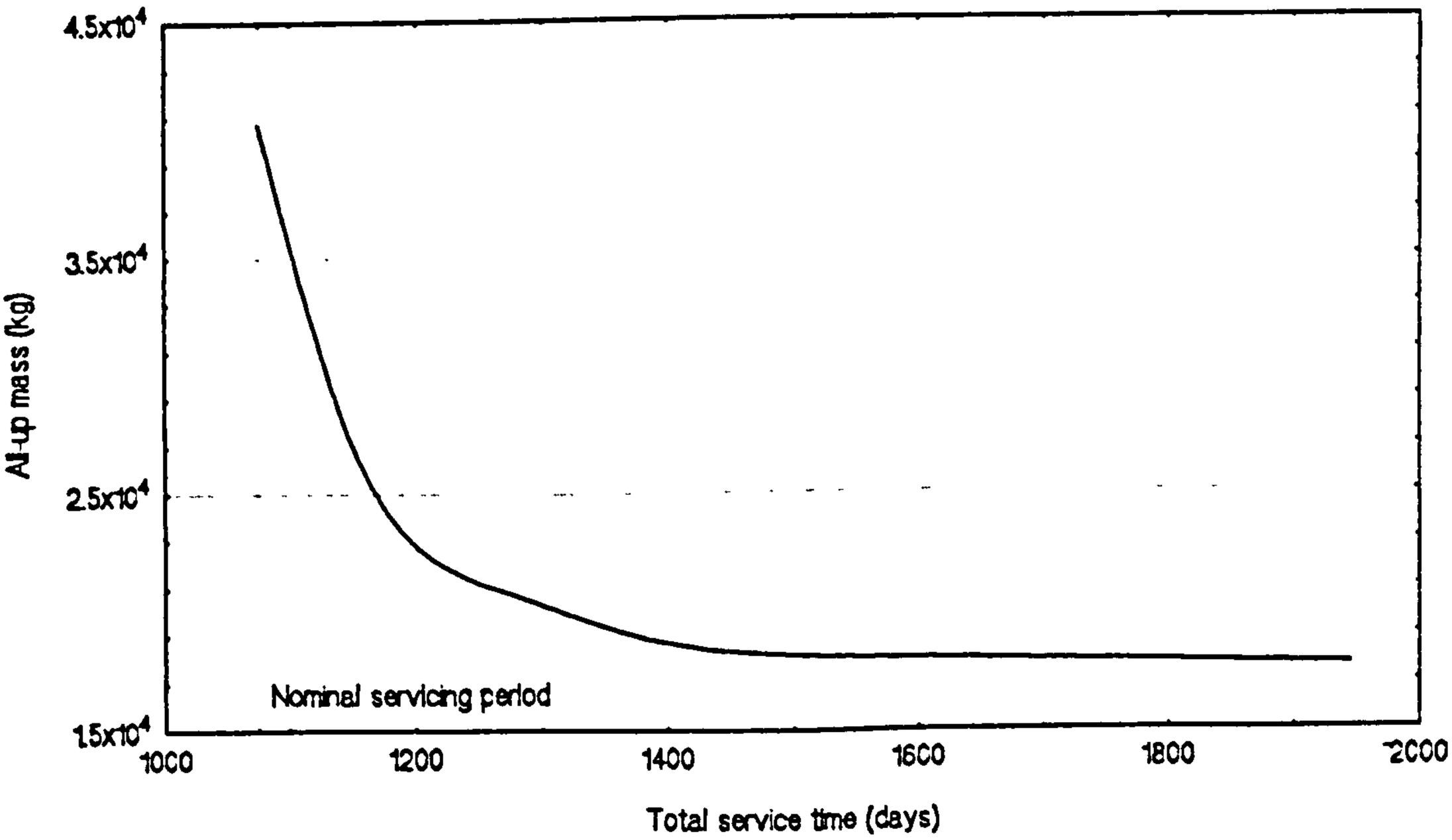

Figure 9.10 All-up mass vs. total service time for eccentric drift orbit transfers.

The most straightforward approach would be to accept the effects of the eccentricity build up and take no steps to correct it. If this is done, however, the manoeuvre must be terminated at an earlier time than previously conceived to prevent re-entry, when the perigee has reached 300 km, for example. This means that the drift orbit will have a smaller differential nodal drift rate and hence the total constellation service period will increase. However, since the propellant required is reduced, the all-up mass of the spacecraft also slightly lessens for long transfer times.

The effect of this strategy is shown in Figure 9.10 on the preceding page where the all-up mass is plotted against total service time for this strategy. All-up mass, rather than propellant mass, is used as the figure of merit here as all the component masses are recalculated in the model rather than just the propellant mass. It can be seen that, in order to even approach the nominal total service period, unfeasibly high all-up masses are required. These are caused by the increase in atmospheric drag as the service vehicle is forced to operate in orbits with lower and lower perigees. However, if longer total servicing times are acceptable then the mass falls to more reasonable figures. This can be illustrated by terminating the manoeuvre when the perigee altitude has reached the original drift orbit altitude, after about 42 days (i.e the perigee altitude is 300 km). If no further decrease in eccentricity is assumed then the differential drift orbit rate falls to 0.27 degrees per day. The effect of this is to increase the single servicing period to approximately 1415 days, an increase of 32% over the target of 1075 days. The all-up mass of the delta spacecraft becomes approximately 18300 kg, some 300 kg lighter than the baseline version from Chapter 8. The all-up mass becomes steadily smaller, the longer the total service period allowed, but realistically useful mass 'gains' are minimal beyond about 2000 days.

A second strategy is to use the baseline vehicle as defined, but to use part of the existing propellant to remove the eccentricity once the service vehicle is in its drift orbit. Equation 6.3 showed that eccentricity can be removed by a tangential thrust reversed at each crossing of the minor axis. The Δv necessary to alter the eccentricity in this way, from e_0 to e_1, is given by

$$\Delta v = \frac{\pi}{4}\left(\frac{\mu}{a}\right)^{0.5}\left(\sin^{-1}e_1 - \sin^{-1}e_0\right) \qquad \text{Eq. 9.1}$$

Eccentricity correction is possible without too much impact on the total service period because it may be performed early during the drift period and takes a comparatively short time in comparison. This approach precludes any increase in the design all-up mass but again leads to the total service period for the constellation being increased. By performing a transfer manoeuvre for 38 days, which takes the the servicing vehicle to an altitude of 360 km, the eccentricity can then be removed in 17 days. Application of this approach leads to a total servicing time of 1260 days, some 17% in excess of the baseline figure. The next logical step is to use additional propellant to remove the eccentricity, although this will be at the expense of increasing the all-up mass.

The effects of the propulsive removal of eccentricity on the all-up mass of the service vehicle are shown overleaf in Figure 9.11, plotted against the curve from Figure 9.10. It can be seen that the advantages of the eccentricity removal approach are very marked at the lower end of the total service time range but that this falls off by the middle of the range. This is explained by the difference in the mass of propellant needed for drag make-up when the eccentricity is not removed (because the perigee must be very low in order to obtain the differential nodal drift rates needed to give the required total service time) and the mass of the propellant needed for eccentricity removal when the propulsive strategy is followed. The difference between the two curves gradually reduces with longer total service times (though the acceptance of the eccentricity gives very small advantages at transfer times larger than 1415 days) since these are obtained by shorter manoeuvres that do not go so low in altitude and do not build up such a high eccentricity and so require minimal additional propellant for drag make-up or eccentricity.

Figure 9.12 overleaf then gives a composite curve derived from most advantageous sections of the two curves. Total service times below 1415 days can only realistically be achieved by propulsive removal of eccentricity. Total service times above this are best obtained not correcting the eccentricity.

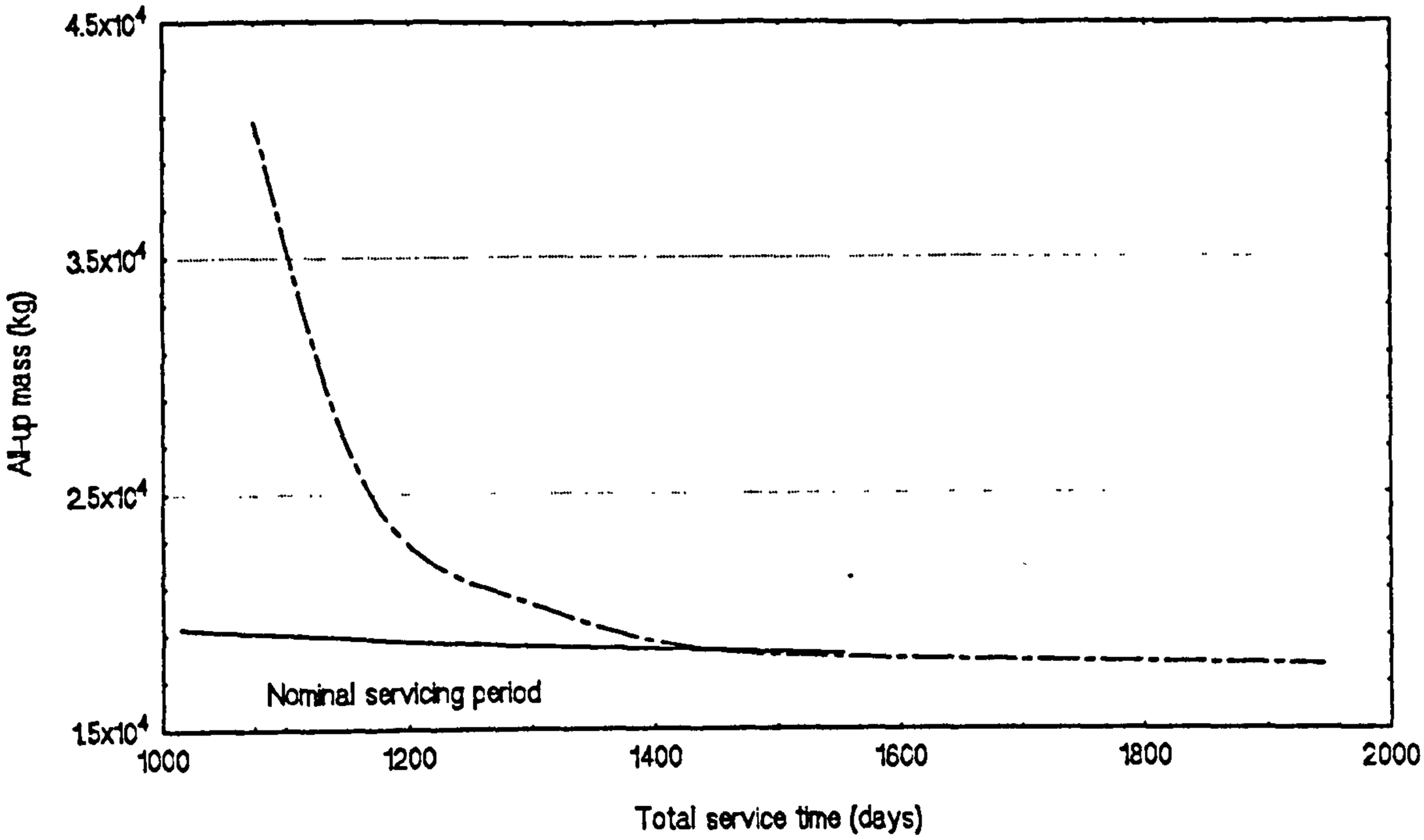

Figure 9.11 All-up mass vs. total service time for both eccentricity strategies.

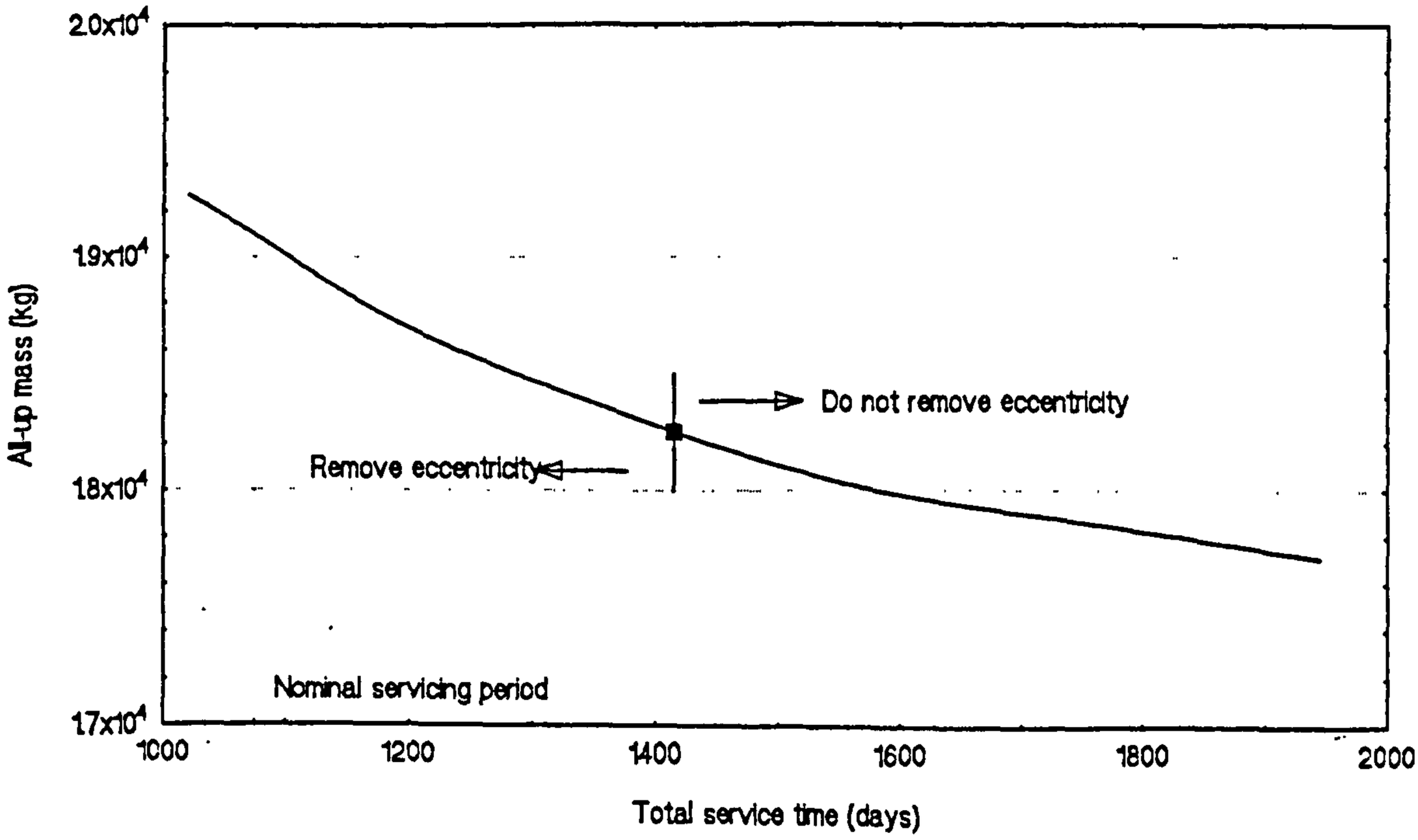

Figure 9.12 All-up mass vs. total service time for composite eccentricity strategy.

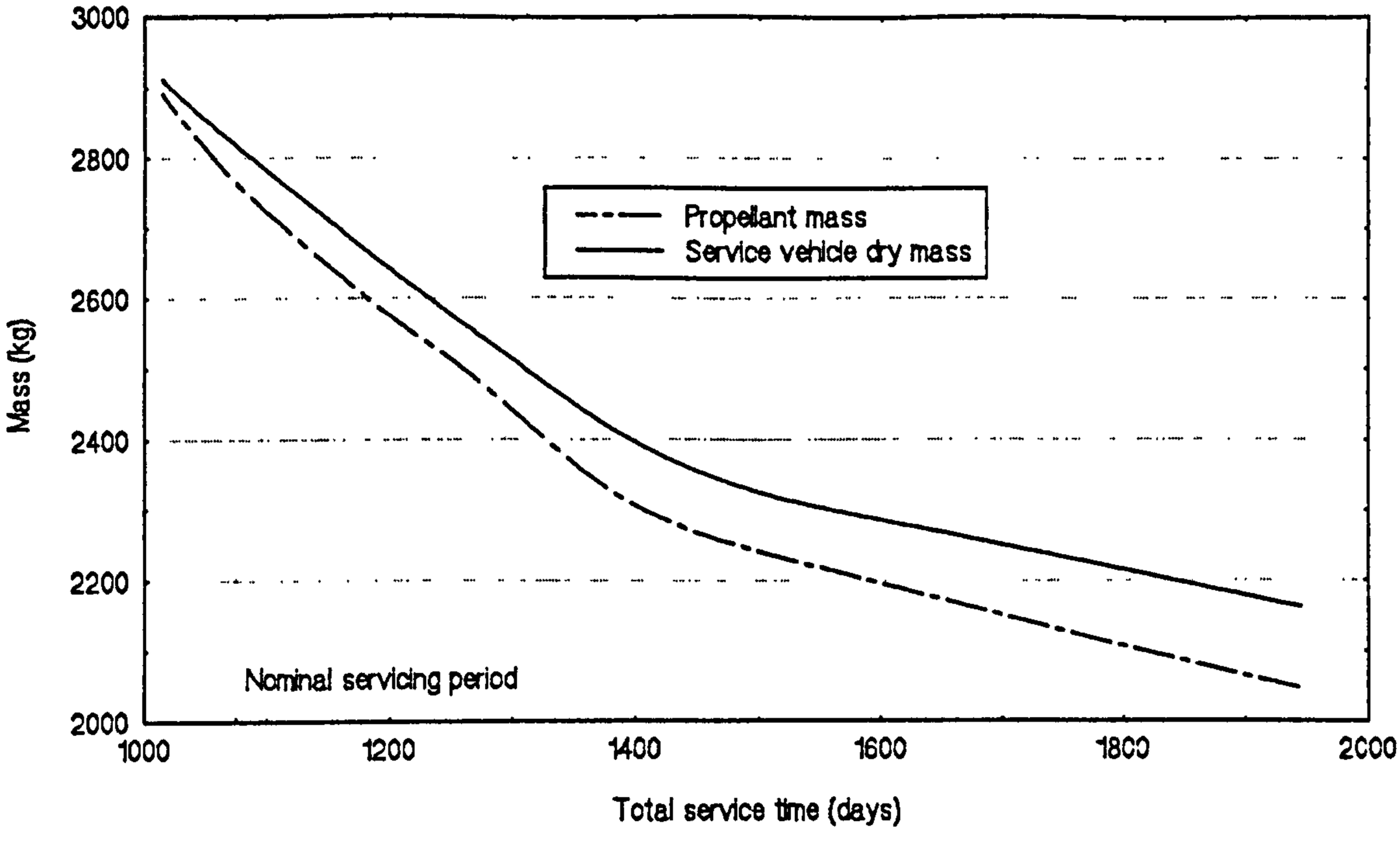

Figure 9.13 Service vehicle dry mass and propellant mass vs. total transfer time for composite eccentricity strategy.

Figure 9.13 on the previous page shows the variation in both service vehicle dry mass and propellant mass for the composite eccentricity strategy.

In order to obtain the nominal servicing period, the additional Δv per manoeuvre necessary is approximately 65 $m.s^{-1}$. Although the one-way manoeuvre Δv is decreased, the total manoeuvre Δv of 395 $m.s^{-1}$, applied over the longer period of 66 days, represents an increase in Δv per transfer of around 20%. This translates to a service vehicle all-up mass increased to 19200 kg, an increase in the baseline mass all-up mass of approximately 3%. As mentioned in Chapter 8, it is not expected that a mass of this amount could be placed directly into EOS orbit though the NLS should be capable of placing around 20000 kg into a 300 km orbit. Allowing for additional Δv to perform the necessary orbit raising, the final all-up mass of the delta service vehicle becomes 19480 kg. For the gamma service vehicle the all-up mass is such that it can be placed directly into EOS orbit so no orbit-raising allowance is needed. The increase is also approximately 3%, giving a total mass of 6630 kg.

For a genuine mission the trade-off between all-up mass and total service time would be driven by numerous factors. There is no specific reason to suppose that the nominal total service time used in this work is anything other than nominal. However, for the sake of consitency the updated configurations for the gamma and delta vehicles to achieve the nominal total service periods are given overleaf in Table 9.1. Although the new figures for the service masses have not changed very much from those given in Chapter 8, it should be noted that this is in part due to the high mass efficiency and the fact that a large amount of the all-up mass is payload. The Δv increase over the earlier figures is approximately 17% in the gamma case and 19% in the delta case.

Additionally, it should be noted both the service vehicle masses and single service cycle periods are subject to uncertainties that can only be determined from further detailed mission simulations. These uncertainties arise from two main sources. Firstly, the eccentricity removal assumes that a reasonable efficacious program for this can be determined. As has already been stated, orbit-Sun geometry plays an

important part in controlling the evolution of eccentricity and, under certain circumstances, it will not be possible to obtain as fast a circularisation as would be desired. This will reduce both the differential drift rate during transfer and increase the amount of time taken to achieve the final drift orbit, so increasing the overall service time.

Conversely, the contribution of atmospheric drag to circularising the orbit has not been included in the analyses above. Again the magnitude of this effect will depend on the orientation of the orbit relative to the Sun (or more particularly, the diurnal bulge). In general, however, this may have some effect on both the all-up mass of the servicing vehicle and the single servicing cycle period, either decreasing the latter for a given period, or decreasing the servicing period attainable by a service vehicle of a given mass.

Table 9.1 - Final service vehicle configuration breakdown

Configuration	Gamma	Delta
No of servicing cycles	3	3
ORU sets carried	1	3
Total Δv ($m.s^{-1}$)	9400	9645
Drift orbit altitude (km)	300	326
Array BOL power (kW)	28.3	82.2
Propulsion system	Ion	Ion
Propellant	Xenon	Xenon
Exhaust velocity ($m.s^{-1}$)	57400	57400
Thrust (N)	0.63	1.9
Payload mass (kg)	4500	13500
Propellant mass (kg)	1020	3100
Service vehicle mass (kg)	1110	2880
All-up mass (kg)	6630	19480

Chapter 10 - Servicing polar platforms using electric propulsion

The future development of space activities and the transformation of these from a specialised area of human activities into a routine one depends on the development of an integrated space infrastructure. This infrastructure will consist of three main parts; in-orbit assets, transportation systems to link these to the Earth and to each other, and communications systems to allow data transfer between the various components. These three parts are all heavily interdependent and, to a large extent, are only valid when considered as a single functional block. The resulting high cost of implementing such a 'total infrastructure' has so far prevented any of the world's governments and space agencies from making significant progress towards this end. With the exception of certain sub-areas, such as the communications satellites industry and the providers of launchers for same, space development currently remains stalled on the threshold of the next stage of its evolution.

Nevertheless, although space infrastructure must sensibly be viewed as a cohesive whole, scaling of the overall architecture may be performed. At the top end is the full infrastructure consisting of a large range of assets such as manned space stations, co-orbiting platforms and man-tended free flyers in low-earth, polar and geostationary orbits with effective and efficient re-useable transportation systems for moving between the Earth and space and between the various in-orbit transportation nodes, the whole welded together by an efficient telecommunications system. At the low end is a more humble arrangement involving a manned space-station, man-tended free flyers and co-orbiting platforms in low-earth orbit only, with additional unmanned platforms in polar and geostationary orbits. At the moment it appears that the next quarter-century of space infrastructure development lies more towards the latter rather than the former, though the evolution of a larger infrastructure in the longer term should obviously not be ruled out.

Largely irrespective of the scope of the infrastructure and the speed at which it develops, in-orbit space transportation systems will be needed to move between whatever in-orbit assets exist. In order to enable worthwhile comparisons to be made of the suitability and comparative merit of different propulsion systems it may be argued that there is a need to move way from specific, narrow-application simulations towards the use of more general software. Axiomatically, such software will be less efficient than existing simulation programs but the move towards an 'industry standard' will be beneficial in the longer term.

The above has provided the stimulus to develop the ORBIT_CALC program. This program, formulated in equinoctial orbital elements to avoid singularities for orbits of small or zero eccentricity, has been designed to be as general as possible. ORBIT_CALC can provide simulations of any near-Earth mission irrespective of the type of propulsion system being used and includes the perturbing effects of atmospheric drag, solar radiation pressure, and Earth asphericity.

Also largely irrespective of the scope of the infrastructure development, the future of polar-orbiting spacecraft seems assured. The growing requirement for detailed Earth resources and environmental information means that this area of space development is both developing commercially at the moment and receiving a broad level of support from the general public.

The next major set of polar spacecraft to have been launched as part of the Freedom/Columbus programme were originally to have been platforms. These, considered as an evolutionary development of current single-use satellites, offer advantages in both lifetime and flexibility of application. These advantages are only available, however, if the capability exists to service and resupply the platforms and so this topic must be examined in the context of the future space infrastructure of which they are part. As stated above, polar platforms will almost certainly be a part of even a minimum future infrastructure. Examination of future space transportation programmes demonstrates that servicing cannot be undertaken by manned means as no launch systems capable of placing humans and payload into suitable polar orbits will exist in the short and medium term future.

It is apparent then that, if polar platforms are to be serviced, autonomous/teleoperative techniques will be required. Even if the future infrastructure is limited, remotely serviced polar platforms appear to offer a useful route to the development of a wide range of 'remote access' technologies that will have a large number of applications through the rest of a future space infrastructure. In particular, they may offer lower cost access to in-space activities by obviating the presence of humans in many spheres of activities.

The servicing of each platform may be accomplished individually but it is more attractive to service a number of them using a single vehicle. To achieve this, however, the vehicle must be capable of making changes in the ascending node of its orbit to move from platform to platform. For chemical propulsion systems the impulsive Δv necessary to do this makes direct nodal alteration impossible at current levels of technology. Given that electric propulsion is known to give high mass efficiency at high mission Δv s this may be expected to offer advantages over chemical propulsion as long as rapid transfer from platform to platform is not needed. Examining the mechanics of low thrust propulsion shows that direct nodal transfers are possible, but that these still require a fairly high Δv.

The asphericity of the Earth causes differential nodal drift between different orbits and this may be used to alter the ascending node, though again this is only an option if rapid transfer is not required. Differential nodal drift (with respect to an arbitrary reference orbit) is caused by the alteration of either or both of the inclination or semimajor axis. In servicing terms, the servicing vehicle is given a different nodal drift rate from that of the constellation of platforms allowing it to move between them. This form of transfer procedure requires an outward manoeuvre to a drift orbit, a period in the drift orbit, and then a return manoeuvre. A drift orbit of greater inclination and lesser radius causes a net eastward change of node while the converse causes a net westward drift.

This form of transfer can be effected using either high- or low-thrust propulsion. For small numbers of transfers of small payloads high-thrust, impulsive transfers to and from the drift orbit may be attractive. Electric propulsion, however, offers significant benefits when repeated transfers of larger

payloads are made and the overall mission Δv is therefore high. Considering quasi-circular orbits it can be shown that optimum nodal transfers can be obtained by use of simple, fixed angle thrust programs. In theory, either eastward or westward transfers are possible. Given the use of solar photovoltaic powered electrically propelled vehicle, however, limitations exist in both transfer directions. As well as being less efficient, westward transfers are limited more fundamentally by the existence of the Van Allen belts. Even moderate changes in altitude lead to prolonged exposure to radiation during the drift orbit period. Even if a hardened service vehicle is a possibility it seems unlikely that platform payloads could be similarly treated without imposing a severe mass penalty. Westward transfers are therefore discounted for this reason.

Eastward transfers are limited by the effects of atmospheric drag since below a certain altitude this will cause the service vehicle to re-enter. The altitude at which this happens is partly dependent on the ballistic characteristics of the service vehicle which is heavily influenced by the power-to-area ratio of the photovoltaic array. The more advanced the technology is, the lower the altitude at which solar-electric vehicles can operate. In this case this is also a function of the drift orbit and the time spent in it. The lower the drift orbit the higher the differential drift rate will be, but the more drag make-up Δv will be needed, thereby increasing the mass of the service vehicle. For any service vehicle and mission configuration there will be an optimum drift orbit altitude. For the vehicles and configuration investigated this altitude was found to be in the vicinity of 300 km.

These results assume that the quasi-circular state is retained throughout the mission. Although this is true, manoeuvre simulations show that, because of the close proximity of the Earth and the non-linear change in atmospheric density with altitude even the small increases in eccentricity caused by the eclipsing of the arrays can cause perigee altitude that will cause the spacecraft to re-enter. This effect can be offset by correcting the eccentricity propulsively for a small increase in all-up mass assuming that the orbit-Sun geometry permits it. This can only determined by more detailed mission simulations. Atmospheric drag may also play a part in decreasing eccentricity, and this too requires additional work

to be carried out before it can be accurately characterised.

For the EOS2 baseline polar platform configuration used here xenon ion propulsion systems emerged as superior in all cases because of their high exhaust velocity and efficiencies combined with reasonable tankage fractions. The two final service vehicle configurations make it is clear that, in terms of overall service vehicle mass and numbers, it is advantageous to use vehicles with as long a life as possible. Vehicle with lifetimes of three servicing cycles are only marginally more massive than those with lifetimes of one servicing cycle. The decision of service vehicle payload capability is not one that can be addressed here since it depends primarily on the results of a trade-off between the upload flexibility required by the polar platform operators and the cost of three times as many ORU launches.

Using realistic values for projected technical developments in electric propulsion against a modest projected future space infrastructure, it has been shown that the servicing of polar platforms by electric propulsion is feasible and that it offers significant advantages in terms of overall mass upload and hence cost.

References

1 SADIN, S.R. Affordability through technology, *Leadership in space for benefits on Earth - Volume 47 in Advances in the astronautical sciences*, ed. Rector, W.F., AAS, 1981, ISBN 0-87703-168-1, pp 155-163.

2 PARKINSON, R.C. The space economy of 2050 AD, JBIS, Vol. 44, pp 111-120, 1991.

3 KLINE, R. A program to develop efficient manned operations in space, *Space Manufacturing 1983 - Volume 53 in Advances in astronautical sciences*, ed Burke, J.D. and Whitt, A.S., AAS, 1983, ISBN 0-87703-189-6, pp. 107-118.

4 RIEDEL, U Evolving a future space infrastructure, British Interplanetary Space Infrastructure Symposium, London, 15 November, 1988.

5 REUTER, K-E. The European long-term space plan, ESA Bulletin, No 54, May 1988, pp. 14-29.

6 VARSI, G. Telerobotics for the efficient utilisation of space, JBIS, Vol 43, pp 273-280, 1990.

7 DICKINSON, A., DINWIDDY, S.E., and SANDBERG, J. The European Data Relay System as part of the in-orbit infrastructure, ESA Bulletin, No 51, August 1987, pp. 47-52.

8 CAVENY, L.H. (ed) *Orbit-Raising and Maneuvering Propulsion: Research Status and Needs - Progress in Astronautics and Aeronautics Vol. 89*, AIAA, 1984, ISBN 0-915928-82-5.

9 FEARN, D.G. A review of future orbit transfer technology, JBIS, Vol 35, pp. 304-325, 1982.

10 GEORGE, D. Advanced space propulsion concepts, IAF paper 86-110.

11 CALUORI, V.A. and SAXTON, D.R. Orbital transfer vehicle - an overview, JBIS, Vol 34, 1981, pp. 171-174.

12 CHARHUT, D.E. and KETCHUM, W.J. Space-based orbital transfer vehicle, Act. Ast., Vol,14., 1986, pp. 105-116.

13 DICKEY, M.R., MATLOCK, R.S and FEIG, J.R. ELITE: An on-orbit demonstration of solar electric propulsion *Astrodynamics 1989 - Volume 71 in Advances in the astronautical sciences*, AAS, 1990, ISBN 0-87703-317-X, pp. 1177-1187.

14 THOMAS, U. and THIRKETTLE, A. The Ariane Transfer Vehicle (ATV) System Studies, ESA Bulletin, No 67, August 1991, pp. 71-77.

15 BARTOLI, C. and BERRY, W. — Review of European electric propulsion, JBIS, Vol 41., Nos. 4 and 5, April/May 1988, pp 147-166.

16 DEININGER, W.D. and VONDRA, R.J. — Spacecraft and mission design for the SP-100 flight experiment, JBIS, Vol. 44, No. 5, May 1991, pp. 217-228.

17 SMITH, H. — *Spacecraft Systems Engineering*, ed. Fortescue & Stark, Wiley, 1990, ISBN 0-471-92794-5, pp 304.

18 FLEETER, R. and WARNER, R. — *Space Mission Analysis and Design*, ed. Wertz & Larson, Kluwer 1991, ISBN0-7923-0970-7, pp 712.

19 LONGHURST, F. — The Columbus system baseline and interfaces, ESA Bulletin, No 50, Amy 1987, pp 88-97.

20 KLINE, R.L., and ADORNATO, R.J. — Satellite servicing from the shuttle orbiter, Earth-Orientated Applications of Space Technology, Vol 2, No 4/4, pp 179-188, 1982.

21 MEISSINGER, H.F. — Cost-effective orbit transfer modes for satellite retrieval and servicing, Proc. First European In-Orbit Operations Technology Symposium, Darmstadt, W. Germany, ESA SP-272, November 1987, pp 29-35.

22 LUTZE, F. — Fuel and time considerations for satellite servicing, AIAA paper 88-4302.

23 PARKINSON, R.C. — The space platform, JBIS, Vol 38, pp 391-394, 1985.

24 SHAPLAND, D. — The Columbus programme - an overview, ESPOIR, Avignon, ESA SP-266, 16-18 June 1986, pp 11-17.

25 SAWDON, F.E., CONCHIE, P.J., and SHELTON, R.M. — The Columbus polar platform, Space Technology, Vol 7, No. 1/2, pp 57-66, 1987.

26 DE VILLIERS, N. — Orbit Configurations, ESPOIR, Avignon 16-18 June 1986, ESA SP-266, pp 49-53.

27 MEISSINGER, H.F., ROSEN, A. and WHEELER, P.C. — Polar platform orbit selection considerations, AAS paper 85-433 in AAS microfiche series, AAS/AIAA Astrodynamics Specialist Conference, Vail, Colorado, August 12-15, 1985.

28 BORIELLO, G., FABRIZI, A., and BALDUCINNI, M. — The propulsion module of the Columbus space platform: trade-offs and design, AIAA paper 86-1200.

29 PALASZEWSKI, B.A. — Advanced propulsion for polar orbiting and co-orbiting free flyers, AIAA paper 86-1564.

30 FECONDA, R.T. and RAUSCHER, R.A. — Space station platforms - propulsion subsystem trades, AIAA paper 86-1591.

31	FEARN, D.G. and WALLACE, N.C.	Advanced propulsion systems for space station applications, JBIS, Vol 40, pp 3-10, 1987.
32	MARTIN, A.R. and CRESDEE, M.T.	The use of electric propulsion on low-earth orbit spacecraft, JBIS, Vol 41, pp 175-182, 1988.
33	KLEMETSON, R.W.	Polar platform servicing performance limitations, AAS paper 85-434, in *Astrodynamics 1985, Vol 58, Advances in the Astronautical Sciences*.
34	KLENAU, W., RIEDEL, U. and EYMAR. P.	European orbit transfer and servicing vehicle, Act. Ast., Vol 14, pp 117-131, 1986.
35	GRAVES C.D. and ROSEN, A.	Orbital servicing from an expendable launch vehicle, IAF paper 89-242.
36	GRAVES, C.D., MEISSINGER, H.F. and ROSEN A.	Servicing of multiple satellites using an OMV-derived transfer vehicle, AAS paper 89-183.
37	MUGELLESI, R.	Launch and retrieval manoeuvres for the agency's free-flying space platform 'Eureca', ESA Journ., Vol 9, pp 39-48, 1985.
38	FISHER, H.T. and FORSBERG, K.J.	The service role of a space station: satellite/platform service and maintenance, AIAA paper 83-7094.
39	QUALLS, G.D. and FEREBEE M.J.	Advanced satellite servicing facilities, AIAA paper 88-4200.
40	BATTIN, R.H.	*An introduction to the mathematics and methods of astrodynamics*, AIAA, 1987, ISBN 0-930403-25-8.
41	CORNELISSE, J.W., SCHOYER, H.F.R. and WAKKER, K.F.	*Rocket propulsion and spaceflight dynamics*, Pitman, 1979, ISBN 0-2736-1141-3.
42	ROTH, E.A.	The gaussian form of the variation-of-parameter equations formulated in equinoctial elements - applications: airdrag and radiation pressure. Act. Ast. Vol 12, No. 10, pp. 719-730, 1985.
43	BROUCKE, R. and CEFOLA, P.	On the equinoctial orbit elements, Cel. Mech. Vol 5, No3, pp 303-310, 1972.
44	CEFOLA, P.J.	Equinoctial orbit elements - applications to artificial satellite orbits, AIAA/AAS Astrodynamics Conference, Palo Alto, Calif, 1972. AIAA Paper No 72-937.
45	WALKER, M.J.H., IRELAND, B and OWENS, J.	A set of modified equinoctial orbital elements, Cel. Mech. Vol 36,pp 409-419, 1985.

46	NASA	Space and planetary environment criteria guidelines for use in space vehicle development, 1982 revision, Volume 1. NASA TM-82748.
47	KING-HELE, D.	*Theory of satellite orbits in an atmosphere*, Butterworth Press, 1964, p.127.
48	NOAA	The US Standard Atmosphere, 1976, NOAA-S/T 76-1562.
49	LAZARI, Y.V.	Computational modelling of the perturbations acting on a close earth satellite, University of Southampton, 1983.
50	WAGNER, C.A.	The gravity potential of the force field of the Earth through the fourth order, NASA TN-D-3317.
51	KING-HELE, D.	*Satellite orbits in an atmosphere: theory and applications*, Blackie, 1987.
52	LADNER, J.E. and RAGSDALE, G.C.	Earth orbital satellite lifetime, NASA TN-1995, 1964.
53	CYGNUS ENGINEERING	Orbital Workbench - Version 1.0, Program Description and User's Manual, Cygnus ENgineering, 918 Leighton Way, Sunnyvale, CA 94087, USA.
54	POESCHEL, R.L. and HYMAN, J.	A comparison of electric propulsion technologies for orbit transfer, *Orbit-Raising and Maneuvering Propulsion: Research Status and Needs - Progress in Astronautics and Aeronautics Vol. 89*, ed. Caveny, L.H., AIAA, 1984, ISBN 0-915928-82-5, pp 203-232.
55	JONES, R.M.	Comparison of potential electric propulsion systems for orbit transfer, J. Spacecraft and Rockets, Vol. 21, No. 1, Feb. 1984, pp 88-128.
56	DEVINCENZI, D.L., ZONDERVAN, K.P., COHEN, R.B., JANSON, S.W., MARVIN, D.C. and CALDWELL, D.J.	Elite systems analysis, AIAA paper 90-2530.
57	CASSADY, R.J.	An analysis of orbit maneuvering capabilities using arcjet propulsion, AIAA paper 88-2832.
58	WILBUR P.J.	Electrostatic thruster capabilities for orbit raising and manoeuvering missions, *Orbit-Raising and Maneuvering Propulsion: Research Status and Needs - Progress in Astronautics and Aeronautics Vol. 89*, ed. Caveny, L.H., AIAA, 1984, ISBN 0-915928-82-5, pp 327-342.

59 SEIKEL, G., YORK, T.M. and CONDIT, W.C. — Applied field magnetoplasmadynamic thrusters for orbit raising missions, *Orbit-Raising and Maneuvering Propulsion: Research Status and Needs - Progress in Astronautics and Aeronautics Vol. 89*, ed. Caveny, L.H., AIAA, 1984, ISBN 0-915928-82-5, pp 203-232.

60 ANGST, S.W. — *Direct Energy Conversion*, Allyn and Bacon, New York, 1982.

61 BERLIN, P — *The Geostationary Application Satellite*, Cambridge University Press, 1988, ISBN 0-521-33525-6.

62 WILLIAMSON, M. — *Dictionary of Space Technology*, Adam Hilger, 1990, ISBN 0-85274-339-4, p. 307.

63 RAUSCHENBACK, H.S. — *Solar Cell Array Design Handbook, Van Nostrand 1980.*

64 STARK, J.P.W. — *Spacecraft Systems Engineering*, ed. Fortescue & Stark, Wiley, 1990, ISBN 0-471-92794-5, p 266.

65 NASA — Solar Array Flight Experiment (SAFE 1) - Final Report, LMSC document F087173, April 1986.

66 KURLAND, R. and STELLA, P. — Status of Advanced Solar Array Program, AIAA paper 88-9050.

67 FLOOD, D.J. — Photovoltaics for high capacity space power systems, Act. Ast., Vol. 19, No. 10, pp. 805-812, 1989.

68 WEINBERG, I. and BRINKER, D.J. — Indium phosphide solar cells, Proc. 21st InterSociety Energy Conversion Conference, Vol. 3, pp 1431-1435, American Chemical Soc., 1986.

69 BURT, E.C.G. — The dynamics of low thrust spacecraft, J. Royal Aeronautical Society, Vol 72, pp 925-940, 1968.

70 EDELBAUM, T.N. — Propulsion requirements for controllable satellites, ARS Journal, August, pp 1079-1089, 1961.

71 ENNIX, K.A., DICKEY, M.R., KLUCZ, R.S. and MATUSZAK, L.W. — Electric Vehicle Analyzer, AIAA paper 90-2573.

72 HOLDAWAY, R. — A theoretical study of satellite emplacement by solar electric propulsion, Ph.D. thesis, University of Southampton, August 1974.

73 SARNECKI, A.J. — Orbit expansion by microthrust: Part 2: Analysis, RAE Technical Report 68008, January 1968.

74 EDELBAUM, T.N., SACKETT, L.L. and MALCHOW, H.L. — Optimal low thrust geocentric transfer, AIAA 10th Electric Conference, Lake Tahoe, Nevada, November 1983.

75 SPONABLE, J.M., and PENN, J.P. — Electric propulsion for orbit transfer: a case study, J. Propulsion, Vol. 5, No. 4, July-August 1989, pp 445-451.

76 O'CONNOR, B. and KORSEMEYER D. — A control methodology for low-thrust orbital transfer, AIAA paper 90-2959.

77 SCOLESE, C.J. — EOS mission design utilizing the space station platforms, AIAA paper 89-0252.

78 ABRAMSON R. — EOS will tell the Earth's story, Aerospace America, May 1990, pp10-11.

79 ISBELL, D. — EOS panel favors shrinking satellites, Space News, Vol. 2, No. 26, July 29 - August 4, 1991.

80 LAWLER, A. — New rocket emphasized in space policy shift, Space News, Vol. 2, No. 26, July 29 - August 4, 1991.

81 ISBELL, D. — Pad reactivation to serve secret satellite needs, Space News, Vol. 2, No. 26, July 29 - August 4, 1991.

82 GUNN, C.R. — Space transportation systems for the 21st Century, Aerospace America, June 1991, pp 32-39.

83 ARIANESPACE — *Ariane 4 Users Guide*, Issue 1, Revision 3, 1985.

84 HERGOTT, R. — Ariane 5 aims for the future, Aerospace America, July 1990, pp 74-75.

85 VEDRENNE, M. — Challenge '95 - The Ariane 5 development programme, ESA Bulletin, No. 52, November 1987, p 12-21.

86 FEUSTEL-BUECHL, J., ISAKEIT, D., and PFEFFER, H. — Wings for European spaceflight - the future of space transportation, ESA Bulletin, No. 66, May 1991, pp 21-28.

87 HEMPSELL, C.M. — European manned in orbit infrastructure - an alternative view, JBIS, Vol 43, pp 459-472, 1990.

88 REINHARTZ, K.K. — European aspects of using the space station, ESA Bulletin No 41, February 1985, pp 42-50.

89 COLUCCI, F. — Informing on the Earth, Space, Vol.7, No. 2, March-April 1991.

90 ESA — *Proceeedings of the second European in-orbit operations technology symposium*, Toulouse, France, ESA SP-297, September 1989

91 MEISSINGER, H.F. — Technology requirements for telerobotic satellite servicing in space, in *Proceeedings of the first European in-orbit operations technology symposium*, Darmstadt, Germany, ESA SP-297, November 1987.

92 CONCHIE, P.J. and WINDSOR, E.P.L. — Polar platform configuration and servicing, Space Technology, Vol.8, No.1/2, pp 37-44, 1988.

93 HATHAWAY, R.G.W. — On-orbit servicing and cost effectiveness of Columbus polar platform concepts, in Proc IGARSS '88 Symp., Edinburgh, Scotland, 13-16 Sept 1988, ESA SP-284.

94 HERMEL, J., MEESE, R.A., ROGERS, W.P., KUSHIDA, R.O., BEATTIE, J.R., and HYMAN, J. — Modular, ion-propelled, orbit-transfer vehicle, JSR, Vol. 25, No. 5, Sept-Oct 1988, pp 368-374.

95 FALKENHAYN, E. — Orbital replacement units design considerations, in Proceeedings of the second European in-orbit operations technology symposium, Toulouse, France, ESA SP-297, September 1989, pp 325-328.

96 ZAFRAN, S., BIESS, J.J. and CALLENS R.A. — Ion propulsion cost effectivity, *Electric propulsion and its applications to space missions - Progress in Astronuatics and Research Status and Needs - Progress in Astronautics and Aeronautics Vol. 79*, AIAA, 1979, pp 391-400.

97 MANVI, R. and FUJITA, T. — Parametric studies of electric propulsion systems for orbit transfer vehicles, AIAA paper 88-2835.

98 BLAIS, T., PAUVERT, C., FEHSE, W. and TOBIAS A. — Investigation and docking and berthing dynamics, in Proceeedings of the second European in-orbit operations technology symposium, Toulouse, France, ESA SP-297, September 1989, pp 325-328.

99 KAUFMAN, H.R. and ROBINSON, R.S. — Large inert-gas thrusters, AIAA paper 81-1540.

100 BURTON, R.L., CLARK, K.E. and JAHN, R.G. — Measured performance of a multimegawatt MPD thruster, JSR, Vol. 20, MAy-June 1983, pp. 299-304.

100 FREE, B.A. — Near-earth electric propulsion transfers with SP 100, AIAA paper 87-0987.

101 SMITH, W.W. and KNOWLES, S.C. — Analysis of electric propulsion concepts for near-term mission application, Joint Army Navy and Air Force Propulsion Conference 1985, Vol. 1, pp 457-467.

102 BEATTIE, J.R., MATOSSSIAN, J.N., and ROBSON, R.R. — Status of xenon ion propulsion technology, AIAA paper 87-1003.